Journal of the
OPTICAL SOCIETY
of AMERICA

VOLUME 37, NUMBER 6 JUNE, 1947

The Upper Atmosphere of the Earth*

E. O. HULBURT
Naval Research Laboratory, Washington 20, D. C.

Interest in the upper atmosphere of the earth has continued to mount rapidly in recent years although during the war period much of the interest was veiled or diverted. Now a sharp stimulus has occurred because devices, such as the V-2 rocket, are available which are able to reach great heights and thereby to provide means of direct experimentation at great heights. It is my plan here to describe briefly present knowledge of the atmosphere up to the ionosphere and to mention the not inappreciable contributions which the V-2 rocket experiments have made already.

DIRECT OBSERVATIONS

DIRECT information about the temperature, pressure, composition, and movement of the air at high altitudes has been obtained from balloons, both free and manned, and from observations of smoke projectiles and meteor trails. The full line curves of Fig. 1 are the temperature-height data[1] to an altitude of 20 km obtained from sounding balloons in Europe at latitude about 48° north. The summer curve is an average of the records of 231 flights and the winter curves of 185 flights; whether they refer to day or to night conditions was not stated. Some data to greater heights are shown in the dotted curves of Fig. 1; these were obtained by our Weather Bureau from balloon flights near sunset at Omaha, Nebraska, latitude 41° north. No full daylight data of the higher levels are yet available because of the difficulty of determining the temperature of the ambient air in full sunlight; nor are full night-time data available either.

It is seen that in temperate latitudes the temperature of the air decreased about 6°C per km until a height of 10 to 15 km was reached with temperatures of −40° to −70°C. Above this height, in winter near sunset the temperature

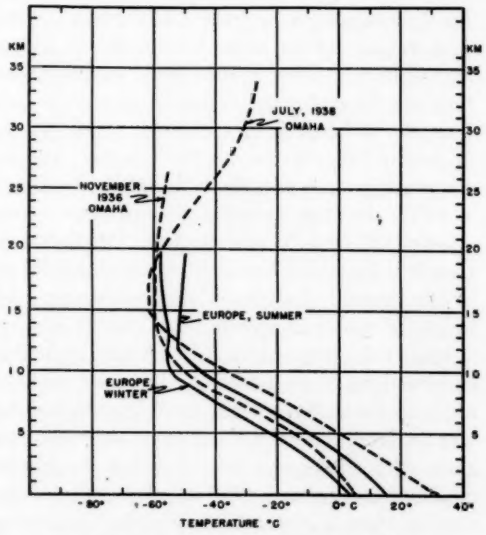

FIG. 1. Temperatures from sounding balloons.

* Presented at the meeting of the Optical Society of America, New York, New York, February 21, 1947.

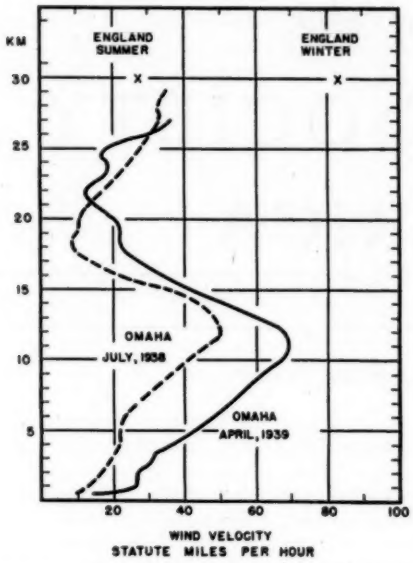

FIG. 2. Winds, curves from sounding balloons, crosses from smoke shells.

remained approximately constant or increased slightly to about 24 km; in summer near sunset it increased considerably from about 20 to 34 km. There are as yet no direct measurements of air temperatures about 35 km.

The region from about 10 to 20 km where the temperature changes little with height is called the "stratosphere" or the "isothermal region." The region above this is called the "upper atmosphere." The stratosphere changes with latitude, its under surface being about 10 km at latitude 60° north or south in summer and approximately 15 km at the equator, the corresponding temperatures being about −45° and −70°C. In temperate latitudes the stratosphere is 5° to 10°C warmer for a low barometer than it is for a high barometer. Nothing is known of the diurnal changes in the temperature and height of the stratosphere.

Wind velocities obtained from sounding balloon observations were found to increase with the altitude above the surface until the stratosphere was entered. There the velocities decreased and then with increasing height began to increase again. Average monthly data[2] for times near sunset from balloon flights near Omaha are shown in the curves of Fig. 2. By means of smoke shells exploded at 30 km over southeast England, Johnson[3] found that the average summer and winter velocities were 27 and 83 miles per hour, respectively; the values are plotted in the crosses of Fig. 2. A maximum value of 147 miles an hour was recorded in winter. The rate of drift of meteor trails was recorded in 26 cases[4] and indicated winds and eddies of over 50 miles an hour, and in two cases of nearly 150 miles an hour. The meteor trails were in levels from about 40 to 110 km; all the trails were immediately distorted and twisted as if by atmospheric currents and turbulance.

With regard to the composition of the atmosphere, the amounts of oxygen up to 29 km and of helium to 21 km have been determined[5] from samples of air obtained in high altitude balloon flights. It was found that the proportions by volume of the respective gases were constant within a few percent at all the heights reached, and were the same as at sea level. The data of Regener for oxygen and of Paneth and Glückauf for helium are plotted in Fig. 3. However, deviations from constancy, small, variable, and real were observed; these appeared to be attributable to irregularities in the lower atmosphere such as weather.

It was discovered by Fabry and Buisson[6] that ozone exists in the upper atmosphere, the amount in a vertical column being from 2 to 4 mm at N.P.T. In a world wide survey in the years 1926 to 1929 observers under the direction of Dobson[7] found that the amount of ozone increased with latitude from about 2 mm at the equator to about 3.6 mm at latitude 68° north and 44°

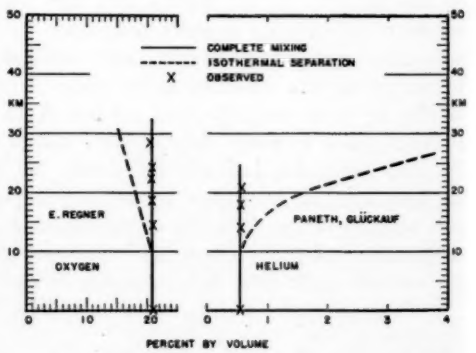

FIG. 3. Oxygen and helium from balloon data.

south. The ozone varied with the season with a maximum in the spring and a minimum in the autumn. It is not known with certainty whether there is a diurnal variation in the ozone content of the atmosphere above any station. A few data[7] indicate that a diurnal variation, if it exists, is small.

Vertical distribution curves of ozone are plotted in Fig. 4; the continuous curves were the direct measurements obtained from balloons;[8] the dotted curves were indirect measurements derived from the "Umkehr" effect.[9] The numbers on each curve were the total amounts of ozone in a vertical column in each case. It is seen that above about 25 km the ozone decreases with height and that the distribution of ozone above 30 km is not clearly known. The amount of ozone in the higher levels has an important bearing on the temperatures of those levels.

THEORETICAL

Theoretical analyses of the atmosphere have had two objectives, (a) to "understand" or "explain" the characteristics, as the composition, pressure, temperature, etc., observed in the lower levels in terms of known or assumed causes, and (b) to extrapolate the theory of the lower levels to higher levels where no direct observations existed in order to determine or predict the characteristics of the unknown levels. Probably the most complete work of this kind was that of Maris and of Gowan published in 1928.[10] Certain of the conclusions are valid today, others may require modification in the light of subsequent data which added to and changed various data which were used. In the following paragraphs are given the essential physics of the theory.

The atmosphere is a mixture of gases held on the surface of the earth by the attraction of gravity. If there were no winds and if the temperature were constant, the atmosphere would be in isothermal equilibrium, each gas would be distributed in height according to the gas laws and the force of gravity, and the proportion of the lighter gases would increase with the height. If the atmosphere were uniformly mixed, as by winds, the proportions of all gases would be the same at all heights.

Assume now that the atmosphere is at a constant temperature at all times, that it is uniformly stirred up, and that it is then kept entirely free from winds while diffusion and gravity work to restore the isothermal equilibrium condition. The lighter gases diffuse upward and the heavier ones downward. The rate of diffusion increases with the altitude and hence the isothermal distribution is attained most rapidly in the high levels and more slowly in the low levels. The level where the region of complete diffusion joins the region of uniform mixing is

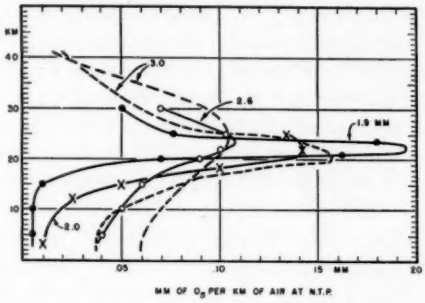

FIG. 4. Vertical distribution of ozone; solid curves from balloon data, dotted curves from "Umkehr" effect.

termed the "diffusion level." Maris showed that for helium at 0°C, for example, the diffusion level was established at 150 km for 0.53 of a day; after one day it descended to 146 km, after two days to 140 km, after five days to 136 km, after a year to 110 km. It was shown that the diffusion level varied with the gas and the temperature, being about 12 km lower and 25 km higher for −50°C and +100°C, respectively, than the level for 0°C. The levels of oxygen, nitrogen, carbon dioxide, and krypton were 5 to 10 km below that of helium.

Now, although the temperature and the amount of wind mixing in the upper atmosphere were not known exactly, it was known that winds exist from sea level to at least 100 km, and it seemed probable that the temperature was not greatly outside the limits of −50° to +100°C. Therefore, the conclusion seemed fairly certain that the diffusion level was probably not below 100 km for all the gases of the atmosphere. This meant that, apart from exceptions discussed below, the composition of the atmosphere was approximately constant from sea level to about 100 km. This is the accepted view at the present time.

The data of Fig. 3 are obviously in support of the conclusion; the dotted curves of Fig. 3 give the proportions of O_2 and He, assuming a diffusion level at 10 km merely to illustrate the fact that the observed data prove that the diffusion level is above 30 km.

Exceptions to the constancy of the composition of the air with altitude are water vapor, ozone, atomic oxygen, atomic nitrogen, and oxides of nitrogen. The first two cannot alter the composition very much, for the total amount of water vapor in a 1 cm^2 vertical column of air can not exceed about 2.6 g; this is the amount calculated on the assumption of saturated water vapor all the way up. The total amount of ozone does not exceed about 4 mm. These are small amounts compared with the 8.3 km of a vertical column of air at N.P.T. from sea level to space. A detailed theoretical discussion of atomic oxygen, atomic nitrogen, and the oxides of nitrogen is beyond the purpose here. Suffice it to say that because of the probability of short ultraviolet solar radiation falling into the atmosphere, it seems certain that oxygen and nitrogen molecules are dissociated and that oxides of nitrogen are formed. But to what extent and in what levels these actions take place is as yet a matter of conjecture.

Theoretical calculations of the temperature of the upper atmosphere have been based on the absorption of solar and earth radiations by the atmospheric gases. The spectrum of the sun was extrapolated into the ultraviolet below 2900A, a region where it was unknown, by assuming that the spectrum was that of a blackbody at 6000°K. Carbon dioxide, water vapor, ozone, and oxygen were considered to be important in regulating the temperature of the atmosphere because of their absorption bands in the spectral region concerned. Of these ozone was the most important because of its ultraviolet band from 2900 to 2300A. All of the bands of all the gases absorb energy from the sun and the earth during the day and the infra-red bands radiate energy at night. The temperature which results depends on the relative rates of absorption and emission and these in turn depend to a large extent on the vertical distribution of ozone.

A distribution with height of the atmospheric gases was assumed. Wind mixing was estimated. Maris[10] calculated that in summer daylight for latitude 50° the temperature increased, from about −40°C at 30 km to +90°C at 100 km, and that in a winter night the temperature remained approximately −40°C at all levels above 30 cm. Gowan[10] obtained roughly similar results; he also calculated the effect of assuming various amounts of water vapor and ozone. The results thus obtained were based on the idea that the maximum of the vertical distribution of ozone was at about 50 km, as was supposed to be the fact in 1928. Later observations showed that the fact was wrong and that the ozone maximum is between 20 and 30 km. Recent evidence, mentioned later, indicates that the sun radiates considerably less than a blackbody at 6000°K in the spectral region of the ultraviolet ozone band 2300 to 2800A. Therefore the numerical theoretical results require revision. Such revision and extension will probably be delayed until further data on the solar spectrum and the upper atmosphere make further excursions into theory profitable.

One may conclude that the theoretical investigations of the upper atmosphere have led to two results, (a) that the composition of the atmosphere is approximately the same throughout the region from 0 to about 100 km, and (b) that somewhere above 30 km the atmosphere grows warmer; but just where this occurs and how much the temperature changes with the day and night, could not be worked out from available data previous to 1946.

It may be remarked that cosmic rays remain aloof in that no important characteristics of the upper air have as yet been attributed to the action of cosmic rays. However, it seems quite possible that chemical or photo-chemical reactions in high levels may be discovered which are dependent upon, or owe their origin to, the high energy radiations.

INDIRECT DATA

If the constitution of the atmosphere is known at all heights, the relation between the pressure and the temperature is known at all heights; therefore the pressure can be calculated from the temperature, and vice versa. Four fields of experimentation which have led to deductions about the upper air temperatures and pressures may be mentioned, (1) sound wave propagation,

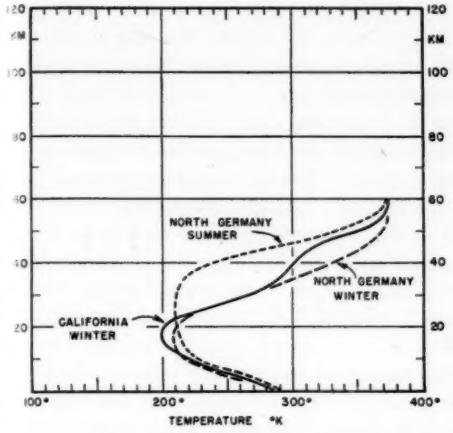

FIG. 5. Temperatures from sound propagation measurements.

(2) atmospheric tides, (3) twilight sky brightness, and (4) meteors.

In the case of sound waves from a sufficiently intense source, as an explosion or gun fire, it was observed[11] that at a distance of 100 to 200 km the sound arrived at a considerably later time than would be expected from the distance and the known velocity of sound. Only a small portion of the abnormally long time could be attributed to winds. In order to account for the long time of transit it was suggested that the sound rays had passed high into the air and had been bent down to the earth again. The suggestion was strengthened by the fact that there was often a zone of silence at 50 to 100 km from the source surrounded by a zone of audibility, and that in the zone of audibility the sound rays descended at angles to the horizontal.

Since the velocity of sound waves in a gas increases approximately with the square root of the absolute temperature and is independent of the pressure, the assumption was made that somewhere in the upper atmosphere the air grew warmer with altitude and that the sound rays were refracted back to the earth by the warmer air. From systematic measurements of the times of transit of the sound waves to various distances and the angles of descent, vertical temperature distributions were worked out by investigators in England,[11] Germany,[12] and America.[13] Some of the results are shown in Fig. 5. Whether these refer to day or night was not stated; no experiments dealing with diurnal changes have yet been published. The course of the vertical temperature distribution curves above the maximum at about 60 km could not be deduced from the sound ray measurements.

It may be mentioned that the velocity of sound would increase with altitude if the average molecular mass decreases with altitude. However, this possibility has seemed remote and has not been entertained in view of the evidence and arguments in favor of a fairly constant atmospheric composition up to about 100 km.

The atmospheric tidal oscillation theory, developed by Laplace, has passed through several interesting phases. The problem was to account for the observed fact that the solar semi-diurnal barometric variation was about 16 times that of the moon, whereas the tide raising force of the moon was twice that of the sun. It was pointed out in 1882 by Sir William Thomson that the solar pressure oscillation could not be a thermal effect, for if it were, the diurnal term should be larger than the semi-diurnal term—in direct contradiction to the facts. As a solution of the problem Kelvin made the suggestion that the atmosphere has a period of free oscillation of nearly 12 hours, so that the solar semi-diurnal tide is magnified by resonance. Analysis showed[14] that in order to obtain the necessary magnification the free period must be within 6 minutes of 12 hours. Further evidence concerning the atmospheric oscillation was adduced from the observed speeds of propagation of the explosion waves from the Krakatoa erruption of 1883 and from the great Siberian meteor of 1908. These each indicated an atmospheric oscillation period of 10.5 hours.[14]

Pekeris[15] investigated the possibility of an atmosphere with two modes of free oscillation of periods 10.5 and 12 hours, respectively. He found that a vertical temperature distribution of the type of curve 1, Fig. 6, would produce such an atmosphere, and that the distributions of the dotted curves 2, 3, and 4 would not produce such an atmosphere. The low temperature of curve 1 at about 80 km was in keeping with a theory of Humphreys[16] that cirrus-like clouds seen on rare occasions at 82 km in the day are composed of ice crystals.

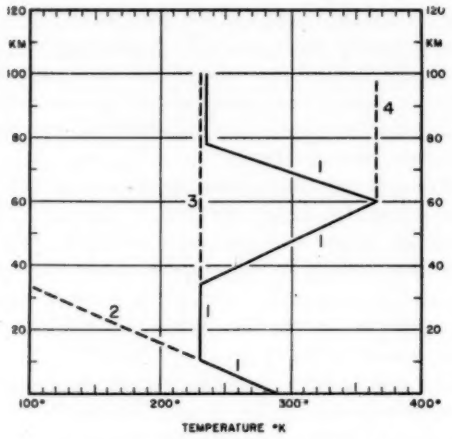

FIG. 6. Temperatures from atmospheric tide theory.

A later contribution to the atmospheric tidal phenomena was made by Appleton and Weekes,[17] who detected and measured a lunar tide in the *E* region of the ionosphere at about 110 km of amplitude about 1 km and with maxima about $\frac{3}{4}$ hour before the lunar transits. They concluded that the magnitude and phase of this tide could not be reconciled with the above theory of atmospheric oscillation. This left the theory in an uncertain state.

The brightness of the zenith sky during twilight was measured in order to determine the pressure and hence the temperature of the air to great heights.[18] The method was as follows: to an observer in twilight the brightness of the zenith sky is mainly a result of the sunlight scattered downward by the vertical column of those air molecules which are in the direct rays of the sun. Since the law of light scattering by air molecules and the intensity of the sun's rays were known, the total number of air molecules in the sunlit vertical column, and hence the pressure, could be calculated from the zenith sky brightness. After sunset, as the angle of depression of the sun below the horizon increases, only the air in increasingly higher levels is lighted by the direct rays of the sun; therefore, the measurement of the zenith sky brightness during the progress of evening twilight yields the pressure at increasingly higher levels. Similarly during morning twilight. Many series of such measurements were carried out near Washington, D. C., U.S.A., latitude 39° north, and Patos, Brazil, latitude 7° south. The result obtained was that the temperature of the twilight atmosphere was constant with height within ±15°C from 20 to 55 km and possibly to 60 km, the temperature being 220°±15°K in these levels. It was further found that the necessary corrections due to multiple scattering, which were also measured, were small at the lower heights but increased rapidly with the altitude, and at about 60 km became so large that the method failed to yield information about the air above 60 km.

Phenomena of meteors have been interpreted as indicating that the density of the air above a level of about 60 km was greater than that calculated from the assumption of a constant air temperature of 220°K from about 40 to 100 km. The increased air density was assumed to be caused by an increase in temperature above the 40 km level. Thus the meteor observations were used to calculate the upper air densities and hence the temperatures. The observed phenomena, both photographic and visual, were the deceleration of the meteor and the heights of the beginning, maximum brilliance, and end of the meteor trails. The air densities were derived from each of these phenomena by means of special detailed theories which assumed a density and size of the meteor and which described the physical actions which occurred when the meteor swept into the atmosphere, lost energy and gave out light. The several theories have been at various times challenged, debated, and modified.

It is beyond my purpose here to describe the several theories. Suffice it to give the results summarized in a recent paper by Whipple.[19] These are shown in Fig. 7 which is redrawn from his Fig. 2. The air densities derived by theory from the meteor observations are plotted as points in Fig. 7. They refer to nocturnal conditions. The smooth curve is that calculated from the temperature height curve 1 of Fig. 6, which has a maximum temperature of 365°K at about 60 km, falling to 184°K at 80 km. Whipple concluded that "a considerable range of solution [of the meteor data] occurs, depending upon the weighting ascribed to the various methods of determining the atmospheric density. The best solution appears to be that [of the smooth curve

of Fig. 7]. . . . It must be noted, however, that a constant atmospheric temperature of about 255°K from 60 to 110 km is not entirely outside the range of solution. . . . The observations of maximum light in photographic meteor trails require a high temperature zone near the 60 km level in the atmosphere, but are better satisfied without the low temperature zone at the 82 km level."

Sound wave propagation suggests a temperature above the stratosphere which rises to about 370°K at about 60 km. The data refer to daytime conditions; there are no data at night. The data permit no conclusion about the temperature above 60 km.

Atmospheric tide theory requires a temperature maximum of about 350°K at about 60 km. Presumably this is an average around the equator; whether there are diurnal variations was not stated. At present the theory is faced with the difficulty that it predicts upper atmospheric tides which are not in agreement with observations of the *E* region of the ionosphere.

Measurements of twilight sky brightness indicate air temperatures during twilight of 220° to ±15°K from about 20 to 55 km; they give no information about the temperature above 60 km, or at other times of day than twilight.

Meteor phenomena at night indicate an increase in temperature with height from about 40 to 60 km, but did not indicate clearly whether the temperature above 60 km remained constant or decreased.

We may comment that although there are some apparent discordant conclusions among these indirect lines of evidence, it appears that none is so constricted that it cannot yield enough to avoid clashing.

TENTATIVE TABLES OF THE UPPER AIR

As a result of the foregoing considerations, tentative tables of the upper atmosphere were drawn up by commissions in England, Germany, and America. The temperature curves are shown in Fig. 8; the American curve, labelled NACA, was prepared by a committee of the National Advisory Committee for Aeronautics.[20] The NACA curve of Fig. 8 was called the "tentative standard" curve; "tentative maximum" and "tentative minimum" curves were also drawn, being respectively 30° to 80°K above and below that of Fig. 8. No seasonal or diurnal variations in the temperatures above 120 km were decided upon.

In the NACA report[20] the composition of the atmosphere was assumed to be approximately unchanged from sea level to 80 km, the mass of the average air molecule being taken to be 28.966 times the mass of the hydrogen atom, or 4.816×10^{-23} g. In the daytime, oxygen was assumed to change linearly with the height from entirely molecular at 80 km to entirely atomic at 100 km; at night the respective levels were 105 and 120 km. From these assumptions of temperature and composition tentative tables of the pressures and densities to 120 km were calculated.

DATA FROM V-2 ROCKET EXPERIMENTS

In 1945 the Army Ordnance Corps obtained a considerable number of V-2 rockets from Germany and planned to fire them in order to gain experience in the performance of the rockets and to obtain data on the upper atmosphere. In the case of their use in upper air research, a collaborative program was commenced in 1946 with the Rocket Sonde Research Section of the Naval Research Laboratory. Other agencies and institutions, such as universities, astronomical observatories, and industries, became interested and a panel was established with membership

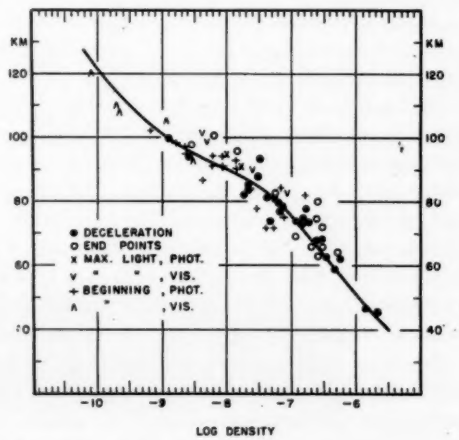

FIG. 7. Atmospheric densities from meteor observations.

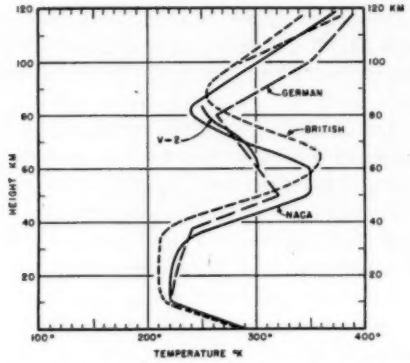

FIG. 8. Tentatively assumed temperature-height curves. The short curve was derived from the V-2 pressure data of October 10, 1946.

restricted to persons actually working in the program. At present the panel consists of representatives of ten institutions.

Special warheads for the V-2 for carrying research apparatus were designed by the Rocket Sonde Section and built at the Naval Gun Factory; telemetering apparatus and other equipment common to most warheads were developed. Each warhead was a specialized short-lived research laboratory. These were supplied to the cooperating institutions, and a program has been carried out in which each institution in turn has undertaken the responsibility of the experiments of each rocket flight. The flights take place at the White Sands proving area in New Mexico, latitude 33° north.

At the present writing new data have been obtained on atmospheric pressures and solar radiations at great heights. Each of these items involved a major effort and was accomplished by specially organized groups at the Naval Research Laboratory. All groups have thus far worked under extreme pressure of time, because the rockets were to be fired according to schedule no matter whether the laboratory warheads were ready or not. The direct data obtained in a few seconds will eventually replace the indirect inferences of years.

We shall make no mention here of the new V-2 cosmic-ray data that have been secured,[21] because as has been said, cosmic rays have not yet been shown to be important in determining the characteristics of the upper air.

Pressure measurements[22] were made during the V-2 rocket flight of October 10, 1946, which took place at 11 A.M., 105th meridian time. The pressure indications of the gauges in the rocket were telemetered to recording apparatus on the ground. Two sets of pressure data were recorded, one set from 0 to 12 km which agreed with known values and one set from about 60 to 85 km. This second set of data is plotted in the dots of Fig. 9 along with the NACA tentative standard day pressure curve. It is seen that the NACA tentative values are about 12 percent below the observed values. Assuming that the composition of the upper air is that of the NACA assumptions, the temperatures were derived from the slope of the observed pressure curve of Fig. 9 and are plotted in Fig. 8. The accuracy of the temperatures obtained in this way is not great, but a critical discussion of the accuracy may be deferred until hopes of further V-2 data are realized.

The V-2 rocket of the flight of October 10, 1946, at 11 A.M. carried a grating spectrograph which photographed solar spectra[23] in the ultraviolet below 3400A up to a height of 88 km. At 11 A.M. the altitude of the sun was 51°; solar activity was low, the terrestrial magnetic character figure being 0.2 for the period 0 to 12 hours on October 10. The rocket ascended to about 160 km and fell to earth in the New Mexico desert about 20 miles from the launching point. Four days later the spectrograph and film container were recovered practically intact.

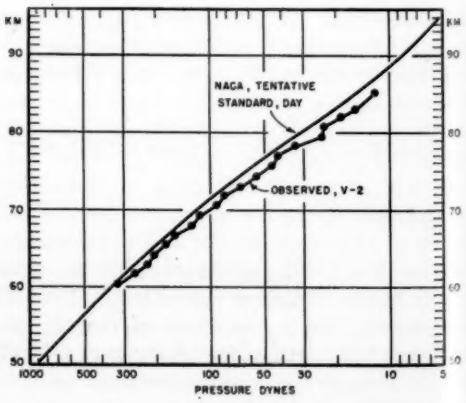

FIG. 9. Pressure data from the V-2 rocket flight of October 10, 1946.

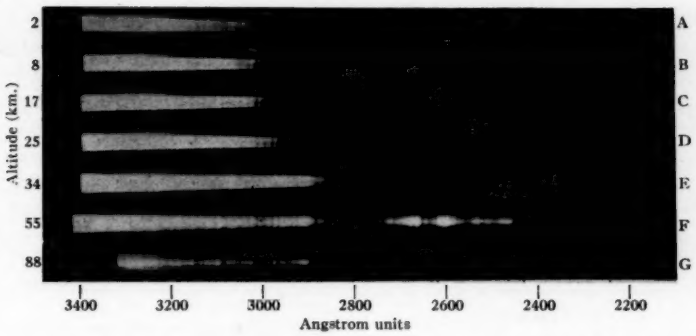

FIG. 10. Solar spectra from the V-2 rocket flight of October 10, 1946.

Upon development 35 spectra were found on the film, the highest being taken at 88 km. Spectra at altitudes above this were not obtained because vibration of the rocket caused the film release mechanism to operate too quickly, with the result that all of the film was exposed on the way up to 88 km. Some of the spectra are shown in Fig. 10, in which all the exposures were 3.6 seconds and the altitudes are above sea level. Up to about 44 km the rocket was stabilized. Above this point it rolled and yawed, and spectra *F* and *G*, Fig. 10, were taken with the sun well off the axis of the spectrograph; *G* at 88 km was so lightly exposed that it showed less ultraviolet than *F* at 55 km. In Fig. 10 the spectra were shaded in printing in order to emphasize the regions of interest as much as possible.

The spectra show a progressive extension into the ultraviolet with increase in altitude. Spectrum *D*, Fig. 10, at 25 km extended to 2925A. Spectrum *E* at 34 km extended to 2650A and showed measurable blackening from about 2260 to 2100 at the short wave-length border of the great Hartley ozone band. Therefore at 34 km there was still enough ozone between the spectrograph and the sun to prevent recording the spectrum in the central region of the band. Spectrum *F* at 55 km showed no evidence of ozone absorption. These solar spectra are the first which have been obtained from above the ozone of the upper atmosphere; they yield a new extension of the solar spectrum into the ultraviolet from about 2900 to 2100A.

The newly revealed portion of the solar spectrum is shown in Fig. 11, in which certain of the absorptions are identified. This is the same spectrum as *F*, Fig. 10, at 55 km; it was shaded in printing. Prominent absorption features are SiI at 2882A, the great magnesium absorptions MgI at 2852A, and the doublet MgII at 2802 and 2795A, and the ultimate lines of FeII at 2410, 2405, 2396, and 2382. A detailed analysis of the spectra is in progress.

The intensity distribution of the sunlight through an amount of overhead atmosphere equivalent to about 1 mm of Hg was determined by careful photographic photometric comparison of the high altitude solar spectra with the spectrum of a calibrated carbon arc. The preliminary results are shown in Figs. 12 and 13 in which the new curve in the region below 3000A was joined to the known curve[24] for

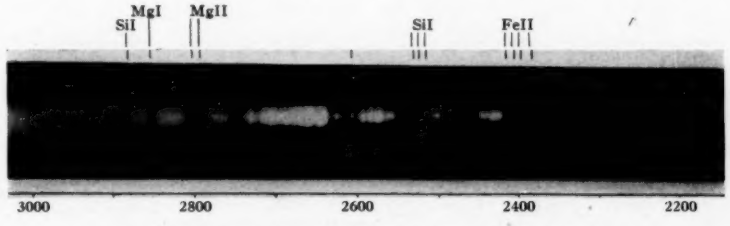

FIG. 11. Ultraviolet solar spectrum from 55 km altitude.

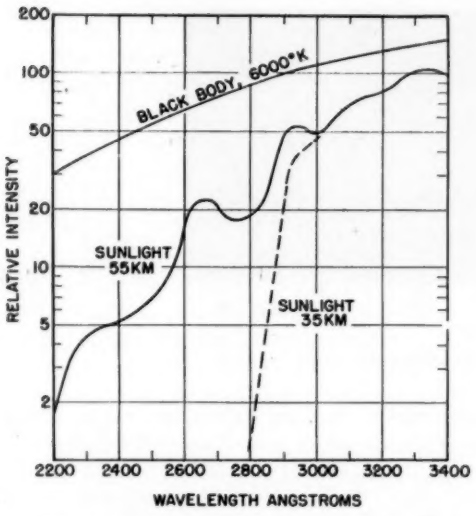

FIG. 12. Ultraviolet solar spectral energy curve.

wave-lengths longer than 3000A for the sun outside the atmosphere. The curve for a blackbody at 6000°K is also plotted in Figs. 12 and 13, and adjusted to pass through the maximum of the solar intensity curve at about 4600A. It is seen that the solar curve falls below the blackbody curve by factors of about 3 and 10 to 20 at 3000 and 2200A, respectively. These new facts will be important in calculating the temperatures of the atmospheric levels where the sunlight is absorbed by ozone.

The determination of the amounts of ozone at various altitudes is in progress. At present all that can be said is that on October 10 approximately 3 percent of the total ozone was above 34 km and less than 1 percent was above 55 km.

The solar spectra obtained thus far offer a little information about oxides of nitrogen in high atmospheric levels. There was no indication in the spectra of the characteristic bands[25] of NO_2 or N_2O_4, nitrogen tetroxide, at 2600 to 2270A. In the case of nitrogen pentoxide N_2O_5 an infra-red atmospheric absorption band at 7.6μ was suggested by Adel and Lampland[26] as being caused by this gas. In the ultraviolet it is known[25] qualitatively that the gas has continuous absorption which increases as the wavelength decreases from 2800 to 2400A. But since quantitative data are lacking, no inferences can be drawn from the solar spectra concerning the presence or absence of N_2O_5 in the high atmosphere. Similarly for nitrous oxide N_2O, which has continuous absorption[25] from 3000 to 1760A probably too weak to be detectable in the high altitude spectra. Thus at present the existence and the distribution of various oxides of nitrogen in the upper atmosphere cannot be determined from the available high altitude spectra.

BIBLIOGRAPHY

The literature on the upper atmosphere is large. The 1523 references in *Terrestrial Magnetism and Electricity, Physics of the Earth Series VIII*, McGraw-Hill Book Company, Inc., 1939, cover many aspects of the subject up to about 1937. More recent references are found in the ten papers of the Gassiot Committee of the Royal Society, *Reports on Progress in Physics*, (Phys. Soc. London 1942–43), Vol. 9, p. 1–100.

The following references are specifically cited in the present report:

(1) W. J. Humphreys, *Physics of the Air* (McGraw-Hill Book Company, Inc., New York, 1940), third edition, Fig. 16, p. 44.
(2) L. F. Hafer, Mon. Weather Rev. **68**,125–129 (1940); J. C. Ballard, *ibid.* **66**, 2–9 (1938).
(3) N. K. Johnson, Nature **157**, 24 (1946).
(4) S. Kahlke, Ann. Hydrogr. **49**, 294–299 (1921); C. C. Trowbridge, Mon. Weather Rev. **35**, 390–397 (1907); data summarized by E. O. Hulburt, Pub. Ast. Soc. Pacific **44**, 178–182 (1932).
(5) A. Lepape and G. Colange, Nature **137**, 459 (1936); F. A. Paneth and E. Gluckauf, Nature **136**, 717–718 (1935); G. A. Prokofiev and others, Nature **133**, 918–919 (1934); E. Regener, Nature **138**, 544 (1936); M. Shepherd, Nat. Geog. Soc., Contrib. Tech. Papers, Stratosphere Ser. No. 2, 117–133 (1936).
(6) C. Fabry and H. Buisson, J. Phys., Paris, **3**, 196–206 (1913); C. Fabry, Proc. Phys. Soc. **39**, 1–14 (1926).
(7) G. M. B. Dobson, Proc. Roy. Soc. **A129**, 411–433 (1930).
(8) E. Regner and V. H. Regner, Physik. Zeits. **35**,788–793 (1934); E. Regner, Beitr. Physik. frei Atmos. **22**,

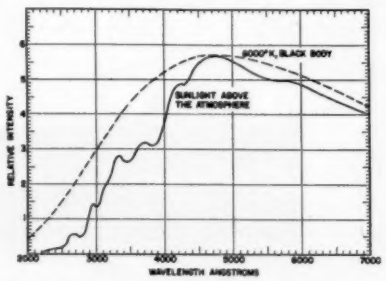

FIG. 13. Solar spectral energy curve.

249–260 (1935); B. O'Brien, F. L. Mohler, and H. S. Stewart, Nat. Geog. Soc. Contrib. Tech. Papers. Stratosphere Ser. No. 2, 71–93 (1936); W. W. Coblentz and R. Stair, Nat. Bur. Stand. J. Res. **26**, 161–174 (1941).
(9) F. W. P. Götz, Erg. Kos. Physik, Leipzig, **1**, 180–235 (1931); F. W. P. Götz, A. R. Meethan, and G. M. B. Dobson, Proc. Roy. Soc. **A145**, 416–446 (1934).
(10) H. B. Maris, Terr. Mag. **33**, 233–255 (1928); **34**, 45–53 (1929); E. H. Gowan, Proc. Roy. Soc. **A120**, 655–669 (1928); **128**, 531–550 (1930).
(11) F. J. W. Whipple, Quart. J. Roy. Met. Soc. **57**, 331–335 (1931); **58**, 471 (1932); **60**, 80–88 (1934).
(12) P. Duckert, Gerlands Beitr. Z. Geophys. **1**, 236–290 (1931).
(13) B. Gutenberg, J. Met. **3**, 27–30 (1946).
(14) G. I. Taylor, Proc. Roy. Soc. **A126**, 169–183 (1929).
(15) C. L. Pekeris, Proc. Roy. Soc. **A158**, 650–671 (1937).
(16) W. J. Humphreys, Mon. Weather Rev. **61**, 228–229 (1933).
(17) E. V. Appleton and K. Weekes, Proc. Roy. Soc. **A171**, 171–187 (1939).
(18) E. O. Hulburt, J. Opt. Soc. Am. **28**, 227–236 (1938).
(19) F. L. Whipple, Rev. Mod. Phys. **15**, 246–264 (1943).
(20) C. N. Warfield, "Tentative Tables for the Properties of the Upper Atmosphere," September 1946, Report of NACA Special Subcommittee on Upper Atmosphere.
(21) S. E. Golian, E. H. Krause, and G. G. Perlow, Phys. Rev. **70**, 223 and 776 (1946).
(22) N. R. Best, E. Durand, D. I. Gale, and R. J. Havens, Phys. Rev. **70**, 985 (1946).
(23) W. A. Baum, F. S. Johnson, J. J. Oberly, C. C. Rockwood, C. V. Strain, and R. Tousey, Phys. Rev. **70**, 781 (1946).
(24) Smithsonian Physical Tables, Table 767 (1933).
(25) H. Sponer and E. Teller, Rev. Mod. Phys. **13**, 75–170 (1941).
(26) A. Adel and C. O. Lampland, Astrophys. J. **87**, 198–203 (1938).

JOURNAL OF THE OPTICAL SOCIETY OF AMERICA VOLUME 37, NUMBER 6 JUNE, 1947

Photographic Measurements of Atmospheric Boil*

L. A. RIGGS, C. G. MUELLER,** C. H. GRAHAM,** AND F. A. MOTE***
Brown University, Providence, Rhode Island

Optical shimmer or "boil" effects are most pronounced over bare ground in bright sunshine. These effects demonstrate that the region of the atmosphere near the ground is an optically heterogeneous medium. Rays of light are variously deviated from moment to moment by every portion of this medium through which they pass. The character and extent of such deviations have been measured in the present experiments with the aid of instantaneous photographs of outdoor targets. In each experiment, 30 or more successive exposures have been made and analyzed in an effort to determine the instantaneous deviation of any point on the target image from its mean position on a reference scale. It has been found that the average deviation, caused by boil, of rays from a point on the target to the camera is in excess of three seconds over level ground in bright sunshine; the maximum deviation may reach nine seconds or more under these conditions. Two separate points on the image are found to suffer the same kind of distortion at the same instant of time if the two points are very close together. The similarity is less marked, however, with points which are farther apart. With points whose separation has an angular subtense at the camera greater than five minutes, the effects of boil upon the two are essentially independent.

INTRODUCTION

THE experiments here reported were performed in connection with a project involving research on the design of telescopic reticles. The aim of the experimenters was to supplement the study of reticle patterns with an investigation into the effects of optical shimmer or boil upon the quality of telescopic images in general. In a project report of August 6, 1945[1] the authors presented the results of this investigation, together with some preliminary considerations of the relation of boil to the performance of stereoscopic rangefinders.

The present experiments employed a photographic method of studying the quality of image in a telescopic system under various atmospheric conditions. The method consisted basically of forming a real image of a distant, outdoor target on a photographic film and making enlarged prints of the film for later study.

* The work described in this report was carried out under a contract between the Office of Scientific Research and Development and Brown University. A first public report of this work was presented at the Winter Meeting of the Optical Society of America, February 20–22, 1947, New York, New York.
** Now at Columbia University, New York, New York.
*** Now at the University of Wisconsin, Madison, Wisconsin.

[1] "Photographic Measurements of Atmospheric 'Boil,' with some Preliminary Theoretical Considerations of the Relation of 'Boil' to Rangefinder Magnification and Baselength." Division 7, N.D.R.C.

A photographic method was used by A. E. Douglass[2] in 1926 to record the appearance of shadow bands caused by atmospheric refraction. His method differs from our own, however, in using a point source of light and recording an image of a portion of the atmosphere directly on a photographic plate. Douglass' method shows the phenomenon of atmospheric refraction as causing light and dark bands of varying density, while our method shows the same phenomenon as a distortion of the image of a target.

The influence of atmospheric distortion on the precision of telescope pointing has been studied in experiments reported by Washer and Williams.[3] These investigators have shown that the probable error, E, of a single pointing is of the order of 0.62 second using a magnification of 37 diameters, "under average daylight conditions and over a terrain that consists partly of park area and partly of city residential and business section." The value of 0.62 second is contrasted with a value of approximately 0.24 second for E when indoor targets are used. The authors attribute the difficulty of outdoor observations to the fact that the observer must set the crosshairs into apparent coincidence with a constantly oscillating image of the target.

Less directly related to our experiments are studies of loss of contrast or detectability in a target seen through haze or fog. Hulburt[4] has analyzed the influence of atmospheric haze in terms of the scattering of light measured by means of a telescopic photometer; and Hardy[5] has shown the extent to which atmospheric haze may reduce the effectiveness of telescopic observation.

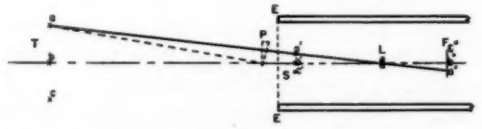

FIG. 1. Diagram showing the relative positions of the target T (three of the nine black, vertical lines are shown at abc); the reference scale, S (with corresponding lines $a'b'c'$); and the combined photographic image $a''b''c''$ formed on a film, F, by the lens, L. The region to the right of EE is enclosed within a railroad tunnel.

PROCEDURE

Basically, the procedure consisted of photographing a black-and-white line target located outdoors at a distance of several hundred meters from the camera, and measuring on the photographs the amount of image distortion which could be attributed to shimmer or boil. It was found necessary to have a reference scale, similar in function to a telescopic reticle or set of crosshairs, in order to determine the absolute magnitude of the deviation of an image point from moment to moment. For this purpose a linear scale was set up at a distance of about 100 meters from the camera in such a way that it was imaged alongside the target on the photographs. The advantage of the scale over a reticle was that any slight vibration or displacement of the camera would affect equally the images of the scale and the target, and hence cause no serious error in measurements of the deviations of the latter. We are reasonably confident, therefore, that the deviations reported below, after due allowance has been made for error in measuring the photographs, are due solely to atmospheric effects.

Figure 1 shows in diagrammatic form the positions of the target, scale, and camera. Also shown is the position of a railroad tunnel which was used in some of the experiments to minimize the effects of boil on the reference scale by shielding from direct sunlight the space between it and the camera.

In each experiment, about 30 successive photographs were made of the target and scale. The camera consisted of a specially adapted telescope objective[6] having a focal length of 128 cm. The aperture was stopped down to a diameter of 2.9 cm in order to secure the depth of focus necessary to include both the target and the scale. Agfa Supreme roll film was used, with exposures of 0.04 second.

The preliminary experiments were conducted at an average height of about 12 meters above a predominantly grassy terrain at the Brown

[2] A. E. Douglass, Photograph of shadow bands. Astrophys. J. **63** (1926), Plate XI *a* following page 188.
[3] F. E. Washer and H. B. Williams, J. Opt. Soc. Am. **36**, 400 (1946).
[4] E. O. Hulburt, J. Opt. Soc. Am. **31**, 467 (1941).
[5] A. C. Hardy, J. Opt. Soc. Am. **36**, 283 (1946).
[6] The telescope was borrowed from the Department of Astronomy at Brown University through the courtesy of Professor Charles H. Smiley.

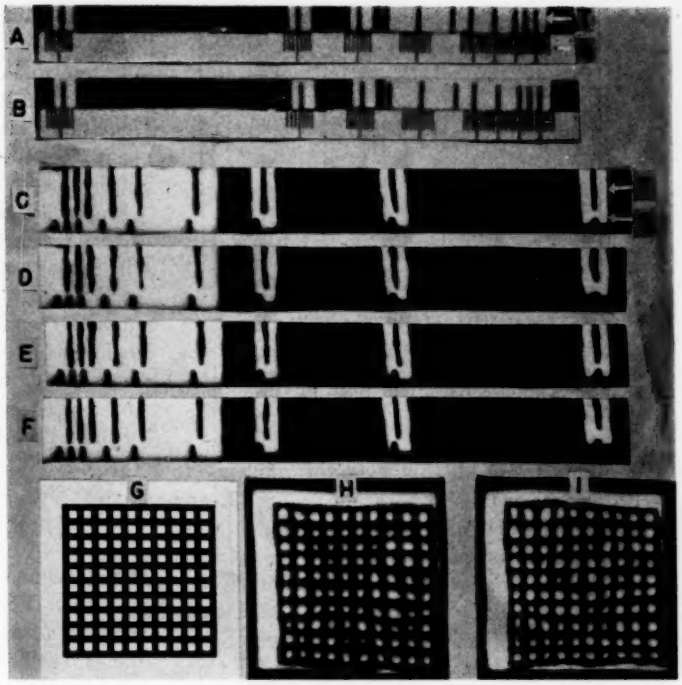

FIG. 2. Image distortion caused by atmospheric boil.

A and B. Row of vertical posts in the target position, *T*, and set of vertical lines in the scale position, *S*. Relatively slight boil; Stadium location; experiment of March 29, 1945.

C, D, E, and F. Corresponding records showing a large amount of boil; tunnel location; experiment of June 19, 1945.

G. Undistorted photograph of a special grid target.

H and I. Telescopic appearance of the grid target in the tunnel location; experiment of June 25, 1945; boil very pronounced.

The angular subtense of the linear scale and target is about 50 minutes at the camera; that of the grid is 6.8 minutes.

University Stadium. Later experiments were done over a railroad right-of-way with no track at Riverside, Rhode Island. In all of the final experiments the camera and scale were set up within the railroad tunnel and the target posts were photographed over a region of railroad right-of-way which was open to direct sunshine. In both the Riverside and the tunnel locations a high degree of boil was assured by working at an average height of about 75 cm above the surface of the bare ground.

RESULTS

Enlarged photographic prints were made from all film records obtained by the procedure above described. Figure 2 shows samples of such prints, in which the effects of boil are seen to include a typical wavy and blurred appearance of all contours and a shift, from moment to moment, of any point on the target with reference to a corresponding point on the scale.

The amounts of shimmer present under the conditions of these experiments have been determined by measuring, on each photographic print, the instantaneous position of a given point on the target with reference to the scale. A frequency distribution of such scale positions is shown in Fig. 3 for one target line in the experiment of June 19, 1945, on which day there was a fairly large amount of shimmer. The average deviation of single measurements from the mean of this distribution is 2.39 seconds of arc. Average deviations in excess of three seconds have been obtained for experiments in which the effects of boil were even more pronounced.

A quantitative approach to the problem of image distortion has been undertaken in the following manner: The image is said to be undistorted (a) if all parts of it remain stationary with respect to the reference scale, or (b) if all parts undergo the same displacement at the same instant with respect to the scale. The degree of distortion is then defined as the degree to which one point on the image is shifted differentially with respect to another point at any given instant of time. Obviously it is this differential shift of separate parts of the image which produces the wavy or warped appearance of a telescopic target in the presence of boil.

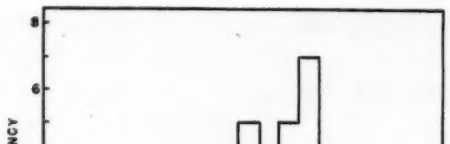

FIG. 3. A frequency distribution of 31 measured positions of a shimmering image of a point on the target. Large amount of boil; experiment of June 19, 1945; tunnel location.

We have applied this type of analysis to records such as those appearing in Fig. 2, and arrive at the following conclusion: When a target post in one region of the scale has been shifted by a certain amount[7] along the scale in one direction, it is likely that the post immediately adjacent to it will show a similar degree of shift in the same direction at the same instant of time. It is less likely, however, that posts more remote from the original one will be similarly shifted; in fact, for posts separated by more than 200 or 300 seconds from one another there appears to be no appreciable relationship between the instantaneous shift of one and that of the other.

Figure 4 presents some samples of the evidence for the above statements. If we call m the algebraic difference between shifts of a given pair of vertical posts at a given instant, we may plot the average value of m for 30 or more photographs as a function of the separation between the posts (angular subtense at the camera). The data of Fig. 4, A show that when no boil is present (weather completely overcast) there is no relationship of the sort described above. In 4, B and 4, D however, it is seen that m is diminished for separations of less than 200 seconds of arc, as compared to a value of about 3.7 seconds for greater separations when a considerable amount of boil is present. With the very large amount of boil in Fig. 4, E, m attains a value of about 4.5 seconds.

The value of m as measured here is inflated to some extent by errors of measurement, which are inevitably large as a result of the blurred appearance of the telescopic image. The magnitude of this factor has been determined by making the usual measurements of m on a series of 40 records, 10 of which were identical enlargements from the same original negative. In these 10 control records, not identified as such by the person making the measurements, the value of m should logically be zero; the values obtained by measurement are shown in Fig. 4, C. It is concluded that the average error, e, of measurements of m is of the order of 1.2 seconds; and that the average amount of distortion or differential shift, d, is related to m approximately by the relation

$$d=(m^2-e^2)^{\frac{1}{2}} \qquad (1)$$

if we assume that m and e are normally distributed. For separations greater than 300 seconds, d has a value of about 3.5 seconds under the conditions of May 12 and June 19, 1945, when a large amount of boil was present (see Fig. 4). For experiments such as that of May 10, 1945, when boil was not present to any appreciable extent, d has a value of less than 1.5 seconds regardless of the separation between points. With the very pronounced boil of June 25, 1945, the value of d reaches about 4.3 seconds.

All of the measurements reported above have been in terms of displacements whose angular subtense was measured at the camera in a horizontal plane. That similar vertical displacements are also found is shown by the distortion of the grid pattern of Fig. 2, H and I. Over the limited area of this surface, 6.8 minutes square, the character and degree of boil effect are not noticeably different whether horizontally or vertically measured. It seems probable that this situation holds only of a target which is sufficiently small so as not to extend vertically through strata of air whose densities are dependent upon their heights above the ground.

DISCUSSION

The present investigation has shown, by the use of an objective photographic method, the average amount of distortion present in a tele-

[7] It is assumed here that the shifts from moment to moment are of a "random" nature and that the "true" or undistorted position of the target post is approximately indicated by the mean position as measured on a set of 30 or more photographs.

scopic image under various degrees of boil or shimmer. Such atmospheric effects are presumably similar to those which would be expected of a set of hypothetical prisms such as the one shown by the dotted lines at P in Fig. 1. The prisms, which occupy the space between the scale and the target, are to be thought of as having constantly changing power, orientation, and size. It is apparent that the effect of any prism is to produce a deviation in the direction of rays entering the camera from any point on the target. The appearance of boil results from the "random" summation of such deviations from instant to instant, and from point to point on the target.

Presumably an observer, in pointing a telescope at a target, must perform a sort of visual integration whereby the telescope cross-hair is brought into coincidence with the mean apparent position of a target point. The exact relation between the amount of distortion as we have measured it, and error of pointing as measured by Washer and Williams, has not yet been determined under comparable conditions of boil. In our experiments, the mean displacement of the target image from its "true" (i.e., mean) position appears to be in excess of three seconds; and the whole extent of the oscillation may be about 18 seconds under conditions when the boil effect is large. Certainly the probable error of a single pointing of a telescope under these conditions would be greatly in excess of the 0.62 second reported by Washer and Williams for an air path which was high above the ground. Furthermore, in our experiments it was not feasible to measure the effects of the atmosphere intervening between the telescopic camera and the scale. Only a direct comparison of observer performance with photographic records made under the same conditions would reveal the exact correspondence between the subjective error and the objectively measured oscillations.

With regard to rangefinder performance, our experiments indicate that atmospheric disturbances affecting the two lines of sight to the instrument may be considered to be independent of one another except for the region near the target on which the two lines are converging. The nature of vernier or stereoscopic observation is such, however, that we should hesitate to

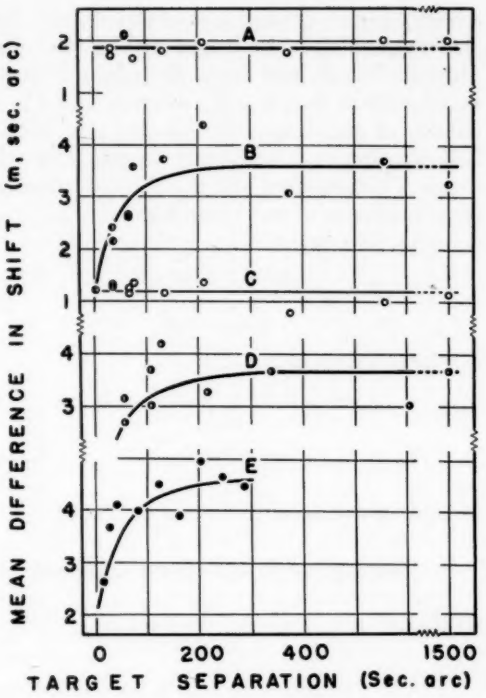

FIG. 4. Differential shift, m, caused by atmospheric boil, between points on the target whose separations are shown.
A. No appreciable boil; Riverside location; experiment of May 10, 1945.
B. Large amount of boil; Riverside location; experiment of May 12, 1945.
C. Control series of measurements on a set of 10 identical prints from one negative; experiment of May 12, 1945.
D. Large amount of boil, experiment of June 19, 1945; tunnel location.
E. Maximal amount of boil; experiment of June 25, 1945; tunnel location.

predict that a given amount of distortion would lead to a certain error of ranging. A "visual integration" must also be involved in establishing a stereoscopic or vernier form of contact, with a target image consisting of two independently oscillating units. Nevertheless, an analysis of the situation existing at a given moment may be of interest.

The standard equation for the error, E, of ranging under ideal conditions of visibility is[8]

$$E=\frac{fR^2}{206{,}000bM} \qquad (2)$$

[8] A. Gleichen, *The Theory of Modern Optical Instruments* (translated by H. H. Ensley and W. Swaine), (His Majesty's Stationery Office, London, 1918).

where f is the variability of observing and R is the range, b the base-length and M the magnification. E, R, and b are all expressed in the same units of length (e.g., meters), and f is in seconds of arc. It may be assumed that optical boil contributes a variability factor, g, to the observer's variability, and that this contribution is proportional to the magnification. The error equation then becomes

$$E=\frac{R^2[f^2+(gM)^2]^{\frac{1}{2}}}{206{,}000bM}. \quad (3)$$

For large values of g and M,

$$[f^2+(gM)^2]^{\frac{1}{2}}\sim(g^2M^2)^{\frac{1}{2}}=gM \quad (4)$$

and

$$E=\frac{R^2g}{206{,}000b}. \quad (5)$$

Equation (5) means that, when a large degree of optical boil is present, magnification has no influence on the error of ranging conceptually regarded as existing for a given instant of time. What influence these instantaneous errors might have on range finding might be answered by an experiment in which photographic analysis is coupled with simultaneous operator performance over the interval of time taken in making range settings.

JOURNAL OF THE OPTICAL SOCIETY OF AMERICA VOLUME 37, NUMBER 6 JUNE, 1947

Multiplier Photo-Tube Characteristics: Application to Low Light Levels*

RALPH W. ENGSTROM
Radio Corporation of America, Lancaster, Pennsylvania

Measurements in such fields as photometry, spectrometry, and astronomy, dealing with very low light levels, may be assisted by the use of photo-multiplier tubes. Spectral characteristics of visible (S-8), blue (S-4), and ultraviolet (S-5) sensitive multiplier tubes are presented. Data are shown illustrating the wide range of linearity of photo-multiplier types 931-A, 1P21, 1P22, and 1P28. The tubes are linear at currents up to the point where space charge in the output stages reduces the ratio of anode current to cathode light flux. Dark currents and the limitations which they introduce in practice are discussed. Fatigue effects are discussed and data shown which indicate good stability at low current levels. The ultimate sensitivity of these tubes when refrigerated to various degrees has been investigated; with suitable precautions, pulses attributable to individual photoelectrons can be counted.

INTRODUCTION

In recent years the availability of multiplier photo-tubes capable of measuring very weak light sources has resulted in a number of important applications in such fields as Raman spectra,[1] spectrographic quantitative analyses,[2–5] radioactive measurements,[6] and astronomy.[7,8] The success of the multiplier photo-tube is principally the result of its tremendous amplification factor which, in addition to its great convenience, permits extension of measurement to lower light fluxes than is possible with a simple photo-tube. This advantage is gained through the elimination of the coupling resistor and the associated Johnson noise.[9–17]

* Presented at the Thirty-First Annual Meeting of the Optical Society of America, New York, New York, October 3–5, 1946.

[1] D. H. Rank, R. J. Pfister, and P. D. Coleman, J. Opt. Soc. Am. **32**, 390 (1942).

[2] D. H. Rank and R. V. Wiegand, J. Opt. Soc. Am. **36**, 325 (1946).

[3] E. A. Boettner and G. R. Brewington, J. Opt. Soc. Am. **34**, 6 (1944).

[4] G. H. Dieke and H. M. Crosswhite, J. Opt. Soc. Am. **35**, 471 (1945).

[5] J. L. Saunderson, V. J. Caldecourt, and E. W. Peterson, J. Opt. Soc. Am. **35**, 681 (1945).

[6] M. Blau and B. Dreyfus, Rev. Sci. Inst. **16**, 245 (1945).

[7] G. E. Kron, Astrophys. J. **103**, 324 (1946).

[8] A. E. Whitford and G. E. Kron, Rev. Sci. Inst. **8**, 78 (1937).

[9] A. M. Glover, Proc. I.R.E. **29**, 413 (1941).

[10] J. A. Rajchman and R. L. Snyder, Electronics **13**, 20 (Dec. 1940).

[11] V. K. Zworykin and J. A. Rajchman, Proc. I.R.E. **27**, 558 (1939).

The purpose of this paper is to make data on the properties of the RCA series of multiplier photo-tubes more generally available. The data include spectral response curves; representative data illustrating the magnitude of fatigue to be expected at various output levels; and a study of the linearity of the tubes with variations in light flux. Emphasis is placed on those properties affecting the measurement of very low light levels and the relative advantages of various methods of utilizing the tubes are presented.

GENERAL CHARACTERISTICS

Gain and Voltage

Schematically illustrated in Fig. 1 is the RCA type of electrostatically focused multiplier photo-tube with the paths of the electrons and secondary electrons indicated as they cascade through the nine dynode stages to the collector anode. The result of this series of secondary-emission multiplications is an over-all gain of approximately one million at 100 volts per dynode stage. Variation of the amplification factor with the voltage per stage is shown in Fig. 2 for a typical 931-A tube. This rapid variation is often useful in that it allows a simple, wide-range gain-control which

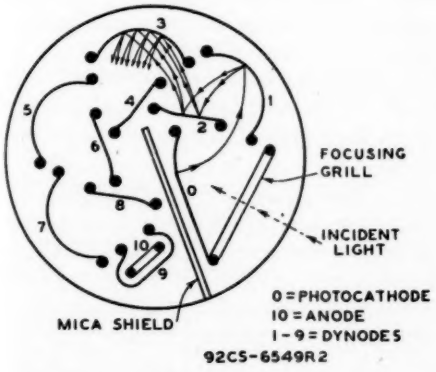

FIG. 1. Schematic arrangement of type 931-A.

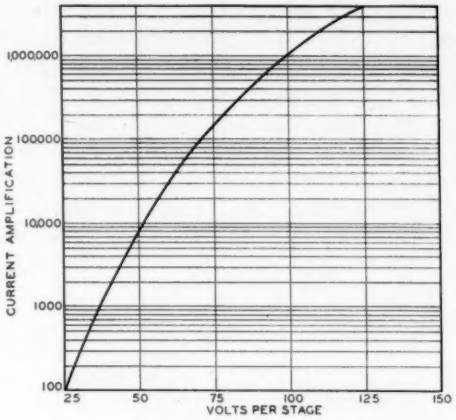

FIG. 2. Average amplification of type 931-A.

may be obtained either by varying the stage voltage of all the dynodes,[18] or that of just one dynode. The first method controls gain by changing the secondary emission per stage; the second controls gain by defocusing the electron stream in one section of the tube. In any case the amplification factor is practically independent of the output stage voltage.

A disadvantage of a gain control sensitive to voltage changes, is that it necessitates a rather well-regulated power supply to prevent the output current of the multiplier tube from being modulated by fluctuations in supply voltage. For low output currents, a fairly compact and inexpensive battery pack can be constructed by use of miniature batteries. An analysis of fundamental electronic regulating circuits, with possible utility in multiplier photo-tube applications, exists in an article by Hunt and Hickman.[19] For the higher output currents a useful circuit may be found in a paper by W. R. Hill.[20] Much of the work that has been done on voltage supplies for the Geiger counter is directly applicable to multiplier tubes. In low current applications in this laboratory a modification of the amplification-bridge type of regulated supply[19] has been found very useful. This circuit has the advantage of providing a positive ground which is desirable in eliminating electrical pick-up. A wide range of regulated

[12] R. B. Janes and A. M. Glover, RCA Review **6**, 43 (1941).
[13] A. Sommer, Elec. Eng. **17**, 164 (1944).
[14] R. C. Winans and J. R. Pierce, Rev. Sci. Inst. **12**, 269 (1941).
[15] F. Preisach, Wireless Eng. **16**, 169 (1939).
[16] C. C. Larson and H. Salinger, Rev. Sci. Inst. **11**, 226 (1940).
[17] W. Shockley and J. R. Pierce, Proc. I.R.E. **26**, 321 (1938).
[18] M. H. Sweet, J. Opt. Soc. Am. **36**, 720 (1946).
[19] F. V. Hunt and R. W. Hickman, Rev. Sci. Inst. **10**, 6 (1939).
[20] W. R. Hill, Proc. I.R.E. **33**, 38 (1945).

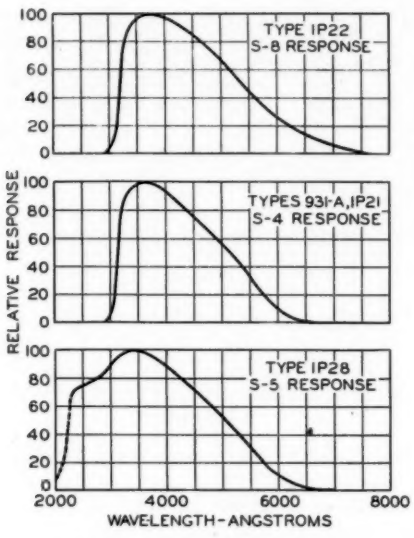

FIG. 3. Spectral response curves.

voltage may be obtained without rebalancing the bridge by choosing a high μ-triode (75 or greater) with a flat amplification factor *versus* plate voltage characteristic.

Spectral Characteristics

At present three types of spectral response are available in the RCA line of multiplier phototubes. Data recently obtained for the S-4, S-5, and S-8 responses with a Bausch and Lomb quartz monochromater are presented in Fig. 3. The S-4 curve, characteristic of a caesium-antimony surface on a nickel base, may be compared with that published earlier by this laboratory.[9] It is not known to what extent the minor differences are attributable to changed and variable manufacturing techniques, or to errors in measurement.

When a caesium-antimony surface is enclosed in an ultraviolet transmitting envelope (Corning 9741 glass), the useful range is extended as shown in Fig. 3 for type 1P28. The ultraviolet cut-off is critically dependent upon the composition and thickness of the glass, so that tube-to-tube variations may be expected.

A caesium-bismuth surface gives the additional red sensitivity of the S-8 response compared to the S-4 curve. This surface, in general, reduces the absolute sensitivity so that a tube with an S-8 response, such as the 1P22, should be chosen only when extension to the red is necessary. The range of response of the S-8 characteristic is approximately that of the eye but the shape of the curve is, unfortunately, quite different.

Color-response variations of these types are of a lesser degree than the rather large tube-to-tube variations of the caesium-oxygen-silver (S-1) types.[21] The S-4 spectral response is particularly stable. Production variations in the response and cut-off characteristics of S-4 types are approximately one-tenth of those of the S-1 types.

Stability

Of great interest to the average user of multiplier tubes is the degree of stability that may be expected in the current output with constant light flux and voltage per stage. Each tube is individual in this respect but a fatigue, characterized by a decrease in sensitivity, is typical. Fatigue is also greater the higher the output current. Illustrating this trend are the data shown in Fig. 4 which were obtained from the average behavior of 10 representative 931-A tubes. In this graph the sensitivity loss in a given time is plotted as a function of the anode current. For each current value at which data were taken, the output current was held constant during the 40-minute test by adjusting the light flux. Sensitivities were recorded at the end of 20 and 40 minutes. The same tubes were used for all the points on the graph; after each 40-minute period

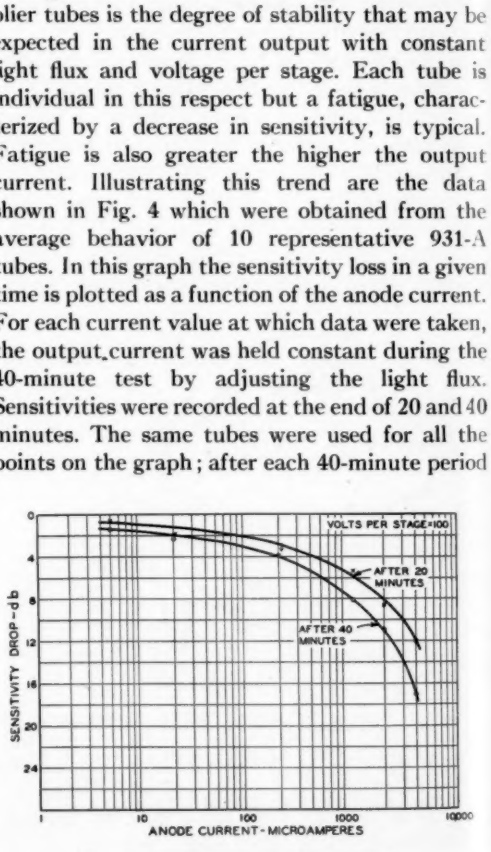

FIG. 4. Sensitivity loss in type 931-A.

[21] H. E. Ives and E. F. Kingsbury, J. Opt. Soc. Am. 21, 541 (1931).

the tubes were stored in darkness for at least one day before being operated at another current value. During this rest period, sensitivity generally recovers to approximately the initial value, except after currents in excess of 1 milliampere, in which case the recovery is incomplete. Loss in sensitivity results almost entirely from the loss in gain in the last few stages of secondary emission.

It is usually advantageous to operate the tube for at least a half-hour at the level of intended operation since the rate of fatigue is greatest during the first half-hour. Operation above 1 milliampere is not recommended because of the excessive fatigue. For most stable operation very low currents are recommended—certainly never over 100 microamperes. How stable the average tube is below 10 microamperes has not been determined, because errors in realigning the light spot and adjusting the voltage were larger with the particular test equipment used than the degree of instability being investigated. At currents less than 1 microampere, however, very little change in sensitivity may be expected.

Linearity

It is well known that photoelectric emission varies linearly with light flux over an extremely wide range. There is likewise no reason to expect secondary emission in the multiplier to be other than linear until space charge distorts the electrostatic fields. Figure 5 illustrates the linearity of output current in an RCA multiplier photo-tube as a function of light flux.

Within an experimental error of 3 percent, the anode current in the range from 10^{-9} to 10^{-3} ampere is proportional to light flux at the cathode. The low levels of light indicated on the graph were obtained by reflection of light consecutively from a pair of convex mirrors. A base of 20:1 in linearity was first established by varying the distance from the light source to the first diverging mirror. In this way any change in light spot or position on the multiplier cathode was made negligible. By means of this 20:1 range neutral filters were calibrated, and used to extend the measurements to the complete range shown in Fig. 5. Since the data for this curve were taken for several tubes, the value of the light flux plotted was arbitrarily adjusted to coincide with the sensitivity of an average tube (10 amperes per lumen), thus permitting a more simple comparison of results.

The last point on the lower end of the curve (Fig. 5) was obtained by counting and measuring the heights of the output pulses from the multiplier, each pulse being an amplified photoelectron. This point, representing a cathode photo-emission of only a few electrons per second, is included on the graph not so much to indicate

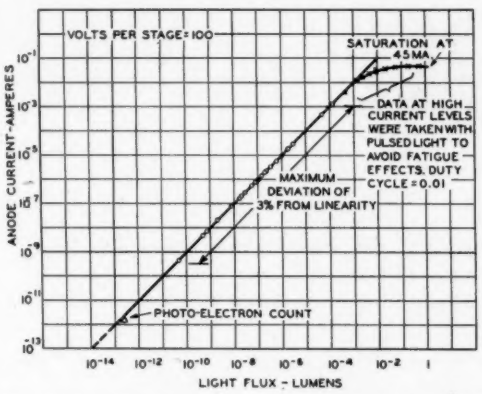
VOLTS PER STAGE = 100
SATURATION AT 45 MA
DATA AT HIGH CURRENT LEVELS WERE TAKEN WITH PULSED LIGHT TO AVOID FATIGUE EFFECTS. DUTY CYCLE = 0.01
MAXIMUM DEVIATION OF 3% FROM LINEARITY
PHOTO-ELECTRON COUNT
ANODE CURRENT-AMPERES
LIGHT FLUX - LUMENS

FIG. 5. Linearity characteristics of RCA photo-multipliers.

the linearity of the multiplier at this level (of which there is very little doubt), but to illustrate the wide range of its applicability.

In order to obtain points in the range from 1 to 45 milliamperes, a technique using pulsed light was employed. Continuous operation at high levels of output current would fatigue the output stages of the multiplier so rapidly that reliable data could not have been obtained. The duty cycle, therefore, was reduced to 0.01 by means of a light-chopper disk. Measurements of the peak current output were then made with a cathode-ray oscillograph. The reduced duty cycle also reduced the bleeder current requirements by a factor of 100. Inter-stage capacitors maintained dynode voltages during the pulse time.

At the top end of the curve a saturation characteristic is observed. The chief limitation of current by space-charge saturation occurs not, as might be expected, at the ninth dynode, but at the surface of the eighth dynode (Fig. 1). This condition is the result of the much closer spacing between dynode 9 and the anode, than between

the dynodes 8 and 9. Calculations from the geometry of the tube and the electrostatic fields (with reference to a rubber dam model) checked quite well with the measured 45-milliampere current maximum at 100 volts per stage. Further confirmation of this point was obtained in the approximate $\frac{3}{2}$-power variation of the saturated current as a function of the voltage per stage.

While these data indicate anode currents as high as 45 milliamperes, it should be emphasized that stability cannot be expected at such levels. These levels are included chiefly for their academic interest and for possible application of the tube in light-pulse detection. The stability of the tube with pulsed light is approximately that of the integrated average current level.

APPLICATION TO LOW LIGHT LEVELS

Dark Current

In any application of the multiplier photo-tube to very low light levels, one of the most important considerations is the dark current of the tube. It is important to understand the source of this current so that operation with maximum sensitivity may be obtained.

Illustrated in Fig. 6 is the anode dark current in microamperes as a function of the voltage per stage. The points were obtained from one tube chosen as typical of the behavior of RCA multiplier photo-tubes. There are three domains in each of which a different type of dark current dominates: (1) ohmic leakage; (2) amplified thermionic emission; (3) regenerative ionization.

At low voltages ohmic leakage is dominant. Leakage current is caused by traces of caesium and other conductive materials on the stem and insulating spacers inside of the tube. Base leakage may also be included in this category. Base leakage is particularly evident if the tube is operated in a very humid atmosphere or in a dirty or dusty locale. As a general rule the leakage in the base itself is less than that inside of the tube. If high humidity causes difficulty it may be advantageous to apply a coating of ceresin wax to the base. In an atmosphere of reduced pressure an electric breakdown may also occur across adjacent pins at high voltage. This type of breakdown is important in airborne equipment.

In the characteristic plotted in Fig. 6 the ohmic leakage is dominant up to about 50 or 60 volts per

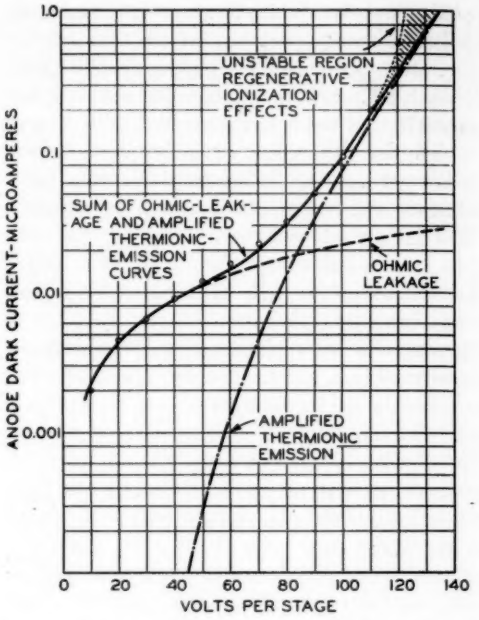

FIG. 6. Dark current in photo-multiplier tubes.

stage. An extrapolated dashed line indicates the calculated continuation of the ohmic leakage. This leakage is directly proportional to the voltage per stage, but the shape of the curve is convex because a logarithmic scale is used for the dark current.

Above 60 volts per stage dark current caused by thermionic emission becomes important. In the sample tube the equivalent thermionic emission at the cathode was 0.6×10^{-14} ampere. This emission is amplified through the tube in the same manner as photo-current; hence, the output current caused by thermionic emission is proportional to the gain characteristic of the multiplier tube, as illustrated by the dot-dash line in Fig. 6. The sums of the values of the extrapolated ohmic-leakage curve, and the values of the amplified thermionic emission curve give the solid line which quite closely fits the observed points and, thus, gives credence to this interpretation.

In almost any method of using the multiplier photo-tube the ultimate limitation to signal detection is thermionic emission. Associated with this component of the dark current is a shot noise resulting from random thermionically emitted

electrons, variably multiplied by the secondary-emission gains of nine stages.

Above about 110 volts per stage, Fig. 6, a third region of dark current begins. Deviation from the ohmic and thermionic dark-current curve is associated with regenerative ionization effects, which cause complete breakdown and an uncontrollable discharge at sufficiently high voltage. For most tubes this breakdown occurs between 140 and 180 volts per stage depending principally on the gain of the tube. In this unstable region, indicated by the shaded area on the graph, dark currents fluctuate violently and if the current is viewed on a cathode-ray oscilloscope, rather large bursts of pulsed noise will be observed in contrast to the fairly steady "rain" associated with thermionic-emission noise. The exact cause of this gaseous noise is not known, but when the gain of the tube has reached a value of 10^7 to 10^8, very little feedback from the anode to the cathode will obviously initiate a self-maintained discharge. This feedback may be caused either by secondary emission from positive ions (of residual gas or vapor), or by photo-emission resulting from light emitted from excited gas, or from fluorescence in the glass or other insulators in the tube. Although the tube has been designed to avoid feedback, it will occur in all tubes when the gain is sufficiently high.

When the tube is operated for optimum signal-to-noise ratio, the region where gas effects become noticeable should be avoided in any system of measurement. If a direct-current method of observation is used, it is best to operate at a stage voltage level where the ohmic leakage is not dominant, since the amplified thermionic emission rises no more rapidly than the useful signal output. Providing the ohmic-leakage component does not vary or drift, as it may in some cases, the fluctuations resulting from thermionic emission are then the chief limitation in the d.c. detection method. In an alternating-current method of observation with a modulated light source, any ohmic leakage becomes secondary to the amplified shot noise associated with the thermionic emission.

Thermionic Emission Noise

Numerous papers written have been to show the nature of, and the limitations imposed by thermionic emission in multiplier photo-tube measurements.[13–15,17] The r.m.s. value of fluctuating output current originated by thermionic emission is closely approximated by the following equation:

$$[(\langle I^2\rangle_{Av})_{\Delta f}]^{\frac{1}{2}} = \mu(2ei_t\Delta f)^{\frac{1}{2}}, \qquad (1)$$

where μ is the gain of the tube, e the electronic charge, i_t the thermionic emission from the cathode, and Δf the band width of the receiving instrument. Neglected in this equation is the noise associated with the thermionic emission from the secondary-emitting surfaces or dynodes. However, since the stage gain is of the order of 4 or 5, this additional noise would only amount to an omission of about 3 percent from Eq. (1).

Another factor omitted from Eq. (1) is the noise associated with the random process of secondary emission. If the number of secondary electrons emitted per primary electron were invariable, the electronic pulses resulting from an electron emitted from the cathode would all be of the same magnitude. But, since the individual dynode secondary-emission yield is statistically variable, the number of electrons in the anode pulses varies, and causes a slight increase[17] in noise, probably of the order of 15 percent over that predicted from Eq. (1). In other respects the noise associated with the random thermionic emission, or photo-emission with the photoelectric current being substituted for i_t, follows Eq. (1) quite accurately, qualitatively and quantitatively.[22]

The essential advantage of the multiplier photo-tube is that the limiting noise in practical measurements can be reduced to that of the thermionic emission as defined in Eq. (1). In a conventional photo-tube the thermionic-emission noise is also present, but in general is exceeded by the Johnson noise of the coupling resistor, or by the shot noise in the first amplifier tube. The multiplier photo-tube raises the photoelectric current above external noise sources with practically no increase in the relative internal noise.

Assuming that the multiplier photo-tube is operated so as to avoid the difficulties of ioniza-

[22] A. M. Glover, R. W. Engstrom, and W. J. Pietenpol, "Final Report on the Investigation and Manufacture of Noise Sources at RCA;" OSRD Report 1060-2, March 7, 1945.

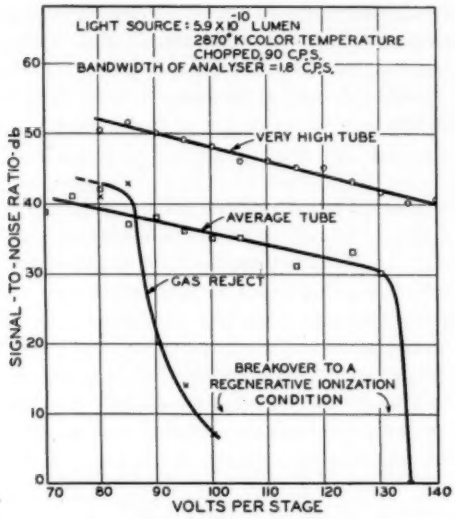

FIG. 7. Sample signal-to-noise curves for RCA photo-multipliers.

tion effects at high voltage, and with analyzing equipment that does not introduce other dominant noise sources, consider the theoretical limits to the detectability of the tube. If the photo-current at the cathode is i_p, the output current produced by the light is

$$I_p = \mu i_p. \tag{2}$$

The anode-noise current will also be increased by the shot effect from the photoelectrons so that the r.m.s.-noise current becomes

$$[(\langle I^2 \rangle_{Av})_{\Delta f}]^{\frac{1}{2}} = \mu[2e\Delta f(i_t + i_p)]^{\frac{1}{2}}. \tag{3}$$

Letting S_n represent the signal-to-noise ratio obtained by dividing Eq. (2) by (3), it follows that

$$S_n^2 = i_p^2/2e\Delta f(i_t + i_p). \tag{4}$$

Equation (4) is also based on the assumptions and omissions inherent in Eq. (1), and refers to the signal-to-noise ratio using a d.c. voltage supply and a d.c. light source. For the purposes of determining the approximate limiting current measurable, Eq. (4) may also be used for order of magnitude if the light is modulated, providing the modulation efficiency is high so that a large d.c. background current is not added. For an accurate determination of signal-to-noise ratio in this case an a.c. form factor determined by the shape of the light-modulation curve would have to be added. If an a.c. voltage supply is used, the signal-to-noise ratio is reduced.[19] It is also advisable to avoid the use of a.c. voltage if gain is important. Voltage limitations apply to the peak a.c. voltage, but average gain would, of course, be considerably less than the maximum during the a.c. cycle.

In the present RCA multiplier photo-tube series, the thermionic emission from the cathode at room temperature is of the order of 10^{-14} ampere. (This emission is 100 to 1000 times lower than the thermionic emission of a Cs-O-Ag tube.) For an arbitrary band width of 1 cycle per second, the factor $2e\Delta f$ is approximately 3×10^{-19} ampere. The limit of detectability under these conditions may then be determined from Eq. (4) to be a cathode photo-current of the order of 5×10^{-17} ampere, corresponding to a light flux of 5×10^{-12} lumen for an average 931-A cathode sensitivity of 10 microamperes per lumen (2870°K).

Methods for improving detectability may be readily deduced from Eq. (4) and are: increase the photo-sensitivity of the cathode, decrease the band width of the measurement, and reduce the thermionic emission. The S-4 spectral characteristic of the 931-A, and 1P21, and the S-5 response of the 1P28, have a very high absolute sensitivity. The 1P21 is probably best in this respect because of higher selection criteria. Some attempt has been made in processing tubes in the RCA laboratory to reduce the thermionic emission, while maintaining good photo-emission, and although indications of improvement were obtained, the problem is still open for solution. It is also possible to manufacture a tube with a smaller cathode area, as has been suggested by G. E. Kron,[7] although this has not as yet been tried. For the user, however, there remain two approaches: reduce band width, and decrease thermionic emission by cooling.

In a light-modulation method the band width is usually determined by that of the a.c. amplifier following the multiplier tube. It is possible, though probably quite difficult, to make an a.c. amplifier with a band width of 0.1 c.p.s. at low audiofrequencies.[23,24] A band width of the order

[23] D. G. Tucker, Elec. Eng. 15, 98 (Aug. 1942).
[24] W. C. Michels and N. L. Curtis, Rev. Sci. Inst. 12, 444 (1941).

of 1 c.p.s., however, is reasonable if negative feedback circuits are employed.[25]

In the measurements described in this paper, a 90 c.p.s. chopped-light source was used and a General Radio type 760A sound analyzer provided a selectivity of 1.8 c.p.s.

For d.c. measurements the band width equivalent is one-fourth the reciprocal of the delay constant of the galvanometer in a direct measuring technique. An accumulation method in which capacitors are charged can be used with a band width inversely proportional to the time of charging. Various types of measurement have been made in this laboratory comparing steady light with chopped-light methods, etc., and they have in all cases quite closely checked Eq. (4). One disadvantage of using the d.c. method with a sensitive galvanometer is that any ohmic leakage in the multiplier will cause an annoying deflection which may vary as leakage paths change.

A third, though not new[26,27] method of utilizing the multiplier photo-tube is as an electron-counting device. In this method pulses in the anode circuit, caused by individual photoelectrons from the cathode, are counted using some electronic counting technique. Band width may be narrowed almost to any extent desired since it is inversely proportional to the time of the count. In the present investigation, elaborate counting equipment was not available and the count was made by observing the pulses on a cathode-ray oscilloscope. Counts longer than about 10 minutes in duration were not attempted, but the improvement expected with this method of narrowing the band width was demonstrated.

Perhaps the greatest possibility of improvement in measureability is obtained through the reduction of the thermionic-emission noise by lowering the tube temperature. If the thermionic emission could be reduced practically to zero, Eq. (4) would become

$$S_n^2 = i_p/2e\Delta f \qquad (5)$$

and the detectable photo-current would be directly proportional to the band width. For Δf equal to 1 c.p.s., the limit would be of the order of 3×10^{-19}-ampere cathode emission. The problem of reducing this level of detection would simply be one of waiting long enough to be statistically sure of the number of pulses per unit time. To determine whether or not the thermionic emission i_t could be reduced indefinitely, was one of the objects of this investigation.

Experimental Signal-to-Noise Ratio

The behavior of RCA multiplier photo-tubes was first studied at room temperature. Figure 7 illustrates sample signal-to-noise behavior of RCA multiplier photo-tubes as a function of voltage per stage. Signal-to-noise on this graph and also on Fig. 8 is in db and is defined by

$$\text{signal/noise (db)} = 20\log_{10}S_n. \qquad (6)$$

The data plotted in Fig. 7 were taken for chopped light (90 c.p.s.) using an a.c. amplifier with a band width of 1.8 c.p.s. The light source was a tungsten lamp operated at 2870°K color temperature. Reduction of the light flux on the multiplier tube to 5.85×10^{-10} lumen was accomplished by a pair of mirrors with convex front surfaces. Three curves are shown which are typical of a very good tube (a 1P21 or an especially good 931-A), an average 931-A, and an out-of-limit tube having excessive gaseous ionization. As the regenerative ionization condition begins, the signal-to-noise ratio falls rapidly, as might be expected. This rapid decline is characteristic of all tubes good or

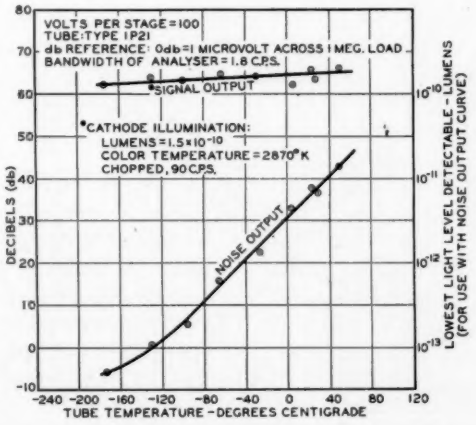

FIG. 8. Signal and noise output of photo-multipliers *vs.* temperature.

[25] F. E. Terman, *Radio Engineers' Handbook* (McGraw-Hill Book Company, Inc., New York, 1943), p. 943.
[26] J. S. Allen, Rev. Sci. Inst. **12**, 484 (1941).
[27] Z. Bay, Rev. Sci. Inst. **12**, 127 (1941).

bad, but the voltage per stage and the gain at which it occurs vary. It may be observed that even the rejected tube is useful with reduced voltage. These data further emphasize the importance of keeping the voltage down if high signal-to-noise ratio is desired. In the flat part of the curves before the onset of the regenerative condition, the signal-to-noise ratio of the 40 db implies a limit of detectability of about 6×10^{-12} lumen at room temperature with a band width of 1.8 c.p.s. This ratio agrees with the prediction of Eq. (4) and supports the assumption that the chief source of noise is amplified thermionic emission. According to Eq. (4), however, the flat part of the curves would be expected to be level and show no downward slope as illustrated. This behavior is very possibly associated with a Schottky or a field-emission effect. The curves show no indication of a decrease in signal-to-noise ratio as the voltage per stage is reduced to lower values than those shown, but, because the gain is also decreased the noise in the coupling resistor and in the first stage of amplification becomes important and obscures the behavior of the multiplier tube. For this reason there is always a minimum gain below which the advantage of the multiplier tube is lost.

Operation at Reduced Temperature

Although the operation of a multiplier phototube at reduced temperatures has been resorted to on numerous occasions,[2, 7, 27, 28] it is accompanied by numerous difficulties. These difficulties are chiefly the results of condensation of water vapor which fogs the light window and causes electrical leakage at the electrical contacts to the tube. Coleman,[29] however, has devised a simple cooling unit utilizing dry ice in which escaping CO_2 prevents condensation of moisture.

For the experimental program undertaken in this laboratory a demountable vacuum chamber was built. This chamber consists of a double-walled flask supported concentrically inside of a larger metal container. The double-walled flask is accessible to the atmosphere through two metal tubes which also support the flask inside the vacuum chamber. Cooling is accomplished by transferring liquid air to the space between the walls of the flask. The inner section of the flask houses the multiplier tube. An opening through the double-walled flask permits light to reach the photo-tube from a window sealed in the outer cylinder. Space on both sides of the liquid-air container is evacuated to less than 1 micron of mercury by means of an oil-diffusion pump. The pressure in the main chamber has to be below about 50 microns to avoid electrical discharge from the multiplier voltage supply; but to avoid thermal loss it is advisable to maintain better than 10 microns. In operation, the principle loss is by radiation. Losses are small enough that once the desired temperature is reached, a liter of liquid air is sufficient to maintain the temperature for 6 to 8 hours. Temperature is measured by means of a thermocouple wrapped around the multiplier tube. When accurate temperature of the cathode has to be known, it is necessary to hold the tube at a constant temperature for several hours to allow the parts inside the tube itself to reach equilibrium. The magnitude and stability of the thermionic dark current is a good indication of equilibrium.

The demountable feature of the apparatus is provided by means of a glycol-phthalate seal which is melted by an electrical heater embedded in the top fitting. Leads from the multiplier are brought out at the top through a large glass stem which is sealed to the metal tubular top. Large spacing in this stem gives good electrical insulation and prevents noise from the socket and connections. This construction is not designed for everyday application, but it serves very well in providing a box with a constant cold temperature, with low thermal loss, and with no difficulty from condensation of moisture either on the base of the tube or on the window.

Measurements of both the sensitivity and noise output were made using this vacuum chamber at temperatures from -175°C to $+50$°C. These measurements are given in Fig. 8 in which both signal and noise are plotted in db with a reference level of 1 microvolt across an input load of 1 megohm (a current of 10^{-12} ampere r.m.s.). Signal-to-noise ratio may be obtained by subtracting the noise ordinates from the signal ordinates at a given temperature. The tube used was a 1P21 at 100 volts per stage. A light flux of

[28] A. Blanc-Lapierre and D. Charles, J. de phys. et rad. 5, 239 (Oct. 1944).
[29] E. F. Coleman, Electronics 19, 220 (June 1946).

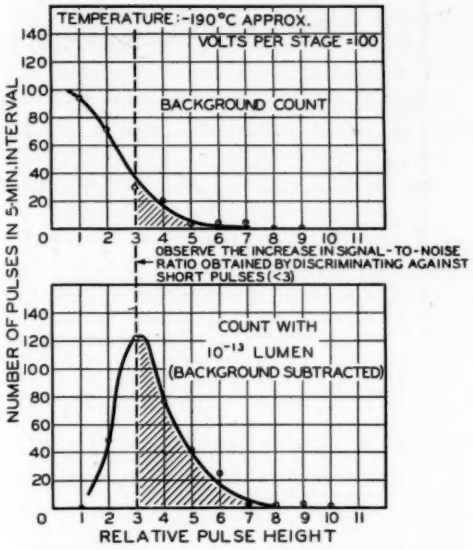

FIG. 9. Pulse-height distribution in photo-multipliers.

1.5×10^{-10} lumen modulated to a 90 c.p.s. square wave was used and data were taken with an a.c. amplifier having a band width of 1.8 c.p.s. Each pair of points on the graph was taken only after at least 4 hours at the indicated temperature. All the data were taken over a period of about two weeks. The order of taking the data was purposely disarranged to avoid any false trend with temperature that might be caused by fatigue or aging effects.

The reduction in noise output in cooling from room temperature to that of liquid air is greater than 40 db, an improvement of 100:1 in the lower limit of light detectability as indicated on the scale at the right-hand side of Fig. 8 which refers to the noise output curve. (Slope of the signal output curve is neglected.) Since the noise current is proportional to the square root of the thermionic emission it is of interest to make a Richardson plot of the noise output data of Fig. 8. The result of this plot is a curve of slope representing a work function of 0.3 volt between +50°C and −50°C and representing a smaller and smaller work function at lower temperatures. A single straight line cannot be made to represent the data. It has been suggested by Rajchman[30] that the curvature may be explained by assuming a non-uniformity of the cathode so that in reality there are several Richardson plots which must be added together and thus produce the curved appearance. It might also be speculated that changes may take place in the complex surface structure of the cathode as the temperature is varied. The sensitivity variation, however, shown on the same graph does not support this suggestion. A field emission current, originating at sharp edges, is also a possible contributor to this behavior. Also difficult to explain is the difference between this measured work function of 0.3 volt and the photoelectric work function of the order of 2 volts. Temperature data on two other tubes give apparent work functions of 0.5 and 1.0 volt.

Sensitivity data as indicated on Fig. 8 show that the sensitivity is essentially independent of temperature. Since the data are plotted on an absolute scale, evidence is thus incidentally presented of the lack of fatigue at these very low current levels. The slight slope to the curve, although barely detectable within the range of experimental error may indicate a temperature coefficient of secondary emission—to the ninth power for the nine stages. The slope may also imply a temperature variation in spectral response of the surface.

Electron Pulse Count

By use of only a broad-band amplifier and a cathode-ray oscilloscope an investigation was made of the general usefulness of the photoelectron-pulse-counting technique. This investigation could only be made at reduced temperatures where the background count was low enough to permit visual count on the oscillograph. In Fig. 9 is a curve of the distribution of pulse lengths as estimated in this manner over a period of 5 minutes for the tube in complete darkness (top curve) and for an illumination of 10^{-13} lumen (lower curve with the dark current subtracted). The different character of the two distribution curves is attributable to the fact that the photocurrent is initiated entirely at the cathode while the dark-current emission may come from the dynodes as well. Electrons originating at the dynodes would result in shorter impulses because of the fewer stages of multiplication. The variable pulse height of the amplified photoelectron count

[30] J. Rajchman, Arch. des Sciences **20**, 231, 267 (1938); 21, 5 (1939).

and part of the variation of the pulse height in the background count are caused by the statistical variations in secondary emission throughout the nine stages of the tube.

Advantage can be taken of this characteristic difference between the background and the photo-originated pulses. By establishing an arbitrary threshold of observation and excluding the shorter pulses—in this case those less than 3 units on the scale—an increase in signal-to-noise ratio can be obtained.** A disadvantage of this method, however, the fact that all photoelectrons are not counted, may be of importance in some applications.

That the pulses observed were actually single amplified electron pulses from the cathode was verified to an accuracy of 25 percent by computing the initiating charge from data on the gain of the tube and the characteristics of the amplifier and oscillograph. The accuracy is about what could be expected from the errors involved in the various factors. The point at the lower left of Fig. 5 represents this datum taken from Fig. 9.

The variation of background pulse count with voltage per stage (excluding pulses of less than three divisions of Fig. 9) is plotted on Fig. 10. Reduction of background count as the voltage is reduced is not the result of decreased pulse heights since the gain of the amplifier has been increased to maintain the same output sensitivity. The number of background counts made in this manner may be reduced to only one or two a minute. This reduction brings the lower limit of detectability in a 5-minute period of observation at 70 volts per stage to about 2×10^{-16} lumen, the equivalent of a cathode photo-current of 2×10^{-21} ampere. (Compare Eq. (4).)

Since the data in Fig. 9 suggest a field-emission effect, it seems advantageous to reduce the voltage still further. (Compare also the slope of the curves of Fig. 7.) The lower limit of usable voltage or gain in the multiplier tube in a pulse-counting application is reached when the photo-electronic output pulse becomes reduced in magnitude to the point where there is confusion from the tube noise and the thermal noise of the coupling resistor.

It may be useful to consider briefly what

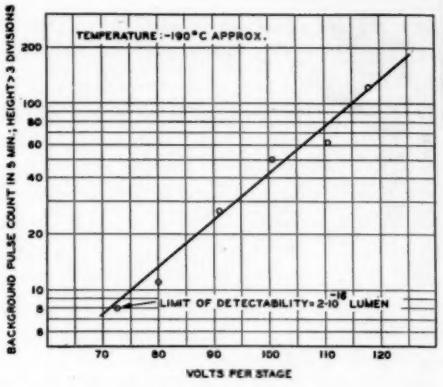

FIG. 10. Background pulse count *vs.* voltage per stage.

factors determine the multiplier gain required to lift the pulse above the noise. Assume the output circuit of the multiplier tube to be a resistance R and a shunt capacitance C. The magnitude of the pulse height in volts across this output resistance is given by

$$V_p=\mu e/C. \tag{7}$$

The r.m.s. value of the thermal noise is

$$(\langle E^2\rangle_{Av})^{\frac{1}{2}}=(kT/C)^{\frac{1}{2}} \tag{8}$$

where k is Boltzmann's constant and T is the temperature in ° K. In order to lift the pulse out of the noise level, with less than one spurious count in 10 minutes, it is estimated (using Equation 3.6–11 of S. R. Rice's paper on "Mathematical Analysis of Random Noise"[31]) that the pulse height must be at least six times larger than the r.m.s. noise voltage. Solving for the minimum gain necessary to accomplish this discrimination gives:

$$\mu=6(kTC)^{\frac{1}{2}}/e. \tag{9}$$

For a temperature of 300°K and a capacitance of 10^{-10} farad a gain of the order of 25,000 is required. This gain requires about 60 volts per stage on an average multiplier photo-tube.

In this account of the minimum permissible gain no consideration has been given either to possible noise in the amplifier following the multiplier tube or to the optimum frequency response of that amplifier. It has been tacitly assumed that the amplifier was noiseless and had an infinite and flat frequency response. In

** This method of improving signal-to-background count has also been suggested by G. E. Kron, reference 7.

[31] S. O. Rice, Bell Sys. Tech. J. **24**, 46 (1945).

practice, noise is introduced by shot noise from the plate and grid currents of the first tube. In an amplifier with a very wide band the noise level of the first tube would exceed the thermal noise in the coupling resistor. However, by limiting the frequency response of the amplifier to a frequency band width a few times $1/RC$ with the coupling resistor R much larger than the equivalent input noise resistance of the first tube (which may be of the order of 10,000 ohms[32]), the noise originating from the amplifier can be made negligible and most of the advantage implied by Eq. (9) can be maintained.

It has been stated by D. O. North[33] that the optimum detection circuit should have a very large input impedance and compensating networks in the amplifier to give a net flat band width much greater than that of the input circuit. With this circuit the minimum multiplier gain could be reduced by a factor of 30 below that predicted by Eq. (9). This improvement is possible since the pulse height out of the amplifier is linearly proportional to the band width of the system[34] while the r.m.s. thermal-noise voltage is proportional to the square root of the band width. Therefore, the minimum gain requirement may be reduced approximately as the square root of the ratio of net band width to $1/RC$ of the coupling circuit. The limitation to increasing the band width is the tube noise. The best compromise indicated is a large input resistance and a very small input capacitance.

[32] E. A. Johnson and A. G. Johnson, Phys. Rev. **50**, 170 (1936).

[33] D. O. North, RCA Laboratories Division, Princeton, New Jersey, private communication 11/8/46.

[34] There is no limitation to the band width of the pulse in the multiplier itself short of 10^8 c.p.s.; see R. D. Sard, J. App. Phys. **17**, 768 (1946).

CONCLUSIONS

Although much of the data presented herein was obtained using a 931-A or 1P21, the general conclusions apply equally to the 1P22 and 1P28. Particular emphasis has been placed on the operation of these multiplier tubes in the detection of very small light flux. For optimum operation, high voltage per stage should be avoided to prevent ionization effects. Thermionic emission, the chief limitation to the detection of low levels of light, may be almost completely eliminated by refrigeration of the tube. Band width of the measuring equipment is always a critical factor in detection. Of the three general methods of applying the multiplier tube, an unmodulated light with d.c. detection is probably the simplest. Modulated light with an a.c. amplifier has the advantage of eliminating the d.c. component of the dark current which may be troublesome. The counting of electron pulses seems to have the greatest possibility of all three methods for the measurement of the lowest light levels.

ACKNOWLEDGMENT

I wish to express my appreciation to Dr. Alan M. Glover for his enthusiastic support and to Mr. Arnold Moore for his assistance particularly on the spectral response curves.

A Logarithmic Photo-Multiplier Tube Photo-Meter*

M. H. SWEET
Ansco Research Laboratories, Binghamton, New York
(Received October 31, 1946)

THE advent and development of photo-multiplier tubes has raised the problem of how best to utilize them in practical circuits. One of the more difficult phases of the problem arises from the fact that they show pronounced fatigue at high current levels (1 ma or more) while their lower limit of practical utility is set by erratic dark current phenomena (which may amount to 0.1 μa or more at 100 volts per stage). If one designs a direct reading instrument to operate in the conventional (linear) fashion, at a constant dynode voltage, then because of the wide range of values to be measured he either encounters fatigue at high light levels or instability at low levels.

In the measurement of optical density, a logarithmic function, one usually encounters a range of light levels of about 1000 to 1 and it is desirable, for practical reasons, to use a direct reading instrument having a uniform density scale. When color film samples are to be measured, the restricted wave-length range available imposes the requirement of very high sensitivity on the receiver. The dynode voltage feedback photometer described below was developed as a solution to this problem.

PRINCIPLES OF OPERATION

The basic principles of operation may be understood by referring to Fig. 1. In this illustration the dynode voltage of the photo-multiplier tube is manually controlled in such a way that the anode current is held constant in the presence of variations in the incident flux intensity. For example, if the tube is excited by light sufficient to cause a current of 1 microampere at 80 volts per stage, if the light level is then increased by a factor of 100, the dynode voltage must be reduced to about 45 volts per stage in order to maintain the original anode current level. The sensitivity of the tube varies with dynode voltage according to the relationship shown in Fig. 2 and since this relationship is substantially loga-

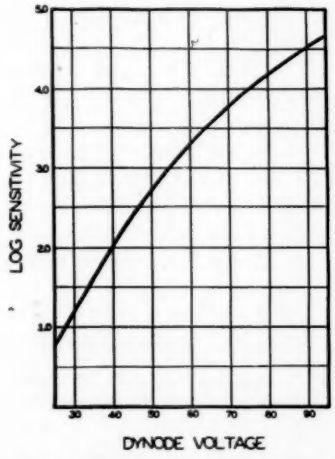

FIG. 2. Relationship between dynode voltage and log sensitivity for typical commercial photo-multiplier tubes.

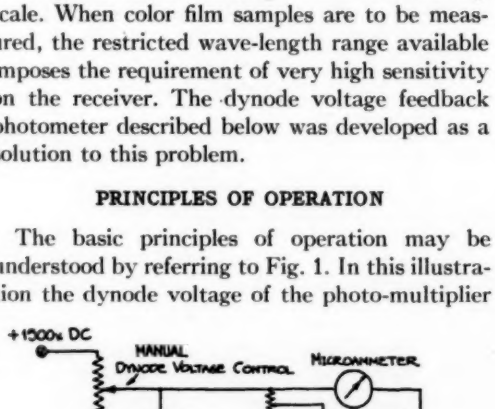

FIG. 1. Basic dynode voltage feedback circuit.

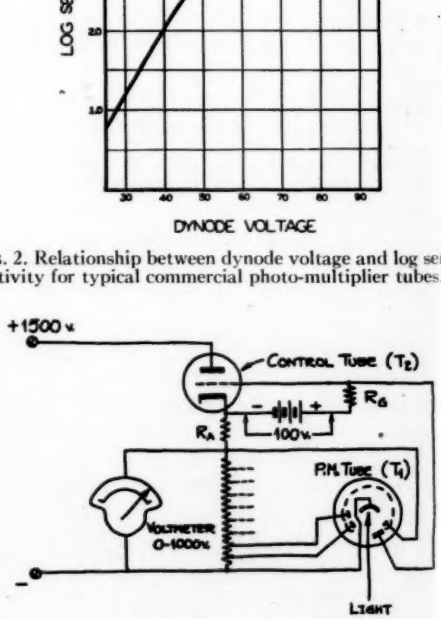

FIG. 3. Simplified diagram of automatic dynode voltage feedback circuit.

* Based on a paper presented at the October 3–5, 1946 meeting of the Optical Society of America in New York.

rithmic, if the dynode voltage at constant anode current is taken as a measure of the incident light, a logarithmic scale will result.

By means of the circuit arrangement shown in Fig. 3, it is possible to maintain the anode current at a constant level automatically. In Fig. 3, the dynode voltage is controlled by the plate-cathode current of a (control) tube whose grid voltage is dependent on the photo-multiplier tube anode current. The electrical polarity is such that increasing photo-multiplier anode current causes the grid to assume a more negative voltage. When light shines on the photo-multiplier cathode, it tends to cause an increase in the photo-multiplier anode current as a consequence of ordinary dynode amplification. However, since the grid of the control tube is thereby driven to a more negative potential, the control tube plate current is decreased and the dynode voltage is reduced to the point where the anode current is maintained at its original level. If we assume the control tube to have an extremely high amplification factor and the grid bias voltage to be very large (positive), then *even a minute percentage change in photo-multiplier tube anode current* will cause the control tube to vary over the extremes of its operating range. Therefore, in actual practice, the anode current at equilibrium will remain approximately constant over the entire range of operation of the instrument and the magnitude of the current will be that required to produce a voltage drop across the grid bias resistor which falls within the critical grid voltage range of the control tube.

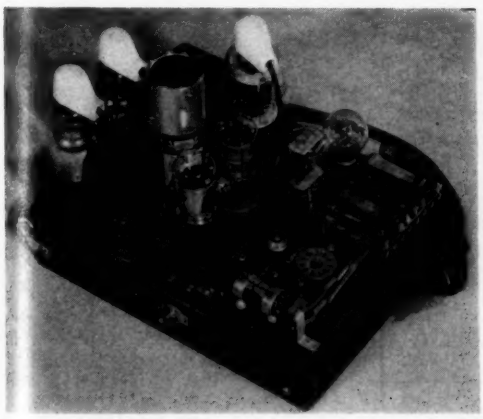

FIG. 4. Power supply and control circuit.

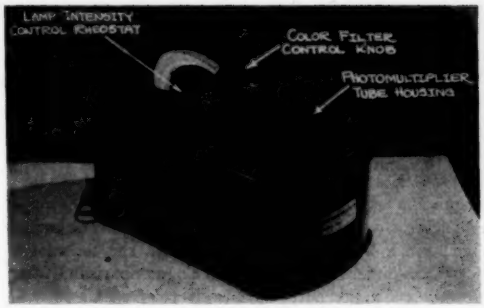

FIG. 5. Color densitometer incorporating dynode voltage feedback.

In over-all effect, the dynode voltages are controlled in such a way as to maintain a constant anode current in spite of light level variations as was done manually in Fig. 1. Therefore, a voltmeter connected as shown will yield a nearly logarithmic direct reading scale in terms of incident light. Figure 4 shows a complete power supply and control unit and Fig. 5 shows a color densitometer employing this circuit.

In a photometer, embodying these principles, containing a well-designed control circuit, the only characteristic of the system which will limit the accuracy, reproducibility, and stability of the instrument is the sensitivity *versus* dynode voltage relationship of the multiplier tube. By the use of this circuit, it is possible to avoid high anode currents at high light levels and low anode currents at low light levels. Therefore, fatigue and dark current effects are reduced to a minimum. An instrument of this type is substantially independent of supply voltage variations and changes in the gain of the control tube. It is virtually instantaneous in response and since it yields a logarithmic voltage output, it is ideally suited to photo-mechanical circuits involving multiplication and division operations.

Circuit details for a practical instrument incorporating these principles are being made available in the current literature.*

* M. H. Sweet, Electronics 19, No. 25, p. 105 (November, 1946).

Stray Light in Optical Systems*

HOWARD S. COLEMAN
Optical Inspection Laboratory, The Pennsylvania State College, State College, Pennsylvania

An objective method has been developed for measuring the stray light in optical systems. Stray light reduces the contrast of image and falsely appears to augment the light transmission of optical system. The method utilizes a photoelectric apparatus to compare the contrast of an image formed by an optical system with the contrast of the object under examination. This comparison, when expressed on a percentage basis, is referred to as "the contrast rendition" of the optical system. The contrast rendition of telescopic, photographic, and microscopic systems has been studied under a variety of conditions. It has been found that the contrast rendition values range from 3 to 100 percent for the systems studied. The contrast rendition of an optical system has been found to depend upon its optical and mechanical design, the use of reflection reducing films, surface defects, the cleanliness of its optical surfaces, the use of lens shades, and the brightness condition of the region surrounding the object under examination. The contrast rendition, for large targets and for a uniform surround, has been found to be independent of the brightness level at which the measurements are made, the contrast of the object, the field angle, and the optical aberrations present in the systems examined. The importance of contrast rendition in telescopic systems has been evaluated using the methods and data of Hardy, Duntley, and Blackwell. This evaluation was made by comparing the computed loss in range that would be caused by an imperfection in contrast rendition with the loss caused by an equal imperfection in light transmission and in magnification for telescopic systems. It was found, for all brightness levels, that the contrast rendition was generally more important than the other two variables. Because of the indicated strong dependence of the range at which targets are visible upon contrast rendition, ranges were computed for specific objects, instruments, and observation conditions, and compared with the results of an extensive visibility field test conducted from aboard ship. The computed and observed ranges were found to be in close agreement. This indicates that the contrast rendition of an optical system is a major factor in determining its performance.

INTRODUCTION

THE "faults" of optical systems have been discussed in detail by many authors. These discussions have usually dealt with the optical aberrations, imperfect light transmission, and the mechanical alignment of the optical parts. There is, however, one fault that has been neglected. This is the non-image-forming (hereafter referred to as stray) light that is scattered by the optical and mechanical parts and from surface defects or lack of cleanliness of an optical system which falls upon the image formed on the photosensitive surface used with the system. Such stray light reduces the contrast of the image, making it more difficult for the photosensitive receptor to distinguish from the background and falsely appears to augment the light transmission. This is shown schematically in Fig. 1. While the existance of this fault is well known, very little has been published concerning it except incidently to other properties of optical systems (e.g. Fabry[1]). It is the purpose of this paper to discuss the general problem of stray light in optical systems of current interest, including telescopic systems, photographic systems, microscopes, and eyepieces.

Recently Hardy,[2] Duntley,[3] and Blackwell[4] have described methods and presented data that

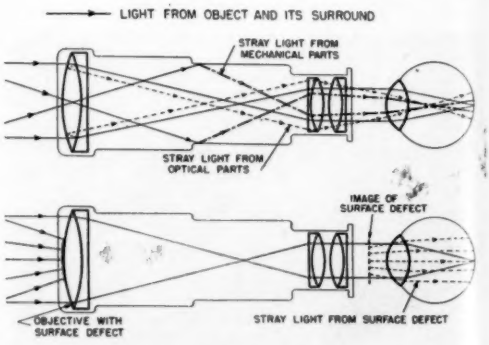
LIGHT FROM OBJECT AND ITS SURROUND
STRAY LIGHT FROM MECHANICAL PARTS
STRAY LIGHT FROM OPTICAL PARTS
IMAGE OF SURFACE DEFECT
OBJECTIVE WITH SURFACE DEFECT
STRAY LIGHT FROM SURFACE DEFECT

FIG. 1. Schematic diagrams of causes of stray light in optical systems.

* The work presented in this paper was performed, in part, as Task C of Contract Nord 7958 between the Bureau of Ordnance of the Navy Department and The Pennsylvania State College and presented at the 16th meeting of the Army-Navy-NRC Vision Committee, 25 June 1946.

[1] C. Fabry, Proc. Phys. Soc. London **48**, 747 (1935).
[2] A. C. Hardy, J. Opt. Soc. Am. **36**, 283 (1946).
[3] S. Q. Duntley, J. Opt. Soc. Am. **36**, 359, 713A (1946).
[4] H. Richard Blackwell, J. Opt. Soc. Am. **36**, 624 (1946).

make it possible to determine the importance of the loss in contrast in images formed by optical systems using the eye as a photo-sensitive receptor. While these data deal with losses in contrast caused by the atmosphere, the results may be generalized to include the loss in contrast of optical images regardless of the cause. An analysis of such data indicates that the amount of stray light normally present in optical systems is of considerable importance. It is evident in the analysis that the type of object and its surround and the brightness level to which the observer's eye is adapted must be taken into account. For example, in addition to the contrast discrimination of the eye varying with brightness as is taken into account in Blackwell's data, the pupil diameter varies considerably as shown in Fig. 2. This latter variation limits, to some extent, the amount of stray light that falls on the retina.

The criterion for determining the importance of stray light has been taken to be the loss in range at which objects are visible that can be attributed to stray light.

In this analysis, the dependence of the range at which objects are detectable for telescopic systems has been computed as a function of light transmission, magnification, and of the contrast of the image presented to the eye. Samples of these computations are shown in Figs. 3–5. A study of the computations indicates that in general, a given reduction in image contrasts

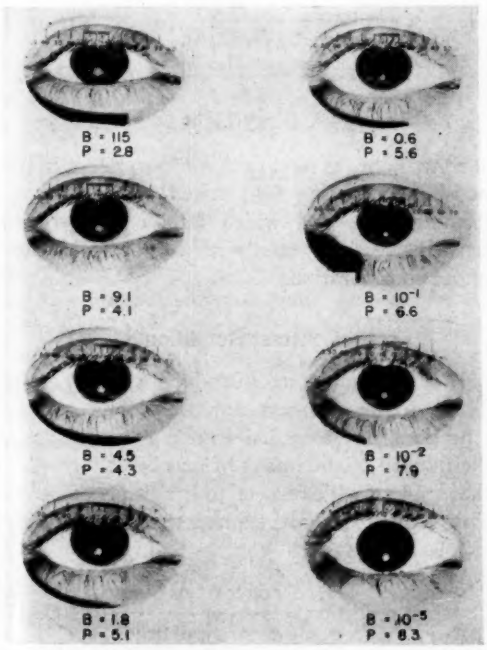

B = brightness in footlamberts; P = pupil diameter in millimeters.

FIG. 2. Flash photographs of the pupil of the human eye adapted to various brightness levels.

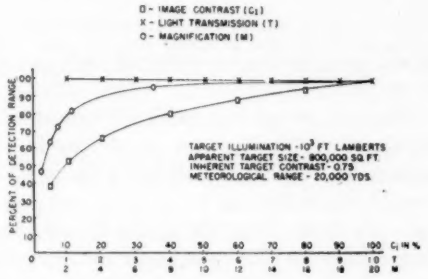
□ - IMAGE CONTRAST (C₁)
X - LIGHT TRANSMISSION (T)
O - MAGNIFICATION (M)
PERCENT OF DETECTION RANGE
TARGET ILLUMINATION - 10³ FT. LAMBERTS
APPARENT TARGET SIZE - 800,000 SQ.FT.
INHERENT TARGET CONTRAST - 0.75
METEOROLOGICAL RANGE - 20,000 YDS.
C₁ IN %
T
M

FIG. 3. Detection range in daylight *vs.* image contrast, light transmission, and magnification for a telescopic system.

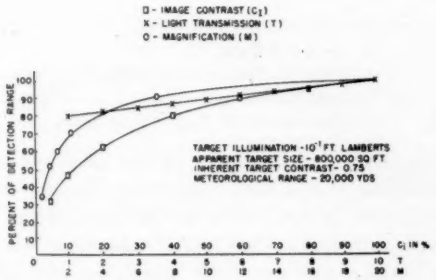
□ - IMAGE CONTRAST (C₁)
X - LIGHT TRANSMISSION (T)
O - MAGNIFICATION (M)
PERCENT OF DETECTION RANGE
TARGET ILLUMINATION - 10⁻¹ FT. LAMBERTS
APPARENT TARGET SIZE - 800,000 SQ.FT.
INHERENT TARGET CONTRAST - 0.75
METEOROLOGICAL RANGE - 20,000 YDS.
C₁ IN %
T
M

FIG. 4. Detection range in twilight *vs.* image contrast, light transmission, and magnification for a telescopic system.

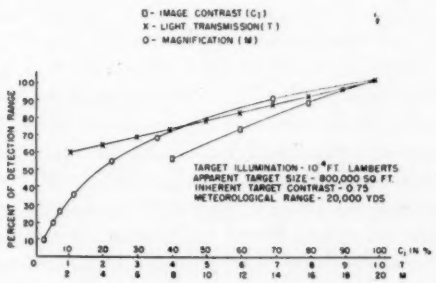
□ - IMAGE CONTRAST (C₁)
X - LIGHT TRANSMISSION (T)
O - MAGNIFICATION (M)
PERCENT OF DETECTION RANGE
TARGET ILLUMINATION - 10⁻⁴ FT. LAMBERTS
APPARENT TARGET SIZE - 800,000 SQ.FT.
INHERENT TARGET CONTRAST - 0.75
METEOROLOGICAL RANGE - 20,000 YDS.
C₁ IN %
T
M

FIG. 5. Detection range in starlight *vs.* image contrast, light transmission, and magnification for a telescopic system.

FIG. 6. Relative loss in detection range caused by a reduction of 20 percent in image contrast, light transmission, and magnification for a 20×telescopic system.

will cause a greater loss in the range at which objects are visible than an equal loss in light transmission or magnification. This is shown schematically in Fig. 6.

In addition to determining the specific losses in range caused by stray light present in optical systems, it is possible to determine the importance of a variety of factors related to stray light. These are:

1. Reflection reducing films.
2. Surface defects.
3. Edge blackening of optical parts.
4. Lens shades.
5. The cleanliness of optical surfaces.

For example, with respect to the importance of cleanliness, it has been found that a single light thumbprint in the center of the front surface of the objective of a 7×50×7.1° telescopic system can reduce the range at which an object is visible at night by as much as 50 percent.

Since the above-mentioned analysis shows stray light to be a controlling factor in the performance of telescopic systems, an experimental check on this conclusion was made. Some of the results of an elaborate field test conducted from aboard ship by the Navy Department were obtained. These results were in the form of the ranges at which targets could be detected under known conditions for a large number of Navy instruments. These ranges were compared with computed ranges based on laboratory measurements of the stray light, light transmission, magnification, and exit pupil for each instrument used in the field test. As indicated in Fig. 7, the results are in unexpectedly close agreement. This agreement indicates that the major factors in controlling the performance of the telescopic systems considered must have been taken into account. It is highly probable that the most important factor considered is the stray light. In this regard a knowledge of the importance of stray light is of particular value since the stray light in many cases can be practically eliminated. This is generally not possible with most imperfections existing in optical systems. Furthermore it should be possible to extend the above analysis on the importance of stray light to other optical systems and other photo-sensitive receptors.

THEORETICAL DISCUSSION OF STRAY LIGHT

In discussing the stray light in optical systems, it is important to define clearly all of the quantities to be used. These may be listed as follows:

1. Stray light.
2. Contrast rendition.
3. The target and its surround.
4. The inherent contrast of the target.
5. The apparent contrast of the target.
6. The contrast of the image of the target.
7. The transmission factor.
8. The scattering coefficient.
9. The contrast rendition equation.

Stray Light

Stray light, as used in this paper, refers to that non-image-forming light mixed with the image-forming light and which falls on the photosensitive receptor used with the optical system under consideration.

Contrast Rendition

It is convenient to introduce a quantity, referred to as contrast rendition. The contrast rendition* of an optical system is a measure of the fidelity of the image of an object formed by that system with respect to brightness contrast. This quantity may be expressed in equation form as follows:

$$\text{Contrast rendition} = \frac{\text{contrast of image}}{\text{contrast of object}} \times 100. \quad (1)$$

* The name "contrast rendition" was suggested by Lt. Commander N. H. Pulling of the Bureau of Ordnance of the Navy Department.

The Target and Its Surround

A test object is used in studying the stray light in optical systems and is referred to as the "target." The target is defined to be a surface under examination differing in brightness with respect to its background. It is sufficiently small (except in the case of point sources) that its presence or absence cannot change the brightness of the field viewed by an optical system by a measurable amount. The background against which the target is viewed is referred to as the "surround." It is helpful to imagine the target and its surround as being a small dark area at the vertex of a large white hemisphere which is concave toward the entrance pupil of the optical system under consideration which is located at the center of the hemisphere.

The Inherent Contrast of the Target

The inherent contrast of the target, C_0, is defined in terms of the brightness of the target, b_0, and the brightness of its surround, B_0, as shown in Eq. (2):

$$C_0=(B_0-b_0)/B_0. \tag{2}$$

This is the contrast an object would have with respect to its background if the distance between the target and the observer is small.

The Apparent Contrast of the Target

If the target is viewed through the atmosphere, or other medium which scatters light along the line of sight of the observer, the contrast that the target appears to have with respect to its surround is referred to as "the apparent contrast" of the target. The apparent contrast of the target, C_a, is related to the apparent target brightness, b_a, and the apparent brightness of the surround, B_a, as shown in Eq. (3):

$$C_a=(B_a-b_a)/B_a. \tag{3}$$

In the laboratory, or for small distances between the observer and the target, the apparent and inherent target contrasts are equal.

The Contrast of the Image of the Target

If the image of the target described above is formed by an optical system, the contrast of the image, C_i, is related to the brightness of the image of the target, b_i, and the brightness of the image of the surround, B_i, as shown in Eq. (4):

$$C_i=(B_i-b_i)/B_i. \tag{4}$$

The Transmission Factor

The transmission factor of an optical system, T, is defined to be the ratio of the brightness of the image of the target, b_i, to the apparent brightness of the target, b_a. This is expressed mathematically in Eq. (5):

$$T=b_i/b_a. \tag{5}$$

It should be recalled that the apparent brightness of the target for small target distances is equivalent to the inherent brightness.

The Scattering Coefficient

The stray light in optical systems must (by definition of the target) originate in the surround. It is therefore desirable to determine the contribution to the over-all brightness of the image received from the surround. This determination is facilitated by the use of a quantity referred to as the "scattering coefficient." Scattering coefficient, K, is defined in terms of the brightness of the stray light present in the image, S, and the apparent brightness of the surround, B_a, as shown in Eq. (6).

$$K=S/B_a. \tag{6}$$

The Contrast Rendition Equation

It is evident that the image of an object formed by an optical system which is free from stray light would have the same contrast the object appears to have. In the presence of stray

CHARACTERISTICS OF SYSTEM	PERFORMANCE	
	COMPUTED	FIELD
4 X 28 X 10°	84%	87%
6 X 33 X 7°	76	76
6 X 33 X 8°	62	56
6 X 42 X 12°	97	100
6 X 50 X 7°	102	80
7 X 50 X 7.1°	100	100
7 X 50 X 10°	100	102
8 X 60 X 8°	113	104
9 X 63 X 57°	119	112
10 X 50 X 7°	111	105
10 X 70 X 7°	116	104
10 X 80 X 7°	118	115
20 X 120 X 3°	163	163
25 X 100 X 3.6°	159	156

BASED ON THE RANGE AT WHICH TARGETS CAN BE DETECTED TAKING THE PERFORMANCE OF THE 7 X 50 X 7.1° BINOCULAR TO BE 100%

FIG. 7. Computed *vs.* field performance of telescopic systems.

light, however, the contrast of the image is less than apparent contrast of the target. This is easily visualized if one imagines the target as a grating consisting of parallel white and dark bands of equal width and the brightness of the white bands equal to the brightness of the surround. The image of such a target in the presence of stray light would have the brightness of both the dark and light portions of the image enhanced by the non-image-forming light. If brightness of the stray light be S, Eqs. (4) and (7) show that the contrast of the image is reduced by its presence.

$$C_i=\frac{(B_i+S)-(b_i+S)}{B_i+S}=\frac{B_i-b_i}{B_i+S}. \quad (7)$$

It should be noted that Eq. (7) applies to the conditions existing on the photo-sensitive receptor of the optical system under consideration. This may be the retina of the human eye, a photographic plate, or a photoelectric element.

Equation (7) may be rewritten in the terms of the apparent brightnesses of the target and its surround by introducing the transmission factor and the scattering coefficient of the system under consideration. This is shown in Eq. (8):

$$C_i=\frac{TB_a-Tb_a}{TB_a+KB_a}. \quad (8)$$

Equation (8) may be transformed into Eq. (9) by dividing both the numerator and the denominator by TB_a.

$$C_i=\frac{TC_a}{T+K}. \quad (9)$$

Equation (9) may be expressed in terms of contrast rendition from Eq. (1) as shown by Eq. (10):

Contrast rendition (C.R.)

$$=\frac{C_i}{C_a}\times 100=\frac{T}{T+K}\times 100. \quad (10)$$

Equation (10) is referred to hereafter as the contrast rendition equation.

Implications from Theory

Equation (10) forms the basis for studying the contrast rendition of optical systems. It has certain implications. These include:

1. The contrast rendition of an optical system depends only upon the light transmission and the scattering coefficient. These quantities depend only upon the brightness conditions of the surround and the design of the optical system.

2. The contrast rendition of an optical system is independent of the contrast of the target. This is of particular importance from an experimental point of view since it is difficult to make measurements using low contrast targets.

3. Since most of the stray light in an optical system originates from the surround, if the surround were reduced to zero, the stray light should be nearly reduced to zero. Thus, in the case of "point" sources, or for targets which are much brighter than the surround, the amount of stray light would be expected to be effectively small.

4. The contrast of an image is not rapidly reduced to zero by increasing the scattering coefficient to a large value. The rate of decrease in image contrast is most rapid for small values (0 to 3) of the scattering coefficient. It should be noted, however, that the scattering coefficient, can become very large (over a hundred) in the case of a non-uniform surround such as observing an airplane near the sun (or the moon at night). It also can be shown that the contrast rendition decreases more rapidly for systems having low transmission factors than those in which the light transmission is high. This is shown graphically in Fig. 8.

5. The transmission factor must be measured in order to determine the scattering coefficient. This is a consequence of the definition of the scattering coefficient, which is arbitrary, but which is believed to be the most desirable form. By defining a modified scattering coefficient as the ratio of the brightness of stray light to the brightness of image-forming light, the contrast rendition equation can be rewritten as shown in Eq. (11). In this case the light transmission factor does not appear explicitly.

Contrast rendition

$$=\frac{1}{1+K'} \text{ where } K' \text{ equals } \frac{K}{T}. \quad (11)$$

6. If most of the stray light in an optical system originates from the sourround, it should

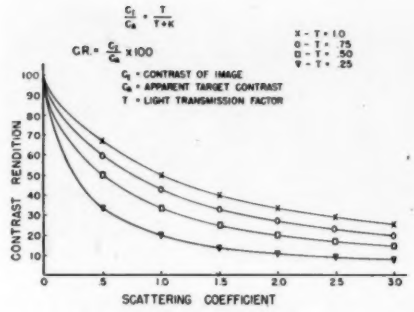
$\frac{C_I}{C_A} = \frac{T}{T+K}$
C.R. = $\frac{C_I}{C_A} \times 100$
C_I = CONTRAST OF IMAGE
C_A = APPARENT TARGET CONTRAST
T = LIGHT TRANSMISSION FACTOR
X - T = .10
O - T = .75
□ - T = .50
▽ - T = .25
CONTRAST RENDITION
SCATTERING COEFFICIENT

FIG. 8. Contrast rendition (C.R.) *vs.* scattering coefficient (K) for various light transmission factors.

be possible to compute its magnitude (for a given optical system) for different types of surrounds from a knowledge of the amount of stray light and from the symmetry and subtense of a particular surround. This is of importance since most conditions under which optical systems are used involve targets with non-uniform surrounds.

EXPERIMENTAL

Introduction

It is the purpose of this section of the paper to describe the apparatus and procedure for making contrast rendition measurements. In principal, the experimental equipment needed to study contrast rendition of optical systems is quite simple. The apparatus includes a target, which in general is a dark or bright surface (usually a black hole) in a 180° white surround. The target may be varied in shape and contrast. An image of the target is formed, by the optical system under consideration, on the entrance pupil of a photoelectric tube which is smaller than the image of the target. There should be no photoelectric response in the case of a black target if the image is as black as the target itself. If on the other hand stray light is scattered over the image of the target, there is a photoelectric response and the magnitude of the response is a measure of the amount of stray light present.

The Apparatus

The forms of the apparatus used to measure the contrast rendition of telescopes, objectives, microscopes, and eyepieces are shown schematically and photographically in Figs. 9 to 16 inclusive.

Since the various arrangements of the contrast rendition apparatus are essentially the same, the following description is primarily concerned with the apparatus used to test telescopic systems.

For discussion purposes it is convenient to imagine the contrast rendition apparatus divided into the following parts:

1. The target.
2. The surround.
3. The off-axis fixture.
4. The image-forming lens.
5. The photoelectric assembly.
6. The recording microammeter.
7. The illumination controls for the surround.
8. The screen used to limit the subtense of the surround.

The Target

The target is usually a black hole in the center of a white disk 8 feet in diameter. The size of the hole may be varied from $\frac{1}{8}$ of an inch to 16 inches. The contrast of the target may be changed by covering the black hole with processed photographic paper of different shades of gray.

While the target used is small with respect to its surround, it is large with respect to the minimum resolvable angle of the optical system under consideration. The target is placed approximately 50 feet from the system under test.

Provision has been made for covering the black hole with a white cover such that the cover in the region of the target is at the same brightness level as the surround. The target and its cover are shown in Fig. 13.

The Surround

In measuring the contrast rendition of telescopic systems, it is convenient to divide the surround into two parts. The first of these, referred to as the small angle surround, covers the central 10° of the field (with respect to the entrance pupil of the instrument under test). The second part, referred to as the wide angle surround, covers the remainder of the field to approximately 180°.

The small angle surround is a white disk 8 feet in diameter located approximately 50 feet from

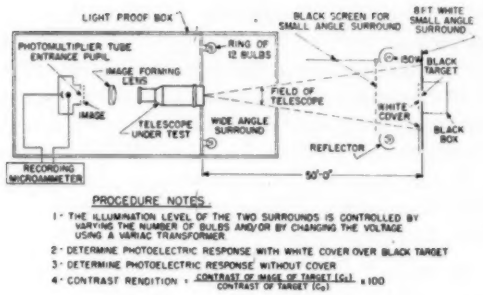
LIGHT PROOF BOX
BLACK SCREEN FOR SMALL ANGLE SURROUND
8 FT WHITE SMALL ANGLE SURROUND
PHOTOMULTIPLIER TUBE ENTRANCE PUPIL
RING OF 12 BULBS
150W
BLACK TARGET
IMAGE FORMING LENS
FIELD OF TELESCOPE
IMAGE
TELESCOPE UNDER TEST
WIDE ANGLE SURROUND
WHITE COVER
BLACK BOX
REFLECTOR
RECORDING MICROAMMETER
50'-0"
PROCEDURE NOTES:
1- THE ILLUMINATION LEVEL OF THE TWO SURROUNDS IS CONTROLLED BY VARYING THE NUMBER OF BULBS AND/OR BY CHANGING THE VOLTAGE USING A VARIAC TRANSFORMER
2- DETERMINE PHOTOELECTRIC RESPONSE WITH WHITE COVER OVER BLACK TARGET
3- DETERMINE PHOTOELECTRIC RESPONSE WITHOUT COVER
4- CONTRAST RENDITION = CONTRAST OF IMAGE OF TARGET (Cᵢ) / CONTRAST OF TARGET (C₀) x 100

FIG. 9. Schematic diagram of contrast rendition apparatus for telescopic systems.

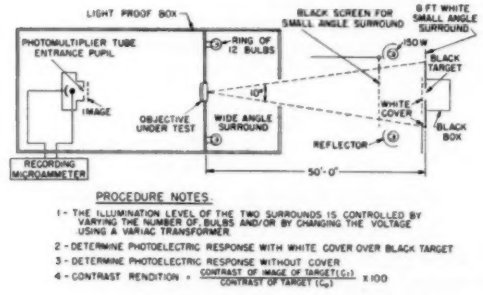
LIGHT PROOF BOX
BLACK SCREEN FOR SMALL ANGLE SURROUND
8 FT WHITE SMALL ANGLE SURROUND
PHOTOMULTIPLIER TUBE ENTRANCE PUPIL
RING OF 12 BULBS
150W
BLACK TARGET
IMAGE
OBJECTIVE UNDER TEST
WIDE ANGLE SURROUND
WHITE COVER
BLACK BOX
REFLECTOR
RECORDING MICROAMMETER
50'-0"
PROCEDURE NOTES:
1- THE ILLUMINATION LEVEL OF THE TWO SURROUNDS IS CONTROLLED BY VARYING THE NUMBER OF BULBS AND/OR BY CHANGING THE VOLTAGE USING A VARIAC TRANSFORMER
2 - DETERMINE PHOTOELECTRIC RESPONSE WITH WHITE COVER OVER BLACK TARGET
3 - DETERMINE PHOTOELECTRIC RESPONSE WITHOUT COVER
4 - CONTRAST RENDITION = CONTRAST OF IMAGE OF TARGET (Cᵢ) / CONTRAST OF TARGET (C₀) x 100

FIG. 10. Schematic diagram of contrast rendition apparatus for telescopic and photographic objectives.

the system under test. This is shown schematically in Fig. 9 and photographically in Fig. 13.

The wide angle surround is a cubical enclosure, with entrance and exit windows which are adjustable in diameter. The cube is 8 feet on a side and is painted white inside and illuminated. This is shown schematically in Fig. 9 and photographically in Fig. 14.

The Off-Axis Fixture

The optical system under test is mounted as shown schematically in Fig. 9 and photographically in Fig. 14. By means of an "off-axis" fixture it is possible to rotate the system under test about its entrance pupil and the photoelectric tube about an axis passing through the exit pupil of the system under test. This type of fixture is required in measuring the contrast rendition of optical systems at various field angles.

The Image-Forming Lens

In the case of afocal instruments, it is often necessary to use an image-forming lens as shown

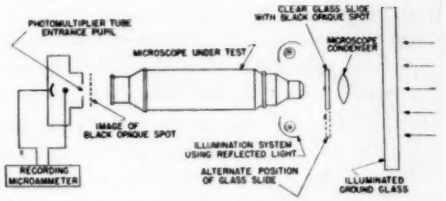
PHOTOMULTIPLIER TUBE ENTRANCE PUPIL
CLEAR GLASS SLIDE WITH BLACK OPAQUE SPOT
MICROSCOPE UNDER TEST
MICROSCOPE CONDENSER
IMAGE OF BLACK OPAQUE SPOT
ILLUMINATION SYSTEM USING REFLECTED LIGHT
ALTERNATE POSITION OF GLASS SLIDE
RECORDING MICROAMMETER
ILLUMINATED GROUND GLASS

FIG. 11. Schematic diagram of contrast rendition apparatus for microscopic systems.

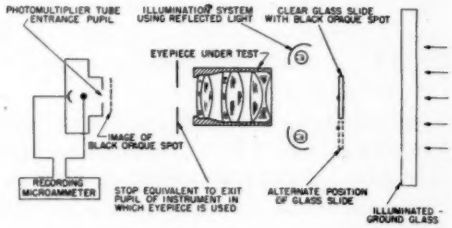
PHOTOMULTIPLIER TUBE ENTRANCE PUPIL
ILLUMINATION SYSTEM USING REFLECTED LIGHT
CLEAR GLASS SLIDE WITH BLACK OPAQUE SPOT
EYEPIECE UNDER TEST
IMAGE OF BLACK OPAQUE SPOT
RECORDING MICROAMMETER
STOP EQUIVALENT TO EXIT PUPIL OF INSTRUMENT IN WHICH EYEPIECE IS USED
ALTERNATE POSITION OF GLASS SLIDE
ILLUMINATED GROUND GLASS

FIG. 12. Schematic diagram of contrast rendition apparatus for eyepieces.

in Fig. 9 and Fig. 15. This lens is used to simulate "the eye" of the optical system and to form an image of the target of a practical size with respect to the size of the entrance pupil of the photoelectric tube. However, the image-forming lens is not entirely essential even in the case of an afocal system since the image can be projected by means of the eyepiece on to the entrance pupil of the photoelectric tube. Measurements have been made on telescopic systems with and without an image-forming lens. Both procedures produced the same contrast rendition values.

In the case of telescopic systems, the image-forming lens is placed in the plane of the exit pupil of the instrument under test and is provided with a set of "pupil" stops to simulate changes in the iris of the eye.

The Photoelectric Assembly

The photoelectric assembly consists of a photomultiplier tube and auxiliary electrical circuits. The entrance pupil of the photo-tube may be varied by means of a set of shim stock diaphragms from 0.3 to 6 mm. The assembly used for testing binoculars is shown schematically in Fig. 9 and photographically in Fig. 15.

The photoelectric tube is of the 1P21 photomultiplying type and utilizes an a.c. circuit

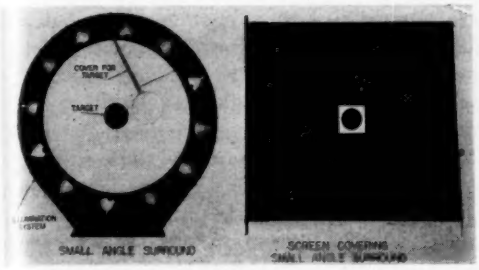

FIG. 13. The small angle surround assembly used in contrast rendition measurements.

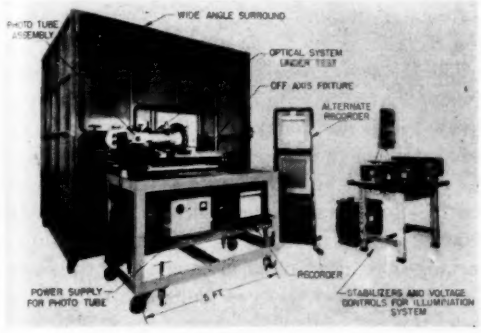

FIG. 14. Contrast rendition apparatus for optical systems of large aperture.

recommended by the manufacturer.[5] The glass envelope is coated with a conducting paint by means of which the electrostatic charges can be drained from the glass envelope thereby increasing the stability of the electrical system. In the region of the photo-sensitive element, the glass envelope has been made diffusing by grinding it with No. 400 carborundum to distribute the light over a larger area to the photo-sensitive surface. Neither of these modifications to the photo-tube are essential.

Mechanical provisions have been made for adjusting photoelectric tube vertically, horizontally, longitudinally, and in azimuth, with respect to the optical axis of the system under consideration.

Recording Microammeter

It has been found convenient to use a recording microammeter to measure the photoelectric responses in making contrast rendition measurements. This provides a permanent record which may be reviewed when desired and makes it possible to make the measurements rapidly using non-technical personnel. A variety of different types of recorders have been used successfully.

The Controls for the Illumination of the Surround

Because of the great sensitivity of the photoelectric system to changes in the voltage impressed on the photo-tube and the illumination system, it has been found desirable to use a fairly constant voltage in the contrast rendition apparatus. It no doubt would be most satisfactory to use batteries for precise measurements but more convenient to use a steady a.c. supply. It has been found possible to stabilize satisfactorily the a.c. line voltage by the use of commercially available stabilizers. This has, however, required

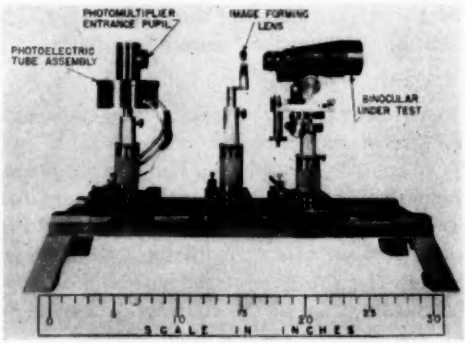

FIG. 15. Contrast rendition apparatus for binoculars.

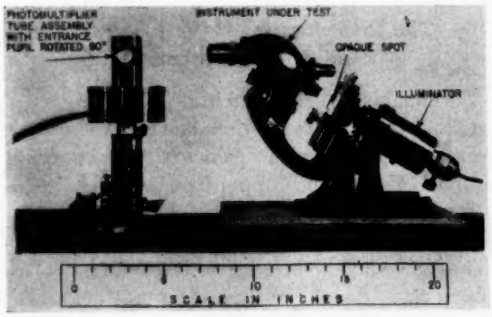

FIG. 16. Contrast rendition apparatus for microscopes.

[5] Radio Corporation of America, Tube Division, Harrison, New Jersey.

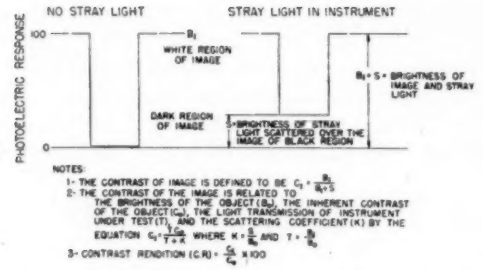
NO STRAY LIGHT
STRAY LIGHT IN INSTRUMENT
PHOTOELECTRIC RESPONSE
100
0
B_1
WHITE REGION OF IMAGE
$B_1 + S$ = BRIGHTNESS OF IMAGE AND STRAY LIGHT
DARK REGION OF IMAGE
S = BRIGHTNESS OF STRAY LIGHT SCATTERED OVER THE IMAGE OF BLACK REGION
NOTES:
1- THE CONTRAST OF IMAGE IS DEFINED TO BE $C_1 = \frac{B_1}{B_1+S}$
2- THE CONTRAST OF THE IMAGE IS RELATED TO THE BRIGHTNESS OF THE OBJECT (B_0), THE INHERENT CONTRAST OF THE OBJECT (C_0), THE LIGHT TRANSMISSION OF INSTRUMENT UNDER TEST (T), AND THE SCATTERING COEFFICIENT (K) BY THE EQUATION $C_1 = \frac{T C_0}{T + K}$ WHERE $K = \frac{S}{B_0}$ AND $T = \frac{B_1}{B_0}$
3- CONTRAST RENDITION (C.R) = $\frac{C_1}{C_0} \times 100$

FIG. 17. Schematic diagram of the type of data obtained in contrast rendition measurements.

the use of separate voltage stabilizers for each of the two surrounds, and for the photoelectric assembly.

The illumination systems of the two parts of the surround may be varied independently. This is accomplished by means of Variac transformers (shown in Fig. 14) and by varying the number and wattage of the incandescant lamps used.

The Screen for Limiting the Angular Subtense of the Surround

Since the amount of stray light introduced into an optical system depends upon the angular subtense of the surround, it is desirable to be able to control the subtense. This is accomplished, schematically, by collapsing the surround from 180° down to the subtense of the target by means of a set of screens of the type shown in Fig. 13. The subtense of the surround is varied in the calibration of the contrast of targets and to study the influence of the surround on contrast rendition.

PROCEDURE

The Procedure for Making Contrast Rendition Measurements

Although the experimental ramifications in making contrast rendition measurements are great, the procedure, in principal, is exceedingly simple. Using the apparatus shown in the preceding figures, the procedure consists of simply measuring the brightness of the image of the target and the brightness of the image of its white cover for a variety of conditions. (The form in which these brightnesses are recorded is shown in Fig. 17.) In practice, however, precise measurements of this type are difficult. These difficulties are largely associated with fluctuations in the photoelectric system, the precise measurement of the brightness condition of the surround, the calibration of the inherent contrast of the target, the stabilization of the a.c. voltages used, and the introduction of stray light into the system under test by the apparatus used. By taking suitable precautions, it has been found possible to make reproducible measurements of contrast rendition to less than 0.5 of a percent. While such precision is not required from a practical point of view in the case of telescopic systems, it may be required for other systems and receptors.

The discussion of the procedure for measuring the contrast rendition of optical systems may be divided into two parts. The first deals with the calibration of the apparatus and the second with the experimental variations used in making the contrast rendition measurements. Since the procedure for measuring the contrast rendition of various optical systems is essentially the same, the present discussion is limited to telescopic systems.

Calibration of the Contrast Rendition Apparatus

The calibration of the contrast rendition apparatus involves the measurement of the brightness at various angles of the surround and of the inherent contrast of the target.

The measurement of the relative brightness at various angles in the surround may be made by means of an off-axis fixture and an optical system known to be practically free from stray light.

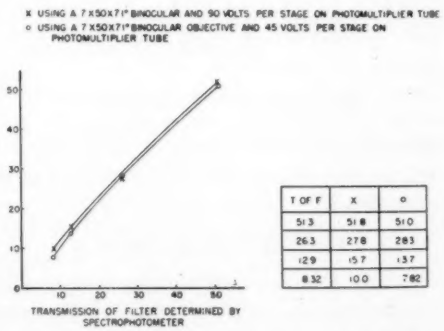

T OF F	X	o
51.3	51.8	51.0
26.3	27.8	28.3
12.9	15.7	13.7
8.32	10.0	7.82

FIG. 18. Test of contrast rendition apparatus for linearity of photoelectric response using neutral Inconel filters.

This measurement is made using the same photoelectric assembly as used in the contrast rendition measurements. The absolute values of the brightness are determined using a modified Macbeth Illuminometer.

The brightness of the small and wide angle surrounds may be varied independently by either changing the number of or the wattage of incandescant lamps used in the illumination system or by changing the voltage across the lamps by means of Variac transformers. Since the same photoelectric assembly is used in both the calibration and contrast rendition measurements, errors in spectral sensitivity can be practically

FIG. 19. 7×50×7.1° binocular used in surface defect test.

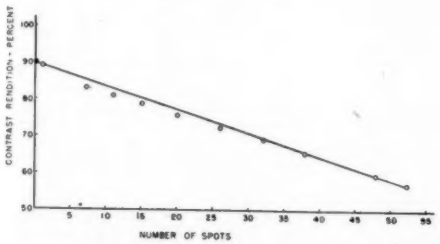

FIG. 20. Contrast rendition *vs.* number of 7-mm oil spots on the front surface of a 7×50×7.1° telescopic system.

TABLE I. The contrast rendition of coated telescopic systems of different design.

Description of system	Contrast rendition
4×16×12°	46%
4×28×10°	85
6×30×8.5°	96
6×33×8°	75
6×42×12°	82
6×50×7°	90
7×50×7°	92
7×50×10°	87
8×60×8°	92
9×63×6°	94
10×50×7°	91
10×70×7°	82
10×70×7°	75
12×34×4.4°	57
12×35×4.2°	69
12×60×3.8°	86
21×76×2.8°	94
10×80×7°	86
20×120×3°	94
25×100×3.6°	92

TABLE II. Contrast rendition of coated and non-coated 7×50×7° binoculars.

Binocular design *A*		Binocular design *B*			
Coated with *S*		Coated with *M*		Non-coated	
Left barrel	Right barrel	Left barrel	Right barrel	Left barrel	Right barrel
91	91	92	93	89	90
91	90	92	91	89	88
91	90	91	92	88	89
91	91	92	92	89	88
89	91	93	93	87	89
92	91	93	92	89	89
92	90	92	91	88	88
92	92	93	92	89	89
93	92	93	92	89	90
90	90	92	93	90	89
Average: 91		92		89	

TABLE III. The contrast rendition of 7×50×7° telescopic systems for targets of different inherent contrast.

Target contrast	Contrast rendition		
	Coated with *M*	Coated with *S*	Non-coated
100.0	90.1	90.0	87.9
93.6	90.1	90.1	87.7
78.4	90.1	90.0	87.9
63.2	90.1	90.0	87.9
50.7	90.1	90.0	87.8
29.6	90.1	90.2	88.0
14.3	90.1	89.6	87.7

TABLE IV. The contrast rendition of a 7×50×7° telescopic system for targets of different subtense.

Target subtense	Contrast rendition	
	Coated	Non-coated
0.10°	89	90
0.15°	90	90
0.20°	90	89
0.40°	91	91

TABLE V. The contrast rendition of coated telescopic systems for various angular subtenses of a uniformly illuminated surround.

Specimen	Contrast rendition		
	Subtense of surround		
	½°	10°	180°
7×35×7.3°	100	98	93
6×42×12°	100	96	81
7×50×7.1°	100	98	93
7×50×10°	100	97	85
10×50×7°	100	96	89
9×63×6°	100	98	94
10×70×7°	100	94	82

TABLE VI. The contrast rendition of coated telescopic systems at different brightness levels of a uniform surround.

Brightness level in footlamberts	Contrast rendition of system 6×42×12°	7×50×7°	7×50×10°	10×50×7°
100.0	84	90	84	88
50.0	83	90	84	88
25.0	84	90	83	88
12.5	84	90	84	88
6.3	84	89	83	87
3.2	84	90	84	88
1.5	84	89	83	88

TABLE VII. The contrast rendition of 7×50×7° telescopic systems at different ratios of the brightness of the wide to small angle surround.

Brightness ratio (B_w/B_s)	Contrast rendition: Coated with *M* Without thumb print	Coated with *M* With thumb print	Coated with *S* Without thumb print	Coated with *S* With thumb print	Non-coated Without thumb print	Non-coated With thumb print
0	98	95	99	93	96	93
1	92	90	90	85	89	83
2	88	84	84	79	83	75
4	80	75	74	68	73	63
8	67	62	60	54	60	48
16	50	45	42	38	43	32
32	34	30	27	25	27	20
64	20	17	15	13	16	11

eliminated even though the change in voltage produces a change in effective wave-length in the illuminating system. In this connection, the photo-multiplier tube has been found to respond nearly linearly of a relatively wide range of voltages impressed on it. This is shown in Fig. 18.

Frequently it is desired to vary the ratio of the brightness of the wide angle surround with respect to the small angle surround. This may be accomplished by changing the brightness of either keeping the other constant. It has been found convenient to vary the brightness of the small angle surround using a Variac transformer in making measurements. This has been found equivalent to the more cumbersome procedure of changing the number of lamps.

The absolute and relative brightness conditions at various points must be checked periodically because of aging of the illumination system and the changes in cleanliness of reflecting surfaces of the surrounds.

Calibration of the Inherent Contrast

The inherent contrast of various targets used in contrast rendition measurements is determined by measuring the contrast of the image with an optical system known to be practically free of stray light and by reducing the subtense of the surround to nearly zero. This latter is accomplished by means of screens of the form shown in Fig. 13 and by turning off the lamps in the wide angle surround. It will be seen from the data that practically all optical systems have a contrast rendition of nearly 100 percent when the subtense of the surround is small.

TABLE VIII. The contrast rendition for a non-coated 7×50×7° telescopic system at different field angles with respect to the optical axis.

Semi-field angle	Contrast rendition
−1.70°	90%
−1.14°	90
−0.63°	91
0.00°	90
+0.63°	91
+1.14°	92
+1.70°	92

TABLE IX. The contrast rendition of 7×50×7° coated telescopic systems for different stops in the exit pupil plane.

Specimen	Contrast rendition: Diameter of stop (mm) None	7.15	2.54
1	93	98	96
2	92	98	97
3	91	98	97
4	92	98	97
5	92	98	96
6	91	98	96
7	92	97	97
8	92	97	96
9	93	98	97
10	93	98	97
Average	92	98	97

TABLE X. Contrast rendition *vs.* ratio of brightness of wide to small angle surround for a non-coated 7×50×7.1° telescopic system with and without scratches on the front surface of the objective.

Brightness ratio (B_w/B_s)	Contrast rendition: Without scratches	With scratches
0	96	96
1	89	82
2	83	71
4	73	56
8	60	40
16	43	24
32	27	15
64	16	8

TABLE XI. The contrast renditions of photographic objectives of different designs at full aperture.

Objective	Focal length (mm)	No. of air-glass surfaces	Contrast rendition Non-coated	Coated
Tessar f:4.5	210	6	90	97
Protar f:18	183	4	96	98
Process f:10	330	8	92	98
Baltar f:2.3	100	8	94	99
Altimar f:5	212	8	93	97
Wide angle f:6.8	88	8	91	95
Metrogon f:6.3	152	10	77	96
Metrogon f:6.3	152	8	88	96

TABLE XII. The contrast rendition of process objectives at f:64 for targets of different inherent contrast.

Target contrast	Contrast rendition Non-coated	Coated
100.0	83.5	97.2
91.0	83.7	96.9
82.4	83.4	97.0
75.0	83.8	96.4
60.2	83.5	97.2
45.1	83.0	96.0
32.1	83.3	96.0
23.0	83.0	96.8
15.2	83.2	96.9

TABLE XIII. The contrast rendition of photographic objectives at different ratios of the brightness of the wide to small angle surround.

Brightness ratio (B_w/B_s)	Tessar f:4.5 E.F.L. = 210 mm		Protar f:18 E.F.L. = 183 mm		Process f:10 E.F.L. = 330 mm	
	Contrast rendition Non-coated	Coated	Non-coated	Coated	Non-coated	Coated
0	98	99	99	100	99	100
1	90	97	96	98	92	98
2	81	94	92	97	85	96
4	69	91	82	95	75	93
8	54	85	76	90	59	85
16	36	75	61	81	42	74
32	22	61	44	70	28	60
64	13	42	28	52	15	43

Conditions Varied in Contrast Rendition Measurements

In studying the contrast rendition of optical systems, it has been found of value to make measurements taking into account the following:

1. The design of the optical system under consideration.
2. Different specimens of the same design.
3. The use of different stops in the optical system.
4. The use of reflection reducing films.
5. The inherent target contrast.
6. The angular subtense of the target.
7. The angular subtense of the surround.

TABLE XIV. The contrast rendition of 210-mm Tessar at f:4.5 for different field angles.

Semi-field angle	Contrast rendition Non-coated	Coated
0	90	97
10	90	97
20	89	97
30	85	95

TABLE XV. The contrast rendition of photographic objectives at different f:numbers.

f:No.	Contrast rendition Baltar E.F.L. = 100 mm Non-coated	Coated	Tessar E.F.L. = 210 mm Non-coated	Coated	Metrogon E.F.L. = 152 mm Non-coated	Coated
2.3	94	99				
4.5	92	98	90	97		
6.3	89	97	90	97	88	96
8.0	88	96	89	97	88	96
11.0	85	96	88	97	88	95
16.0	84	94	87	97	87	95
32.0			87	97	86	95

TABLE XVI. The contrast rendition of a 300 mm f:4.5 non-coated Tessar with and without a light thumb print on the center of its front surface.

f:No.	Contrast rendition Without print	With print
4.5	93	91
5.6	94	92
8.0	94	89
11.0	94	85
16.0	93	80
22.0	93	77
32.0	93	75

TABLE XVII. The contrast rendition of a non-coated 100 mm f:2.3 Baltar for lens shades of different angular subtense.

Total angular subtense of shade	Contrast rendition f:2.3	f:5.6	f:11
No shade	94	89	87
40°	97	94	93
30°	97	95	94
20°	98	96	94
10°	98	97	96

8. The brightness condition of the surround with respect to the target.
9. Surface defects and the lack of cleanliness of the optical surfaces.
10. Different intended adjustments of the optical system under test.

In the general study of contrast rendition all of these conditions are being considered in detail

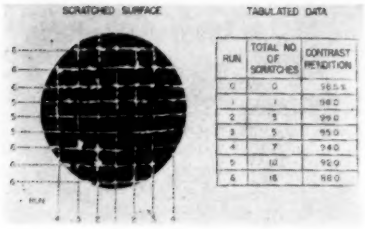

FIG. 21. Contrast rendition *vs.* surface defects in the front surface of a 7×50×7.1° binocular objective.

for a large number of optical systems in which nearly half a million measurements have been made thus far.

CONTRAST RENDITION DATA

The data are presented in graphic and tabular form. These include contrast rendition values for a variety of conditions for telescopic systems, photographic objectives, telescopic objectives, microscopic systems, and eyepieces.

TABLE XVIII. The contrast rendition of coated telescopic objectives of different designs.

Designation	No. of air glass surfaces	Contrast rendition
5×35×13°	6	85%
7×50×7.1°	2	98
6×30×8.5°	2	98
10×45×4.3°	2	98
20×64×2°	2	99
10×38×4°	2	99

TABLE XIX. The contrast rendition of 7×50×7.1° telescopic objectives of the same design.

Contrast rendition		
Coated	Non-coated	Uncoated
99	99	99
99	99	98
99	99	99
99	99	99

TABLE XX. The contrast rendition of coated and non-coated 5×35×13° telescopic objectives having six air-glass surfaces.

Target contrast	Contrast rendition	
	Coated	Non-coated
100.0	84.4	70.5
90.7	84.3	71.0
82.3	84.3	70.4
74.8	84.0	70.7
59.5	83.8	71.0
44.9	84.4	70.7
33.0	84.3	70.8
22.8	84.3	70.4
14.8	84.4	70.4

Contrast Rendition Data for Telescopic Systems

The contrast rendition data for telescopic systems are presented in Tables I to X inclusive and in Figs. 19 and 20. Unless otherwise specified, the contrast rendition data were obtained under the following conditions:

1. For a 180° uniform surround.
2. At a brightness level of 100 footlamberts.
3. With carefully cleaned optical surfaces.
4. With coated optics.

TABLE XXI. The contrast rendition of 7×50×7.1° binocular objectives of various field angles.

Semi-field angles	Contrast rendition		
	Coated with *M*	Non-coated	Uncoated
0°	98	98	98
2°	98	98	98
4°	98	98	98
6°	98	98	98
8°	98	98	98
10°	98	98	98
12°	98	98	98

TABLE XXII. The contrast rendition for various ratios of brightness of the wide to small angle surround for 5×35×13° telescopic objectives having six air-glass surfaces.

Brightness ratio (B_w/B_s)	Contrast rendition			
	Coated		Non-coated	
	Without thumb print	With thumb print	Without thumb print	With thumb print
0	99	97	99	97
1	85	82	71	67
2	74	71	57	51
4	59	56	39	36
8	42	39	25	21
16	25	24	14	12
32	14	14	7	7
64	8	8	4	3

TABLE XXIII. The contrast rendition of microscopes of different design.

Designation of design	Contrast rendition		
	Focal length of objective		
	4 mm	16 mm	32 mm
1	87	97	97
2	61	86	68
3	91	98	94
4	92	97	97
5	88	95	95

5. At full exit pupil.
6. For a target having an inherent contrast of 100 percent.
7. For targets subtending an angle of $\frac{1}{4}°$ with respect to the center of the objective of the instrument under test.

Contrast Rendition Data for Photographic Objectives

The contrast rendition data for photographic objectives are presented in Tables XI to XVII inclusive. Unless otherwise specified, the data were obtained under the following conditions:

1. Using a 180° uniform surround.
2. At a brightness level of 100 footlamberts.
3. With carefully cleaned optical surfaces.
4. With coated optics.

TABLE XXIV. Contrast rendition of monocular microscopes of the same design.

Specimen	Contrast rendition, Focal length of objective 4 mm	16 mm	32 mm
1	86	96	96
2	92	97	97
3	92	98	95
4	93	96	98
5	93	98	97
6	93	97	95

TABLE XXV. The contrast of a monocular microscope for six different 32-mm objectives of the same design.

Specimen	Contrast rendition
1	90%
2	87
3	90
4	88
5	89
6	89

TABLE XXVI. The contrast rendition of the left barrel of a binocular microscope for targets of different inherent contrasts.

Target contrasts	Contrast rendition
92%	96%
83	98
78	96
74	97
60	98
46	98
38	97

TABLE XXVII. The contrast rendition of the left barrel of a binocular microscope for reflection and transmission targets.

Focal length of objective	Contrast rendition, Reflection, Without thumb print	Reflection, With thumb print	Transmission, Without thumb print	Transmission, With thumb print
16 mm	92%	77%	95%	81%
32 mm	89	64	90	65

TABLE XXVIII. The contrast rendition of the left barrel of a binocular microscope for uniformly illuminated surrounds of different sizes.

Diameter of surround	Contrast rendition (using 32 mm objective)
12.7 mm	85%
9.50	88
6.35	89
5.08	89
4.06	90
3.81	90
3.37	91
2.54	92
1.85	94
1.32	96
0.64	97

TABLE XXIX. The contrast rendition of the left barrel of a binocular microscope for different field positions.

Position	Contrast rendition (using 32 mm objective)
Left edge	87%
Half to left	88
Center	89
Half to right	90
Right edge	91

TABLE XXX. The contrast rendition of the left barrel of a binocular microscope for different condenser stops.

Diameter of condenser stops	Contrast rendition, Focal length of objective 4 mm	16 mm	32 mm
30 mm	88	90	87
25	89	90	87
20	89	91	87
15	89	90	87
10	88	90	87
5	82	91	87
1		88	91

TABLE XXXI. The contrast rendition of the left barrel of a binocular microscope for a light thumb print covering $\frac{1}{3}$ of the front surface of each objective.

Focal length of objective	Contrast rendition, Without thumb print	With thumb print
4 mm	79%	74%
16	87	85
32	90	50

TABLE XXXII. The contrast rendition of coated eyepieces of different design.

Description	No. of air-glass surfaces	Contrast rendition
9×5×37°	4	95%
7.1×7×65°	6	97
7.1×7×65°	6	98
7.1×7×67°	6	98
7.1×7×65°	6	97
7.1×7×65°	6	97
6.3×15.3×11°	4	93
9.7×4.5×43°	4	97
10.9×7×72°	6	97
13.8×4×40°	4	96
7.1×5.8×36°	4	98
11×3.6×41°	4	95
12.8×3×40°	4	98
16.2×2.4×34°	4	98

5. For a target having an inherent contrast of 100 percent.

6. For targets subtending an angle of 2° with respect to the center of the objective under test.

Contrast Rendition Data for Telescopic Objectives

The contrast rendition data for telescopic objectives are presented in Tables XVIII to XXII inclusive and in Fig. 21. These data were taken under the same conditions as the photographic objectives. All of the telescopic objectives, with the exception of one, are cemented doublets. The exception, a four-element lens with six air-glass surfaces, is however likely to be the type of objective used in future designs and therefore is given special attention.

Contrast Rendition Data for Microscopes

The contrast rendition data for microscopes are presented in Tables XXIII to XXXI inclusive. Unless otherwise specified, the data were obtained under the following conditions:

1. Along the optical axis.
2. Using a uniform surround ten times the field of the microscopes.
3. Using a transmission target $\frac{1}{10}$ the field of the microscope.
4. Using the condenser at full aperture.

Contrast Rendition Data for Eyepieces

The contrast rendition data for eyepieces are presented in Tables XXXII to XXXVIII inclusive. Unless otherwise specified, the data were obtained under the following conditions:

1. Along the optical axis.
2. Using a uniform 50° surround.
3. Using a 2° target.
4. Using a stop equivalent to the exit pupil of the instrument for which the eyepiece was designed.
5. Using coated optics.

DISCUSSION AND CONCLUSIONS

It is evident from the preceding data that there is a certain degree of imperfection in all of the optical systems studied. The magnitude of this imperfection is seen to depend upon the design and the conditions under which the optical system is used. In the case of current high grade optical systems, in the normal state of adjustment, contrast rendition values range from 4 to 100 percent. These values depend upon the brightness condition of the region surrounding the target. In the case of a target having a dark surround the values range from 96 to 100 percent. In the case of a uniform surround the values range from 46 to nearly 100 percent. In the case in which the brightness of the 10° region surrounding the target is 1/64 as bright as the remainder of the surround, the values range from 4 to 52 percent. The question is raised as to what magnitude of imperfection in contrast rendition is of practical concern? This appears to depend upon the type of optical system. For example in the case of visual instruments it can be shown that an imperfection of less than 2 percent can be neglected. In the case of photographic systems an imperfection of 1 percent cannot be neglected judging from recent photographs[6] illustrating the importance of reflection reducing films. This indicates that each optical

TABLE XXXIII. The contrast rendition 7.1×7×65° eyepieces of the same design.

Specimen	Contrast rendition
1	97%
2	94
3	93
4	96
5	96
6	97

[6] "Lens coating does make a difference," P.S.A.J. 13, 34 (1947).

system should be considered on its own merits and under specific conditions in which it is used. There are, however, a few general conclusions that can be made. These include:

1. The concept of contrast rendition is valuable in predicting the performance of optical systems.

2. The contrast rendition is imperfect, to some degree, for all optical systems, and under most of the conditions in which they are used.

3. The contrast rendition of an optical system depends upon its optical and mechanical design, the nature of the surround in which it is used, the cleanliness of the optical surfaces, and the use of reflection reducing films.

4. The contrast rendition is substantially the same for specimens of the same design.

5. The contrast rendition is largely independent of the target contrast, the brightness level, the field angle, and the optical aberrations present for the optical systems and target subtenses considered here.

6. The contrast rendition of optical systems is, in general, improved by the use of reflection reducing films. In this connection, however, there appears to be little gain in contrast rendition by using reflection reducing films in connection with 7×50 binoculars. The light transmission, however, is increased from 54 to 74 percent by the use of the films.

7. The contrast rendition of an optical system is improved by the use of lens shades which effectively reduce the angular subtense of the surround with respect to the entrance pupil of the system under consideration.

8. The loss in range caused by an imperfection of 10 percent in contrast rendition for carefully cleaned 7×50 binoculars may be at least as high as 25 percent.

9. The loss in range caused by imperfect contrast rendition of telescopic systems is greater than similar losses in light transmission and magnification.

10. The loss in range caused by a single light thumb print placed in the center of the front surface of the objective of a 7×50 telescopic system may be as much as 50 percent in detecting

TABLE XXXIV. The contrast rendition of non-coated and coated 7×50×7.1° binocular eyepieces.

Contrast rendition	
Non-coated	Coated
97	97
94	95
97	98
97	96
Average = 96	Average = 97

TABLE XXXV. The contrast rendition of a 7.1×7×65° eyepiece for targets of different inherent contrast.

Target contrast	Contrast rendition
94	97%
85	97
78	97
71	96
65	98
59	97
52	96
37	97
30	97

TABLE XXXVI. The contrast rendition of a 7.1×7×65° eyepiece at different field angles.

Semi-field angles	Contrast rendition	
	Non-coated	Coated
0	96	98
5	96	98
10	98	98
15	98	98
20	98	98
25	98	98

TABLE XXXVII. The contrast rendition of a 7.1×7×65° eyepiece for stops of different diameters placed in the plane of the exit pupil.

Stop diameter	Contrast rendition	
	Non-coated	Coated
5.5 mm	95	97
7.2	96	98
11.0	96	98
12.5	96	98
15.8	97	98
18.3	97	98
25.4	96	98
51.0	53	51

TABLE XXXVIII. The contrast rendition of a 7.1×7×65° eyepiece with and without clean optics.

Location of thumb print	Contrast rendition	
	Non-coated	Coated
None	96	98
Eye lens	81	90
Field lens	92	94

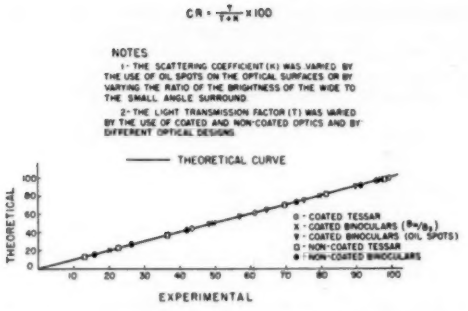
CR = T/(T+K) x 100
NOTES
1- THE SCATTERING COEFFICIENT (K) WAS VARIED BY THE USE OF OIL SPOTS ON THE OPTICAL SURFACES OR BY VARYING THE RATIO OF THE BRIGHTNESS OF THE WIDE TO THE SMALL ANGLE SURROUND
2- THE LIGHT TRANSMISSION FACTOR (T) WAS VARIED BY THE USE OF COATED AND NON-COATED OPTICS AND BY DIFFERENT OPTICAL DESIGNS
THEORETICAL CURVE
THEORETICAL
EXPERIMENTAL
0 - COATED TESSAR
X - COATED BINOCULARS (B=/B2)
9 - COATED BINOCULARS (OIL SPOTS)
□ - NON-COATED TESSAR
● - NON-COATED BINOCULARS

FIG. 22. A comparison of theoretical and experimental contrast rendition values for various scattering coefficients and light transmission factors.

objects at night and as much as 10 percent of the range at which targets may be detected in daylight.

11. In general, contrast rendition of non-coated photographic objectives becomes more imperfect as the aperture stop is decreased.

12. By taking into account the contrast rendition, light transmission, magnification, and exit pupil diameter it is possible to predict the performance of telescopic systems with considerable accuracy with respect to the range at which targets are detectable.

13. Within the limits of the experiments described in this paper, the theoretical treatment of contrast rendition is adequate. A comparison of experimental contrast rendition values with theoretical values computed from Eq. (10) is shown in Fig. 22.

14. Stray light is caused by undesirable reflections from the optical and mechanical surfaces and from surface defects and lack of cleanliness of the optical parts. For the optical system studied, the stray light reflected from the mechanical parts is greater than that reflected from the optical surfaces.

15. In general, the principal source of stray light is from the region surrounding the target.

16. The contrast rendition of visual optical systems depends upon the diameter of the pupil of the eye, the exit pupil, the diameter of the eye lens, and the eye relief.

17. The loss in contrast rendition caused by surface defects or lack of cleanliness is directly proportioned to the area of the defect.

Miscellaneous Comments

1. It would be desirable to extend the methods described by Hardy in predicting the performance of telescopic systems to other optical systems. It seems particularly desirable to make such an extension into photographic systems and systems which use photoelectric receptors of various kinds.

2. The importance of surface defects on the performance of optical instruments appears to be negligible and is only a sign of good workmanship.

3. With respect to the aberrations present, the actual resolving power of the telescopic systems in Table II range from 44 to 92 percent and from 10 to 92 percent the field angles indicated in Table VIII. For these particular telescopic systems, the contrast rendition does not vary by more than 2 percent. It should be noted however, that this apparent independence of contrast rendition upon optical aberrations applies onlto targets that are large in subtense with respect to the minimum resolvable angle of the system under consideration. In the event the targets are comparable in subtense with the minimum resolvable angle, the loss in resolution caused by an imperfection in contrast rendition would be the same as an equivalent loss caused by a reduction in test object contrast.

ACKNOWLEDGMENT

The author is indebted to a considerable number of individuals for encouragement, suggestions, and assistance in connection with the preparation of this paper and the experimental measurements. These are: Dr. T. Smith, National Physical Laboratory, London; Professor A. C. Hardy, Massachusetts Institute of Technology, Cambridge, Massachusetts; Dr. Theodore Dunham, Jr., Chief 16.1 of the NDRC, Cambridge, Massachusetts; Commander S. S. Ballard, Lt. Commander N. H. Pulling, and Lt. Commander M. J. Jennings, Navy Department, Washington, D. C.; Dr. R. Tousey and Dr. D. M. Packer, Naval Research Laboratory, Washington, D. C.; Professor S. Q. Duntley, Massachusetts Institute of Technology, Cambridge, Massachusetts; Mr. Richard Blackwell, University of Michigan, Ann Arbor, Michigan; Lt. W. S. Verplanck, and Cap-

tain C. W. Schilling, Naval Medical Research Laboratory, New London, Connecticut; Dr. A. F. Turner, Bausch & Lomb Optical Company, Rochester, New York; Mr. A. H. Bennett, American Optical Company, Buffalo, New York; Dr. Harold Moulton, American Optical Company, Southbridge, Massachusetts; Dr. I. C. Gardner, National Bureau of Standards, Washington, D. C.; Dean F. C. Whitmore, Dr. M. F. Coleman, Mr. S. W. Harding, and Mr. D. G. Clark, The Pennsylvania State College, State College, Pennsylvania.

JOURNAL OF THE OPTICAL SOCIETY OF AMERICA VOLUME 37, NUMBER 6 JUNE, 1947

Reflection and Transmission Interference Filters

Part I. Theory

L. N. HADLEY AND D. M. DENNISON
University of Michigan, Ann Arbor, Michigan

(Received February 1, 1947)

An interference filter of the reflection type consists in its simplest form of a perfectly reflecting mirror on which is placed a thin layer of a dielectric material. The outer surface of the dielectric is coated with a very thin metallic film. When properly constructed such a filter reflects 100 percent of radiation at the frequencies $2n\nu_0$, and 0 percent of radiation at the frequencies $(2n+1)\nu_0$.

A transmission filter consists of a thin dielectric layer, both sides of which are coated with very thin metallic films. A well made filter will transmit up to approximately 40 percent of the incident radiation at the frequencies $n\nu_0$. The transmission bands can be made quite narrow, and the transmission between the maxima may be less than 1 percent although it does not fall to zero.

The theory, which consists of a straightforward application of the Maxwell equations, is initially applied to a single metallic film backed by dielectric media. The reflection and transmission coefficients, as well as the phase shifts, are obtained and are given in terms of the thickness and the optical constants of the film.

The reflection coefficient for the reflection filter is developed next and is expressed as a function of the properties of a single metallic film. The general formula is quite complicated but degenerates to a simple form when the wave-length becomes long (i.e. for the infra-red region). By using the filter at oblique incidence it is shown that polarized radiation may be produced.

The transmission filter is studied and its properties may again be formulated in terms of the properties of a single metallic film. The values of the optical constants are deduced, which lead to the construction of an efficient transmission filter. Silver films have approximately these values in the visible region of the spectrum, but fail to possess them either in the ultraviolet or in the infra-red region. The theory shows that when the filter is tilted so that the angle of incidence is no longer normal, the transmission band shifts towards shorter wave-lengths, and splits into two bands, one of which is polarized parallel and the other perpendicular to the plane of incidence. This phenomenon is observed with experimental filters.

1. INTRODUCTION

FILTERS which isolate a particular wave-length region of the spectrum have long been an indispensable tool for certain branches of spectroscopy. Many different types of filtering systems have been devised and have included simple dye filters, the very effective but expensive polarization filters, Christiansen filters, and residual ray plates, to mention only a few.

During and following the war two new types have appeared, (a) the reflection interference filter,[1] which makes use of the absorbing properties of a semi-conducting layer placed a quarter-wave-length in front of a perfectly reflecting

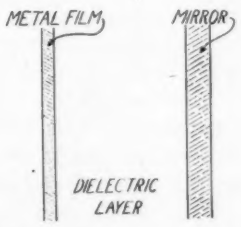

FIG. 1. Arrangement of various layers in the reflection filter.

[1] L. N. Hadley and D. M. Dennison, Phys. Rev. **69**, 258 (1946).

mirror, and (b) the transmission interference filter,[2] which consists essentially of a Fabry-Perot etalon with a spacing of the order of a few wave-lengths.

The reflection filter was used extensively in the short radio wave-length region during the war. For this region it was constructed by supporting a carbon-impregnated canvas sheet of proper resistance a quarter-wave-length above a plane metal surface. The adaptation of this filter for the infra-red and optical regions involves the same principle, but requires considerably different techniques. A good front surface mirror (Fig. 1) forms the plane metal surface, and the carbon-impregnated canvas sheet is replaced by a thin semi-transparent metallic film, which has the same resistive property. The metallic film is supported by a dielectric layer which is usually produced by evaporation.

The transmission filter (Fig. 2), which was developed in Germany, consists of two thin semi-transparent metallic layers parallel to each other and separated, as mentioned above, by a distance of the order of a few wave-lengths. A dielectric layer is again used as the means of separating the metal layers. The filter is mounted on some transparent supporting substrate, such as a glass plate.

The typical optical properties of these filters are shown in Figs. 3 and 4. Figure 3 is a plot of the reflection coefficient as a function of frequency for the reflection filter. A minimum reflection coefficient of zero is obtained for some frequency ν_0 (the frequency for which the spacing between mirror and semi-transparent film is $\lambda_0/4$), and for all odd multiples of this frequency. A maximum reflection coefficient of 100 percent is obtained at zero frequency, and at the even multiples of the fundamental frequency ν_0. The exact shape of this curve will be given in detail in a later section.

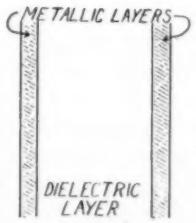

FIG. 2. Arrangement of the various layers in the transmission filter.

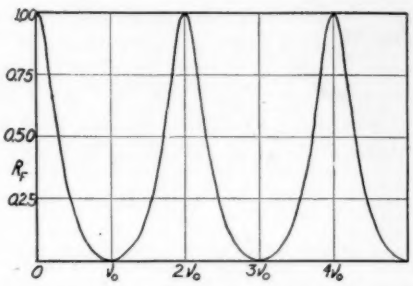

FIG. 3. Reflection coefficient *vs.* frequency of radiation for the reflection filter. Resistance of metal film is 377Ω/□, dielectric constant of dielectric layer is unity.

In contrast to the maximum and minimum reflection coefficients of 100 and 0 percent, respectively, for the reflection filter, the maximum transmission coefficient for the transmission filter is of the order of 30 to 40 percent, and the minimum transmission coefficient can be made to be considerably less than one percent, but cannot in principle be zero. The maxima occur at zero frequency, and at some frequency ν_0 (the frequency for which the spacing between films is $\lambda_0/2$), and at all integral multiples of ν_0. An interesting feature of the transmission filter is that the transmission band, in the visible region, may be made to be of the order of 100A wide, where the width is defined as the distance between the points of half-maximum intensity on either side of the band.

The optical properties of each of these filters may be expressed as a function of wave-length, and of the other parameters of the system. These parameters are the thickness Δ, and index of refraction n of the dielectric layer; the thickness s, index of refraction η, and extinction coefficient κ of the semi-transparent metal layers; the angle of incidence θ; and in the case of the reflection filter, the properties of the reflecting mirror.

When the wave-length region is far longer than the wave-lengths at which electronic resonances

[2] J. A. Sanderson and R. L. Ueberall, Report H-2731, Navy Department, Office of Research and Inventions, N.R.L.

occur in metals, the parameters η and κ may be conveniently replaced by ϵ, μ, and σ, where ϵ is the permittivity, μ is the permeability, and σ is the conductivity of the metal.[3] It is well known that the use of the constants ϵ, μ, and σ, to express the optical properties of metals, is quite valid for all wave-lengths longer than about 10μ, and, for some materials, the expressions obtained are reasonably accurate even for wave-lengths approaching the visible region.

The general relationship between the constants η and κ, and the constants ϵ, μ, and σ, is obtained from the wave-propagation constant, which is usually written as

$$k^2=\omega^2\epsilon\mu+i\omega\mu\sigma.$$

The propagation constant for free space is

$$k_0^2=\omega^2\epsilon_0\mu_0,$$

where $\omega=2\pi\nu$, and ν is the frequency of the radiation. The ratio of k to k_0 is then,

$$\frac{k^2}{k_0^2}=(\eta+i\kappa)^2=\frac{\epsilon\mu}{\epsilon_0\mu_0}+i\frac{\mu\sigma}{\omega\epsilon_0\mu_0}.$$

For simplicity we will consider only non-magnetic metals so that μ may be replaced by μ_0 throughout. Hence

$$\eta+i\kappa=\left[\frac{\epsilon}{\epsilon_0}+i\frac{\sigma}{\omega\epsilon_0}\right]^{\frac{1}{2}}.$$

This gives

$$\eta^2=\frac{\left(1+\dfrac{\sigma^2}{\omega^2\epsilon^2}\right)^{\frac{1}{2}}+1}{2\epsilon_0/\epsilon}, \tag{1}$$

and

$$\kappa^2=\frac{\left(1+\dfrac{\sigma^2}{\omega^2\epsilon^2}\right)^{\frac{1}{2}}-1}{2\epsilon_0/\epsilon}. \tag{2}$$

For wave-lengths of the order of 10μ and longer, and for metallic materials, the term $\sigma^2/\omega^2\epsilon^2$ is much larger than unity,[4] and for this case Eqs. (1) and (2) reduce to

$$\eta=\kappa=[\sigma/2\omega\epsilon_0]^{\frac{1}{2}}. \tag{3}$$

[3] The conductivity of an evaporated metallic film is generally considerably lower than that of the bulk metal, although it approaches the bulk conductivity as the film becomes thick.

[4] H. Murmann, Zeits. f. Physik **54**, 741 (1929).

The expressions (1) and (2) are not valid in general for radiation of visible and ultraviolet frequencies, since the electronic absorption frequencies lie in this range. These absorptions give rise to dispersion, and consequently the conductivity must be replaced by a new complex conductivity.

The equations developed here, however, will be expressed in terms of the propagation constant, written in the form $k=(2\pi/\lambda)(\eta+i\kappa)$, and thus will be valid for all wave-length regions. The appropriate degenerations for the long wave-lengths of the infra-red may be easily performed. Excellent work has been done by many investigators in determining η and κ for various metals in the optical region of the spectrum. Two papers, which have special application for our problem are those of F. Goos[5] and H. Murmann[6] on the reflection and transmission coefficients of thin silver films.

The solution of the filter problem is straightforward but not simple, since there are a number of regions of space to be considered. The procedure will be to write down the expressions for travelling waves in each of the regions, apply the appropriate boundary conditions between regions, and thereby determine the characteristics of the filters as a function of the properties of the component films.

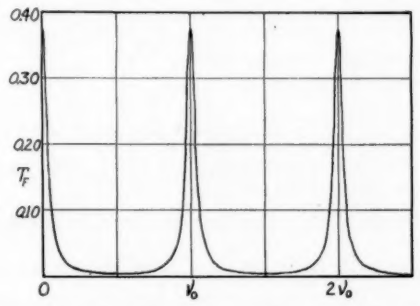

FIG. 4. Transmission coefficient *vs.* frequency of radiation for the transmission filter. The constants of the films are chosen such that the reflection and transmission coefficients for a single metal film are 0.80 and 0.122, respectively.

It is proposed that the present article will deal with the theory of interference filters, and that a second article (Part II) will describe the con-

[5] F. Goos, Zeits. f. Physik **100**, 95 (1936).

[6] H. Murmann, Zeits. f. Physik **101**, 643 (1936).

struction of actual filters and their experimental properties. Before proceeding to a discussion of filter theory it will be advantageous to consider the case of a single metallic layer.

2. OPTICAL PROPERTIES OF A SINGLE METAL LAYER

Consider a plane metal layer of thickness s in the x-direction, and of infinite extent in the yz-plane. Let the region of negative x be a semi-infinite dielectric space with the real index of refraction n_1, and the region $x>s$ be a semi-infinite dielectric space with the real index of refraction n_3 (Fig. 5). It will later be advantageous to consider that the two dielectric regions I and III are finite, although very thick compared with a wave-length of the radiation. The angle θ, without subscript, will be reserved to describe the incident or emergent angle outside the dielectric regions. Region I will be characterized by a propagation constant $k_1=2\pi n_1/\lambda$; region II by $k_2=2\pi(\eta+i\kappa)/\lambda$; and region III by $k_3=2\pi n_3/\lambda$. The direction of propagation will be

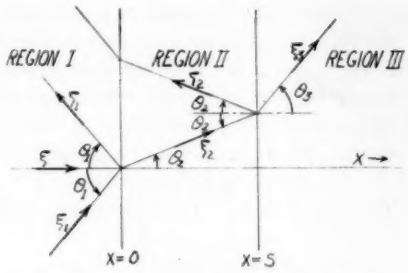

FIG. 5. Geometry used in the discussion of the single metal film.

defined in the various regions by the unit vectors ξ_i and ζ_i. Let plane electromagnetic radiation from region I be incident upon the left side of region II, and let the wave normal make an angle θ_1 with the x axis in region I. Since in general the wave will be partially reflected at the boundary between regions I and II, the expression for the wave in region I may be written as the sum of an incident and a reflected wave of the form:

$$E_{\mathrm{I}}=E_{11}\exp(ik_1\xi_1\cdot r-i\omega t)+E_{12}\exp(ik_1\zeta_1\cdot r-i\omega t), \tag{4}$$

$$H_{\mathrm{I}}=k_1/\omega\mu_0[\xi_1\times E_{11}\exp(ik_1\xi_1\cdot r-i\omega t)+\zeta_1\times E_{12}\exp(ik_1\zeta_1\cdot r-i\omega t)]. \tag{5}$$

Similarly in region II

$$E_{\mathrm{II}}=E_{21}\exp(ik_2\xi_2\cdot r-i\omega t)+E_{22}\exp(ik_2\zeta_2\cdot r-i\omega t), \tag{6}$$

$$H_{\mathrm{II}}=k_2/\omega\mu_0[\xi_2\times E_{21}\exp(ik_2\xi_2\cdot r-i\omega t)+\zeta_2\times E_{22}\exp(ik_2\zeta_2\cdot r-i\omega t)]. \tag{7}$$

In region III there is no reflected wave, and consequently

$$E_{\mathrm{III}}=E_{31}\exp(ik_3\xi_3\cdot r-i\omega t), \tag{8}$$

$$H_{\mathrm{III}}=k_3/\omega\mu_0[\xi_3\times E_{31}\exp(ik_3\xi_3\cdot r-i\omega t)]. \tag{9}$$

The boundary conditions are that the tangential components of E and H are continuous across all boundaries. There are then two cases of special interest: (a) E is normal to the plane of incidence, and (b) E is parallel to the plane of incidence. The boundary conditions may be expressed in the form,

$$\left.\begin{aligned}\xi\times E_{\mathrm{I}}&=\xi\times E_{\mathrm{II}}\\ \xi\times H_{\mathrm{I}}&=\xi\times H_{\mathrm{II}}\end{aligned}\right\}\text{ at } x=0, \tag{10, 11}$$

for the boundary between regions I and II, and

$$\left.\begin{aligned}\xi\times E_{\mathrm{II}}&=\xi\times E_{\mathrm{III}}\\ \xi\times H_{\mathrm{II}}&=\xi\times H_{\mathrm{III}}\end{aligned}\right\}\text{ at } x=s, \tag{12, 13}$$

for the boundary between regions II and III.

Case (a): E is Normal to the Plane of Incidence

It is convenient to express the boundary equations for H in terms of E. This may be done by use of Eqs. (5), (7), and (9). Equation (11), then, has the following form, where the exponential terms disappear since $x=0$ for this boundary.

$$\xi\times[\xi_1\times E_{11}+\zeta_1\times E_{12}]k_1/\omega\mu_0=\xi\times[\xi_2\times E_{21}+\zeta_2\times E_{22}]k_2/\omega\mu_0.$$

Upon expanding the vector products this gives

$$[(\xi\cdot E_{11})\xi_1-(\xi\cdot\xi_1)E_{11}+(\xi\cdot E_{12})\zeta_1-(\xi\cdot\zeta_1)E_{12}]k_1 =[(\xi\cdot E_{21})\xi_2-(\xi\cdot\xi_2)E_{21}+(\xi\cdot E_{22})\zeta_2-(\xi\cdot\zeta_2)E_{22}]k_2. \quad (14)$$

Since the media are all isotropic

$$\xi\cdot E_{11}=\xi\cdot E_{12}=\xi\cdot E_{21}=\xi\cdot E_{22}=0; \quad (15)$$

and from Fig. 5

$$\xi\cdot\xi_1=\cos\theta_1, \quad \xi\cdot\xi_2=\cos\theta_2, \quad \xi\cdot\xi_3=\cos\theta_3. \quad (16)$$
$$\xi\cdot\zeta_1=-\cos\theta_1, \quad \xi\cdot\zeta_2=-\cos\theta_2,$$

The resulting boundary equations (10) and (11) then become

$$E_{11}+E_{12}=E_{21}+E_{22}, \quad (17)$$

and from (14), (15), and (16)

$$(E_{11}-E_{12})k_1\cos\theta_1=(E_{21}-E_{22})k_2\cos\theta_2. \quad (18)$$

A similar procedure for Eqs. (12) and (13) leads to

$$E_{21}\exp(ik_2s\cos\theta_2)+E_{22}\exp(-ik_2s\cos\theta_2)=E_{31}\exp(ik_3s\cos\theta_3), \quad (19)$$

$$[E_{21}\exp(ik_2s\cos\theta_2)-E_{22}\exp(-ik_2s\cos\theta_2)]k_2\cos\theta_2=k_3\cos\theta_3E_{31}\exp(ik_3s\cos\theta_3). \quad (20)$$

From Eqs. (17), (18), (19), and (20) the amplitude ratios E_{31}/E_{11} and E_{12}/E_{11} may be determined

$$t_\perp{}^R\exp(iu_\perp{}^R)\equiv E_{31}/E_{11}=\frac{4\alpha_2\exp(-ik_3s\cos\theta_3)}{(1+\alpha_1)(1+\alpha_2)\exp(-ik_2s\cos\theta_2)-(1-\alpha_1)(1-\alpha_2)\exp(ik_2s\cos\theta_2)}, \quad (21)$$

$$r_\perp{}^R\exp(iy_\perp{}^R)\equiv E_{12}/E_{11}=\frac{(1-\alpha_1)(1+\alpha_2)\exp(-ik_2s\cos\theta_2)-(1+\alpha_1)(1-\alpha_2)\exp(ik_2s\cos\theta_2)}{(1+\alpha_1)(1+\alpha_2)\exp(-ik_2s\cos\theta_2)-(1-\alpha_1)(1-\alpha_2)\exp(ik_2s\cos\theta_2)}. \quad (22)$$

The superscript R on the symbols $t_\perp$, $u_\perp$, $r_\perp$, and $y_\perp$ indicates that the corresponding wave is traveling from region I into region III of Fig. 5. In all of the formulas which follow a superscript R means that the wave is traveling from left to right while a superscript L means that the wave is traveling from right to left. The angles u and y are the respective phase shifts of the transmitted and the reflected rays. The terms α_1 and α_2 are abbreviations

$$\alpha_1\equiv k_2\cos\theta_2/k_1\cos\theta_1, \quad \text{and} \quad \alpha_2\equiv k_2\cos\theta_2/k_3\cos\theta_3.$$

The angles θ_1, θ_2, and θ_3 may be eliminated by use of the refraction law.

$$k_1\sin\theta_1=k_2\sin\theta_2=k_3\sin\theta_3=k\sin\theta,$$

where k is the propagation constant for free space, and θ, referred to earlier, is the angle between the direction of propagation and the x axis in free space outside the dielectric regions. When this is done, and when the k's are replaced by the optical constants, the expressions for α_1 and α_2 become

$$\alpha_1\equiv(\eta^2-\kappa^2-\sin^2\theta+2i\eta\kappa)^{\frac{1}{2}}/(n_1{}^2-\sin^2\theta)^{\frac{1}{2}}\equiv(a+ib)/p,$$

$$\alpha_2\equiv(\eta^2-\kappa^2-\sin^2\theta+2i\eta\kappa)^{\frac{1}{2}}/(n_3{}^2-\sin^2\theta)^{\frac{1}{2}}\equiv(a+ib)/q,$$

where a, b, p, and q are

$$a=\frac{1}{\sqrt{2}}\{[(\eta^2-\kappa^2-\sin^2\theta)^2+4\eta^2\kappa^2]^{\frac{1}{2}}+(\eta^2-\kappa^2-\sin^2\theta)\}^{\frac{1}{2}}, \tag{23}$$

$$b=\frac{1}{\sqrt{2}}\{[(\eta^2-\kappa^2-\sin^2\theta)^2+4\eta^2\kappa^2]^{\frac{1}{2}}-(\eta^2-\kappa^2-\sin^2\theta)\}^{\frac{1}{2}}, \tag{24}$$

$$p=(n_1^2-\sin^2\theta)^{\frac{1}{2}}, \tag{25}$$

$$q=(n_3^2-\sin^2\theta)^{\frac{1}{2}}. \tag{26}$$

It will be convenient to use the abbreviation

$$\rho=a^2+b^2. \tag{27}$$

To determine the reflection and transmission coefficients it is necessary to find the time average of the normal component of the Poynting vector. For the reflection coefficient this is $R_\perp{}^R=E_{12}E_{12}^*/E_{11}E_{11}^*$ since both E_{11} and E_{12} are in the same medium. The transmission coefficient is

$$T_\perp{}^R=E_{31}E_{31}^*k_3\cos\theta_3/E_{11}E_{11}^*k_1\cos\theta_1.$$

The actual calculation of these is a tedious but elementary algebraic task, and only the results will be given here

$$R_\perp{}^R=\left\{\left[\left(\frac{\rho}{p^2}+1\right)\left(\frac{\rho}{q^2}+1\right)-\frac{4a^2}{pq}\right]\cosh\frac{4\pi bs}{\lambda}+\left[\frac{2a}{q}\left(\frac{\rho}{p^2}+1\right)-\frac{2a}{p}\left(\frac{\rho}{q^2}+1\right)\right]\sinh\frac{4\pi bs}{\lambda}\right.$$
$$\left.-\left[\left(\frac{\rho}{p^2}-1\right)\left(\frac{\rho}{q^2}-1\right)+\frac{4b^2}{pq}\right]\cos\frac{4\pi as}{\lambda}+\left[\frac{2b}{q}\left(\frac{\rho}{p^2}-1\right)-\frac{2b}{p}\left(\frac{\rho}{q^2}-1\right)\right]\sin\frac{4\pi as}{\lambda}\right\}\Big/D_\perp, \tag{28}$$

$$T_\perp{}^R=8\rho/pqD_\perp, \tag{29}$$

$$D_\perp=\left\{\left[\left(\frac{\rho}{p^2}+1\right)\left(\frac{\rho}{q^2}+1\right)+\frac{4a^2}{pq}\right]\cosh\frac{4\pi bs}{\lambda}+\left[\frac{2a}{q}\left(\frac{\rho}{p^2}+1\right)+\frac{2a}{p}\left(\frac{\rho}{q^2}+1\right)\right]\sinh\frac{4\pi bs}{\lambda}\right.$$
$$\left.-\left[\left(\frac{\rho}{p^2}-1\right)\left(\frac{\rho}{q^2}-1\right)-\frac{4b^2}{pq}\right]\cos\frac{4\pi as}{\lambda}+\left[\frac{2b}{q}\left(\frac{\rho}{p^2}-1\right)+\frac{2b}{p}\left(\frac{\rho}{q^2}-1\right)\right]\sin\frac{4\pi as}{\lambda}\right\}. \tag{30}$$

The phase angles $y_\perp{}^R$ and $u_\perp{}^R$ of the reflected and transmitted waves, may be computed by finding the ratio of the real and imaginary parts of E_{12}/E_{11}, and of E_{31}/E_{11}, respectively. $y_\perp{}^R$ is the phase of the reflected wave relative to the incident wave as measured at the boundary between I and II. $u_\perp{}^R$ is the corresponding phase of the transmitted wave as measured at the boundary II, III. These angles will play an important role in determining the properties of the actual filters.

One obtains

$$\tan y_\perp{}^R=\frac{\frac{4ab}{pq}\left(\cosh\frac{4\pi bs}{\lambda}-\cos\frac{4\pi as}{\lambda}\right)+\frac{2b}{q}\left(\frac{\rho}{p^2}+1\right)\sinh\frac{4\pi bs}{\lambda}-\frac{2a}{q}\left(\frac{\rho}{p^2}-1\right)\sin\frac{4\pi as}{\lambda}}{\left(\frac{\rho}{p^2}+1\right)\left(\frac{\rho}{q^2}-1\right)\cosh\frac{4\pi bs}{\lambda}-\left(\frac{\rho}{p^2}-1\right)\left(\frac{\rho}{q^2}+1\right)\cos\frac{4\pi as}{\lambda}}, \tag{31}$$

$$+\frac{2a}{p}\left(\frac{\rho}{q^2}-1\right)\sinh\frac{4\pi bs}{\lambda}+\frac{2b}{p}\left(\frac{\rho}{q^2}+1\right)\sin\frac{4\pi as}{\lambda}$$

$$u_\perp{}^R=\tan^{-1}b/a-2\pi qs/\lambda+\tan^{-1}\delta,$$

where

$$\delta=\frac{\left(1+\frac{a^2-b^2}{pq}\right)\sin\frac{2\pi as}{\lambda}\cosh\frac{2\pi bs}{\lambda}-\frac{2ab}{pq}\cos\frac{2\pi as}{\lambda}\sinh\frac{2\pi bs}{\lambda}+\left(\frac{a}{p}+\frac{a}{q}\right)\sin\frac{2\pi as}{\lambda}\sinh\frac{2\pi bs}{\lambda}-\left(\frac{b}{p}+\frac{b}{q}\right)\cos\frac{2\pi as}{\lambda}\cosh\frac{2\pi bs}{\lambda}}{\frac{2ab}{pq}\sin\frac{2\pi as}{\lambda}\cosh\frac{2\pi bs}{\lambda}+\left(1-\frac{a^2-b^2}{pq}\right)\cos\frac{2\pi as}{\lambda}\sinh\frac{2\pi bs}{\lambda}+\left(\frac{b}{p}+\frac{b}{q}\right)\sin\frac{2\pi as}{\lambda}\sinh\frac{2\pi bs}{\lambda}+\left(\frac{a}{p}+\frac{a}{q}\right)\cos\frac{2\pi as}{\lambda}\cosh\frac{2\pi bs}{\lambda}}. \tag{32}$$

The corresponding expressions when the wave is traveling from region III into region I, namely $R_\perp{}^L$, $T_\perp{}^L$, $y_\perp{}^L$, and $u_\perp{}^L$ are obtained from the above formulas by merely interchanging p and q, since the indices of refraction n_1 and n_3, which characterize regions I and III, appear only in p and q.

It should be noted that $T_\perp{}^R$ is symmetrical in p and q and hence the transmission coefficient is independent of the direction of propagation of the wave as it must be. The reflection coefficient and consequently the loss of energy in the film, is however dependent upon the direction.

Before discussing the expressions for reflection and transmission derived so far, it will be advantageous to present the corresponding formulas for the case when the electric vector of the incident wave is parallel to the plane of incidence.

Case (b): *E* is Parallel to the Plane of Incidence

In this case it is convenient to express E in terms of H. The procedure is similar to that used earlier, and the boundary equations are

$$\begin{gathered}H_{11}+H_{12}=H_{21}+H_{22},\\(H_{11}-H_{12})k_2\cos\theta_1=(H_{21}-H_{22})k_1\cos\theta_2,\\H_{21}\exp(ik_2s\cos\theta_2)+H_{22}\exp(-ik_2s\cos\theta_2)=H_{31}\exp(ik_3s\cos\theta_3),\\[H_{21}\exp(ik_2s\cos\theta_2)-H_{22}\exp(-ik_2s\cos\theta_2)]k_3\cos\theta_2=k_2\cos\theta_3H_{31}\exp(ik_3s\cos\theta_3).\end{gathered}$$

The equations for the ratios H_{31}/H_{11} and H_{12}/H_{11} are identical in form with Eqs. (21) and (22).

$$t_{11}\exp(iu_{11}{}^R)\equiv H_{31}/H_{11}=\frac{4\beta_2\exp(-ik_3s\cos\theta_3)}{(1+\beta_1)(1+\beta_2)\exp(-ik_2s\cos\theta_2)-(1-\beta_1)(1-\beta_2)\exp(ik_2s\cos\theta_2)}, \tag{33}$$

$$r_{11}{}^R\exp(iy_{11}{}^R)\equiv H_{12}/H_{11}=\frac{(1-\beta_1)(1+\beta_2)\exp(-ik_2s\cos\theta_2)-(1+\beta_1)(1-\beta_2)\exp(ik_2s\cos\theta_2)}{(1+\beta_1)(1+\beta_2)\exp(-ik_2s\cos\theta_2)-(1-\beta_1)(1-\beta_2)\exp(ik_2s\cos\theta_2)}, \tag{34}$$

where

$$\beta_1\equiv k_1\cos\theta_2/k_2\cos\theta_1,\quad \beta_2\equiv k_3\cos\theta_2/k_2\cos\theta_3$$

and in terms of the optical constants η and κ

$$\begin{aligned}\beta_1&=[(\eta^2-\kappa^2-\sin^2\theta+2i\eta\kappa)^{\frac{1}{2}}n_1{}^2/(\eta^2-\kappa^2+2i\eta\kappa)(n_1{}^2-\sin^2\theta)^{\frac{1}{2}}]=n_1{}^2(c+id)/p,\\ \beta_2&=[(\eta^2-\kappa^2-\sin^2\theta+2i\eta\kappa)^{\frac{1}{2}}n_3{}^2/(\eta^2-\kappa^2+2i\eta\kappa)(n_3{}^2-\sin^2\theta)^{\frac{1}{2}}]=n_3{}^2(c+id)/q,\end{aligned}$$

c and d are abbreviations for

$$c\equiv[a(\eta^2-\kappa^2)+2b\eta\kappa]/(\eta^2+\kappa^2)^2, \tag{35}$$

$$d\equiv[b(\eta^2-\kappa^2)-2a\eta\kappa]/(\eta^2+\kappa^2)^2, \tag{36}$$

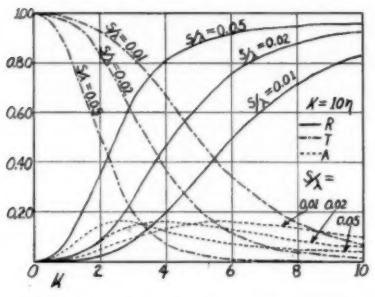

FIG. 6. Reflection, transmission, and absorption coefficients as a function of κ for a single metal film in air. Normal incidence. $\kappa=10\eta$.

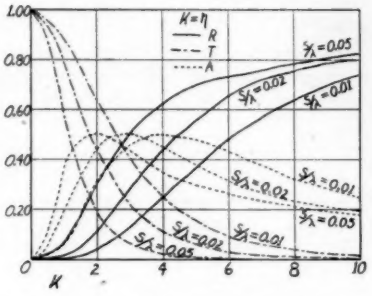

FIG. 7. Reflection, transmission, and absorption coefficients as a function of κ for a single metal film in air. Normal incidence. $\kappa=\eta$.

and

$$c^2+d^2=\rho/(\eta^2+\kappa^2)^2. \tag{37}$$

a, b, p, q, and ρ have the same meanings as before. From these the transmission and reflection coefficients for this polarization may be written. These will not be given explicitly since the form of the equations is identical with Eqs. (28), (29), and (30), where the a and b in the coefficients are replaced by c and d, respectively, q is replaced by q/n_3^2, p by p/n_1^2 and ρ is replaced by $\rho/(\eta^2+\kappa^2)^2$. The a and b terms in the arguments of the hyperbolic and trigonometric functions, however, remain the same.

The interpretation of the general equations for the reflection and transmission coefficients of the dielectric-backed metallic layer is rather difficult, for in the general case both R and T are functions of η, κ, λ, s, n_1, n_3, and θ, and the equations are transcendental. Some simplification occurs if the equations are written for normal incidence, and for $n_1=n_3=1$. In this case

$$R_\perp{}^R=R_\perp{}^L=R_\parallel{}^R=R_\parallel{}^L=R_0 \quad \text{and} \quad T_\perp=T_\parallel=T_0;$$

$$R_0=\left\{[(\eta^2+\kappa^2+1)^2-4\eta^2]\left(\cosh\frac{4\pi\kappa s}{\lambda}-\cos\frac{4\pi\eta s}{\lambda}\right)\right\}\Big/ D_0,$$

$$T_0=8(\eta^2+\kappa^2)/D_0,$$

$$D_0=[(\eta^2+\kappa^2+1)^2+4\eta^2]\cosh\frac{4\pi\kappa s}{\lambda}+4\eta(\eta^2+\kappa^2+1)\sinh\frac{4\pi\kappa s}{\lambda}$$

$$-[(\eta^2+\kappa^2-1)^2-4\kappa^2]\cos\frac{4\pi\eta s}{\lambda}+4\kappa(\eta^2+\kappa^2-1)\sin\frac{4\pi\eta s}{\lambda}.$$

The curves of Figs. 6 and 7 give some indication of the variation of R_0 and T_0 with η, κ, and s/λ. In order to reduce the number of variables, we have taken two cases: $\kappa=\eta$, and $\kappa=10\eta$. For each of these the reflection, transmission and absorption ($A_0=1-R_0-T_0$) are plotted as functions of κ. The parameter s/λ is given the series of values 0.01, 0.02, and 0.05. One feature of particular interest is the difference in the absorption coefficient between the set of curves for which $\kappa=\eta$ and those for which $\kappa=10\eta$. For $\kappa=\eta$ the maximum absorption is 0.50. This value of the absorption coefficient occurs for rather small values of κ, and the absorption coefficient is then considerably larger than the transmission coefficient and remains so for all higher values of κ. When $\kappa=10\eta$ the maximum absorption is lower (about 15 percent) and there is then a considerable range of κ in which the transmission coefficient is equal to or larger than the absorption coefficient. The reflection coefficient is also relatively high in this region. This will have a great significance when we come to the equations for the

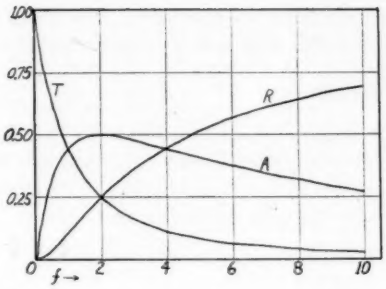

FIG. 8. Reflection, transmission, and absorption coefficients as a function of f for a single metal film in air. Infra-red approximation: $\kappa=\eta=(\sigma/2\omega\epsilon_0)^{\frac{1}{2}}$, and $s\ll\lambda$.

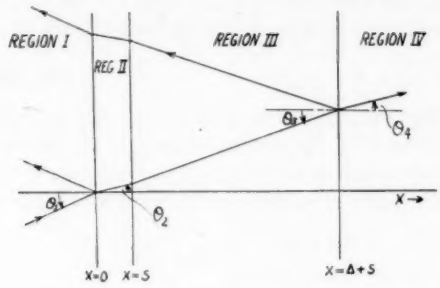

FIG. 9. Geometry used in the discussion of the reflection filter.

transmission filter since the curves of Fig. 6 approximate the behavior of silver films in the optical region while those of Fig. 7 are more characteristic of the infra-red region.

In the infra-red region when the wave-length is sufficiently long the η and κ become large compared with unity and both approach the value $(\sigma/2\omega\epsilon_0)^{\frac{1}{2}}$. This, together with the assumption of a thin film introduces further simplifications. It will be useful to give the complete set of formulas for these conditions which are now not limited by the conditions of normal incidence or of air dielectrics on either side of the film.

$$R_{\perp}{}^{R}=[(1/p)-(1/q)+(f/pq)]^2/[(1/p)+(1/q)+(f/pq)]^2, \tag{38}$$

$$T_{\perp}{}^{R}=T_{\perp}{}^{L}=[(4/pq)]/[(1/p)+(1/q)+(f/pq)]^2, \tag{39}$$

$$A_{\perp}{}^{R}=[(4f/pq^2)]/[(1/p)+(1/q)+(f/pq)]^2. \tag{40}$$

For the other polarization

$$R_{\shortparallel}{}^{R}=[(n_1{}^2/p)-(n_3{}^2/q)+(fn_1{}^2n_3{}^2/pq)]^2/[(n_1{}^2/p)+(n_3{}^2/q)+(fn_1{}^2n_3{}^2/pq)]^2, \tag{41}$$

$$T_{\shortparallel}{}^{R}=T_{\shortparallel}{}^{L}=[4n_1{}^2n_3{}^2/pq]/[(n_1{}^2/p)+(n_3{}^2/q)+(fn_1{}^2n_3{}^2/pq)]^2, \tag{42}$$

$$A_{\shortparallel}{}^{R}=[4fn_1{}^2n_3{}^4/pq^2]/[(n_1{}^2/p)+(n_3{}^2/q)+(fn_1{}^2n_3{}^2/pq)]^2, \tag{43}$$

$$f=\sigma ks/\omega\epsilon_0=(\mu_0/\epsilon_0)^{\frac{1}{2}}\sigma s=120\pi\sigma s, \tag{44}$$

and

$$p=(n_1{}^2-\sin^2\theta)^{\frac{1}{2}}, \quad q=(n_3{}^2-\sin^2\theta)^{\frac{1}{2}}.$$

The corresponding expressions for $R_{\perp}{}^{L}$, $A_{\perp}{}^{L}$, $R_{\shortparallel}{}^{L}$, and $A_{\shortparallel}{}^{L}$ may be obtained from the above by interchanging p and q, and n_1 and n_3. It should also be pointed out that Eqs. (38) through (43) are independent of the frequency of the radiation.

From Eq. (44) it is seen that, for $f=1$, $1/\sigma s=(\mu_0/\epsilon_0)^{\frac{1}{2}}=120\pi$ ohms. The physical meaning of this can be shown in the following way. The familiar equation for the electrical resistance of a conductor is $r=1/\sigma\times(L/A)$ where L is the length of the conductor, and A is its cross-sectional area. If the shape of the conductor is taken to be a square slab of side L and thickness s, and if the resistance is measured between opposite side of the square, then the above expression becomes

$$r=1/\sigma\times(L/sL)=1/\sigma s. \tag{45}$$

Hence it is possible to express the resistance of such a thin metal film in terms of ohms per square, abbreviated $\Omega/\square$. Obviously the dimension of the square is unimportant, since this dimension disappeared from Eq. (45). Because of the specific number, $(\mu_0/\epsilon_0)^{\frac{1}{2}}=377$ ohms, which appears it is also possible to use the ratio $f=377/r$ as a measure of the resistance of the film. The curves of Fig. 8

show the variation of R, A, and T with f for normal incidence, and for $n_1=n_3=1$. For $f=2$, which corresponds to a resistance of 189Ω/□, the absorption in a metallic film is at a maximum of 0.5.

3. THE REFLECTION FILTER

The reflection filter is somewhat more complex than the single film, in that there are four regions of space (Fig. 9), and consequently three pairs of boundary equations. These equations are similar to the equations of Section 2, and one case will be discussed in detail—that in which E is perpendicular to the plane of incidence. The final result also will be given for the other polarization.

$$\left.\begin{aligned} &E_{11}+E_{12}=E_{21}+E_{22}\\ &E_{11}-E_{12}=\alpha_1(E_{21}-E_{22}) \end{aligned}\right\} \text{ at } x=0,$$

$$\left.\begin{aligned} &E_{21}\exp(ik_2 s\cos\theta_2)+E_{22}\exp(-ik_2 s\cos\theta_2)=E_{31}\exp(ik_3 s\cos\theta_3)+E_{32}\exp(-ik_3 s\cos\theta_3)\\ &E_{21}\exp(ik_2 s\cos\theta_2)-E_{22}\exp(-ik_2 s\cos\theta_2)=1/\alpha_2[E_{31}\exp(ik_3 s\cos\theta_3)-E_{32}\exp(-ik_3 s\cos\theta_3)] \end{aligned}\right\} \text{ at } x=s,$$

$$\left.\begin{aligned} &E_{31}\exp[ik_3(\Delta+s)\cos\theta_3]+E_{32}\exp[-ik_3(\Delta+s)\cos\theta_3]=E_{41}\exp[ik_4(\Delta+s)\cos\theta_4]\\ &E_{31}\exp[ik_3(\Delta+s)\cos\theta_3]-E_{32}\exp[-ik_3(\Delta+s)\cos\theta_3]=\alpha_3 E_{41}\exp[ik_4(\Delta+s)\cos\theta_4] \end{aligned}\right\} \text{ at } x=\Delta+s,$$

where α_1 and α_2 have the same meaning as before, except that region I will be free space, and consequently $n_1=1$, and $\alpha_3=k_4\cos\theta_4/k_3\cos\theta_3$. As in the earlier discussion the dielectric will be assumed lossless, that is, k_3 will be taken to be real.

From the above set of equations the ratio E_{12}/E_{11} may be found, and the result may be written in terms of quantities previously obtained in Section 2.

$$\frac{E_{12}}{E_{11}}=\frac{r_\perp^R\exp(iy_\perp^R)-r_{M\perp}g_\perp\exp[i(x_\perp+z_\perp+2k_3\Delta\cos\theta_3)]}{1-r_{M\perp}r_\perp^L\exp[i(x_\perp+y_\perp^L+2k_3\Delta\cos\theta_3)]} \tag{46}$$

where $r_\perp^R\exp(iy_\perp^R)$ and $r_\perp^L\exp(iy_\perp^L)$ are the reflected amplitudes for the metallic layer, region II, as given in Section 2. $r_{M\perp}\exp(ix_\perp)$ is the reflected amplitude for the mirror layer, region IV. g is an abbreviation for a combination of terms which has not appeared before. It is

$$g_\perp\exp(iz_\perp)=r_\perp^R r_\perp^L\exp[i(y_\perp^R+y_\perp^L)]-t_\perp^R t_\perp^L\exp[i(u_\perp^R+u_\perp^L)],$$

where

$$\tan z_\perp=\frac{r_\perp^R r_\perp^L\sin(y_\perp^R+y_\perp^L)-t_\perp^R t_\perp^L\sin(u_\perp^R+u_\perp^L)}{r_\perp^R r_\perp^L\cos(y_\perp^R+y_\perp^L)-t_\perp^R t_\perp^L\cos(u_\perp^R+u_\perp^L)}.$$

The reflection coefficient for the filter may be written at once. It is Eq. (46) multiplied by its complex conjugate

$$R_F=\frac{(r^R-r_M g)^2+4r^R r_M g\sin^2\left(\dfrac{2\pi q\Delta}{\lambda}+\dfrac{x-y^R+z}{2}\right)}{(1-r_M r^L)^2+4r_M r^L\sin^2\left(\dfrac{2\pi q\Delta}{\lambda}+\dfrac{x+y^L}{2}\right)}. \tag{47}$$

A general discussion of this expression is somewhat difficult since it depends in a complicated fashion upon the optical constants of the film. The form of the reflection curve usually obtained, however, is similar to that shown in Fig. 2 except that the maximum reflection will be slightly less than 100 percent and the minimum reflection may be considerably greater than 0 percent.

Since it is believed that these filters will find their greatest usefulness in the infra-red region of the spectrum, we shall proceed immediately to that degeneration. When the wave-length of the radiation is long, say 10μ or more, it has been shown that $\eta=\kappa=(\sigma/2\omega\epsilon_0)^{\frac{1}{2}}$ and that the thickness of the metallic film will become very small compared with the wave-length. r^R, r^L, and T

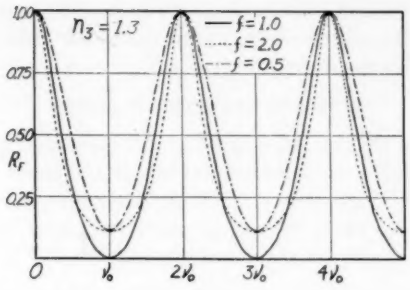

FIG. 10. Reflection coefficient of reflection filter as a function of frequency. Index of refraction of dielectric layer is 1.3. Curves are given for $f=0.5$, 1.0, 2.0.

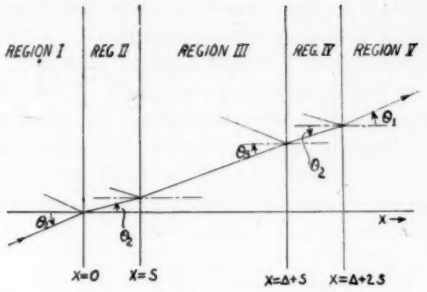

FIG. 11. Geometry used in discussion of transmission filter.

may be replaced by the expressions developed in Section 2 for this case. If r_M is taken to be unity (perfect mirror) and $\theta=0$, Eq. (47) becomes

$$R_F=\frac{(1-f)^2+n^2\cot^2(2\pi n\Delta/\lambda)}{(1+f)^2+n^2\cot^2(2\pi n\Delta/\lambda)}, \qquad (48)$$

where the index of refraction n of the dielectric layer is written without subscript, since it is the only dielectric layer to be considered. It corresponds, however, to the n_3 of Section 2.

From this it is easily seen what conditions are required for the metallic film and for the dielectric layer in order to give zero-reflection coefficient, since this expression becomes zero when $f=1$ and $2\pi n\Delta/\lambda=(2m+1)\pi/2$ where m is an integer. It will be recalled that $f=1$ corresponds to a resistance of 377Ω/□. The condition on the phase angle gives $\Delta=(2m+1)\lambda/4n$. For this value of Δ the expression for R_F becomes unity when λ is such that $2\pi n\Delta/\lambda=m\pi$. The reflection coefficient of such a filter is plotted as a function of frequency in Fig. 10. n is taken to have the value 1.3. ν_0 is the frequency for which $\Delta=\lambda_0/4n$. Also shown are the curves for which $f=0.5$ and for $f=2.0$. It is interesting to note that the value of f required to give zero-reflection coefficient at ν_0 is independent of the index of refraction of the dielectric layer although the shape of the curve does depend somewhat upon n. As n increases from unity the width of the transmission region becomes broader and the absorption valleys narrower. With this as a background of the type of phenomenon to be expected from the reflection filter, it is now easy to examine some of the more complex features.

Oblique Incidence

The form of the two equations obtained for oblique incidence is identical with that of Eq. (48)

$$R_{F\perp}=\frac{(1-f/p)^2+(q^2/p^2)\cot^2(2\pi q\Delta/\lambda)}{(1+f/p)^2+(q^2/p^2)\cot^2(2\pi q\Delta/\lambda)},$$

$$R_{F\parallel}=\frac{(1-fp)^2+(n^4p^2/q^2)\cot^2(2\pi q\Delta/\lambda)}{(1+fp)^2+(n^4p^2/q^2)\cot^2(2\pi q\Delta/\lambda)},$$

where $p=\cos\theta$ (since $n_1=1$) and $q=(n^2-\sin^2\theta)^{\frac{1}{2}}$.

Hence for oblique incidence, in order to obtain zero-reflection coefficient the filter must be designed for a particular angle of incidence and a particular polarization. If for example the filter is to have zero-reflection coefficient for $E_\perp$ at $\theta=60°$ then $f=\frac{1}{2}$ (resistance of 754Ω/□). The minimum reflection coefficient $R_{F\parallel}$ for the other polarization is then $(1-fp)^2/(1+fp)^2=0.36$. Such a filter may consequently be used to produce polarized light.

Effect of Imperfect Mirror

If we return to Eq. (47) and simplify it to normal incidence, and $n=1$, it becomes (again in the infra-red approximation)

$$R_F=\frac{[f-r_M(2-f)]^2+[f+r_M(2-f)]^2\cot^2\dfrac{2\pi n\Delta}{\lambda}}{[2+f+r_Mf]^2+[2+f-r_Mf]^2\cot^2\dfrac{2\pi n\Delta}{\lambda}}.$$

This becomes zero, as before, if simultaneously the first term in the numerator is set equal to zero, and the argument of the cotangent becomes

$(2m+1)\pi/2$. The second of these conditions is identical with that obtained previously. The first condition gives $f=2r_M/(1+r_M)$. Hence if the mirror has a reflection coefficient of less than unity, this may be compensated by an appropriate decrease in f, so that the reflection coefficient of the filter may still be made zero. Under these conditions the maximum reflection coefficient of the filter becomes

$$R_{F\,\max}=(2r_M/1+2r_M-r_M^2)^2.$$

For any reasonable value of r_M, say $r_M\geq 0.9$ ($R_M\geq 0.81$), this last expression may be replaced by $R_{F\,\max}\cong r_M^2=R_M$, where R_M is the reflection coefficient of the mirror alone.

4. THE TRANSMISSION FILTER

For the transmission filter there are five regions of space to be considered (Fig. 11) and hence four pairs of boundary equations. These equations for the case where the electric vector is perpendicular to the plane of incidence are as follows:

$$\left.\begin{aligned} E_{11}+E_{12}&=E_{21}+E_{22}\\ E_{11}-E_{12}&=\alpha_1(E_{21}-E_{22})\end{aligned}\right\}\text{ at } x=0,$$

$$\left.\begin{aligned} &E_{21}\exp(ik_2s\cos\theta_2)+E_{22}\exp(-ik_2s\cos\theta_2)=E_{31}\exp(ik_3s\cos\theta_3)+E_{32}\exp(-ik_3s\cos\theta_3)\\ &E_{21}\exp(ik_2s\cos\theta_2)-E_{22}\exp(-ik_2s\cos\theta_2)\\ &\qquad=(1/\alpha_2)[E_{31}\exp(ik_3s\cos\theta_3)-E_{32}\exp(-ik_3s\cos\theta_3)]\end{aligned}\right\}\text{ at } x=s,$$

$$\left.\begin{aligned} &E_{31}\exp[ik_3(\Delta+s)\cos\theta_3]+E_{32}\exp[-ik_3(\Delta+s)\cos\theta_3]\\ &\qquad=E_{41}\exp[ik_2(\Delta+s)\cos\theta_2]+E_{42}\exp[-ik_2(\Delta+s)\cos\theta_2]\\ &E_{31}\exp[ik_3(\Delta+s)\cos\theta_3]-E_{32}\exp[-ik_3(\Delta+s)\cos\theta_3]\\ &\qquad=\alpha_2[E_{41}\exp[ik_2(\Delta+s)\cos\theta_2]-E_{42}\exp[-ik_2(\Delta+s)\cos\theta_2]]\end{aligned}\right\}\text{ at } x=\Delta+s,$$

$$\left.\begin{aligned} &E_{41}\exp[ik_2(\Delta+2s)\cos\theta_2]+E_{42}\exp[-ik_2(\Delta+2s)\cos\theta_2]=E_{51}\exp[ik_1(\Delta+2s)\cos\theta_1]\\ &E_{41}\exp[ik_2(\Delta+2s)\cos\theta_2]-E_{42}\exp[-ik_2(\Delta+2s)\cos\theta_2]\\ &\qquad=(1/\alpha_1)E_{51}\exp[ik_1(\Delta+2s)\cos\theta_1]\end{aligned}\right\}\text{ at } x=\Delta+2s.$$

The quantity of chief interest to be obtained from this set of equations is E_{51}/E_{11} since the square of its absolute value is equal to the transmission coefficient.

$$E_{51}/E_{11}=\{16\alpha_1\alpha_2\exp[-ik_1(\Delta+2s)\cos\theta_1]\}/D_\perp,$$

where the denominator $D_\perp$ is given by

$$\begin{aligned}D_\perp=&[(1+\alpha_1)(1+\alpha_2)\exp(-ik_2s\cos\theta_2)-(1-\alpha_1)(1-\alpha_2)\exp(ik_2s\cos\theta_2)]^2\exp(-ik_3\Delta\cos\theta_3)\\&-[(1+\alpha_1)(1-\alpha_2)\exp(-ik_2s\cos\theta_2)-(1-\alpha_1)(1+\alpha_2)\exp(ik_2s\cos\theta_2)]^2\exp(ik_3\Delta\cos\theta_3).\end{aligned}$$

By combining this with the expressions obtained for the reflected and transmitted amplitudes of a dielectric-backed metallic layer, the following result is obtained for the transmission coefficient of the filter

$$T_{F\perp}=\frac{T_\perp^2}{(1-R_\perp{}^L)^2+4R_\perp{}^L\sin^2\left[\dfrac{2\pi\Delta(n_3-\sin^2\theta)^{\frac{1}{2}}}{\lambda}+y_\perp{}^L\right]},\tag{49}$$

where $T_\perp$ and $R_\perp{}^L$ are the coefficients for a single dielectric-backed metallic layer, and $y_\perp{}^L$ is the phase shift of the reflected amplitude at the dielectric-to-metal boundary. (It will be recalled that the reflection coefficient and the phase shift, but not the transmission coefficient depend upon the direction of propagation of the wave. In the case at hand, the superscript L indicates that these quantities are to be determined for a wave traveling from a region of dielectric constant n_3 toward a region of dielectric constant n_1.) The quantity n_3 is the index of refraction of the middle dielectric layer.

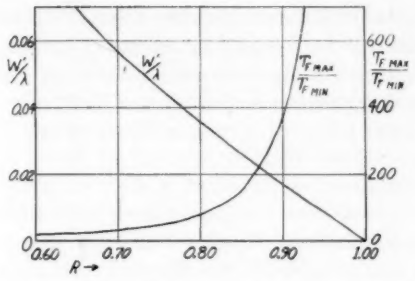

FIG. 12. Band width and ratio of $T_{F\max}/T_{F\min}$ as functions of R for the transmission filter.

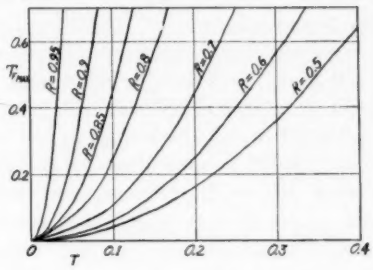

FIG. 13. $T_{F\max}$ as a function of T for various values of R.

The transmission coefficient for the other polarization may be obtained in an analogous way and is identical in form with Eq. (11).

$$T_{F\text{II}}=\frac{T_{\text{II}}^2}{(1-R_{\text{II}}{}^L)^2+4R_{\text{II}}{}^L\sin^2\left[\dfrac{2\pi\Delta(n_3-\sin^2\theta)^{\frac{1}{2}}}{\lambda}+y_{\text{II}}{}^L\right]}. \tag{50}$$

The maximum transmission is obtained when the argument of the sine is $m\pi$, where m is an integer and is (at normal incidence)

$$T_{F\max}=[T^2/(1-R^L)^2]=[T^2/(T+A^L)^2]. \tag{51}$$

The quantity A^L is the absorption in the film for a wave moving in the left direction. Minimum transmission is obtained when the argument of the sine is $(2m+1)\pi/2$, and is

$$T_{F\min}=T^2/(1+R^L)^2. \tag{52}$$

The width of the transmission band is defined as twice the wave-length interval between the positions of half-maximum transmission and maximum transmission, and is given by

$$W=[2\lambda_{\max}/(m\pi-y_0{}^L)]\sin^{-1}[1-R^L/2(R^L)^{\frac{1}{2}}], \tag{53}$$

where $y_0{}^L$ is the limiting value of $y_{\perp}{}^L$ and $y_{\text{II}}{}^L$ for normal incidence.

From the last of these equations it may be seen that the band width decreases for increasing reflection coefficient. Hence for a narrow band, it is desirable for the reflection coefficient to be as large as possible. The absorption coefficient, however, is not a negligible factor for these films, so that in order to keep the maximum transmission up to a reasonable value, a compromise must be made between band width and maximum transmission. From the second form of Eq. (51) it appears that the transmission coefficient of the single film must be large compared to the absorption coefficient in order to maintain a high transmission for the filter.

To illustrate the way in which R and T determine the characteristics of a transmission filter, the curves of Figs. 12 and 13 have been plotted. The band width W and the ratio $T_{F\max}/T_{F\min}$ depend only on R^L, and these are plotted in Fig. 12. The band width for the fundamental transmission band has been chosen, and the ordinate is the ratio of band width to the wave-length of the fundamental, W'/λ_0. The contribution of $y_0{}^L$ to the phase shift has been neglected for this curve, and the band width is then called W'.

For example, to obtain a ratio $W'/\lambda_0=0.025$ the reflection coefficient must be 0.85, and the ratio $T_{F\max}/T_{F\min}$ is then 150. If the value of $T_{F\max}$ is to be kept reasonably large, say 0.40, then from the curves of Fig. 13 we see that the transmission of the single film must be around 0.10 and, thus, the absorption of the film cannot be greater than 0.05. Recalling now the curves of Section 2, these values of $R=0.85$, $T=0.10$, and $A=0.05$ can be achieved by a film in which $\kappa=7$, $\eta=0.35$, and $s/\lambda=0.02$.

More generally, it is possible to build a transmission filter which has a narrow band pass

$(W'/\lambda_0 \leq 0.05)$, a high ratio of maximum to minimum transmission $(T_{F\,\max}/T_{F\,\min} \geq 100)$, and a relatively high maximum transmission $(T_{F\,\max} \geq 0.25)$ if the following conditions hold: $\kappa \gtrsim 5$, $\eta \leq 0.1\kappa$, $s/\lambda \leq 0.02$. Silver has these properties over most of the visible region, and is used for the metal layers in such filters for this region. In the near infra-red, however, the index of refraction η rises sharply and soon becomes the same order of magnitude as the extinction coefficient κ. Also in the near ultraviolet the index of refraction becomes equal to or larger than the extinction coefficient, and consequently silver is not a satisfactory metal to use in either of these regions.

Published values of optical constants determined from bulk metal are not necessarily valid for the thin films required for these filters. The films are usually obtained by vacuum evaporation or by sputtering, and the physical properties are in general quite different from the properties of the bulk metal.

The effect of the phase shift at reflection (y^L) is not negligible for these films, and may be as much as one radian for silver films in the visible region. The principal effect of this phase shift, at least in what has been discussed so far, is that the band width is somewhat increased. This has importance only for the fundamental pass band, and possibly for the first or second overtone bands. Beyond these, $m\pi$ is large enough to overshadow the contribution of y_0. It does however modify the effective thickness of the dielectric layer. For the fundamental band at normal incidence, $2\pi n\Delta/\lambda_0 + y_0 = \pi$ and consequently the dielectric thickness is $\Delta = \lambda_0(1 - y_0/2\pi)/2n$.

A further consequence of the phase shift y^L is that a splitting of the transmission band occurs when light is passed through the filter obliquely. In this case the phase shift depends both upon the polarization and upon the angle of incidence. In addition to the splitting, there is a shift in the wave-length of both maxima, resulting chiefly from the presence of the angle of incidence θ in the first term of the argument of the sine (Eqs. (50) and (51)).

TABLE I. Observed wave-length shift and splitting as a function of angle of incidence for a typical filter $(m=2)$.

θ	$\lambda_\perp$	$\lambda_\parallel$	$\delta\lambda$
0°	6311A	6311A	0A
15°	6216	6203	13
30°	5972	5879	93
45°	5679	5483	196
60°	5293	4971	322

The experimental effect is very striking. At normal incidence, the transmitted light exhibits a single transmission band which usually appears to be quite narrow. As the filter is rotated so that the light no longer passes through it normally the band shifts towards shorter wave-lengths and splits into two bands. The splitting is small compared with the shift. A test shows that the short wave-length component of the doublet is polarized with electric vector parallel to the plane of incidence.

The observed shift and splitting for a typical filter are given by the experimental data of Table I.

Since the maximum transmission for each polarization occurs when the argument of the sine is $m\pi$, we may write

$$2\pi\Delta(n_3^2 - \sin^2\theta)^{\frac{1}{2}}/\lambda_{\perp\,\max} + y_\perp{}^L = 2\pi\Delta(n_3^2 - \sin^2\theta)^{\frac{1}{2}}/\lambda_{\parallel\,\max} + y_\parallel{}^L = m\pi.$$

The observed splitting is small compared to the wave-length, and hence the above expression may be developed to obtain,

$$\lambda_{\parallel\,\max} - \lambda_{\perp\,\max} \equiv \delta\lambda$$

$$= \frac{\lambda_{\parallel\,\max}\lambda_{\perp\,\max}}{2\pi\Delta(n_3^2 - \sin^2\theta)^{\frac{1}{2}}}(y_\parallel{}^L - y_\perp{}^L) \cong \lambda_m \delta y^L/m\pi. \quad (54)$$

The problem of fitting the experimental data describing an actual filter to the theoretical equations in order to obtain the optical constants of the metallic layer is a difficult one, and will be reserved for Part II which will deal with experimental filters. As an example, however, the properties of a filter have been calculated, using a set of optical constants which are believed to be representative for silver films in the visible region; namely $\eta = 0.6$, $\kappa = 6$, $s/\lambda = 0.02$. The dielectric constants of regions I and V are taken to be unity while that of region III is 1.3. The pertinent optical constants of the single film become $R^L = 0.707$, $T = 0.140$, and $y^L = 0.44$. The calculated maximum transmission of the filter is

0.23 and the minimum transmission is 0.007. (incidentally, one may remark that this would constitute a useful filter although the maximum transmission is somewhat low.) If the first-order maximum transmission occurs at 5000A, the band width would be 650A and the thickness of the dielectric $\Delta=1660$A. If on the other hand the filter were constructed so that the second-order maximum fell at 5000A, the corresponding figures would be $W=300$A and $\Delta=3600$A.

In the infra-red region where $\kappa=\eta=(\sigma/2\omega\epsilon_0)^{\frac{1}{2}}$ and where s/λ is very small, the expression for the transmission coefficient readily degenerates to the following simple form. At normal incidence

$$T_P=\frac{1}{(f+1)^2+\frac{f^2}{4}(f+2)^2\sin^2\left(\frac{2\pi n_3\Delta}{\lambda}\right)},$$

where $120\pi/f$, as earlier, is equal to the $\Omega/\square$ of each silver film. The transmission curves for such an infra-red filter are plotted in Fig. 14 for the two values $f=1$ and $f=4$. It is seen that neither of these filters would be particularly useful. The dilemma is that f must be small if the maximum transmission of the filter is to be reasonably large, and that f must be large if the minimum transmission is to be reasonably small.

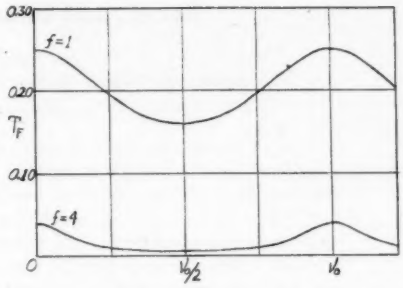

FIG. 14. Transmission coefficient of transmission filter (infra-red approximation) *vs.* frequency. Curves are given for $f=1$ and for $f=4$.

Recent and Unusual German Lens Designs

EDWARD K. KAPRELIAN
Photographic Branch, Squier Signal Laboratory, Fort Monmouth, New Jersey
(Received February 18, 1947)

Some of the unusual lenses in the Carl Zeiss collection and those found in captured German equipment are shown diagrammatically, and constructional formulas and performance data are supplied. Many of the objectives are the Zeiss V (versuch—trial) lenses constructed to such formulas as appeared promising. Most of the lenses fail to fall in any of the usual classifications. Wide angle types include an f:2.8 distortionless objective and a 210° objective of the reversed telephoto type. The long focus objectives include the 300 cm f:25 telephoto lens used in the FK 3-m infra-red camera for photographing England from the French Coast. Wide aperture types include modifications of the triplet, Gauss and Sonnar types. Among these are objectives of f:1 and f:1.5 aperture used in the Bildwandler (infra-red image converter), and which possess focal lengths of from 9 to 40 cm. Experimental objectives utilizing one or more aspherical surfaces are described. References are made to the appropriate prior art.

THE extensive lens collection of the Zeiss museum, containing samples of almost every objective produced at the Zeiss works during the past forty years, and now being studied at Signal Corps Engineering Laboratories, provides an accurate index of the lens design activities of this firm both before and during the war.

Included in the collection are several hundred V (versuch) lenses. These are experimental lenses produced from computations which appeared promising. Some V lenses are prototypes of later, commercially issued lenses, others were never pursued beyond the experimental stage. Among the V lenses are objectives having exceptionally wide angles of view and others of extreme aperture or great focal length, which constitute valuable sources of design data. The lenses described have been chosen from the Zeiss collection and from captured military equipment. Constructional data for the conventional 100-mm focal length are included in some instances. The formulas have been obtained from partially illegible documents and, while every care has been exercised in their reproduction, and they appear to contain no gross errors, they are presented without guarantee of accuracy.

WIDE ANGLE TYPES

That Zeiss was active in the design of extremely wide angle lenses long prior to the war is evident from the serial numbers of the experimental lenses, which indicate that one important phase of this work was begun shortly after the publication of the Hill Sky Lens patent (1924) and, reaching a peak during 1935–1937, continued well into the war period. The outstanding wide angle objective used by Germany during the war was the Pleon lens produced in some quantity for aerial photography by the Luftwaffe, and was the outcome of work done, for the most part, prior to 1938.

One wide angle lens of unusual construction is the V1940 No. 4 (Fig. 1) having an aperture of f:2.8 and focal length of 7.5 cm. This lens is comprised of eight elements and presents a construction not shown in available literature, and which fails to fall in any of the usual classifications. This objective possesses good spherical and axial chromatic corrections and covers a field of approximately 70 degrees with little astigmatism or coma. Of particular interest is the fact that distortion is almost entirely absent, mainly because of the balance of powers of the first and last elements. Detailed constructional data for this objective have not been determined.

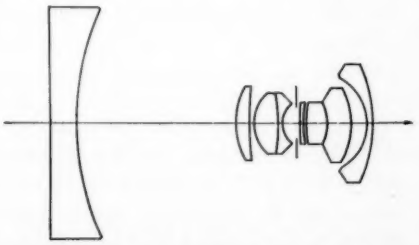

FIG. 1. Zeiss V1940, No. 4, f:2.8, F=7.5 cm, No. 2659275.

Another wide angle lens is V1939 No. 17 (Fig. 2) of 10-cm focal length and an aperture of f:5.6. This design does not appear in the literature; since the doublet is negative it may be considered a modified Cooke Triplet. The lens covers satisfactorily a half-angle of 45 degrees. The field is entirely flat, spherical and chromatic corrections are good, and the objective is fairly free of coma. Detailed constructional data for this lens have not been determined.

Another wide angle lens designated V1935 No. 2 (Fig. 3) is unusual in that the front element is strongly concave to the subject, apparently for the purpose of reducing distortion. Except for the compound rear component, which is slightly negative in power, the construction is similar to that shown by Merte.[1] This sample, having a focal length of 10 cm and an aperture of f:6.2, covers satisfactorily a half-angle of 45 degrees with good spherical and chromatic correction and with distortion not exceeding one percent.

One series of lenses termed "Sphaerogon" (Fig. 4) apparently had passed the experimental or "V" stage and was produced in apertures of f:7 and f:8 in focal lengths of from 1.6 cm to 12 cm. This objective comprises a negative front component of three cemented elements and a positive rear component of three elements of the Dagor type with the inner element detached. The Sphaerogon is an extension of the Hill Sky Lens[2] and possesses, in common with all reversed telephoto lenses, a large amount of distortion. This objective appears to combine the rear component of one system of Merte[3] with the front negative triplet of a wide angle objective by Richter,[4] the latter incidentally disclosing, with slight variations, the structure of the wide angle Pleon lens. The Sphaerogon possesses considerable spherical aberration but is well corrected chromatically. The field is quite flat to about 55 degrees semi-field, deteriorating considerably at 70 degrees semi-field because of astigmatism and curvature.

Similar in type to the Sphaerogon, the V1936 No. 18 (Fig. 5) has an aperture of f:6.8 and a focal length of 1.6 cm. In this lens the negative front component of the Sphaerogon has been divided and the positive rear component made more complex. Its total angle of view of 210 degrees exceeds that of any anastigmat previ-

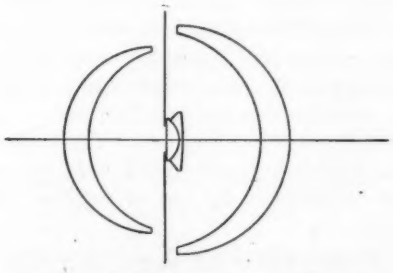

FIG. 2. V1939, No. 17, f:5.6, F=10 cm.

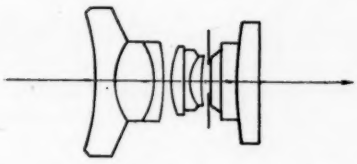

FIG. 3. V1935, No. 2, f:6.2, F=10 cm.

	n_D	V			
1.	1.60000	60.9	r_1 = 64.0	t_1 = 8.1	s_1 =0.80
2.	1.48880	69.9	r_2 = 24.2	t_2 =11.3	s_2 =2.70
3.	1.60000	60.9	r_3 = 32.3	t_3 = 3.2	
4.	1.67024	47.2	r_4 = 41.3	t_4 = 7.75	
5.	1.54753	45.9	r_5 = 20.7	t_5 = 0.95	
6.	1.46580	65.4	r_6 = 577.8	t_6 = 3.7	
7.	1.67024	47.2	r_7 = 9.5	t_7 = 4.0	
8.	1.60729	49.3	r_8 = 23.9	t_8 = 7.0	
9.	1.46580	65.4	r_9 =1616.2	t_9 = 9.0	
			r_{10} = 689.0		
			r_{11} = 418.4		
			r_{12} = 802.1		

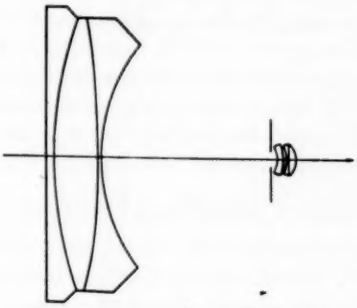

FIG. 4. Sphaerogon, f:7, F=4.1 cm.

	n_D	V			
1.	1.62022	60.3	r_1 = ∞	t_1 = 7.35	s_1 =51.4
2.	1.62363	35.9	r_2 =269.5	t_2 =31.8	s_2 = 1.23
3.	1.63826	55.7	r_3 =159.3	t_3 = 7.35	
4.	1.51746	56.5	r_4 =147.2	t_4 = 7.10	
5.	1.55092	45.4	r_5 = 42.9	t_5 = 2.2	
6.	1.60284	60.6	r_6 = 19.8	t_6 = 6.37	
			r_7 = 15.1		
			r_8 = 94.3		
			r_9 = 21.4		

[1] U. S. Pat. 2140024 (1938).
[2] Brit. Pat. No. 225398 (1924).
[3] U. S. Pat. No. 2126126 (1938).
[4] U. S. Pat. No. 2247068 (1941).

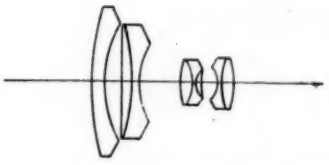

FIG. 5. V1936, No. 18, f:6.8, F=1.6 cm.

	n_D	V			
1.	1.62060	60.2	r_1 =653.0	l_1=14.7	s_1= 36.2
2.	1.63598	35.4	r_2 =460.0	l_2=43.7	s_2=104.0
3.	1.62060	60.2	r_3 = ∞	l_3=14.4	s_3= 7.45
4.	1.61250	58.7	r_4 =475.0	l_4= 5.6	
5.	1.53353	55.6	r_5 =236.0	l_5= 1.9	
6.	1.49687	64.9	r_6 = 39.0	l_6= 4.9	
7.	1.51482	54.6	r_7 =102.0	l_7= 2.2	
8.	1.58960	61.3	r_8 = 12.4	l_8= 8.55	
			r_9 = 47.5		
			r_{10}= 48.0		
			r_{11}= 92.0		
			r_{12}= 35.7		

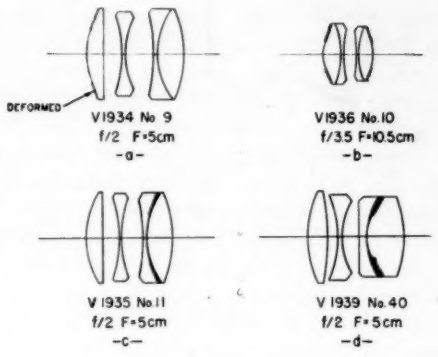

FIG. 6.

ously known, with the possible exception of the system shown by A.E.G.[5] Spherical and chromatic corrections are fair. The field is curved toward the lens from 20 degrees to 70 degrees semi-field and curved away from the lens from 70 degrees to the edge of the field.

USE OF ASPHERICAL SURFACES

As early as 1901 Zeiss had produced, experimentally, objectives of familiar construction employing one or more deformed surfaces. While aspherical surfaces are not feasible to produce commercially, they offer the advantages of increased aperture and fairly wide field in relatively simple systems. Apparently no experimental work had been done with aspherical surfaces after 1939, and none of the large aperture objectives found in captured equipment utilized such surfaces. Because of their complicated nature, constructional data for the aspherical objectives described have been omitted.

In V1934 No. 9 (Fig. 6a) the familiar Tessar construction, through deformation of the first surface, attains an aperture of f:2. There is considerable spherical aberration present. The semi-field is flat to 15 degrees with considerable coma present.

V1936 No. 10 (Fig. 6b) is an objective comprising two cemented pairs, both outer crowns being deformed as indicated. Operating at f:3.5 and with a focal length of 10.5 cm, the lens possesses a flat semi-field of 30 degrees with very little spherical aberration and good chromatic correction.

[5] Ger. Pat. No. 620538 (1935).

In V1935 No. 11 (Fig. 6c) the aperture of f:2 is reached in a 5-cm Tessar construction through deformation of the sixth surface. Although spherical aberration is well corrected, there is considerable coma present in the 18-degree semi-field which is fairly flat.

This concept of deforming a cemented surface has been modified somewhat in V1939 No. 40 (Fig. 6d) by utilizing as the aspherical surface the cemented face of the rear crown. Here the computations have apparently been quite thorough; the optical properties of the cement as well as its thickness have been considered with exactness. The thin meniscus of cement actually behaves as a fifth, thin, aspheric element in the system, its n_D and V being quite different from those of the elements it joins. The lens displays little spherical aberration, fair achromatization, and a flat semi-field of 18 degrees.

TELEPHOTO TYPES

Telephoto lenses appear to have been a type which, despite many modifications and computations, retained a relatively uncomplicated structure; almost every experimental telephoto lens in the collection contains four elements and is of moderate or small aperture. Apparently all German telephoto lenses used in military applications of photography are of definite prewar design.

The longest all-refracting objective used appears to have been a telephoto objective of f:25 and focal length of 300 cm (Fig. 7) computed in 1936 and used in the FK 3-m infra-red camera. The relatively small aperture permits excellent

correction while maintaining a compact arrangement; the distance from the focal plane to the front vertex is only 145 cm. This objective apparently was not originally intended for infra-red work, and focusing on a target at a given range, and with a given filter-emulsion combination, is accomplished by moving the lens along an arbitrary scale in accordance with a chart which indicates the arbitrary settings as a function of the target distance and the wave-length range (filter and emulsion combination). The lens is intended to cover about 3 degrees total field (5″×7″ negative size) and resolves 12 lines per mm on the axis and not less than 8 lines mm anywhere in this field. Infra-red cameras of much greater focal length (17 meters and 28 meters) were used by Germany, but these utilized spherical mirrors with or without telenegative components and possessed very small relative apertures.

The Telikon (Fig. 8), with a focal length of 75 cm and a relative aperture of f:6.3, possesses the important and desirable optical characteristics, in a telephoto lens, of short focal-plane-to-front-vertex distance and a fairly wide angle of view. The design of this lens, issued by Zeiss under the designation Bauart blc and used by the Luftwaffe in large numbers for aerial photography, is credited to Richter.[6] It was produced in focal lengths of 50 cm and 75 cm using the identical glasses disclosed in the patent and with almost no change in other constructional data. The 75-cm Telikon is capable of covering a 15° semi-field and resolves about 60 lines/mm on the axis and not less than 20 lines/mm within this semi-field.

WIDE APERTURE TYPES

A study of the collection discloses that while many computations were made on the Sonnar type and its derivatives, and lenses of this general construction were used for military purposes, many modifications of the Gauss type were computed and constructed, particularly for infra-red applications. This is particularly true regarding objectives used with the larger Bildwandlers (image converters) which are similar in principle to our sniperscope and which operate in the infra-red region in the neighborhood of one micron wave-length. It is surprising to note the extensive employment of complex refracting systems of large aperture and considerable focal length when the difficulty of producing large refracting elements and the tactical disadvantage of the great weight of these systems are considered in contrast with the simpler Schmidt systems of equivalent performance. Most wide aperture experimental designs for infra-red applications have relative apertures between f:1 and f:2; with the exception of modifications of the R-Biotar, almost no designs of greater aperture than f:1 were produced. Almost without exception all large aperture infra-red objectives were computed after 1941. All objectives intended for infra-red use were provided with low reflection coatings having maximum effectiveness in the neighborhood of one micron wave-length.

Infra-red objective Bauart blc (Fig. 9) with an aperture of f:1.5 and focal length of 40 cm may be considered an extension of the triplet type. Intended for use with a harbor installation infra-red viewing device, its rear element (8) is made of a dense red filter glass and is strongly negative in power in order to produce a curved field conforming to the curved sensitive surface of the image converter tube. Element 7 is a

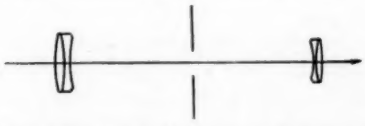

FIG. 7. *IR* Fernobjektiv, f:25, F=300 cm.

	n_D	V			
1.	1.57043	57.6	r_1=14.0	t_1=0.5	s_1 } =13.8
2.	1.61300	37.1	r_2=11.8	t_2=0.4	s_2 }
3.	1.52057	57.0	r_3=67.6	t_3=0.2	
4.	1.62363	36.8	r_4= 4.3	t_4=0.4	
			r_5= 3.7		
			r_6= ∞		

[6] U. S. Pat. No. 2239538 (1941).

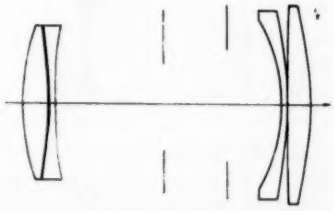

FIG. 8. Telikon f:6.3, F=75 cm.

	n_D	V		
1.	1.60801	46.0	r_1=21.1	t_1=32
2.	1.72825	28.3	r_2=40.1	s_1= 0.1
3.	1.60801	46.2	r_3=40.2	t_2= 1.2
4.	1.72825	28.3	r_4=71	s_2=30.4
			r_5=13.0	t_3= 1.0
			r_6=70	s_3= 0.1
			r_7= ∞	t_4= 1.9
			r_8=33.2	

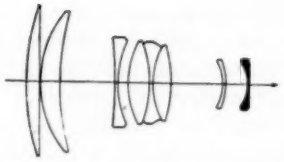

FIG. 9. U.R. Objektiv f:1.5, F=40 cm.

	n_D	V		
1.	1.61844	60.4	r_1 =113.49	t_1= 5.95
2.	1.61844	60.4	r_2 = ∞	s_1= 0.19
3.	1.72828	28.3	r_3 = 48.02	t_2= 8.85
4.	1.61844	60.4	r_4 =125.3	s_2=26.06
5.	1.72828	28.3	r_5 =134.0	t_3= 1.42
6.	1.61844	60.4	r_6 = 44.43	s_3= 4.12
7.	1.72828	28.3	r_7 = 41.33	t_4= 9.97
8.	*RG*8		r_8 = 46.28	t_5= 1.16
			r_9 = 30.17	t_6= 8.50
			r_{10} = 60.51	s_4=24.45
			r_{11} = 20.81	t_7= 1.16
			r_{12} = 32.21	s_5=10.02
			r_{13} = 17.61	t_8= 0.70
			r_{14} =324.8	

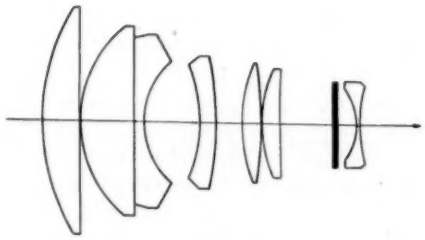

FIG. 10. U.R. Objektiv B f:1, F=25 cm.

	n_D	V		
1.	1.61995	60.5	r_1 = 90.5	t_1=17.3
2.	1.61995	60.5	r_2 = ∞	s_1= 0.04
3.	1.72857	28.3	r_3 = 51.6	t_2=26.1
4.	1.72857	28.3	r_4 = ∞	t_3= 3.0
5.	1.61995	60.5	r_5 = 33.5	s_2=26.5
6.	1.61995	60.5	r_6 = 48.5	t_4= 7.2
7.	*RG*8		r_7 =112.1	s_3=11.4
8.	1.75184	27.6	r_8 = 66.5	t_5= 8.6
			r_9 =245.0	s_4= 1.0
			r_{10} = 60.4	t_6= 8.0
			r_{11} =707.0	s_5=24.0
			r_{12} = ∞	t_7= 2.0
			r_{13} = ∞	s_6= 9.0
			r_{14} = 24.5	t_8= 1.0
			r_{15} = 75.0	

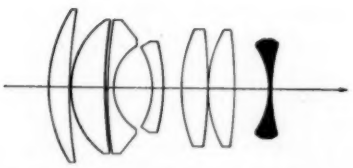

FIG. 11. U.R. Objektiv A f:1, F=9 cm.

	n_D	V		
1.	1.62123	60.4	r_1 = 72.8	t_1=14.5
2.	1.62123	60.4	r_2 = 237.9	s_1= 0.1
3.	1.73083	28.3	r_3 = 53.6	t_2=24.7
4.	1.73083	28.3	r_4 =1416.4	s_2= 0.1
5.	1.61931	60.5	r_5 =1416.4	t_3= 4.0
6	1.61931	60.5	r_6 = 32.3	s_3=29.5
	*RG*8		r_7 = 42.9	t_4= 7.2
			r_8 = 71.4	s_4=12.2
			r_9 = 167.6	t_5=18.7
			r_{10} = 82.7	s_5= 0.1
			r_{11} = 69.8	t_6=14.8
			r_{12} =3429.6	s_6=45.3
			r_{13} = 45.3	t_7= 2.2
			r_{14} = 98.4	

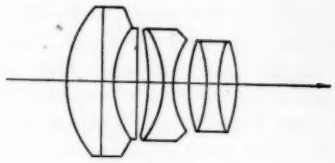

FIG. 12. V1938, No. 16, f:1.5, F=7 cm.

	n_D	V			
1.	1.67060	47.2	r_1 = 59.9	t_1=14.0	s_1=4.9
2.	1.53103	49.0	r_2 = ∞	t_2= 2.8	s_2=8.8
3.	1.62090	60.4	r_3 = 33.4	t_3=17.8	
4.	1.69922	30.1	r_4 =459	t_4= 9.8	
5.	1.64775	33.8	r_5 = 78.8	t_5= 2.1	
6.	1.62090	60.4	r_6 = 32.3	t_6=11.2	
7.	1.53103	49.0	r_7 = 33.9	t_7= 1.1	
8.	1.67060	47.2	r_8 = 98	t_8=10.5	
			r_9 = 35.2		
			r_{10} = 36.4		
			r_{11} =102		

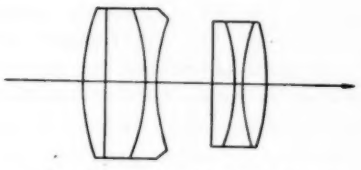

FIG. 13. V1938, No. 10, f:2.8, F=8 cm.

	n_D	V		
1.	1.67215	47.1	r_1=35.2	t_1= 8.7
2.	1.46550	65.2	r_2 = ∞	t_2=12.2
3.	1.64853	33.7	r_3=38.9	t_3= 3.2
4.	1.67215	47.1	r_4=27.9	s = 6.2
5.	1.52991	51.1	r_5=24.9	t_4= 5.0
6.	1.67215	47.1	r_6=40.2	t_5= 1.2
			r_7=30.0	t_6= 7.5
			r_8=70.0	

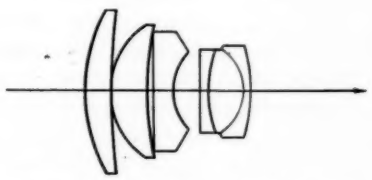

FIG. 14. V1939, No. 33, f:1.4, F=5 cm.

	n_D	V		
1.	1.67190	47.1	r_1 = 75.5	t_1=10.2
2.	1.62270	53.0	r_2 =462.0	s_1= 0.4
3.	1.72820	28.4	r_3 = 39.0	t_2=17.1
4.	1.53103	49.0	r_4 =293	s_2= 1.7
5.	1.65821	50.9	r_5 = ∞	t_3= 4.0
6.	1.58923	61.1	r_6 = 25.6	s_3=16.6
			r_7 = ∞	t_4= 2.7
			r_8 = 55.8	t_5=21.6
			r_9 = 23.9	t_6= 5.0
			r_{10} = 72.5	

"closure" element for protecting the inner surfaces when the filter is removed. The objective is practically entirely free of spherical aberration at wave-lengths in the region of one micron and possesses a reasonably flat field of 10 degrees. Between 730 millimicrons and 1080 millimicrons the change in focal length of the 40-cm objective is less than one millimeter. It is of interest that, except for the filter element, only two types of

glass have been used in the construction of this objective. Infra-red objective B (Fig. 10) possesses the greatest focal length (25 cm) among the f:1 infra-red lenses and was used with infra-red image converting devices. It is a modified Gauss type with a field flattener, directly in front of which is placed a plane-parallel infra-red filter. This objective displays substantially no spherical aberration and has a substantially flat semi-field of approximately 5 degrees.

Another large aperture infra-red objective (Fig. 11) was that used with the tank mounted Bildwandler and which has a focal length of 9 cm and a relative aperture of f:1. Similar to objective B, except for incorporating the filter and the field flattener in a single element, it is free of measurable spherical aberration and displays little astigmatism over the usable semi-field of 8 degrees.

Another large aperture design of 7-cm focal length and f:1.5 aperture is V1938, No. 16 (Fig. 12) which may be considered a modification of the Cooke Triplet, in which each collective lens is replaced by a cemented triplet and the dispersive lens is replaced by a cemented doublet. This objective possesses a very flat semi-field of 15 degrees with very little astigmatism. Spherical and chromatic aberrations are well corrected. Only small amounts of coma are evident within the 15-degree semi-field.

V1938 No. 10 (Fig. 13) has a relative aperture of f:2.8 and appears to represent an attempt, during the period prior to the use of reflection reducing coatings, to eliminate glass-air surfaces

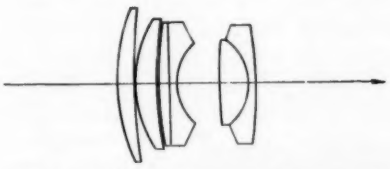

FIG. 15. V1942, No. 9, f:1.5, F=5 cm.

	n_D	V		
1.	1.62210	58.1	r_1 = 66.5	t_1=10.1
2.	1.67060	47.2	r_2 =430.1	s_1= 0.1
3.	1.48793	69.9	r_3 = 35.2	t_2=11.7
4.	1.73910	28.3	r_4 = 80.6	s_2= 1.0
5.	1.70162	41.2	r_5 = 84.9	t_3= 6.6
6.	1.64288	47.8	r_6 =823.2	t_4= 1.7
			r_7 = 23.2	s_3=20.4
			r_8 =162.5	t_5=16.5
			r_9 = 21.3	t_6= 2.9
			r_{10} =128.8	

FIG. 16.

to the greatest extent possible. It is similar to the Zeiss Herar designed by Huber[7] except for the addition of another crown (element 4) to the rear component. It possesses a flat semi-field of 22 degrees and has little coma. Spherical and chromatic corrections are good.

A modification of the f:1.5 50-mm Sonnar is shown in V1939, No. 33 (Fig. 14) in which an air space has been substituted for the usual fluor crown element. At full aperture this objective performs satisfactorily over a total angle of 42 degrees, the aberrations being well corrected except for considerable coma. Astigmatism is virtually absent within a 15-degree semi-field.

A further modification of the Sonnar type is shown in V1942, No. 9 (Fig. 15) in which the broken contact provides a meniscus air space in front of the fluor crown element. The corrections of this 50-mm, f:1.5 sample are reasonably good except for considerable lateral chromatic aberration, and definition is acceptable over a total angle of 42 degrees by usual standards. It is interesting to note (Fig. 16) that this lens, in common with others in the collection, is mounted in a micrometer mount to permit trial and error changes in spacing between two or more elements for determining the position of optimum performance.

[7] U.S. Patent No. 2124301 (1938).

A Photoelectric Lens Bench

W. HERRIOTT
Bell Telephone Laboratories, New York, New York
(Received March 21, 1947)

A photo-multiplier tube and a cathode-ray oscilloscope have been incorporated in lens testing apparatus to provide a visual trace representing the spatial distribution of energy in the image formed by the lens under test.

THE conventional lens testing bench provides means for microscopic examination of the image formed by a lens under test. Either a collimator or a distant illuminated slit or pinhole provides essentially parallel light entering the lens. A nodal slide is usually provided to permit ready measurement of oblique aberrations. Provision is made for both axial and lateral movement of the microscope in order that spherical aberration, axial color, curvature of field, and distortion can be measured in addition to the oblique aberrations, namely, coma, astigmatism, and lateral color. Suitable scales are provided for measurement of all aberrations.

The lens bench is used to determine the deficiencies of a lens system in terms of its component aberrations, and these aberrations are frequently expressed in graphical form. Such data are of great value to the lens designer but have little interest to the lens user, as they give almost no information regarding the spatial distribution of light or energy within an image. Reference is frequently made to a "circle of confusion" of a given size. This is misleading, since a large portion of the energy may lie within a small fraction of the area within the circle. The need for exact information on the structure of small images formed by lenses of high relative aperture has led to the application of electro-optical scanning methods to lens testing, as described below.

In the photoelectric lens bench shown in Fig. 1, the microscope is replaced by an image-scanning unit which comprises a narrow, vibrating slit and a photo-multiplier tube, together with graduated means for moving the unit both axially and laterally. The output of the multiplier tube is applied to the Y or vertical deflection circuit of a cathode-ray oscilloscope. The vibrating slit is actuated at power line frequency (60 cycles) by the moving coil of a small loudspeaker unit. The speaker unit also drives the moving coil of a second speaker unit which serves as a generator and develops a voltage proportional to the slit velocity.

By integrating this voltage with a resistance-capacity network, a voltage is obtained which is proportional to the slit displacement. This voltage is applied to the X or horizontal deflection plates of the oscilloscope. Since the instantaneous voltage and slit displacement are proportional, values of X on the oscilloscope will at all times represent the position of the vibrating slit.

A high speed relay is connected across the output of the photo-multiplier. It is actuated by the power line so as to short the oscilloscope during the motion of the slit in one direction, thus furnishing a zero line for amplitude measurements.

The vibrating slit is narrow, having a width of .01 mm or less, depending on the size of image being scanned. A short narrow vertical slit (or pinhole), used at the focus of a collimating telescope, gives essentially parallel light to the lens under test. The vibrating slit is parallel to the collimator slit and scans the image of it formed by the lens. A ribbon filament lamp is normally used to illuminate the collimator slit, although an arc lamp gives increased signal from the multiplier tube. This is desirable where lenses are examined with light filters having low transmission. The relative spectral sensitivity of the photo-multiplier is not important where narrow band-pass light filters are used, as long as it covers the desired region. Filter loss is compensated by changing the voltages applied to the multiplier until unit output is secured, as shown by the amplitude of the trace on the oscilloscope. The energy distribution of the

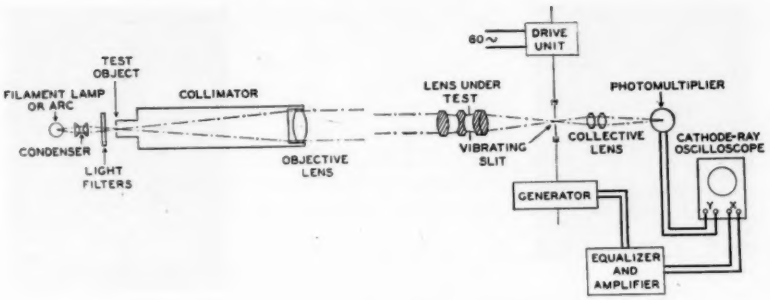

FIG. 1. Photoelectric lens bench.

source, the spectral transmission curve of the filter, and the spectral sensitivity curve of the photo-multiplier must be considered in interpreting the traces secured.

An off-axis image can be scanned tangentially as well as radially. This offers additional information regarding astigmatism and coma.

Figures 2 and 3 show the on-axis performance of an f:2.8, 4.5-inch E.F. lens designed for and tested at a magnification of 3.5 and having chromatic correction at 5000A and 7000A. Figure 2 was taken through a Wratten No. 16 (yellow) filter and Fig. 3 through a Wratten No. 47 (blue) filter. The distance between perforations represents 0.4 mm in the image plane at the longer conjugate focus of the lens. It is seen that the image formed in yellow light is much narrower than that formed in blue light, where the color curve of the lens is rising steeply. To secure best focus at each filter condition, the scanning slit was moved 2.29 mm away from the lens for the blue filter condition. This represents 0.19 mm undercorrection for the blue at the short conjugate. Slight decentering of the lens is shown by lack of symmetry in the flare at the sides of the main image.

A photoelectric lens bench as described above was constructed at these laboratories to test certain lenses for a television application. It was desired to determine the equivalent amplitude *versus* frequency characteristic of a lens when considered as a circuit element in a television transmission system. In this case the test objects consisted of Levy screens having from 25 to 225 lines per inch. A portion of the image was scanned both on axis and at 10 degrees off-axis and the resulting signal amplitudes determined from the oscilloscope trace. Figures 4 and 5 show the performance of the above-mentioned f:2.8 lens on axis and 10 degrees off axis. A Wratten No. 22 (orange) filter was used, and the lens was stopped down to f:4. A 150-line Levy screen was used, and its image was formed at a reduction of 3.5 times. This 525-line per inch image was scanned by the vibrating slit. The figures show that a loss of signal amplitude occurs even on axis and that this loss is greater off axis as would be expected. Similar patterns are readily secured using Levy screens having different numbers of lines to the inch, and it is a relatively simple matter to construct an amplitude-frequency response characteristic for any lens used in a given television system. The photoelectric lens bench has greatly simplified the securing of such data.

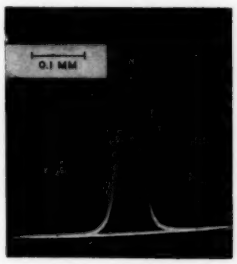

FIG. 2. Cathode-ray tube display of the distribution of energy in an image formed by a lens in yellow light.

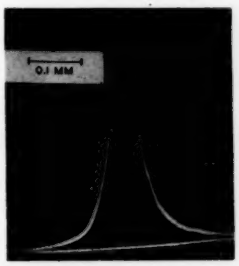

FIG. 3. Cathode-ray tube display of the distribution of energy in an image formed by a lens in blue light.

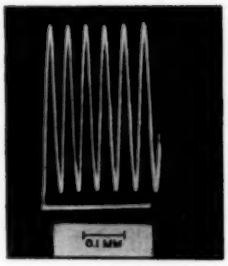

FIG. 4. Light modulation in the image of a grating formed by a lens on axis.

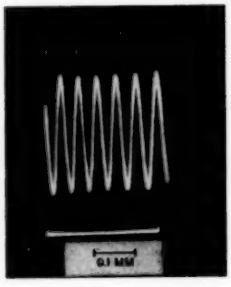

FIG. 5. Light modulation in the image of a grating formed at 10 degrees off axis.

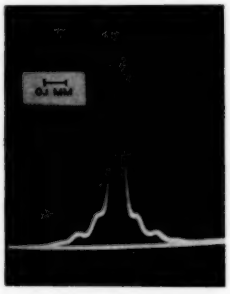

FIG. 6. Diffraction spectra present when a coarse grating is placed over the lens under test.

Figure 6 shows first-, second-, and third-order spectra formed when an 8-mesh screen is placed immediately in front of the lens referred to above.

Photographs of the image pattern as it appears on the oscilloscope tube are readily made. The oscilloscope screen was of the P-1 type (green), and exposures of 1/25 second were made at a magnification of 0.5 on Kodak 35-mm Super-XX film at a lens opening of f:3.5. Photographs serve for measurement and for record purposes.

The photoelectric lens bench offers convenient and accurate means for lens inspection. Space requirements are small, inspection can be done in a lighted room, and the necessary adjustments and measurements are easily and rapidly made. Errors of manufacture that affect image quality result in a change of shape or position of the oscilloscope trace. The shift of an image due to decentering, for instance, can readily be measured if it amounts to 0.01 mm. Decentering also produces a curious warping of the trace as the scanning slit is moved axially through the plane of best focus.

Future developments in television may impose requirements on lens performance that are met by few lenses now commercially available. In the past it has been assumed that lenses introduced little or no degradation in over-all system performance.

The equipment herein described is in current use in these laboratories for determining the performance of available lenses in terms normally employed by the circuit engineer.

The author wishes to acknowledge valuable assistance given by his associates on matters relating to electrical circuits employed in this equipment.

JOURNAL OF THE OPTICAL SOCIETY OF AMERICA VOLUME 37, NUMBER 6 JUNE, 1947

Light Scattering by Spherical Particles*

DAVID SINCLAIR†
Department of Chemistry, Columbia University, New York, New York
(Received March 6, 1947)

The Mie theory of light scattering by a spherical isotropic particle of any radius is briefly described. Equations are given for the angular distribution of intensity, and for the total energy scattered by transparent particles or scattered and absorbed by absorbing particles. It is shown experimentally and by comparison of the equations that both the Mie and the Rayleigh equations for the angular distribution of intensity yield results which are too great by a factor of two when the particle is illuminated by natural light.

Graphs are included giving some of the results of a recently published series of scattering calculations made by The Mathematical Tables Project of the National Bureau of Standards.

A second factor of two occurs in the measurement of the scattering cross section of very large spheres where scattering becomes analogous to diffraction. It is shown theoretically that when the radius of the sphere is at least 25 times the wave-length the scattering cross section is equal to twice the geometric cross section. This result is confirmed experimentally when the observation is made at a distance from the sphere large enough so that the diffracted light is excluded from the measuring device.

INTRODUCTION

THE theory of scattering by a spherical isotropic particle of radius approximately equal to the wave-length of the incident light was first developed in a usable form by G. Mie[1] in 1908. Previously, Rayleigh[2] had derived his well-known equations for scattering by small particles, not necessarily spherical, of radius much less than the wave-length. Since that time, additional investigations, both theoretical and experimental, have been made by Debye,[3] Love,[4] Blumer,[5] Jobst,[6] Engelhard and Friess,[7] Ray,[8] Bromwich,[9] Stratton and Houghton,[10] Ruedy,[11] LaMer and Barnes[12] and others. The complete theory is given in a compact form by Stratton.[13]

During the experimental investigation of light scattering by oil fog, certain difficulties were encountered in the application of the theory, and results were obtained which indicated some discrepancies in the theory and in its past interpretation. It is the purpose of the present paper to indicate these discrepancies and to describe some of the more interesting experimental results obtained.

In addition there is included a description of scattering calculations based on the Mie theory (made by The Mathematical Tables Project of the National Bureau of Standards) which were used to check the theory and experiments.

The equations of the Mie theory, which were found most useful in interpreting the experimental measurements, were the following:

Suppose a plane wave of light incident on a sphere of radius, r, very small compared to the wave-length. The total light energy scattered per second per unit intensity of illumination (unit energy per unit cross-sectional area) is:

$$S=24\pi^3\left(\frac{m^2-1}{m^2+2}\right)^2\frac{V^2}{\lambda^4}. \qquad (1)$$

* This article is based on work performed for the Office of Scientific Research and Development under Contract OEMsr-148 with Columbia University. Publication assisted by the Ernest Kempton Adams Fund for Physical Research of Columbia University.

† Now at the Johns-Manville Research Laboratory, Manville, New Jersey.

[1] G. Mie, Ann. d. Physik **25**, 377 (1908).

[2] Lord Rayleigh, *Scientific Papers* (Cambridge University Press, 1899), Vol. I, pp. 92–93, Vol. IV, p. 400.

[3] P. Debye, Ann. d. Physik **30**, 57 (1909).

[4] A. E. H. Love, Proc. Lond. Math. Soc. **30**, 308 (1899); 31, 489 (1899).

[5] Hans Blumer, Zeits. f. Physik **32**, 119 (1925); **38**, 304 and 920 (1926); **39**, 195 (1926).

[6] G. Jobst, Ann. d. Physik **76**, 863 (1925).

[7] H. Engelhard and H. Friess, Kolloid Zeits. **81**, 129 (1937).

[8] B. Ray, Proc. Indian Assoc. Cultivation Sci. **7**, 1 (1921).

[9] T. J. Bromwich, Phil. Trans. **220A**, 189 (1920).

[10] J. A. Stratton and H. G. Houghton, Phys. Rev. **38**, 159 (1931).

[11] R. Ruedy, Can. J. Research **19A**, 117 (1941).

[12] V. K. LaMer and M. D. Barnes, J. Colloid Sci. **1**, 71 and 79 (1946).

[13] J. A. Stratton, *Electromagnetic Theory* (McGraw-Hill Book Company, Inc., New York, 1941), p. 563.

Here V is the volume of the sphere, λ the wavelength of the light in the surrounding medium, and m the real or complex refractive index of the particle relative to the real refractive index of the medium. S is the scattering cross section of the sphere. Equation (1) is in the form given by Rayleigh and it applies only when $r \ll \lambda$.

For spheres of any size the general form of Eq. (1) is:

$$S=\frac{\lambda^2}{2\pi}\sum_{n=1}^{\infty}\left(\frac{a_n{}^2+p_n{}^2}{2n+1}\right). \tag{2}$$

The a_ns and p_ns are complex functions of the parameter $\alpha=2\pi r/\lambda$ and the index of refraction m. For transparent (non-absorbing) spheres m is real, and Eq. (2) yields the total amount of light abstracted from the incident beam. For absorbing spheres m is complex, and Eq. (2) yields only that part of the light which is scattered by the sphere.

For absorbing spheres, the total light abstracted from the incident beam (i.e., both scattered and absorbed) per second per unit intensity of illumination is:

$$S_e=\frac{\lambda^2}{2\pi}Re\left[\sum_{n=1}^{\infty}(-1)^n i(a_n+p_n)\right]. \tag{2a}$$

S_e is defined as the extinction cross section and *Re* stands for the real part of the expression in the brackets.

The sum in Eq. (2) has been calculated for a variety of values of α and m (real) by The Mathematical Tables Project of the National Bureau of Standards. Tables of these calculations have recently been published.[14]

The Mathematical Tables Project has also calculated the extinction cross section, S_e, from Eq. (2a), for a variety of absorbing particles. These calculations have not as yet been published.

The above equations hold for incident light of any state of polarization. However, the intensity scattered in a given direction varies with the state of polarization of the incident light.

[14] V. K. LaMer and D. Sinclair, "Verification of Mie Theory," O.S.R.D. No. 1857; Department of Commerce Office of Publication Board, Report No. 944.

When the incident light is plane polarized the intensity scattered at an angle ψ when $r \ll \lambda$ is:

$$I_\psi=\frac{9\pi^2}{R^2}\left(\frac{m^2-1}{m^2+2}\right)^2\frac{V^2}{\lambda^4}\sin^2\psi. \tag{3}$$

R is the distance from the sphere to the point of observation, which must be very large compared to the radius of the sphere. ψ is the angle between the direction of propagation of the scattered light and the electric vector in the incident light. The scattered light is plane polarized with its electric vector lying in the plane defined by the electric vector in the incident light and the direction of propagation of the scattered light.

SCATTERING OF UNPOLARIZED LIGHT

When the incident light is unpolarized, and $r \ll \lambda$, the intensity scattered in the direction θ is:

$$I_\theta=\frac{9\pi^2}{2R^2}\left(\frac{m^2-1}{m^2+2}\right)^2\frac{V^2}{\lambda^4}(1+\cos^2\theta). \tag{4}$$

θ is the angle between the directions of propagation of the incident and scattered light.

The theory predicts and observation confirms that the light scattered by spheres of any size is composed of two incoherent, plane polarized components whose planes of polarization are mutually perpendicular. For the extremely small spheres to which Eq. (4) applies, the $\cos^2$ term in the parenthesis gives the relative intensity of the scattered component whose electric vector lies in the plane defined by the incident and scattered beams (hereafter referred to as the plane of observation). The term corresponding to the factor unity in the parenthesis refers to the scattered component whose electric vector is perpendicular to the plane of observation. When $\theta=90°$ it is seen that the scattered light is plane polarized with its electric vector perpendicular to the incident beam, a well-known result.

Equation (3) (but not Eq. (4)) is in the form given by Rayleigh. It should be emphasized that both equations refer to unit intensity of illumination. Experimental and theoretical investigations showed that the value usually given in the literature for the intensity scattered by particles illuminated by unpolarized light is too large by a factor of two, as described below.

For a sphere whose radius is of the same order of magnitude as the wave-length the equation corresponding to Eq. (4) is given by Mie as follows:

$$I_\gamma = \frac{\lambda^2}{4\pi^2 R^2}(i_1+i_2). \qquad (5)$$

The angular distribution functions i_1 and i_2 are complex functions of α, m, and γ ($\gamma = 180° - \theta$). Their values have been calculated by The Mathematic Tables Project for several values of α and m (real), for values of γ from 0° to 180° in steps of 10°.[14]

The functions i_1 and i_2 are proportional to the intensities of the two incoherent, plane polarized components in the scattered light. i_1 is the component whose electric vector is perpendicular to the plane of observation, and i_2 is polarized perpendicular to i_1. When the sphere is illuminated by unpolarized light of two (2) units of energy per unit cross-sectional area, the scattered intensity is given by Eq. (5). (When the incident light is plane polarized the scattered light is elliptically polarized, and i_1 and i_2 do not in general give its components.)

The calculations in the Tables[14] show that *one-half* the integral of Eq. (5) is equal to the scattering cross section given by Eq. (2).

The integral of Eq. (5) is:

$$\int_0^\pi \frac{\lambda^2}{4\pi^2 R^2}(i_1+i_2)2\pi R^2 \sin\gamma d\gamma = \frac{\lambda^2}{2\pi}\int_0^\pi (i_1+i_2)\sin\gamma d\gamma. \qquad (6)$$

The values of the integral:

$$\tfrac{1}{2}\int_0^\pi (i_1+i_2)\sin\gamma d\gamma$$

are given in the Tables.[14] It will be seen that they agree to better than 1 percent with the values of the sum in Eq. (2). Evidently Eq. (6) is equal to twice S, so that Eq. (5) gives twice the true value of I_γ.

The error occurred in the theory, derived for plane polarized light, when transferring to unpolarized light. The error was originally made by Rayleigh[2] who added the intensity I_ψ (Eq. (3)) to the intensity, I_χ, scattered from another incident beam of unit intensity but polarized at right angles to the beam giving rise to I_ψ, to obtain the equation for the intensity, I_θ, scattered by a particle illuminated by unpolarized light. Here ψ, χ, and θ are the angles between the scattered ray and the rectangular coordinate axes, for which $\sin^2\psi+\sin^2\chi = 1+\cos^2\theta$. Therefore:

$$I_\psi + I_\chi = \frac{9\pi^2}{R^2}\left(\frac{m^2-1}{m^2+2}\right)^2 \frac{V^2}{\lambda^4}(1+\cos^2\theta). \qquad (7)$$

This is twice the value of I_θ given by Eq. (4), and evidently refers to two units of intensity in the incident unpolarized light. Equations (2) and (2a) of Mie's theory are correct since they were derived throughout for the case of plane polarized light.

Rayleigh's error was first pointed out by Stiles[15] in a paper which was brought to our attention after reference 14 was distributed. The error has been repeated in a number of texts. For example, in the *Handbuch der Physik*,[16] the error is compensated by making an improper integration over the sphere. The double value is also given by Blumer,[5] Gans,[17] and Born.[18] Humphreys,[19] however, multiplies Eq. (7) by the factor ½ to obtain the correct intensity. When the incident light is plane polarized the correct intensity is given by Wolfson,[16] Gans,[17] Born,[18] and Bromwich.[9]

The fact that Eq. (6) gives double the scattered intensity was observed during measurement of the intensity distribution of the light scattered by a stearic acid fog of uniform droplet size. The fog of supercooled, transparent droplets of known radius and concentration was observed while streaming out of the fog generator,** in the form of a cylindrical jet about 1 cm in diameter. The concentration was low enough so that the scattering was incoherent and the effect of each of the n droplets per unit volume was superposed. A suitable volume was uniformly illuminated by unpolarized white light, and the intensity scat-

[15] W. S. Stiles, Phil. Mag. **7**, 204 (1929).
[16] G. Wolfson, *Handbuch der Physik* **XX**, 314.
[17] Richard Gans, *Handbuch der Expt. Physik* **XIX**, 368.
[18] Max Born, *Optik* (Julius Springer, 1933), p. 376.
[19] W. J. Humphreys, *Physics of the Air* (McGraw-Hill Book Company, Inc., 1940), p. 561.

** The method of producing such a fog will be described in a forthcoming issue of the Journal of Colloid Science.

tered into a given small solid angle was measured with a photometer. The measurements were made through a roughly monochromatic filter ($\lambda = 0.524 \pm 0.01$ micron) at angles θ from 3° to 175°, at frequent intervals. The intensities were then integrated over a sphere and the magnitude of the scattering cross section, S, obtained by comparison with the brightness of a diffuse reflector of known reflectivity.

The results are given in Fig. 1. The ordinates are the "scattering area coefficient," defined as: $K_s = S/\pi r^2$, i.e., the ratio of the scattering cross section to the geometric cross section. The abscissae are the values of $\alpha = 2\pi r/\lambda$. (When $\lambda = 0.524$ micron, $r = \alpha/12$ micron.) The dotted curve shows the experimental results obtained on the uniform droplet size stearic acid fog, real refractive index 1.43. The dashed curve shows the values obtained for K_s by taking Eq. (2) or *one-half* of Eq. (6) from the Tables for real index 1.44. The agreement between the observed and calculated results is considered to be satisfactory. The discrepancies are caused by the difficulties inherent in this type of measurement.

For transparent materials, the scattering cross section can be obtained more readily by measuring the transmission. Measurements at various concentrations showed that the transmission, T, could be expressed by the equation:

$$T = \frac{I}{I_0} = e^{-Snl}. \tag{8}$$

Here I_0 is the incident and I the emergent intensity, n the particle number concentration, and l the length of path in the aerosol.

A beam of approximately monochromatic light from a Hilger monochromator was passed through a uniform particle size aerosol of known concentration. The transmission was measured with a photo-cell, as a function of particle size and wave-length, and the scattering cross section calculated from Eq. (8). Measurements were made at values of T from about 0.9 to 0.3 for a path length of 1 meter. Good agreement was obtained between the experimental values of S and the theoretical values obtained from the Tables for oleic acid (index 1.46), petroleum-diol (index 1.50), and sulfur (index 2.0). The measurements on oleic acid and sulfur are described in reference 14.

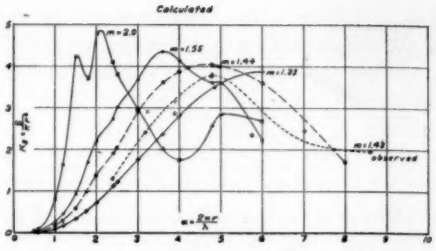

FIG. 1. Scattering area coefficient—K_s.

To sum up: Eq. (2) for the scattering cross section is in agreement with experimental measurements for values of α up to 12, but equations involving the angular distribution of intensity, such as Eqs. (5) and (6), yield results which are twice too high.

THE SCATTERING CROSS SECTION

Figure 1 also shows the calculated values of the scattering area coefficient, K_s, as a function of α for $m = 1.33$, 1.55, and 2.0 obtained from the Tables. It will be seen that K_s has its maximum value of 4 or greater at values of α which decrease with increasing refractive index. There is also a second maximum at a greater value of α. Numerous minor peaks occur, particularly at the higher refractive indices. These minor peaks have recently been confirmed experimentally[12] for a suspension of sulfur particles in water (relative refractive index $m = 1.50$).

The Mie equations hold theoretically for any value of α. Unfortunately, when α is greater than 10 or 12, the practical difficulties of calculation become excessive as a result of the slow convergence of the series in Eqs. (2) and (2a). Debye[3] has, however, developed approximation formulae with which the scattering cross section can be calculated for large values of α.

Stratton and Houghton,[10] applying these approximation methods to Eq. (2a), have calculated the scattering cross section for a wide range of α values for water drops of real refractive index 1.33. Below $\alpha = 6$ their values for the scattering cross section agree excellently with those of Fig. 1 for index 1.33. The second maximum occurs at $\alpha = 15$, and for very large values

of α the scattering cross section approaches $2\pi r^2$. It should be noted that Stratton and Houghton plotted a curve for K *vs.* α where $K = S/2\pi r^2$, i.e., one-half the scattering area coefficient defined above.

Jobst,[6] applying the same approximation methods to Eq. (2a), finds that the scattering cross section of large totally reflecting metallic spheres approaches the value $2\pi r^2$. (For this type of sphere as well as for transparent spheres, the scattering cross section can be obtained from either Eq. (2) or (2a) since the absorption is zero.) Similarly, Jobst finds that the extinction cross section of large absorbing gold spheres is also $2\pi r^2$.

Jobst plotted a curve for $A/\pi r^2$ where A is equal to one-half the extinction cross section, S_e, given by Eq. (2a). Jobst adjusted the incident intensity so that for very large spheres $A/\pi r^2$ would be equal to unity, in agreement with geometric optics. However, both Mie's and Stratton's equations clearly refer to unit intensity. Jobst's equations refer to unit amplitude, i.e., an intensity of one-half.

From the point of view of geometric optics it appears strange that the scattering cross section of a very large sphere is $2\pi r^2$, twice its geometric cross section. However, experimental as well as theoretical considerations have shown this to be true.

The problem may be considered from two points of view: (1) the Mie theory is wrong for large values of α (although correct for small α's), or (2) the theory is entirely correct, but for large spheres it is difficult or impossible to perform experiments to verify it.

In a mathematical analysis of the problem Brillouin[20] integrates the light scattered by a perfectly reflecting sphere in two parts, (1) that scattered into a small solid angle about the forward direction, and (2) that scattered in all other directions. He finds that for spheres for which $\alpha = 160$ ($r = 13$ microns at $\lambda = 0.524$ micron) the light scattered into a small cone of half-angle $\theta = 7°$ about the forward direction is approximately equal to the light scattered in all other directions. The scattering cross section of the sphere is found to be πr^2 for light scattered at angles $0 < \theta \leq 7°$ and πr^2 for light scattered at angles $7° < \theta \leq \pi$. Thus the total scattering cross section is $2\pi r^2$.

Scattering by large spheres is analogous to diffraction by an opaque circular disk. The angle θ within which one-half the scattered light from the sphere falls is roughly equal to the angular divergence of the diffraction pattern produced by an opaque circular disk of radius, r, when illuminated by a plane wave. For example, the angular divergence, θ, of the radius of the fifth black ring (within which practically all the diffrated light falls) is $\theta = 2.62(\lambda/r)$. For green light of wave-length $\lambda = 0.524$ micron and $r = 13$ microns, $\theta = 6°$, in close agreement with $\theta = 7°$ for a perfectly reflecting sphere of 13 microns radius.

The total light contained in the diffraction pattern produced by an opaque circular disk is, according to Babinet's principle, equal to that contained in the diffraction pattern produced by a circular aperture of the same radius as the disk, i.e., πr^2 times the incident intensity. But the disk also intercepts an equal amount of light, so that its "extinction" cross section is $2\pi r^2$, equal to the extinction cross section found by Jobst for large gold spheres, by Jobst and Brillouin for perfectly reflecting spheres, and by Stratton and Houghton for large water drops.

The value of the scattering or extinction cross section observed experimentally would depend upon the method. For large spheres of 15 microns radius the scattering method of Fig. 1 would yield a value in the neighborhood of πr^2, since half the light (at $\lambda = 0.524$ micron) is scattered (diffracted) within a cone of half-angle $5\frac{1}{2}°$, and it is practically impossible to approach closer than 3° without including some of the incident light in the measurement. On the other hand, a transmission measurement making use of Eq. (8) is less severely limited, since the collector can always (theoretically) be placed so far from the sphere that a negligible part of the diffracted light reaches it.

A transmission measurement of this type was made on lycopodium spores lightly sifted on to a glass plate. The radius of these spores, measured with a microscope, was 15.0 ± 1.0 microns. A count of the number of spores per unit area of plate was made microscopically. This number replaces the factor nl in Eq. (8). The plate was

[20] L. Brillouin, Applied Math. Panel N.D.R.C., Reports Nos. 87.1 (Dec. 1943), 87.2 (April 1944).

mounted in a vertical position and illuminated by a parallel beam of white light. Sharp diffraction rings were observed, from whose size the spore radius was calculated in close agreement with the microscope measurement. A photronic cell of about 2 inches diameter and the green filter were used to measure the transmission of the spore covered glass plate at $\lambda = 0.524$ micron. The reading of the photo-cell increased by the factor 2.1 when the distance from the plate was decreased from 18 ft. to 6 in. The extinction cross section calculated by means of Eq. (8) was nearly $2\pi r^2$ at 18 ft. and πr^2 at 6 in.

At the distance of 6 in. all the diffracted light was collected by the photo-cell, and only the intercepted light was measured. At the distance of 18 ft. the half-angle subtended by the photo-cell at a point of the plate was about 1/4°. The amount of green light diffracted within this angle by an opaque disk of 15 microns radius is about $1/16\pi r^2$, so that at this distance the expected value of the scattering cross section is $31/16\pi r^2$. A similar measurement on spheres of 1.5-cm radius would require a distance of about 3 miles between the plate and collector.

It thus appears that the Mie theory is correct, and the theoretical scattering cross section is $2\pi r^2$ for large spheres when both the diffracted and intercepted light are considered. In most practical measurements, however, only the intercepted light can be detected, the diffracted light being indistinguishable from the incident beam.

ACKNOWLEDGMENT

This work was done under the supervision of Professor Victor K. LaMer whose continued interest and enthusiasm provided a constant incentive. The writer is also indebted to Drs. J. Q. Umberger and Seymour Hochberg and Mr. Irwin Wilson for their assistance in performing the experiments.

JOURNAL OF THE OPTICAL SOCIETY OF AMERICA VOLUME 37, NUMBER 6 JUNE, 1947

Method of Computing Correction Plate for Schmidt System for Near Projection, with Special Reference to System for Television Projection

H. S. FRIEDMAN
Kollmorgen Optical Corporation, Brooklyn; New York
(Received March 12, 1947)

The image formed on the cathode-ray tube face in television is projected upon a near screen by an optical system, which is an extension of the classic Schmidt camera, consisting of a large aperture spherical mirror and a plano-aspherical correcting plate at the center of curvature of the mirror. The aspherical surface is the last surface of the system and is so shaped that the center of the field is completely freed from spherical aberration for some wavelength. A method of computing the aspherical surface in this or a similar system is described. A method of determining the chromatic aberration due to the plate and of selecting the constants of the system so that the plate assumes a form of minimum chromatic error is described. The computation of the sin condition of the system is described and also the trace, in the tangential plane, of rays from off-axis portions of the field from which the nature of the off-axis imagery is deduced as well as the curvature of the tube face required to produce a flat image on the screen. Ray trace formulas through the aspherical surface only are given. The trace of rays reflected or refracted at spherical surfaces is assumed to be accomplished by conventional methods.

THE system under consideration, in general, is one in which rays originating from an object plane are reflected or refracted by spherical surfaces and finally refracted by an aspherical surface to incidence on a near image plane. The surface is so figured that the center of the field is completely freed from spherical aberration. Tracing of ray paths other than through the figured surface is accomplished by conventional trigonometric ray trace methods. The following method is concerned only with the ray trace through the figured surface.

Figure 1 shows an optical system for the projection upon a near screen of the television image, formed on a cathode-ray tube face by means of a large aperture spherical mirror and

a plano-aspherical correction plate placed at the center of curvature of the mirror and figured on the side nearest the screen. The system[1] is an extension of the classic[2] Schmidt objective for imaging a far target.

The cathode-ray tube behaves like a diffusing surface, the brightness of which can be increased only at considerable expense. The light-gathering power of the mirror is very great for such objects, compared with the conventional small projection lens, which is ordinarily used at relatively lower speeds, but in conjunction with a condensing system which concentrates a good deal of light on a film and directs most of it through the projection lens. Systems such as shown in Fig. 1 have been designed for speeds as high as f:0.7.

Since the bundles or cones of rays, corresponding to all the object or image points in the field, pass through a common opening or stop at the center of curvature of the mirror, the chief rays of the bundles are all approximately normal to the mirror, and the bundles are all incident on the mirror in approximately the same manner. This tends to make the imagery uniform over the field and to eliminate astigmatism and coma. The curvature of the field which is characteristic of the system is eliminated on the screen by appropriately curving the tube face or object plane. The spherical aberration which would appear over the whole field, in the absence of the correction plate, is substantially eliminated by its presence.

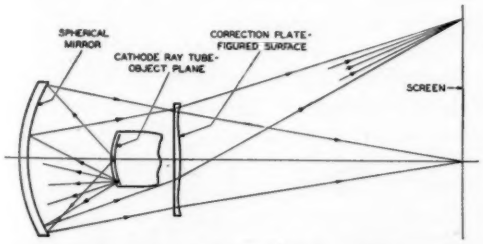

FIG. 1. Schmidt system for television projection upon a near screen. The correction plate, with figured surface shown exaggerated, is at the center of curvature of the spherical mirror.

[1] I. G. Maloff and D. W. Epstein, "Reflective Optics In Projection Television," Proc. Nat. Elec. Conf., 190 (Oct. 5–7, 1944).

[2] Frank Allen Lucy, "Exact and Approximate Computation of Schmidt Cameras. I. The Classical Arrangement," J. Opt. Soc. Am. **30**, 251 (1940).

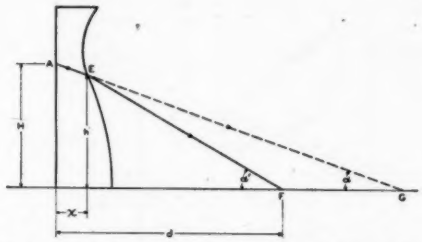

FIG. 2. Refraction at the aspherical surface of the correction plate of an extra-axial ray from the axial object point on the tube face. AEG is the ray after refraction by the plano surface and EF after refraction by the aspherical surface. F is the location of the screen.

The spherical aberration is completely eliminated at the center of the field by equalizing the optical path lengths of all the rays from the axial object point. That is, for any such ray, the sum of the segments of path length in successive optical media, each multiplied by the index of refraction of the medium in which it lies, is the same as for any other such ray. Since the object plane lies on the inner face of the tube, the segments lying in the tube face itself should be considered.

Chromatic aberration, due to refraction by the correction plate is present but can be minimized by proper selection of the constants of the system, i.e., mirror curvature and aperture, location of tube face and screen, and thickness and refractive index of the correction plate. If the constants are selected so that a ray from the axial object point, incident on the correction plate at a certain height above the axis, requires that the plate at that zone cause no angular deviation of the ray in order that it arrive at the center of the screen, then the correction plate will assume a convex shape at the center and a concave shape at the periphery and the chromatic error will be at a minimum. In the case of systems in the neighborhood of 6× magnification, satisfying current television design requirements, the height is about 85 percent of the useful half-diameter of the plate.

When the constants of the system are selected, the correction surface can be computed. In Fig. 2, AEG is an extra-axial ray, from the axial object point O (not shown in figure), after refraction by the plano surface of the correction plate. The axial optical path from O to F is computed, and the extra-axial path for any other

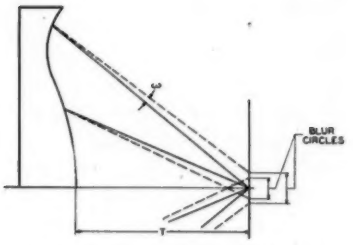

FIG. 3. Chromatic aberration due to refraction by the correction plate. The solid rays correspond to the wave-length for which the system is fully corrected for spherical aberration at the center of the field. The dashed rays correspond to another wave-length.

ray from O is computed from O to A. The difference K between the two is found. Then:

$$K=nAE+EF, \tag{1}$$

where n is the refractive index of the plate.

$$nAE=nx/\cos\alpha, \tag{2}$$

$$EF^2=(H-x\tan\alpha)^2+(d-x)^2. \tag{3}$$

Combining and simplifying:

$$x^2+2[\cos^2\alpha/(n^2-1)][H\tan\alpha+d-nK/\cos\alpha]x +[\cos^2\alpha/(n^2-1)][K^2-H^2-d^2]=0. \tag{4}$$

Since α, H, and K are determined by the trigonometric ray trace preceding the correction surface, and d and n are constants of the system, the coefficient of x and the constant term can be evaluated and the quadratic solved for x. The expressions are arranged for rapid and convenient evaluation on a standard computing machine.

Then

$$h=H-x\tan\alpha. \tag{5}$$

Thus the coordinates of the correction surface are found by Eqs. (4) and (5).

If the constants of the system have been selected as described before, the correction curve will assume a form such as shown in Fig. 3. The solid line rays are completely corrected for spherical aberration, a certain index of refraction n having been assumed for the plate, corresponding to wave-length λ. For a wave-length λ', corresponding to refractive index n', which is larger (say) than n, the chromatic deviation of the plate is shown by the dashed rays producing blur circles on the image plane as shown. The dashed rays are bent downward from the corresponding solid rays by the convex portion of the plate and upward by the concave portion. If the angular chromatic deviation ω is known, the radius of the blur circle can be estimated. If the radii of the blur circles for all the rays computed are plotted against the corresponding zone heights on the aspherical surface, the largest circles produced by the convex and concave portions of the plate can be determined, which, if the constants of the system have been properly selected, will be equal, and the chromaticity will be at a minimum. If the blur circles in question are not equal, it is desirable to vary one or more constants of the system, the location of the tube for example, and recompute the aspherical surface. With only a few rays for two trials, a form adjusted for minimum chromatic error can be interpolated. It remains however to evaluate ω for any ray.

Before evaluating ω, the slope of the normal to the correction surface at the zone in question is found. In Fig. 4, the angle α which a ray forms with the axis before refraction by the aspherical surface is known from the trigonometric ray trace. The angle α', formed after refraction is found from

$$\tan\alpha'=h/(d-x). \tag{6}$$

The deviation of ray AEG in Fig. 4 is therefore:

$$\delta=\alpha'-\alpha. \tag{7}$$

The angles of incidence and refraction of the ray at the figured surface are ϕ and ϕ'.

$$\phi=\phi'-\delta, \tag{8}$$

$$\sin\phi'=n\sin\phi, \quad \text{(Snell's law)} \tag{9}$$

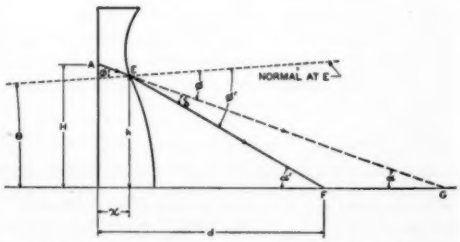

FIG. 4. The normal to the correction surface at a point for which the coordinates have been computed. AEG and EF show the path of an extra-axial ray from the axial object point, before and after refraction at the aspherical surface as in Fig. 3. ϕ and ϕ' are the angles of incidence and refraction, respectively, formed with the normal.

whence

$$\sin\phi = \sin\delta/(n^2-2n\cos\delta+1)^{\frac{1}{2}}, \qquad (10)$$

and

$$\theta = \phi - \alpha, \qquad (11)$$

which defines the normal.

In systems such as we have under consideration, the correction surface is very flat and θ is small for any zone. The plate may therefore be regarded as a thin wedge of angle θ at any zone with deviation $(n-1)\theta$. If the system is corrected for wave-length λ, then the difference between the deviations at some zone for rays corresponding to wave-lengths λ and λ', is

$$\omega = \theta(n_\lambda - n_{\lambda'}). \qquad (12)$$

If the screen distance T in Fig. 3 is large compared with the correction plate diameter, then the radius of the blur circle is

$$r = \omega T, \qquad (13)$$

where ω is in radians.

It should be noted that since ω is proportional to θ, the correction plate shape for minimum chromatic error can be selected on the basis of the values of θ without the necessity of computing ω or the blur circle radii, i.e., by selecting the shape for which the largest positive and negative values of θ are equal. However, it is necessary to compute θ in any case and the computation for the blur circles is easy and contributes data of interest.

The question of off-axis imagery arises. Although it was stated that the system is substantially free of coma and oblique spherical aberration, it is desired to find as nearly as possible the extent to which it is so. For a first indication the sin condition is examined. For all the rays proceeding from the axial object point to F, in Fig. 4, the ratio $\sin\alpha'/\sin\alpha_1$ is evaluated where α_1 is the angle formed by the axis and the ray from the axial object point; α' is determined by Eq. (6) above. If the ratio is constant for all zones, the system is free of coma. This applies only to third-order aberrations and not to the entire field.

To find the exact nature of the off-axis imagery, it would be necessary to trace the paths of all useful rays from off-axis object points through the system to the screen. The incidence of these

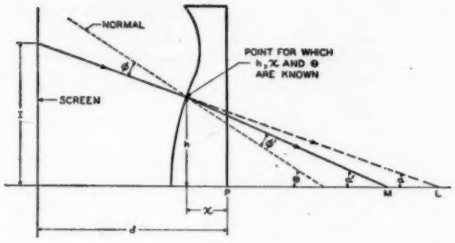

FIG. 5. Ray trace from an extra-axial point on the screen, backwards towards the correction plate. A ray from a selected height I is directed to L, through a previously defined point on the correction surface, and refracted by the aspherical surface to M. ϕ and ϕ' are the angles of incidence and refraction respectively formed by the ray with the normal.

rays on the correction surface would be determined by the conventional ray trace, and it would be necessary to deduce the equation of the aspherical surface from the points for which the coordinates are known in order to carry the trace through the aspherical surface. This would be a laborious process. An idea of the extra-axial imagery in the tangential plane can be had by the device of computing backwards from points on the screen through the system to the object plane or tube face. This is a relatively easy undertaking as illustrated in Fig. 5, since rays can be directed from the screen to points on the aspherical surface for which the coordinates and the slope of the normal are known.

If a ray in Fig. 5 from a height I on the screen is directed to a point on the aspherical surface for which h, x, and θ are known, then the angle a between the ray and the axis is found from

$$\tan a = (I-h)/(d-x). \qquad (14)$$

The angle of incidence on the plate is

$$\phi = \theta - a. \qquad (15)$$

The angle of refraction ϕ' is found from

$$\sin\phi' = \sin\phi/n, \qquad (16)$$

where n is the refractive index.

The angle between the axis and the refracted ray is

$$a' = \theta - \phi'. \qquad (17)$$

The distance of the point of incidence of the refracted ray, on the axis, from the plano surface of the plate is

$$PM = (h/\tan a') - x. \qquad (18)$$

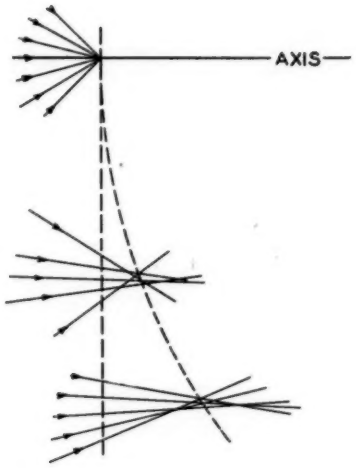

FIG. 6. Blur patterns formed by the system at the tube face, from cones of rays proceeding from points on the screen and directed backwards through the correction plate, mirror and tube face in the same order. The central and a peripheral and intermediate image points are shown. The dashed straight line is the first order image plane and the dashed curve indicates the optimum tube face shape.

The refracted ray is sufficiently described by PM and a' so that its course through the remainder of the system and its incidence on the tube face can be determined by conventional ray trace methods for spherical surfaces. A sufficient number of rays can be directed from a point on the screen to known points on the aspherical surface so that the tangential section of the useful cone of light may be traced through the system.

When sufficient rays are thus traced, a large scale drawing, such as shown in Fig. 6, can be made, showing the incidence of the rays on the tube face, the trace of the rays having been carried through the refracting surfaces of the tube face. The best curvature for the tube face can be approximated by drawing a circular curve which cuts the smallest sections through the several ray patterns. An aspherical curve may be so drawn if desired. The method of tracing two rays through the center of the plate and through the zone where the normal is horizontal, which is sometimes used, will not yield as accurate a picture of the nature and location of the blur which constitutes the image point for a particular part of the field.

After the shape of the tube face has been selected as just described, it is not necessary to retrace the cones of rays from off-axis points on the screen to the tube face, Since the tube face, in the form originally selected for the computations, even though roughly approximated, and the finally selected tube face lie in or close to the focal surface, their effects on the imagery are substantially the same; and changing the shape of the tube face is analogous to shifting a plate near an image plane into the plane. Nor is it necessary to recompute the coordinates of the aspherical surface of the correction plate. The spherical aberration caused by the axial portion of the tube face varies inconsequentially with moderate variations in the shape of the tube face.

An extension of the method described for tracing the tangential sections of cones of rays from extra-axial points on the screen, can be made for the sagittal section by similarly directing rays in that section to points on the correction surface for which h, x, and θ' are known. This should result in a still more accurate determination of the optimum curvature of the tube face but adds considerably to the labor of computing.

The advantage of computing backwards from extra-axial points on the screen as described, rather than forwards from the tube face, is that, aside from obviating the necessity of determining the equation of the curve of the correction surface, only a single set of computations is necessary to give the blur patterns from which the optimum curvature of the tube face is approximated. If computations are made from extra-axial points on the tube face towards the screen, several sets of computations would have to be made from tube faces of various curvatures until, by interpolation or directly, the smallest sections of the blur patterns for the various image points were found to lie on a flat plane corresponding to the screen.

In conclusion it is suggested that improvement of the extra-axial imagery should result from the use of a correction plate, aspherical on both sides. A plate based on a spherical surface instead of a plano might also be better than the conventional form.

JOURNAL OF THE OPTICAL SOCIETY OF AMERICA VOLUME 37, NUMBER 6 JUNE, 1947

Light Distribution in the Optical Image*

M. HERZBERGER
Kodak Research Laboratories, Rochester, New York
(Received February 19, 1947)

A method is proposed for obtaining information about the light distribution in an optical image. The characteristic function of the optical system is approximated by a polynomial, containing terms up to the fifth or seventh order. The coefficients of this function having been found, a large number (about 100) of rays from an object point are chosen, so that they are evenly spaced in the aperture of the system. By means of the function, the intersection points of the rays can be calculated in any desired image plane, to a close approximation. The intersection points were plotted, representing each ray by a small dot. The figures show that these plots are very similar to photographs of the image of a point light source. The image of a line element can be obtained by integration of a series of such figures.

IN designing an optical system it is the aim of the optical designer to get as much information as possible about the image-forming qualities of the optical system before actually making it. This paper is intended to help him obtain a more comprehensive knowledge than that permitted by the methods now in use. The usual method of judging optical systems is based upon a generalization of the Seidel theory which gives very incomplete information. If the lens under investigation has a small aperture and a small field, the image-forming qualities can be described by five quantities: spherical aberration, coma, astigmatism, curvature of field, and distortion, following Seidel's terminology.

These errors have some meaning for finite aperture and field. If the rays from an object point on the axis (at a finite or infinite distance) are considered, the distance of the intersection point of a ray with the axis from the Gaussian focus may be called *spherical aberration*. Abbe's sine condition gives information about coma, more exactly, the asymmetry of the image of a point near the axis. But these are actually general functions of the aperture, and are not proportional to the square of the aperture, as in Seidel's theory. Astigmatism, curvature of field, and distortion have less meaning for image formation for systems of finite aperture and field; however, we desire a generalization of these terms. If we consider only the rays through the center of the entrance pupil, the so-called *principal rays*, we see that these rays make an optical projection of the object on the image plane. This projection may be distorted or undistorted; in any case, we obtain a measure of distortion as a function of the field angle. The rays from a given object point off the axis are tangential to their caustic surface at two points in the image space. If we again consider only the principal rays, or rather, the two points which lie on every principal ray of the system, we see that these points form two surfaces, the so-called *meridional* and *sagittal* surfaces. Astigmatism, as well as the two surfaces, is a function of the field angle.

These five aberrations are the quantities usually computed. It is possible to measure these quantities for a given optical system, and R. Kingslake,[1] in particular, has devised ingenious methods of doing so. However, it is not theoretically possible to find from these data a picture of light distribution in the image, because they are based on the tracing of a few rays in the meridional plane only, and the influence of the skew rays is almost entirely neglected (the computation of sine condition and sagittal astigmatism yields only first-order information in that direction).

* Presented before L'Institut d'Optique, Paris, France, October, 1946; and before the Optical Society of America, New York, New York, October, 1946. After finishing this paper, the author's attention was drawn to a paper by D. Hawkins and C. E. Linfoot in the December, 1945, issue of the Monthly Notices of the Royal Astronomical Society, in which spot diagrams were used to indicate the light distribution in the image of a Schmidt camera. It might, however, be difficult to apply this very ingenious method to the design of instruments with a sizable number of surfaces. The method applied here has been used in these Laboratories since 1939. The author feels that the approximation methods and the image error theory connected with it still warrant its publication.

[1] R. Kingslake, Trans. Opt. Soc. **27**, 221 (1925).

This paper is intended to remedy this deficiency, and to show how one may visualize the light distribution. A certain amount of skew-ray tracing seems necessary, and suggestions will be made on the interpretation of results of such calculations.**

The intersection of the image rays with a series of parallel planes in the image spaces is given by one of Hamilton's characteristic functions (or, better, by Bruns' modification). From the data of the ray computation,[2] we calculated the coefficients of the development of the so-called "mixed characteristic," taking as variables the coordinates of the object point and the coordinates, x_p', y_p', of the intersection of the image ray with the exit pupil.[3] Having made these calculations for four object points, $\xi=0$, $\eta=0$ (the axis point); $\xi=\sin 10°$, $\eta=0$; $\xi=\sin 18°$, $\eta=0$; $\xi=\sin 24°$, $\eta=0$; we can obtain the coefficients analytically as functions of the object angle and the position in the exit pupil. From this analytical function can now be calculated the intersection point of any desired ray with one or more planes in the image space.

The rays from the axis point fill a circular exit pupil, the radius of which is given by the aperture of the system. The rays from an off-axis point do not fill a circular aperture because of vignetting. The vignetting can be taken into account in the following way: On projecting the first surface optically into the image space, we have three circular apertures, the exit pupil, and the first and last surfaces of the lens, which limit the "cone" of light, and whose centers lie on the axis. We can find the light beam which goes to an image point by projecting these three circles from the image point on the exit pupil. The area common to the three concentric circles thus obtained is the vignetted aperture, which varies from angle to angle.

To obtain the light distribution in the image, we now assume a number of evenly distributed points at close intervals in the exit pupil and compute by formula the intersection of these rays with one or more planes in the image space. The plotting of these points gives a picture of the light distribution in the image, which, in comparison with Wolfe's actual photographs, is fairly close to the actual image.

Although this method is quite satisfactory for giving an idea of the light distribution in the image (it is easy from there to obtain an idea of the images of lines), there is the objection that it cannot be tied up easily with the new theory of image errors. Mathematical investigation shows that the use of angular coordinates of a different type of characteristic function permits an easier coordination of coefficients with finite-image error theory. Therefore, in the second part of the paper we outline this theory, which is based upon the fact that there exists a characteristic function, $D(\xi, \zeta, \xi', \zeta')$, such that the intersection of the rays with the meridian plane is given by

$$h=\frac{\partial D}{\partial \xi'}, \quad z=-\frac{\partial D}{\partial \zeta'}. \tag{0, 1}$$

The coefficients of D are also calculated from the ray-trace data. The coefficients tell us immediately about the symmetry of the image in question, as will be shown below. Having found these coefficients, we can assume a large number of rays in the image space, defined by their

** The results obtained theoretically by the methods contained here were tested practically as described in a publication by L. A. Jones and R. N. Wolfe, J. Opt. Soc. Am. **35**, 559 (1945). In their paper a method was developed to measure the energy distribution in the optical image. As an example, a certain lens (5-H-30) having an aperture of f:5, and a focal length of 306.5 mm, was investigated, the images of a point source were photographed for various image planes and various angles, and the light distribution in the image was analyzed. Figure 1 of their paper is a sample of the pictures analyzed. At the same time, we calculated the spot diagrams for the same lens. The methods were worked out in 1939 and are now released for publication. The pictures attached contain the calculated images and the photographs of a light source made by Wolfe at that time. The spot diagrams were made by W. Litten, in the following manner: A camera back carrying 35-mm film was attached to the table of a measuring microscope. In the model used, the microscope tube was stationary, while the table moved in two directions. The eyepiece was replaced by a right-angle prism, and a Kodatron flashlamp was set up several feet away, pointing toward the microscope. The microscope object was set to focus on the film the image of a circular aperture in front of the lamp, the aperture being large enough to give dots of a suitable size on the film. In use, the calculated coordinates of a ray-intersection point were set on the two scales of the traveling stage, and the exposure button of the flashlamp was pressed to record the dot on the film. The whole work was done in a darkroom, with baffles placed where necessary to prevent light from the lamp from reaching the film directly.

[2] For the purpose of this investigation, we traced a much larger number of rays than were actually necessary, in order to get an idea of the accuracy of the method.

[3] For the case of a photographic objective, the object is usually at infinity, and the coordinates of an object point are therefore angles.

direction cosines, and can calculate h and z for each ray. From h and z may be computed the intersection points of the rays in a series of image planes.

The ray through the center of the exit pupil has a finite value, ξ_0, ζ_0. The rays are then chosen in such a way that the values, $\xi-\xi_0$, $\zeta-\zeta_0$, are evenly distributed with respect to the vignetted aperture projected to infinity. If the points are chosen dense enough, we shall obtain a picture comparable to the photographic image of a point light source, with the advantage that the coefficients of the characteristic function give an easy geometric interpretation for finite aperture and stop.

We shall find that in a good image the coordinates thus chosen are not entirely independent, which means that the determinant of the least squares normal equations becomes small. In this case, the solution of these equations needs more decimal places than are available on commercial calculating machines. The author has therefore developed a novel method of solving the normal equations, which might be of value for other applications in which a large number of unknowns occur.

The lens investigated was an f:5 objective with a well-corrected field of 20 degrees, and a focal length of 306 mm.

PART I: THE LIGHT DISTRIBUTION IN THE IMAGE AS A FUNCTION OF THE PUPIL INTERSECTION

Given an optical system which is rotationally symmetrical, we select the origin of one Cartesian coordinate system on the object side at the entrance pupil, and the other on the image side at the exit pupil. An arbitrary ray is then given by its direction cosines, ξ, η, $\zeta=(\eta^2-\xi^2-\eta^2)^{\frac{1}{2}}$, in the object space, and the coordinates, x_p', y_p', of its intersection point with the exit pupil, or, in the case of a rotationally symmetrical system, by the symmetric functions,

$$a=\tfrac{1}{2}(\xi^2+\eta^2),\quad b=\xi x_p'+\eta y_p',\quad c=\tfrac{1}{2}(x_p'^2+y_p'^2). \tag{I, 1}$$

The general theory then enables us to compute the direction cosines of the image ray, if the characteristic function is given, as

$$\begin{aligned}\xi'&=\frac{\partial W}{\partial x_p'}=W_b\xi+W_c x_p',\\ \eta'&=\frac{\partial W}{\partial y_p'}=W_b\eta+W_c y_p',\\ \zeta'&=(\eta'^2-\xi'^2-\eta'^2)^{\frac{1}{2}},\end{aligned} \tag{I, 2}$$

where the subscripts c and b indicate differentiation with respect to c and b. The point of intersection with a plane at a distance k from the exit pupil is given by

$$\begin{aligned}x_k'&=x_p'+k\frac{W_b\xi+W_c x_p'}{\zeta'},\\ y_k'&=y_p'+k\frac{W_b\eta+W_c y_p'}{\zeta'}.\end{aligned} \tag{I, 3}$$

Without loss of generality, we can assume that the (infinite) object point lies in the meridian plane; this means that for $\eta=0$, (I, 1) and (I, 2) become

$$a=\tfrac{1}{2}\xi^2,\quad b=\xi x_p',\quad c=\tfrac{1}{2}(x_p'^2+y_p'^2), \tag{I, 4}$$

and

$$\xi'=W_b\xi+W_c x_p',\quad \eta'=W_c y_p'. \tag{I, 5}$$

The meridian rays are defined by setting $y_p'=0$.

Developing W with respect to b and c, we obtain

$$\begin{aligned}W=w_0&+w_2b+w_3c+\tfrac{1}{2}(w_{22}b^2+2w_{23}bc+w_{33}c^2)\\&+\tfrac{1}{6}(w_{222}b^3+3w_{223}b^2c+3w_{233}bc^2+w_{333}c^3)\\&+\frac{1}{24}(w_{2222}b^4+4w_{2223}b^3c+6w_{2233}b^2c^2\\&\qquad+4w_{2333}bc^3+w_{3333}c^4).\end{aligned} \tag{I, 6}$$

Most of the seventh-order terms can be neglected, and frequently the fifth-order terms do not contribute much to the whole. A number of these coefficients can be obtained from the meridional trace alone. For the latter we have $y_p'=\eta'=0$, and

$$\begin{aligned}\xi'=w_2&+(w_3+w_{22}\xi^2)x_p'+\tfrac{1}{2}(3w_{23}+w_{223}\xi^2)\xi x_p'^2\\&+\tfrac{1}{6}(3w_{33}+6w_{223}\xi^2+w_{2222}\xi^4)x_p'^3\\&+\frac{1}{24}(15w_{223}+10w_{2223}\xi^2)\xi x_p'^4\\&+\tfrac{1}{8}(w_{333}+3w_{2233}\xi^2)x_p'^5\\&+\frac{7}{148}w_{2333}\xi x_p'^6+\frac{1}{48}w_{3333}x_p'^7,\end{aligned} \tag{I, 7}$$

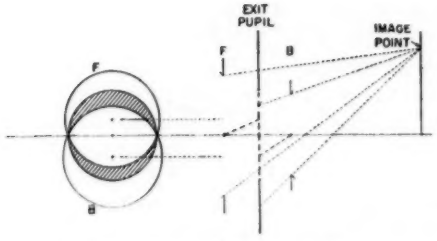

FIG. 1. The projected apertures.

which permits us to obtain eight combinations of the fourteen variables. The remaining six must be obtained from the trace of a small number of skew rays, by using the method of least squares.

Having calculated the coefficients of W, Eq. (I, 5) allows us to compute the image coordinates for any ray given by its object direction and the points of intersection in the exit pupil.

We could calculate the geometric-optic light density at each point, which is equal to the reciprocal of the functional determinant of (I, 3) with respect to x_p' and y_p' (as suggested by Hamilton). This density is infinite at all points of the caustic, and, by drawing curves of constant density, we can make a "contour map" of the light, according to geometrical optics. However, the following method has been found to result in a representation which is more easily compared with the photographic image of a point object than the density diagram. We choose a number of points evenly spaced over the portion of the exit pupil which is filled with light (vignetted aperture), and calculate the rays from the object points ($\xi=5,\ 10,\ 15,\ 20°;\ \eta=0$) through the evenly spaced points of the exit pupil by means of Eq. (I, 3).

The vignetted aperture differs from angle to angle. For an infinite object (i.e., where the entering light rays are parallel), the vignetting is most easily calculated in the entrance pupil. The bundle of rays is usually limited by the front window, the back window, and the (variable) aperture in the diaphragm plane. We project[4] the back window and diaphragm into the image space, thus obtaining three circles whose centers lie on the axis: one representing the front window, one the exit pupil, and the third the back window (see Fig. 1). A beam of light from the image point projects the image of the front and back window on the exit pupil, where each forms a circle with its center off the axis. The area which is common to these three circles represents the vignetted aperture.

Analytically, we obtain the aperture in the following manner: If the images of the front window, the back window, and the exit pupil have the radii, r_F, r_B, and r_p, respectively, and if k_F' and k_B' are the distances from the center of the exit-pupil circle, the centers of the front-window and back-window circles to the image plane, and if h is the image height, we have the equations of the circles projected on the entrance pupil

$$\left(x'-h'\frac{k'}{k'-k_F'}\right)^2+y'^2=\left(\frac{k'}{k_F'}r_F\right)^2,$$

$$x'^2+y'^2=r'^2, \quad \text{(I, 8)}$$

$$\left(x'-h'\frac{k'}{k'-k_B'}\right)^2+y'^2=\left(\frac{k'}{k_B'}r_F\right)^2.$$

Figure 2 shows the vignetting diagrams for 0°, 10°, and 24° with the points chosen for the spot diagram. A triangular pattern would have been more appropriate, but for simplicity of computation a square pattern was chosen. Of course, the distribution of points in the final spot diagram shows the influence of this pattern, and a little imagination must be used in viewing the diagram, particularly in smoothing out the contours of the spot diagram.

In Figs. 3 to 7 are plotted the intersection points of the chosen rays for a number of parallel planes. Above them are photographic images of a point light source made by R. N. Wolfe, of

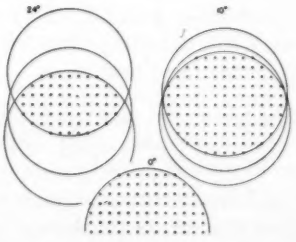

FIG. 2. Vignetting diagram for three angles.

[4] Projection is here used in the sense of Gaussian optics, which is completely satisfactory for our vignetting diagram.

FIGS. 3 to 7. Comparison of spot diagrams with star-image photographs.

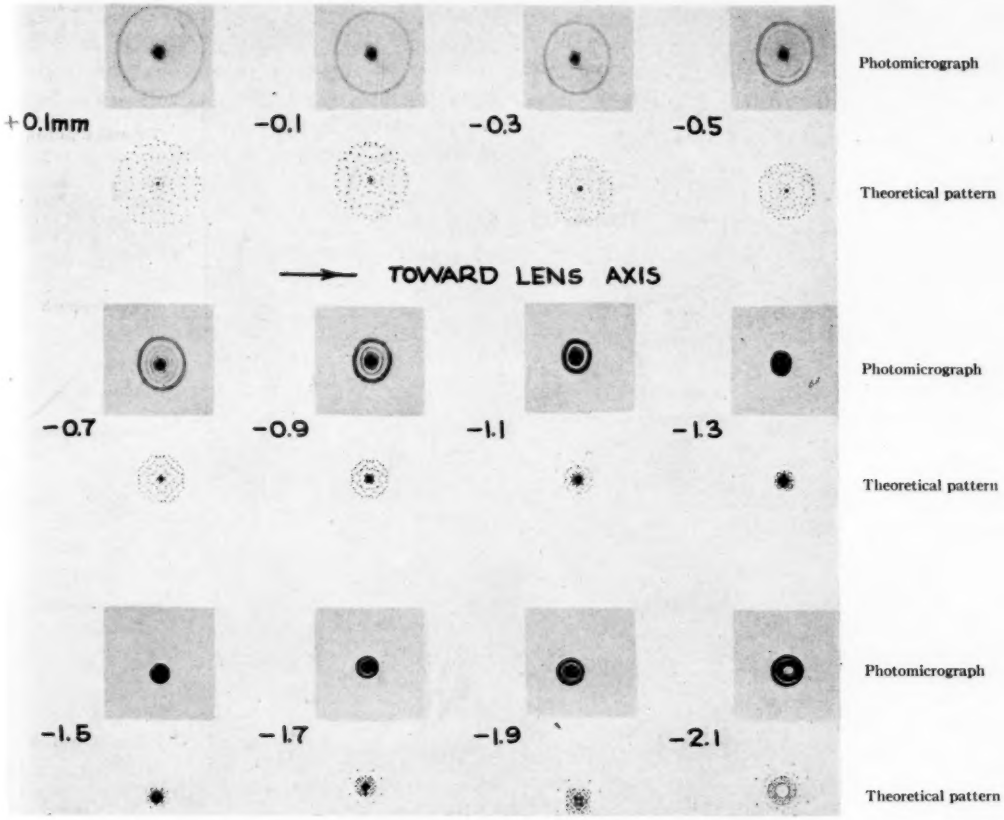

FIG. 3. Image of point source—12″ f:5.0 5-H-30 lens. 0°

these Laboratories. The similarity is especially striking, since the method used in the calculation of the diagrams was inferior to the one described here, because, for the diagrams, the fifth- and seventh-order errors had been neglected.

PART II: THE SPOT DIAGRAM AND THE DIAPOINT THEORY

During the last five years the author has developed a new theory of image errors, based upon the degree of symmetry of the manifold of image rays. It is desirable to coordinate the elements of this theory with the coefficients in the development of W. This can be done easily for the aberrations of the third order, but it leads to a very difficult problem in the investigation of finite aperture and field. Thus, the author has developed a different method of computing the spot diagrams described in Part I, a method which permits a ready understanding of the geometrical meaning of the various coefficients in the approximation development. The use of Bruns' characteristic will be abandoned, and the so-called *diacharacteristic* function, which was introduced by the author[5] in 1939, will be applied.

The points where the rays from an infinite object point ($\xi=\eta=0$) intersect the meridional plane will be called the *diapoints* of the object points. From Eqs. (I, 5) and (I, 3) we have, for

[5] M. Herzberger, J. Opt. Soc. Am. **26**, 197 (1936).

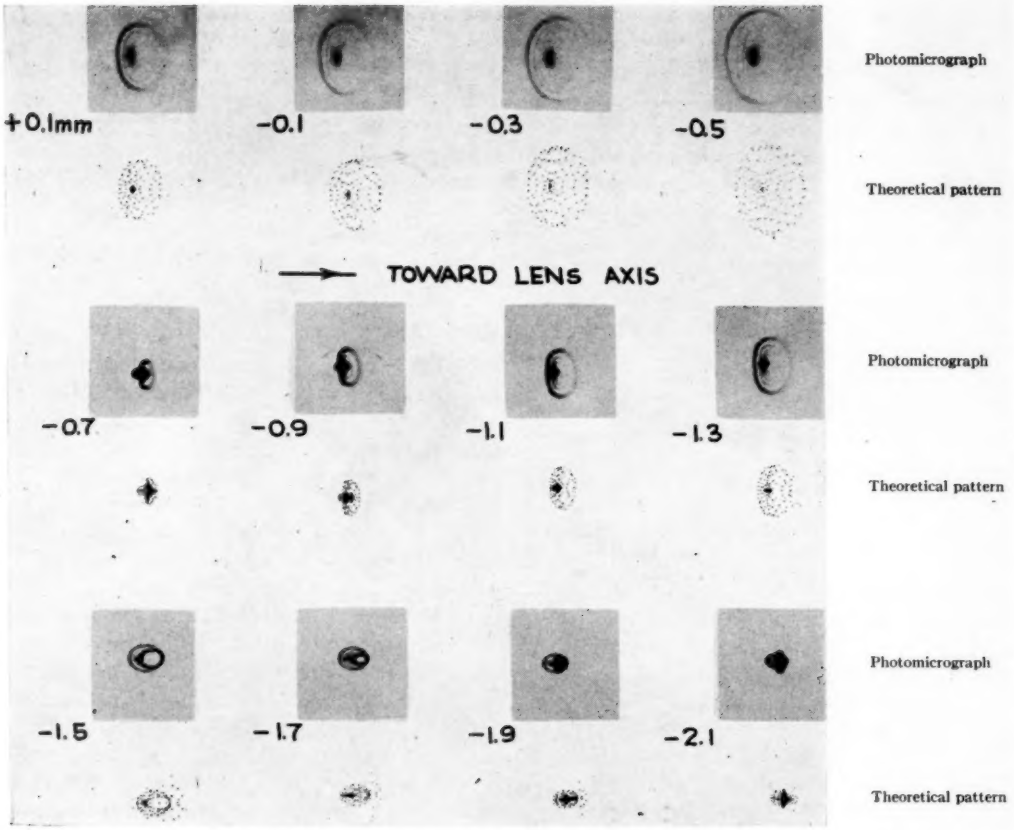

FIG. 4. Image of point source—12″ f:5.0 5-H-30 lens. 5°

the coordinates of the diapoints,

$$k_D' = -\frac{\xi'}{W_c}, \qquad \text{(II, 1)}$$

$$x_D' = -\frac{W_b}{W_c}\xi, \quad y_D' = 0, \quad z_D' = -\frac{1}{W_c}.$$

In place of the variables x_p' and y_p', we introduce the new variables, ξ' and ζ', which will be used together with ξ and ζ. Since we shall investigate the neighborhood of the principal ray given by ξ_0', $\zeta_0' = (\eta'^2 - \xi_0'^2)^{\frac{1}{2}}$, $\eta_0' = 0$, we can introduce

$$v = \xi' - \xi_0', \quad w = \zeta' - \zeta_0', \qquad \text{(II, 2)}$$

as variables. According to Hamilton's theory, we can find a characteristic function, $D(v, w)$, so that the coordinates of the diapoint are given by

$$x = \frac{\partial D}{\partial v}, \quad z = -\frac{\partial D}{\partial w}, \qquad \text{(II, 3)}$$

with

$$D = d_1 v + d_2 w + \tfrac{1}{2}(d_{11}v^2 + 2d_{12}vw + d_{22}w^2) + \tfrac{1}{6}(d_{111}v^3 + 3d_{112}v^2 w + 3d_{122}vw^2 + d_{222}w^3) + \frac{1}{24}(d_{1111}v^4 + \cdots); \qquad \text{(II, 4)}$$

where again fifth- and seventh-order terms can be used, if necessary.

The coefficients of the characteristic are obtained by demanding that for the rays traced,

$$(x - D_v)^2 + (z + D_w)^2 = \text{minimum}. \qquad \text{(II, 5)}$$

The calculation of the vignetting diagram is only slightly more complicated than it was in the previous case. Again, we have three apertures in the image space: the exit pupil, the back window, and the image of the front window. The rays from the Gaussian image point through any one of these circles form a cone whose generators or limiting rays have the direction cosines:

$$\eta=\frac{-y'}{(h'^2+r'^2+k'^2-2h'x')^{\frac{1}{2}}},$$
$$\xi'=\frac{h'-x}{(h'^2+r'^2+k'^2-2h'x')^{\frac{1}{2}}} \qquad \text{(II, 6)}$$
$$\zeta=\frac{k'}{(h'^2+r'^2+k'^2-2h'x')^{\frac{1}{2}}},$$

in which h' is the image height, k' is the distance of the image to the plane of the circle, r' is the radius of the circle, and x, y are the coordinates of the point on the circle of radius, r'.

Elimination of x' gives an equation of the second order for ξ' and ζ',

$$(r'^2+k'^2-h'^2)\zeta'^2+2h'k'\zeta'=k'^2. \qquad \text{(II, 7)}$$

This, together with

$$\xi'^2+\zeta'^2=1, \qquad \text{(II, 8)}$$

determines the area in ξ' and ζ' for the rays through the circle.

If we carry out this process for all three apertures, we obtain a region in the $\xi'-\zeta'$ plane which is common to all these areas, namely, the vignetting diagram (Fig. 8). By choosing values

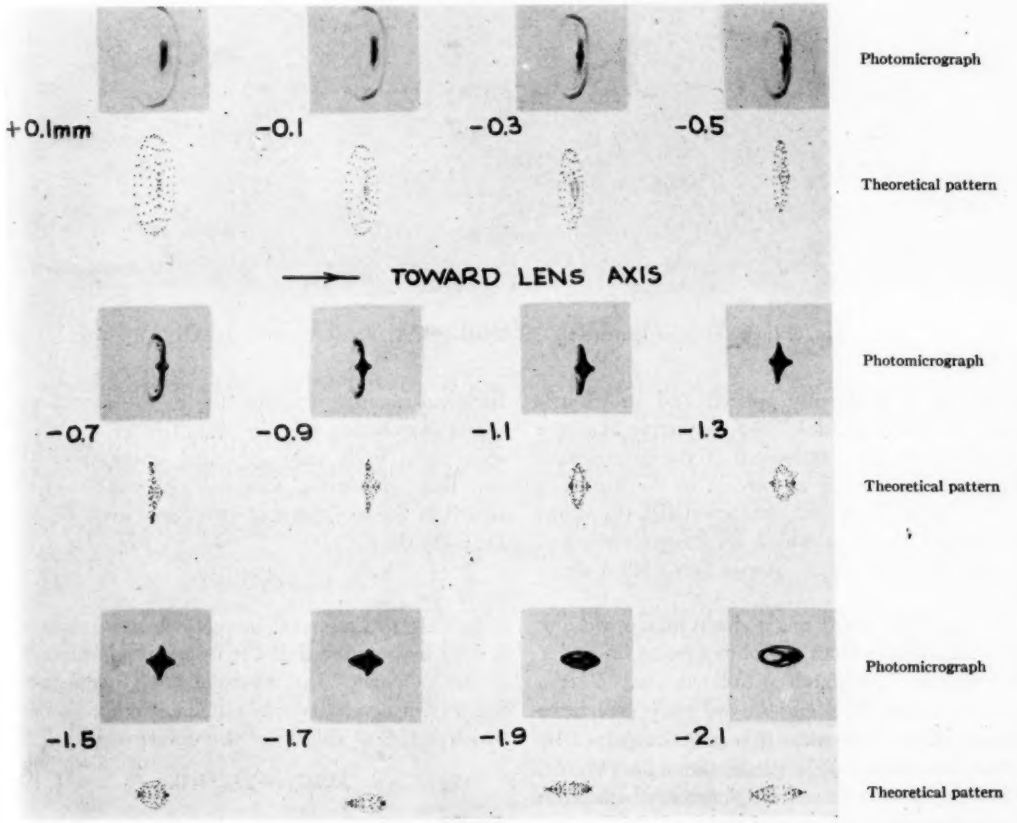

FIG. 5. Image of point source—12″ f:5.0 5-H-30 lens.

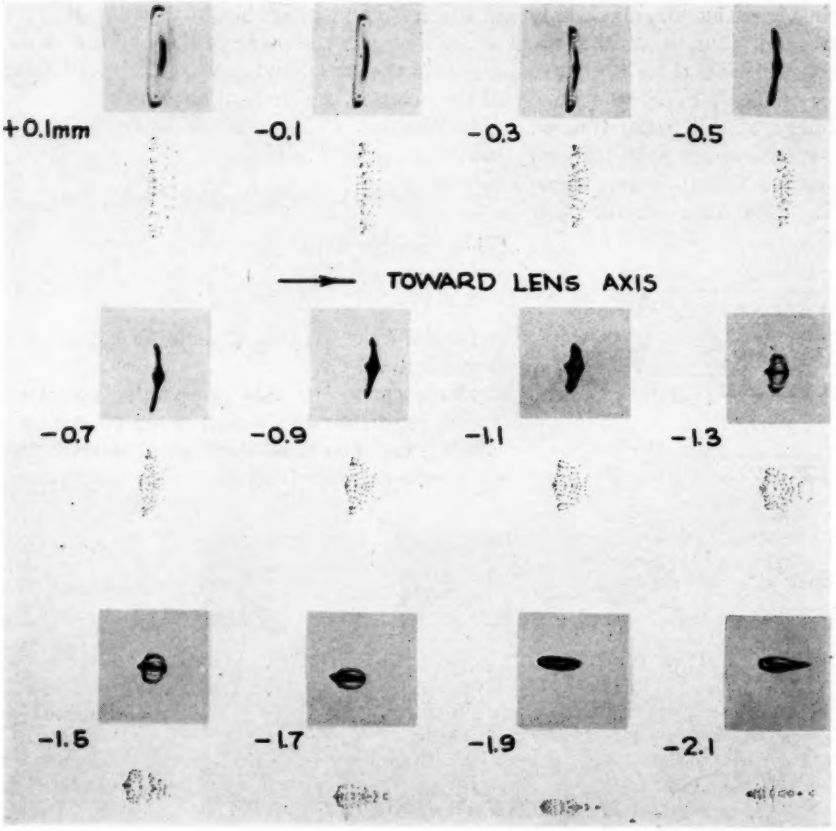

FIG. 6. Image of point source—12″ f:5.0 5-H-30 lens. 15°

of ξ' and ζ' uniformly spaced and sufficiently dense in the permissible area, we arrive at a new spot diagram, the equivalent of the former spot diagram. Continuing as before, we see that our knowledge of the mixed characteristic, W, allows us to trace the rays which we have chosen and to plot their points of intersection with a series of planes.

If the object point has a sharp image, we find that, for all rays from the object point, h' and z' are constant. Although it follows that D is a linear function of v and w, we may still have "image errors," because this point may not lie in the Gaussian image plane (field curvature), or its height may differ from $f' \tan \sigma$, which is the requirement for undistorted imagery.

If the image is not sharp, it should be symmetrical about a straight line in the meridional plane, so that it has the qualities of a general axis point with only spherical aberration. We call this *symmetrical imagery*, the condition for which is the existence of two constants, C_1 and C_2, such that

$$D_v = C_1 D_w + C_2. \qquad \text{(II, 9)}$$

In case symmetrical imagery is not achieved, it may be possible that the image is symmetrical about a curve, the so-called *half-symmetrical imagery*, a necessary and sufficient condition for which is the vanishing of the determinant,

$$D_{vv} D_{ww} - D_{vw}^2 = 0. \qquad \text{(II, 10)}$$

In this case, we speak of *errors of asymmetry*, meaning the deviation of the curved axis from a

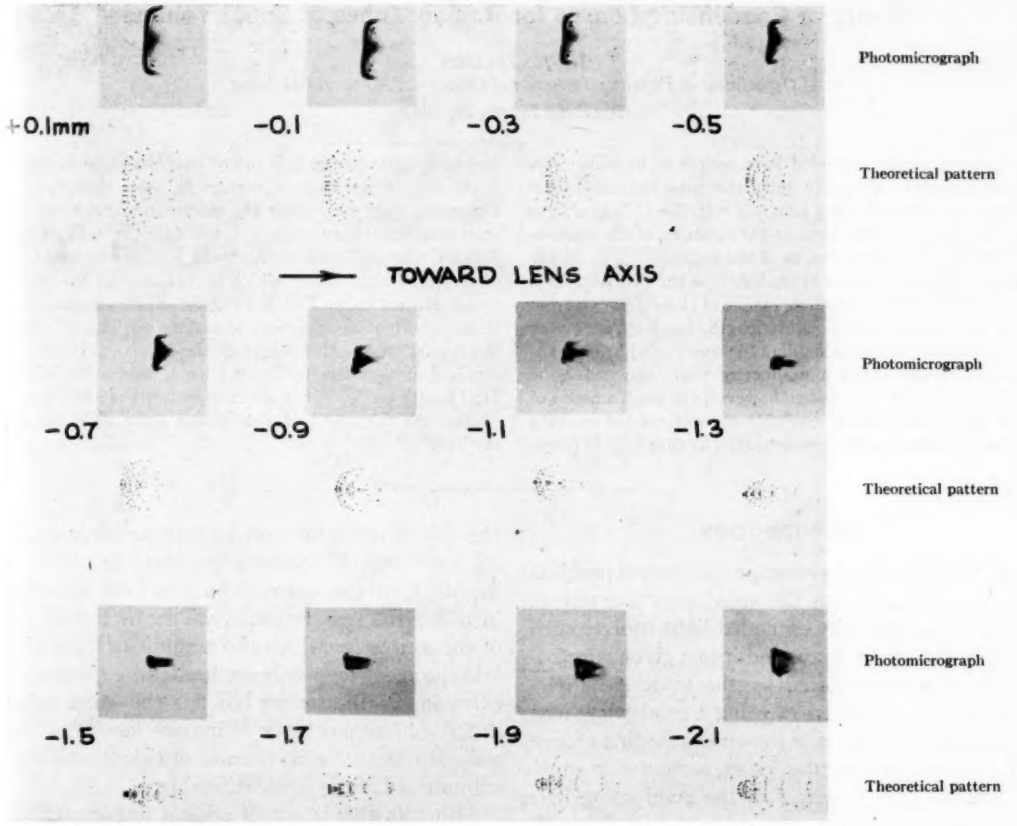

FIG. 7. Image of point source—12″ f:5.0 5-H-30 lens. 20°

straight line. The right side of (II, 10), if not zero, gives a measure for the deformation error. In the case of symmetrical and half-symmetrical imagery, the diapoints form the axis of symmetry, so that a graphical picture of the errors of symmetry of a system may be obtained by plotting these diapoints.

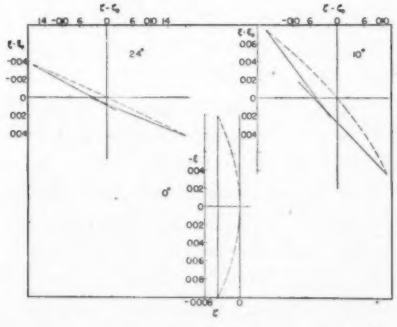

FIG. 8. Vignetting diagram for ξ and ζ.

The method developed here allows us to examine the geometrical-optical image of a point. Although it is not difficult to predict with accuracy from these pictures the imagery of straight lines or the resolving power of the system from points and lines, a more detailed analysis will be contained in a forthcoming paper.

ACKNOWLEDGMENT

I wish to acknowledge the help of my assistants: H. O. Hoadley, who helped with the preparation of the manuscript, and especially H. Jenkins, who worked out in detail the enormous number of numerical calculations for this paper.

Theory of Condensing Lenses for Raman Tubes of Small Volume*

J. RUD NIELSEN
Department of Physics, University of Oklahoma, Norman, Oklahoma

(Received March 29, 1947)

For a spatially extended light source of uniform cross section, such as a Raman tube, the most favorable focal length of the condensing lens is $F=hf/(b-s)$, where $2h$ is the extension of the source in the direction of the spectrograph slit, f the focal length of the collimator lens, $2b$ the height of the prism, and $2s$ the length of the slit. With such a condensing lens, placed a distance of $(h+s)f/(b-s)$ from the slit, the greatest possible length, $l_{max}=h^2f/bs$, of the source is fully effective in filling the spectrograph. This was proved by the writer a number of years ago under the assumption that $h \gg s$. Often, however, the small amount of the scattering material available necessitates the use of a Raman tube of small cross section. The case $h \leqq s$ is therefore investigated here. It is shown that the theorem stated holds also in this case. However, in order that the full amount of light may enter the spectrograph, some of the scattered light must pass out through the wall of the Raman tube and pass through the condensing lens at a distance from the center which is greater than the radius of the Raman tube. This has certain disadvantages. It is therefore often advantageous to make $h=s$, in which case the maximum effective length of the Raman tube can be attained more satisfactorily by using a condensing lens of focal length $sf/(b+s)$ immediately in front of the slit and placing the front end of the Raman tube right against the lens.

INTRODUCTION

A NUMBER of years ago the general problem of determining the maximum amount of light that a spatially extended light source, such as a Raman tube, may send into a given spectrograph was investigated by the writer.[1] In particular, the advantage of using a condensing lens was studied, and it was shown that with a source of uniform rectangular cross section the most favorable focal length F of the condensing lens is equal to $hf/(b-s)$, where f is the focal length of the collimator lens of the spectrograph, $2b$ the height of the prism (or of the rectangular collimator aperture), $2s$ the length of the spectrograph slit, and $2h$ the height of the source, i.e., its extension parallel to the slit. It was assumed that the height, rather than the width $2g$ of the source, is the limiting factor, as will generally be the case. For a circular Raman tube of internal radius r, it is usually accurate enough to put $h=g=2^{-\frac{1}{2}}r$. With such a condensing lens, placed so that its distance z from the slit is equal to $(h+s)f/(b-s)$, the length of the source which is fully effective in filling the spectrograph with light has its greatest possible value h^2f/sb. The diameter of the condensing lens must be sufficiently large, and the source must be placed on the axis of the collimator in such a position that its back end is focussed on the slit. By the length, l, of the source which is fully effective in filling the spectrograph, we mean the length of the source for which the amount of light sent into the spectrograph is not limited by the lateral extension of the source but has the same value as for a luminous layer of infinite lateral extension. If the source is of uniform brightness, this amount of light is proportional to l.

Although this is not of critical importance, it is usually advantageous to design a Raman tube (or other "end-on" source) and its condensing lens in such a manner that the Raman tube has the maximum length that is fully effective with the cross section chosen. When that is done, the amount of light sent into the spectrograph is proportional to, and the required exposure time inversely proportional to, the square root of the volume of the scattering material, whereas otherwise the exposure time will increase more rapidly when the volume is reduced.

In the writer's previous paper—which will be referred to as I in what follows—the variation of the fully effective length l with the focal length F of the condensing lens and the distance z of the latter from the spectrograph slit was investigated only for the case in which h is considerably larger than s. Since it has become increasingly necessary to work with Raman tubes of very small volume, it is of interest to extend

* Paper presented at the winter meeting of the Optical Society of America, February 20–22, 1947, New York, New York.

[1] J. Rud Nielsen, J. Opt. Soc. Am. **20**, 701 (1930).

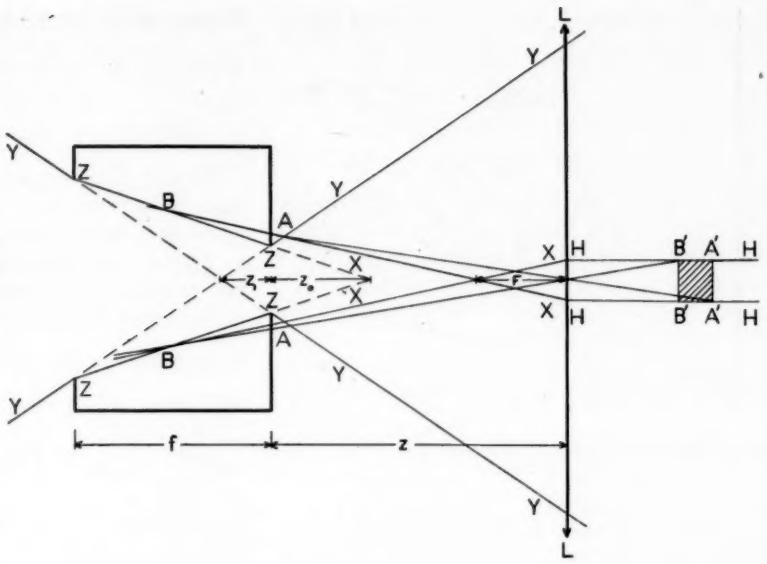

FIG. 1. Determination of fully effective length of source. Drawing is compressed in direction of the z-axis.

the work to the case $h \leqq s$. This will be done in the present paper.

FORMULAS FOR FULLY EFFECTIVE LENGTH

The determination of l as a function of F and z for fixed values of h, s, f, and b is carried out almost as in I, where proof was given for the validity of the procedure. Figure 1 illustrates the derivation for a certain set of values of F and z. For convenience of drawing, the figure is greatly compressed along the axis. HH is the top or bottom boundary of the light source; LL is the condensing lens of focal length F and distance z from the slit. The image of any point on the boundaries HH of the source will lie on the planes XX passing through the focus of the condensing lens. The spectrograph collimator is shown to the left in the figure. The lines YY and ZZ indicate planes passing through the upper and lower edges of the collimator aperture and the ends of the slit. The planes ZZ cut each other a distance $z_0 = sf/(b-s)$ in front of the slit, and the planes YY cut each other a distance $z_1 = sf/(b+s)$ behind the slit. The points A and B where XX cut either YY (in front of the slit or behind the collimator lens) or ZZ (between slit and collimator) are determined and also their image points A' and B'. The fully effective part of the source (hatched in Fig. 1) is that which lies between A' and B'. The distance l between A' and B' is found by means of the simple lens formula. In the case illustrated in Fig. 1, A lies in front of the slit and B between the slit and the collimator. If the distance z between the slit and the condensing lens is increased sufficiently, B will move to the left and lie on YY behind the collimator. A similar change in the positions of A occurs when the focal length F of the condensing lens is decreased. On the other hand, if z is decreased to a certain value A and B will join each other at the end points of the slit, and l will have become zero. If z is further reduced XX will cut neither YY outside the collimator nor ZZ inside the collimator, and l will remain zero, i.e., no part of the source will be fully effective. An increase in F will have similar effect.

In Table I are listed the expressions found for l. Each formula holds for one of the regions I, II, III, or IV of F, z-space shown in Fig. 2. For convenience, the scale for z is $\frac{1}{5}$ of that for F.

The values of F and z used in drawing Fig. 1 are represented by a point lying in Region IV. The line $z = (h+s)F/h$, which separates Region I from Region II and II from IV, represents sets of values of F and z for which one or both of the points A and B in Fig. 1 lie at an endpoint of the slit. The line $z = (b+h)F/h - f$, which sepa-

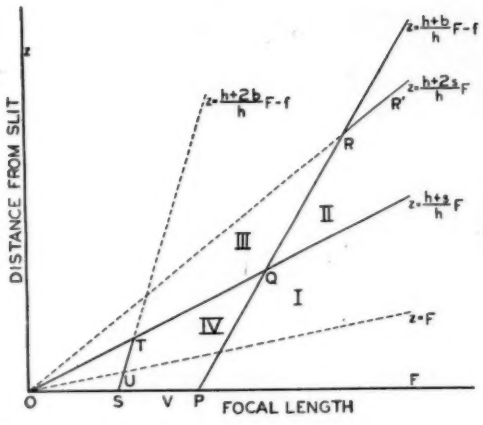

FIG. 2. Regions and points in F, z-space. Scale for z is one-fifth of that for F.

rates II from III and IV from I, represents sets of F, z values for which one or both of the points lie at the edge of the collimator aperture.

The two lines cut each other in a point Q having coordinates $F=hf/(b-s)$ and $z=(h+s)f/(b-s)$. The line $z=(b+h)F/h-f$ cuts the F-axis in a point P having coordinates $F=hf/(h+b)$ and $z=0$.

GREATEST VALUE OF FULLY EFFECTIVE LENGTH

The problem is to determine the value of F and z for which the fully effective length l of the Raman tube has its greatest value. Since l is given by different expressions in the four regions shown in Fig. 2, these regions must be considered separately.

Region I.—In this region $l=0$ throughout. This does not mean, of course, that all sets of F, z-values in this region are equally ineffective but rather that for no set is any part of the source fully effective. The somewhat formal character of the criterion used here for the effectiveness of an end-on source or a Raman tube is clearly illustrated by the fact, which will be proved below, that the point in F, z-space for which l has its maximum value is on the border of Region I.

Region II.—In order to investigate the variation of l over this region it is convenient to introduce the variable $u=z-F$ and to regard l as a function of u and F. We find from (2)

$$l(F,u)=(z_0+z_1)(hu-sF)F/s(u-z_0)(u+z_1). \quad (6)$$

Differentiation with respect to F gives

$$(\partial l/\partial F)_u=(z_0+z_1)(hu-2sF)/s(u-z_0)(u+z_1), \quad (7)$$

and

$$(\partial^2 l/\partial F^2)_u=-2(z_0+z_1)/(u-z_0)(u+z_1). \quad (8)$$

Thus, l, regarded as a function of F for constant u, will have a maximum or a minimum when $hu-2sF=0$, i.e., along the straight line $z=(2s+h)F/h$ which passes through the origin and cuts the upper borderline $z=(h+b)F/h-f$ of Region II in the point

$$F=hf/(b-2s), \quad z=(h+2s)f/(b-2s),$$

and

$$u=2sf/(b-2s), \quad (9)$$

indicated by R in Fig. 2.

Since $u>z_0=sf/(b-s)$ in the entire Region II, $(\partial^2 l/\partial F^2)_u$ is negative at any point on the line RR'. It follows that, when u is regarded as a constant parameter $>2sf/(b-2s)$, $l(F,u)$ is a maximum on the line RR'. Its value there, obtained by substituting $u=2sF/h$ into (6), is

$$l_{RR'}=\lambda_1(u)h^2(z_0+z_1)/4s^2, \quad (10)$$

where

$$\lambda_1(u)=u^2/(u-z_0)(u+z_1). \quad (11)$$

Since the derivative

$$d\lambda_1/du=-u((z_0-z_1)u+2z_0z_1)/(u-z_0)^2(u+z_1)^2 \quad (12)$$

is negative for all the values of u considered, $l_{RR'}$ is greatest for the lowest value of u, i.e., at

TABLE I. Fully effective length for different regions in F, z-space.

Region	l	
I	0,	(1)
II	$\left(\frac{z+(1+h/s)z_1}{z-F+z_1}-\frac{z-(1+h/s)z_0}{z-F-z_0}\right)F$,	(2)
III	$\frac{2hz_1F}{s(z-F+z_1)}$,	(3)
IV	$\left(\frac{z-(1+h/s)z_0}{z-F-z_0}-\frac{z+(1-h/s)z_1}{z-F+z_1}\right)F$,	(4)

where

$$z_0=sf/(b-s), \text{ and } z_1=sf/(b+s). \quad (5)$$

the point R. When this value of u, given by (9), and the expressions (5) for z_0 and z_1 are substituted in (10) the value for l at the point R is found, after some reduction, to be

$$l_R = 2h^2f/3bs. \tag{13}$$

We next have to consider the part of Region II which lies below the line $u = 2sf/(b-2s)$ passing through R. It is easily verified that $(\partial l/\partial F)_u < 0$ throughout this space, so that for a given u, l will have its greatest value on the borderline QR. On this line the fully effective length is

$$l_{QR} = 2h^2f/b(b+s-hf/F), \tag{14}$$

which increases with decreasing F. Thus, the greatest value of l in the entire Region II is found at the point Q where F has its smallest value, $hf/(b-s)$. It is

$$l_Q = h^2f/bs. \tag{15}$$

Region III.—The expression (3) increases with decreasing z for all constant values of F. The greatest value of l in this region will therefore occur on the borderlines to Regions II and IV. One of these has already been considered. On the line OQ separating Regions III and IV

$$l_{OQ} = 2h^2z_1/s(s+hz_1/F). \tag{16}$$

This increases with increasing F and reaches its greatest value at the point Q. For l_Q we get again (15).

Region IV.—It is convenient also to introduce here the variable $u = z - F$.

We get from (4)

$$l(F, u) = ((z_0+z_1)sF - (z_0-z_1)hu - 2hz_0z_1)F/s(u-z_0)(u+z_1), \tag{17}$$

$$(\partial l/\partial F)_u = (2(z_0+z_1)sF - (z_0-z_1)hu - 2hz_0z_1)/s(u-z_0)(u+z_1), \tag{18}$$

$$(\partial^2 l/\partial F^2)_u = 2(z_0+z_1)/(u-z_0)(u+z_1). \tag{19}$$

Thus a maximum or a minimum of $l(F, u)$, regarded as a function of F with the constant parameter u, occurs where

$$2(z_0+z_1)sF - (z_0-z_1)hu - 2hz_0z_1 = 0$$

or

$$u = 2bF/h - f, \quad z = (2b+h)F/h - f.$$

This is a straight line which cuts the boundaries of Region IV in the points S and T having coordinates

$$F = hf/(2b+h), \quad z = 0, \quad u = -hf/(2b+h) \tag{20}$$

and

$$F = hf/(2b-s), \quad z = (h+s)f/(2b-s), \quad u = sf/(2b-s), \tag{21}$$

respectively. It is readily shown that when $h \leqq s$ (19) is negative for all points between S and T. Thus, along all lines $u =$ constant cutting ST, l has a maximum on ST. This maximum is found to be

$$l_{ST} = \lambda_2(u)sh^2f/2b(b^2-s^2), \tag{22}$$

where

$$\lambda_2(u) = (u+f)^2/(z_0-u)(u+z_1). \tag{23}$$

The derivative,

$$d\lambda_2/du = 2b^2fu(u+f)/(b^2-s^2) \times (z_0-u)^2(u+z_1)^2, \tag{24}$$

is positive for $u > 0$ and negative for $u < 0$. The smallest value of λ_2, and hence of l_{ST}, therefore occurs at the point U where the line $u = 0$ cuts ST. The value of l_{ST} at this point is

$$l_U = h^2f/2bs. \tag{25}$$

The greatest values of λ_2, and hence of l_{ST}, occur at the endpoints S and T. We find

$$l_S = 2sh^2f/b(4s^2-h^2) \tag{26}$$

and

$$l_T = 2h^2f/3bs = l_R. \tag{27}$$

For $h < s$, $l_T > l_S$, whereas these two values are equal when $h = s$.

We have now considered the part of Region IV which lies between the lines $u = hf/(2b+h)$ and $u = sf/(2b-s)$. It remains to consider the parts for which $sf/(2b-s) < u \leqq sf/(b-s)$ and $-hf/(h+b) \leqq u < -hf/(2b+h)$. Both of these areas lie to the right of the line ST where $(\partial l/\partial F)_u < 0$, as is seen from (18). In searching for the greatest value of l, it is therefore sufficient to consider points lying on the boundary lines TQ and SP. The points lying on TQ were considered as belonging to Region III, so there remains only to study the variation of l over the segment SP of the F-axis.

Substituting $z = 0$ and (5) in (4) we get

$$l_{SP} = 2sf(hf-(b+h)F)F/((b-s)F+sf) \times (sf-(b+s)F), \tag{28}$$

TABLE II. Fully effective length at selected points in F, z-space for $h<s$.

Point	F	z	l
P	$hf/(b+h)$	0	0
Q	$hf/(b-s)$	$(h+s)f/(b-s)$	h^2f/bs
R	$hf/(b-2s)$	$(h+2s)f/(b-2s)$	$2h^2f/3bs$
S	$hf/(2b+h)$	0	$2h^2sf/b(4s^2-h^2)$
T	$hf/(2b-s)$	$(h+s)f/(2b-s)$	$2h^2f/3bs$
U	$hf/2b$	$hf/2b$	$h^2f/2bs$
V	$\frac{[s^2(b+h)-bs(s^2-h^2)^{\frac{1}{2}}]f}{2bs^2+b^2h+sh^2}$	0	$\frac{2[s(b+h)-b(s^2-h^2)^{\frac{1}{2}}]^2f}{b[(b+s)(s+h)^{\frac{1}{2}}-(b-s)(s-h)^{\frac{1}{2}}]^2}$

which, for $h<s$, goes to zero when F approaches $hf/(b+h)$, i.e., when the point $(F, 0)$ approaches P. It is not difficult to show that l_{SP} is a maximum when F has the value

$$F'=[s^2(b+h)-sb(s^2-h^2)^{\frac{1}{2}}]f/(2bs^2+b^2h+s^2h), \quad (29)$$

which corresponds to a point V on the segment SP. Substituting (29) in (28) we find, after some reduction,

$$l_V=2f[s(b+h)-b(s^2-h^2)^{\frac{1}{2}}]^2/b[(b+s)(s+h)^{\frac{1}{2}}-(b-s)(s-h)^{\frac{1}{2}}]^2. \quad (30)$$

It can be shown that, for $h<s$, this is smaller than l_Q.

The values of the fully effective length, found for $h<s$ for the special points marked in Fig. 2, are summarized in Table II. We see that, as in the case $h>s$ treated in I, the fully effective length has its greatest value h^2f/bs when $F=hf/(b-s)$ and $z=(h+s)f/(b-s)$.

The case $h=s$ requires a small amount of special consideration. As h approaches s, F' approaches the value $sf/(b+s)=z_1$ which is the ordinate of the point P when $h=s$. Thus, the point V merges with P. It is readily shown that l_V increases monotonously as the ratio h/s is increased. In the limit l_V approaches the maximum value

$$l_1=sf/b. \quad (31)$$

This is equal to the value found for l_Q when $h=s$. In this case, the greatest possible value l_1 of the fully effective length of the source can be attained in two different ways, either by letting $F=sf/(b-s)$ and $z=2sf/(b-s)$ or by letting $F=sf/(b+s)$ and $z=0$. The results obtained for $h=s$ are summarized in Table III.

DISCUSSION

It will be seen from the formulas given here, and from Tables II and III, that the fully effective length does not vary greatly over considerable areas of F, z-space. Thus, there is a great deal of latitude in the design of Raman tubes and condensing lenses. It is an interesting fact that the optimum point Q in F, z-space, and for $h=s$, also the equally favorable point V, lie on the border of Region I in which $l=0$. Of course, although l is discontinuous at these points, there is no discontinuity in the amount of light which enters the spectrograph.

The foregoing analysis leads to the same expressions for the maximum fully effective length and the optimum focal length as found in I. For $h=s$, it gives an alternative choice for F and z. As in I, it has been assumed that the index of refraction of the luminous source is nearly equal to that of air. If the Raman tube contains a liquid the value of $l_{\max}$ will be increased.

It should be pointed out that in order that the full amount of light may get into the spectrograph, some of the scattered light, especially from the back end of the Raman tube, must pass out through the wall of the Raman tube and pass through the condensing lens at a distance from the center which is greater than the radius of the Raman tube. If the glass of the wall contains inhomogeneities, or if there is dust on the outside wall, a disturbing amount of unshifted light may thus get into the spectrograph. The use of a Raman tube with $h<s$ in the standard manner (represented by the point Q) is therefore not entirely satisfactory. This objection is not valid when $h\gg s$, for, in this case, the amount of light going outside the front aperture of the Raman tube is so small that it can be masked off with negligible decrease in the amount of light utilized in the spectrograph.

Using the approximate relation $h=r/2^{\frac{1}{2}}$ between h and the internal radius of the Raman tube, we find $V=2\pi h^2l$ for the volume of the latter. If it is desired to design a Raman tube so that its length is equal to h^2f/bs, the maximum fully effective length, we have two relations between the four quantities V, l, h, and s. Two of these quantities can therefore be chosen at

w ll. In many cases V is given by the amount of a ailable material. Usually, l is next chosen so as to give an exposure time that is not inconveniently long. If V is small, the values thus determined for h and especially for s will be small, and the spectral lines will be short. The resulting spectrum will not lend itself well to photometry. If it is required to make accurate measurements of the intensity distribution in the spectrum, s, rather than l, must be chosen together with V. If V is very small, say of the order of one milliliter or less, the case $h<s$ may then arise. When the value of h obtained in one or the other of these ways lies fairly close to the corresponding value of s, it will usually be most satisfactory to make adjustments such that h and s become equal and to use a condensing lens of focal length $sf/(b+s)$ placed immediately in front of the slit with the front end of the Raman tube against the lens.

TABLE III. Fully effective length at selected points in F, z-space for $h=s$.

Point	F	z	l
P	$sf/(b+s)$	0	0
Q	$sf/(b-s)$	$2sf/(b-s)$	sf/b
R	$sf/(b-2s)$	$3sf/(b-2s)$	$2sf/3b$
S	$sf/(2b+s)$	0	$2sf/3b$
T	$sf/(2b-s)$	$2sf/(2b-s)$	$2sf/3b$
U	$sf/2b$	$sf/2b$	$sf/2b$
V	$sf/(b+s)$	0	sf/b

Index to the Literature on Spectrochemical Analysis

THE American Society for Testing Materials through its Committee E-2 on Spectrographic Analysis has sponsored the publication of two indexes on the Literature on Spectrochemical Analysis. One, issued in 1940, covered the years from 1920 to 1939; the second, now available, covers the period from 1940 to 1945, inclusive. The first index has almost 1500 references on such subjects as light sources, quantitative analysis, etc. The second index (Part II) has almost a thousand contributions to literature in this field and there is an important addition, namely brief abstracts of the material. This was done because of the scarcity of many of the journals in which the articles appeared, on account of wartime problems. The work of maintaining and compiling these indexes is carried out under the direction of Bourdon F. Scribner and William F. Meggers, National Bureau of Standards.

Each of the publications has a detailed subject index. Copy of Part II of the index, covering 200 pages, in heavy paper cover, can be procured at $3.00 each. Part I, a 100-page publication, is available at $1.50. For both parts the price is $3.75. They can be obtained from A.S.T.M. Headquarters, 1916 Race Street, Philadelphia 3, Pennsylvania.

The Visibility of Lines and Squares at High Brightnesses[1]

SELIG HECHT, SHERMAN ROSS,[2] AND CONRAD G. MUELLER[3]
Laboratory of Biophysics, Columbia University, New York, New York

Field experiments show that a wire may be seen against a sky of high brightness when its diameter subtends only half a second of visual angle. For this the wire must be at least one degree long. Shorter wires must be thicker. Silhouetted squares may be seen at angles of only 18 seconds. Considering length and width, squares are more efficient visual targets than fine lines by about a factor of 3.

I. PREVIOUS WORK

At the limits of visibility most objects become blobs whose shapes lie between the two extremes of a long line and a radially symmetrical disk or square. The visual angle at which these two types of target can just be resolved is in some uncertainty, to judge by the diverse values already published.

For a single dark line against a luminous background Aubert (1865) records a minimum visual angle of 6 seconds, while Hartridge (1922) gives 3.6 seconds. However, Barnard (1897–8) found the thickness to be 0.44 second, while Lowell (1903) gives values between 0.73 and 1.13 seconds depending on the certainty of seeing. Pickering (1915) similarly records minimal angles between 0.82 and 1.15 seconds for different degrees of certainty.

More recently Hecht and Mintz (1939) found that the angle varies with brightness, and that at a maximum indoor brightness of 30 footlamberts they could resolve binocularly a line subtending only 0.5 second. From their data it seems likely that at still higher brightnesses the angle would be slightly but not much less. In addition, Byram (1944) has shown for a similar target that the just resolvable angle varies with the pupil size. For the maximum pupil (2.43 mm diameter) at a brightness of 5000 footlamberts Byram records an angle of slightly over 0.5 second.

For a dark spot on a luminous background the values are much larger, as is to be expected; but in addition the published figures vary much less widely from one another. Thus Hueck's (1840) measurements of 30 seconds agree with those of Aubert (1865) who gives values between 25 and 29 seconds, not too far from the more recent measurements of 30.1 to 33.6 seconds recorded by Pickering (1915). Byram (1944) has shown that the angle varies with pupil size and that with a pupil of 2.43 mm and a brightness of 1200 millilamberts, the disk diameter is just over 31 seconds.

II. PRELIMINARY OBSERVATIONS

We were able to make field measurements of the visual angle for the resolution of lines and squares by means of the parachute training towers at Camp Lejeune, North Carolina. The ground for several miles around the towers is flat, and the towers are easily seen from appropriate vantage points. Moreover, surrounding the towers for a diameter of about a mile is a cleared level area only partly overgrown with low brush. Targets suspended from the towers can therefore be viewed against the sky from measured distances under controlled conditions.

Even casual observation shows that the values of 3 to 6 seconds as the resolution angle for a line cannot be correct. The $\frac{5}{16}$-inch cable which raises and lowers the parachutes can easily be seen against the sky at a distance of about three-fourths of a mile. At this point the cable thickness subtends about 1.5 second of arc. However, a black wire half as thick ($\frac{5}{32}$ inch) can also be seen at this distance. We suspended 125 feet of such a wire from the parachute attachment block and kept it taut by tying a heavy weight to its free end. The wire was seen at all times against the daylight sky, even at a distance of 0.7 mile.

Similar tests with a $\frac{1}{16}$-inch black wire found us

[1] Part of this work was done under a contract, recommended by the Committee on Medical Research, between the Office of Scientific Research and Development and Columbia University. The measurements were made at Camp Lejeune, North Carolina, in the Summer of 1945. Opinions here expressed are those of the authors and are not official with the Navy Department. Publication assisted by the Ernest Kempton Adams Fund for Physical Research of Columbia University.

[2] Ensign, U.S.N.R.; now at Bucknell University, Lewisburg, Pennsylvania.

[3] Ensign, U.S.N.R.

(SH and CGM) able to see it at half a mile with almost complete certainty. At 0.7 mile recognition was uncertain, while at 0.6 mile we could see the wire frequently enough to judge that we were near the threshold of resolution for such a test object. These dimensions yield values of the order of 0.5 second visual angle.

III. EXPERIMENTS

Using the parachute towers and the procedure to be described in Section IV, we made determinations of several aspects of the visibility of lines and squares and of the influence that wearing neutral tint sunglasses had on them.

1. We measured the visual angle which a single black line must subtend in order to be recognized against the daylight sky. Under the present circumstances this reduces to determining the frequency with which the presence of a wire can be correctly ascertained from different distances.

2. We determined what effect the wearing of neutral tint sunglasses ($N-1$) has on this visual angle. The sunglasses are the plastic brow-rest neutral variety made by the Polaroid Corporation. On the average they transmit 12 percent of the light. The measurements with sunglasses were made at the same time as the first project which served as control.

3. We ascertained the influence of the length of line on the visual capacity to resolve its width. The question may be formulated in this way. How long need a line be so that making it any longer will not influence the ability of the eye to pick it up against the sky?

4. We measured the visual angle which a square must subtend when its presence can be recognized as silhouetted against the daylight sky.

5. We determined the effect that wearing sunglasses had on this visual angle. This too was determined simultaneously with project 4 which served as control.

IV. ARRANGEMENT AND PROCEDURE

For present purposes the parachute tower is to be considered merely as a vertical support 250 feet high having two horizontal arms at the top which project about 20 feet on each side. Each arm has a block which may be raised and lowered, and to which a black wire can be attached. At its other end the wire has a heavy iron weight, so that when the wire is raised by the block on the projecting arm, it is held stretched and steady. The structure and arrangements are shown in Fig. 1.

For the measurements of a single line a black $\frac{1}{16}$-inch wire was used. Micrometer determinations of its thickness showed it to be very uniform at 0.066 inch, with no deviation greater than 0.6 percent.

When the block is raised and the weight at the end of the wire is about 2 feet from the ground, the weight cannot be seen at distances greater than a few hundred feet from the tower. This is because of the low shrubbery between weight and observer, and even more because of the distant background trees in front of which the weight seems to disappear.

The wires from the two arms are not identical in length. Because of the shape of the background trees the segment of the wire visible against the sky on the left arm occupies 35 mils (2°) while the comparable segment on the right occupies only 30 mils (1.7°).

An observer on the ground beyond 200 feet can see the attachment block rising to a given distance above the ground. He cannot see the bottom of the attached wire nor the weight tied to it. Thus the block may have a wire suspended from it, or it may not, and it is the task of the observer to decide which is the case. Each observation is an independent judgment of the presence or absence of the wire.

In our first tests with the wire, each block was up for 2 minutes, during which time the observer

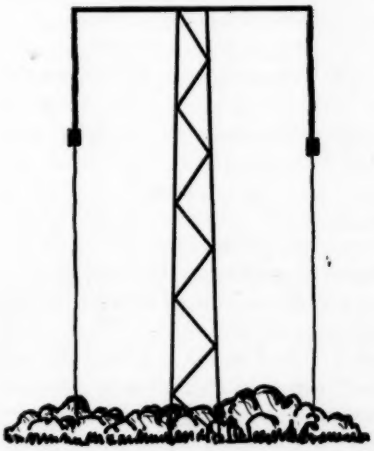

FIG. 1. Schematic view of parachute tower and background trees. The tower is 250 feet from the ground and the arms extend 20 feet to either side. To the heavy rectangular block there may be attached a wire whose presence is to be observed. The wire is held taut by a heavy weight at its bottom; the weight is invisible against the background of trees.

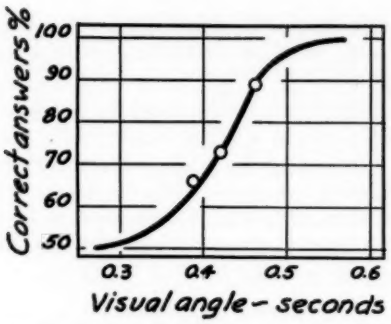

FIG. 2. Visual angle of suspended wire and the frequency of correctly recognizing its presence.

had to make up his mind. This interval proved too long and was reduced first to 1½ minutes, and then to 1 minute. Even 1 minute was more than adequate since most observers make a proper judgment in a few seconds, and repeated looking and straining only result in fatigue rather than improved performance.

In most instances we used both projecting arms of the tower, alternating them. The block with or without suspended wire would be up on one side while preparations were being made on the other side. This would then be raised while the first arm was again being prepared. The sequence of presence or absence of the wires was unknown to any observer and was determined entirely by SR who with an assistant manipulated the tower machinery for raising and lowering the blocks. The schedule of presentations was randomized, and chance success was 50 percent.

All measurements with the wire were made from three distances directly north of the tower. The nearest distance was 2458 feet and had been accurately surveyed. The other two were 225 and 450 feet farther north. These we measured with a steel tape from the surveyed position.

For measurements with squares we used only the left arm of the tower. The targets were blackened cylinders 2.0, 2.5, and 3.0 inches in diameter; the height of each cylinder was the same as its diameter. When suspended vertically and seen in silhouette such cylinders look like squares, regardless of their rotation on the vertical axis. The cylinders were joined by a $\frac{1}{32}$ inch wire, which is invisible at the distance (2458 feet) of the observers.

The targets were presented in any or all of three specified positions along the suspended wire; these three positions could be easily identified by their proximity to obvious portions in the structural details of the tower. The presence of a target in any position was completely independent of the presence of targets in the other two positions. The presentation of a target in each position was random and each position was treated separately, so that chance success for it was 50 percent.

All observations with the wires and squares were made binocularly.

Brightness measurements of the background sky were made every fifteen minutes during the course of any experiment with a Macbeth Illuminometer. On most experimental days the sky was a clear blue, and there was little variation in its brightness of about 1000 millilamberts. When white clouds were part of the background, the brightness was generally about 2000 millilamberts, but sometimes it rose to twice this value. This high value occurred during part of the measurements on thin lines and for two days on which preliminary runs were made with square targets. The final runs with square targets were made against a clear blue sky.

V. FIRST MEASUREMENTS WITH WIRES

Before describing the final measurements made with and without sunglasses we wish to give the results found by five observers in a preliminary trial at a distance of 2458 feet. The observations were made on a brilliantly sunny afternoon with the sky a pale blue and a brightness of 1400 footlamberts. The subjects had all had some experience in scientific work and ranged in age between 18 and 50 years. The data are given in Table I.

It is clear that one can make an almost perfect

TABLE I. Frequency of correctly judging the presence of a 0.066-inch wire at a distance of 2458 feet. Sky brightness 1400 footlamberts.

Subject	Left side		Right side	
	No. of observations	No. correct	No. of observations	No. correct
DH	8	7	8	8
WNN	10	9	10	8
JFR	10	10	10	7
CGM	10	10	10	10
SH	10	10	10	9
Total	48	46	48	42

TABLE II. Recognition of 0.066-inch black wire as influenced by distance, sunglasses, and position. Sky brightness very nearly 4000 footlamberts.

Circumstances	Number of correct responses											
Distance from wire	2458 feet				2683 feet				2908 feet			
Visual angle of wire	0.461 sec.				0.422 sec.				0.389 sec.			
Sunglasses	without		with		without		with		without		with	
Position of wire	left	right	left	right	left	right	left	right	left	right	left	right
Subjects												
CGM	3	3	3	3	1	3	3	2	2	2	3	3
SH	3	3	3	2	2	3	2	3	2	2	2	2
HP	3	1	3	3	3	2	2	3	3	1	2	2
ATK	3	3	3	2	2	3	3	1	3	2	1	0
NA	3	3	3	3	2	3	3	3	2	2	3	3
JAM	2	3	3	3	2	3	2	1	2	2	2	3
CLB	3	3	2	2	1	3	1	2	2	1	3	2
AHM	2	2	1	3	1	3	2	2	1	1	2	2
NL	3	3	2	2	3	1	1	2	2	1	1	3
JFR	3	3	3	3	2	3	1	3	2	2	2	1
Total, $n=30$	28	27	26	26	19	27	20	22	21	16	21	21
Total, $n=60$	55		52		46		42		37		42	
Total, $n=120$	107				88				79			
Total percent correct	89				73				66			

judgment of the presence of the wire at this distance. The visual angle subtended by the wire is 0.461 second of arc.

From Table I it appears that the 35 mils long wire on the left side can be seen somewhat more easily than the 30 mils wire on the right. More extensive observations did not bear this out. However, it may vary with different observers. We shall consider this in detail later.

VI. DISTANCE, SUNGLASSES, AND FINE LINES

The final measurements of the frequency of correctly seeing a fine wire at different distances with and without sunglasses were made with ten subjects all of whom had had some scientific experience. They were made when there were thin clouds in the sky late on a sunny morning so that the brightness of the sky background was very nearly 4000 footlamberts.

The observers began at the first position of 2458 feet from the tower. The blocks were raised alternately, each for a minute and a half, and each observer made a judgment as to whether there was a wire attached to the block. Each block went up three times, and the judgments were binocularly with the naked eyes.

Remaining in the same position, the subjects put on the sunglasses, and after allowing a few minutes for adaptation went through a similar sequence of observations.

The group then moved to a distance of 2683 feet from the tower and a series of six measurements was made first without sunglasses and then with them. Finally, the observers moved to 2908 feet from the tower, and the series was repeated as before, first without sunglasses and then with them. Thus at three different distances each subject made three judgments each of the left target and of the right target, and then repeated both with sunglasses on.

The results are given in detail in Table II from which several things become clear at once. Apparently the position of the target is unimportant. Therefore, the length of the wire between 30 and 35 mils does not influence its capacity to be recognized. Adding the number of correct judgments for all the left (35 mils) presentations gives 135 correct out of 180 trials, or 75 percent. Similarly the total of correct right (30 mils) judgments is 139 out of 180 trials, or 77 percent. The difference is negligible; its critical ratio is 0.40, which means that it has a 70 percent chance of being purely fortuitous.

Table II also shows that the sunglasses have no influence on the visibility of a fine wire at this high brightness of background sky. Adding all the values without glasses gives 138 correct

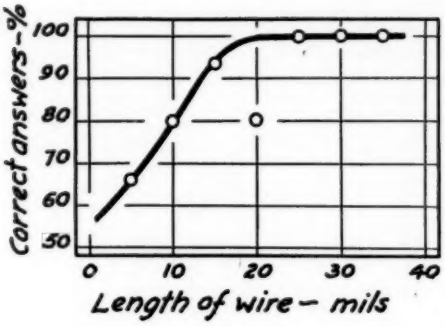

FIG. 3. Influence of angular length of wire on the frequency of correctly recognizing its presence. Width of wire occupies visual angle of 0.461 second.

judgments out of 180 trials, or 77 percent. Adding all the values with glasses gives 136 correct judgments out of 180 trials, or 76 percent. The difference of 1 percent is meaningless; it has a critical ratio of 0.20, which is interpreted as an 84 percent probability of being pure chance.

Since neither the position of the target nor the sunglasses influence the measurements, all the data at a given distance from the target may be combined. Table II then shows that distance does influence the frequency of seeing the wire.

The precise relation between distance and frequency of seeing may best be presented graphically as in Fig. 2. Here we have plotted the three values from Table II as percent correct answers against visual angle in seconds of arc subtended by the diameter of the wire. Through the points we have drawn the best frequency curve extending between 50 and 100 percent correct responses.

Figure 2 shows that for the wire to be seen with perfect certainty it has to subtend about 0.51 second of arc; that is, it would have to be about 2000 feet away. To be seen with only 95 percent certainty, it needs to subtend a visual angle of only 0.48 second. With 75 percent certainty the wire can be seen at a visual angle of 0.43 second.

VII. INFLUENCE OF LENGTH

Common experience indicates that the length of a linear target influences its visibility. In the measurements of Hecht and Mintz the diameter of the field was about 7° visual angle, and the wire was the same length. In Byram's work the length of the line was 1°, and in our own measurements it was between 1.7° and 2°. Since the minimum resolvable diameter in all three investigations is approximately the same it follows that even a 1° length does not decrease visibility.

We set out to discover the necessary minimum length by determining the frequency of seeing the $\frac{1}{16}$-inch wire for different lengths of wire when it is viewed from a distance of 2458 feet. We used five subjects and the experiment was made in the early afternoon of a sunny day against an almost clear blue sky of 2000-millilambert brightness. The procedure was as before except that each presentation lasted only one minute. Five presentations were made for each side of the tower, the two sides alternating.

The original wires were 125 feet long, but because of the background an observer could see only a segment of the left wire 35 mils long and 30 mils of the right wire. After five observations had been made of each side, the wires were shortened by 10 mils each, so that they presented segments of 25 and 20 mils, respectively. Each observer then made five determinations on each side as before. Then 10 more mils of wire were removed to yield visible segments of 15 and 10 mils length, and the observations were repeated as before. Finally an additional 10-mil length was removed from the left wire, which now showed only a 5-mil segment, and the observations repeated on that side alone.

The details of the experiment are given in Table III. From the results it appears that for segments between 15 and 35 mils, length does not influence the frequency of correct responses to the presence of the wire. The frequency of correct answers fluctuates enough from length to length in this range so that no clear trend is visible.

TABLE III. Length of wire and visibility. Diameter of wire is 0.461 second of arc.

Subject	Number of correct responses 35 mils	30 mils	25 mils	20 mils	15 mils	10 mils	5 mils
NA	5	5	5	4	4	4	4
HP	4	3	4	5	3	1	3
SW	5	5	5	4	5	5	4
CGM	5	5	5	4	5	3	2
SH	4	4	5	3	5	2	3
Total $n=25$	23	22	24	20	22	15	16
Percent correct	92	88	96	80	88	60	64

However, below 15 mils, the frequency of correct answers drops sharply, and one may therefore set 15 mils as the value of the necessary segment.

Nevertheless, even for longer segments there are enough errors to keep the values from perfect certainty. The average of all the values between 15 and 35 mils is 88.8 percent correct, which is identical with the 89 percent correct answers found in Table II, with the 10 observers in the preceding experiment using only the 35- and 30-mil segments. Evidently this is the average frequency for an angle of 0.461 second, and no matter how long the wire is, it will not be seen with a greater frequency by a random group of moderately trained subjects.

Examination of Table III reveals that three of the five subjects made perfect scores with the 35-, 30-, and 25-mil lengths. Two of these three observers had participated in the experiment described in Table II and had made perfect scores for the 35- and 30-mil lengths at an angle of 0.461 second. Moreover, four other observers recorded in Table II had also secured perfect scores under these conditions. Evidently the lower than perfect certainty recorded by the group as a whole is due to the few individuals whose vision is not quite as good as that of the majority.

Because of this lowering of the average, we have considered separately the results of the three individuals (NA, SW, and CGM) who made perfect scores for 35 and 30 mils in Table III. Their averages are plotted in Fig. 3. Neglecting the obviously aberrant point at 20 mils, we have drawn a smooth curve through the other points. As in Table III there is a decided drop in the frequency of correct answers between 15 and 20 mils.

The data are not adequate for a fine determination of the critical length; but in Fig. 3 the curve becomes maximal at about 18 mils. Since each mil equals 3.43 minutes of arc, one may put this critical length at just above 1 degree. Evidently for a fine line to be recognized with maximum frequency, its length must cover about two-thirds the rod-free area of the fovea.

TABLE IV. Influence of size and sunglasses on frequency of recognition of silhouetted squares. Distance of observers, 2458 feet. Sky brightness, about 1000 millilamberts.

Size		Frequency of correct answers out of 144 trials			
		without sunglasses		with sunglasses	
inches	seconds	number	percent	number	percent
3.0	21.0	142	98.6	134	93.1
2.5	17.5	133	92.4	116	80.6
2.0	14.0	106	73.6	78	54.2

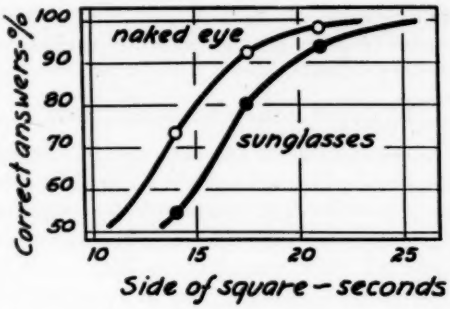

FIG. 4. Influence of wearing neutral sunglasses (transmission of 12 percent) on the visibility of small squares viewed against the sky. The sky brightness is just about 1000 millilamberts.

VIII. SQUARES AND SUNGLASSES

The measurements with squares were made essentially like those with fine lines. Four observers, all well-trained, served as subjects; one (CGM) had worked in the fine line series, while the other three were new. Observations were made during a period of three weeks, on afternoons of clear blue sky only and a brightness of about 1000 millilamberts.

For each size target each observer made a total of 36 judgments without sunglasses and 36 judgments with sunglasses. The data for all observers have been combined and are presented in Table IV.

The measurements are quite regular as is seen when they are plotted in Fig. 4. Contrary to the findings in the experiment with linear targets, sunglasses definitely influence the visibility of the squares in this experiment. Comparison of the two curves in Fig. 4 shows that to see a square through the sunglasses with the same certainty as without the glasses requires on the average an increase of 17.5 percent in the linear dimension of the square.

For the unencumbered eyes Fig. 4 shows that a silhouetted square can be seen with complete certainty if one side subtends a visual angle of 22

seconds; with 95 percent certainty it must subtend 18 seconds; and with 75 percent certainty, 14 seconds.

IX. SUNGLASSES AND BRIGHTNESS

The difference in the effect of wearing sunglasses in the two experiments needs some consideration, else the results might appear entirely fortuitous.

Sunglasses can cause a decrease in visual acuity because of their reduction in light intensity and/or because of their optical imperfections. The fact that there was no reduction in the visibility of single lines in the first experiment shows that optical imperfections if they existed were of no importance. One must therefore conclude that a reduction in brightness from 4000 millilamberts to about $\frac{1}{8}$ this value, that is to 500 millilamberts, produces no change in visual acuity.

The bundle of light from the test object which reaches the retina is limited by the pupil of the eye. Because the targets are so small and so far away the area of this beam as it passes through the sunglasses is practically the same size as the pupil. Moreover, the shape of the target, because of the small size and large distance, does not alter the area of this beam as it is cut by the glasses. Therefore, if sunglass imperfections do not affect the optics of a single line, they will not distort the image of a square. As a result one must look elsewhere for the cause of reduction of the visibility of squares by sunglasses.

The other factor concerned is light absorption, and this is probably the reason. The background brightness for the line measurements was 4000 millilamberts, while the brightness for the square measurements was only 1000 millilamberts. The sunglasses transmit about $\frac{1}{8}$ of the light. The measurements therefore tell us that whereas there is no appreciable change in visibility between 500 and 4000 millilamberts, there evidently is a 17.5 percent difference between 125 and 1000 millilamberts.

Previous work by Lythgoe (1932) and by Shlaer (1937) bear this out. Shlaer's data (his Table I) show that while there is no change in visual acuity between 5000 and 500 millilamberts, there is a loss of 12.2 percent from 1000 to 100 millilamberts. Similarly Lythgoe's measurements (his Fig. 6) show a loss of 10 percent in visual acuity between 1000 and 100 footlamberts. These reductions are of the same order of magnitude as those we found with sunglasses and the small targets.

X. LINES AND SQUARES

Judged by the measurements presented here, the human eye has a high visual acuity indeed for single test objects. Our single line data confirm the measurements of Barnard, of Hecht and Mintz, and of Byram. The data with squares, however, are smaller than those given by previous observers from Hueck to Byram. Our values of about 20 seconds for perfect recognition are by no means the best performance. Additional measurements with a single square and more prominent localization of it seemed to show that one can see even smaller sizes; but the observations are too few to be included here.

It is instructive to determine which target is the more effective visual stimulus,—a compact one like a square or a linear one like a wire. The solid visual angle occupied by the 22 second square is nearly 500 square seconds. The corresponding dimensions of the line are a width of 0.5 second and a required length of about 1 degree. The solid angle is therefore 1800 square seconds. The compact target is obviously the more effective stimulus.

This knowledge is of value in the construction of signals out of a given amount of material such as cloth, paint, or dye. Clearly it is of great advantage to make the signal compact rather than linear.

SUMMARY

1. The visibility of targets was studied at the limits of their resolution as viewed in silhouette against the open sky, and the influence of sunglasses on this visibility was determined. Two kinds of test objects were investigated representing the extremes between which most targets fall. One was a long wire; the other was a square. Measurements were made of the frequency with which the presence of the target was correctly recognized in relation to the visual angle which it subtended.

2. The wire can be seen with perfect certainty when it subtends a visual angle of only 0.51 second of arc; with 95 percent certainty at an

angle of 0.48 second; and with a 75 percent certainty at 0.43 second. These values are roughly equivalent to seeing a $\frac{1}{16}$-inch wire half a mile away.

3. The length of the wire also influences its visibility. For maximum recognition the length of the wire must occupy at least 18 mils. This is just over 1 degree visual angle, and covers about two-thirds the vertical diameter of the rod-free area of the fovea.

4. The presence of a silhouetted square can be recognized with perfect certainty when one side subtends a visual angle of 22 seconds; with 95 percent certainty at an angle of 18 seconds; and with 75 percent certainty at 14 seconds. These are roughly equivalent to seeing a 3-inch square at half a mile.

5. A square is the more efficient distant visual stimulus than a line. To be seen with complete certainty a square must occupy almost 500 square seconds visual angular area, whereas a line requires about 1800 square seconds. For signal recognition purposes it is obvious that a radially symmetrical target is to be preferred to a linear one.

6. The use of neutral tint sunglass transmitting about 12 percent of the light had different effects on the visibility of the two targets. The wire could be seen just as well with as without the glasses, while the visibility of the squares was reduced by about 17 percent. The difference in the two instances probably depends on the background brightness. In the wire measurements it was reduced by the glasses from 4000 to 500 millilamberts; in the square measurements from 1000 to 125 millilamberts. Such effects of brightness on visual acuity is in keeping with previously well-established measurements.

BIBLIOGRAPHY

H. Aubert, *Physiologie der Netzhaut* (E. Morgenstern, Breslau, 1865), p. 235.

E. E. Barnard, "A micrometrical determination of the dimensions of the planets and satellites of the solar system made with the 36-inch refractor of the Lick Observatory," Pop. Astron. **5**, 285 (1897–1898).

G. M. Byram, "The physiological and photochemical basis of visual resolving power," Part I and Part II, J. Opt. Soc. Am. **34**, 571 and 718 (1944).

H. Hartridge, "Visual acuity and resolving power of the eye," J. Physiol. **57**, 52 (1922).

S. Hecht and E. U. Mintz, "The visibility of single lines at various illuminations and the retinal basis of visual resolution," J. Gen. Physiol. **22**, 593 (1939).

A. Hueck, "Von den Grenzen des Sehvermögens," Arch. f. Anat. u. Physiol. p. 82, (1840).

P. Lowell, "Experiment on the visibility of fine lines in its bearing on the breadth of the 'canals' of Mars," Bull. Lowell Obs. **1**, No. 2 (1903).

R. J. Lythgoe, "The measurement of visual acuity," Great Britain Med. Res. Council, Special Report Series No. 173 (1932).

W. H. Pickering, "Report on Mars, No. 11," Pop. Astron. **23**, 569 (1915).

S. Shlaer, "The relation between visual acuity and illumination," J. Gen. Physiol. **21**, 165 (1937).

Letters to the Editor

Stray Radiation in Littrow-Type Spectrometers Which Employ Collimating Mirrors

HAROLD W. STRAAT

Bausch and Lomb Optical Company, Rochester, New York

March 26, 1947

THE Littrow-type spectrometer which employs a concave mirror as a collimating means has become widely used in instrumentation in the ultraviolet, visible, and infra-red portions of the spectrum. Many instruments of this type perform poorly because of the presence of stray light within the system. Various techniques are employed to minimize this effect, as in infra-red spectrometry, where a lithium fluoride or quartz "dark slide" is frequently used.

A study of the situation will indicate that most of this stray radiation may be almost completely eliminated by the correct geometrical placement of the optical elements involved in the system. The stray radiation within the

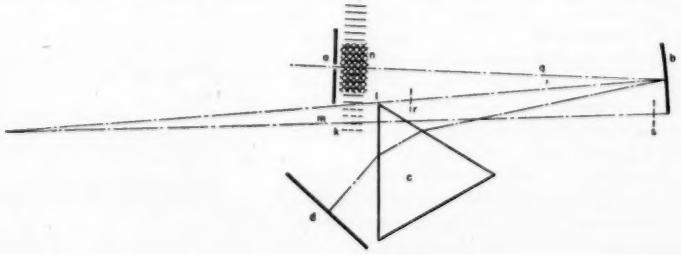

FIG. 1.

FIG. 2.

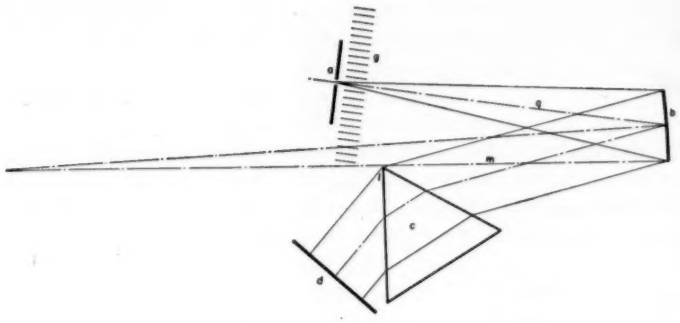

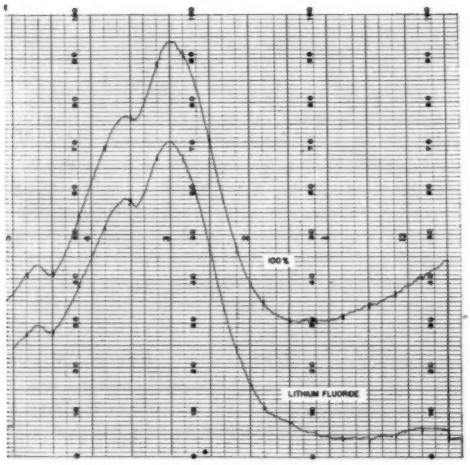

FIG. 3.

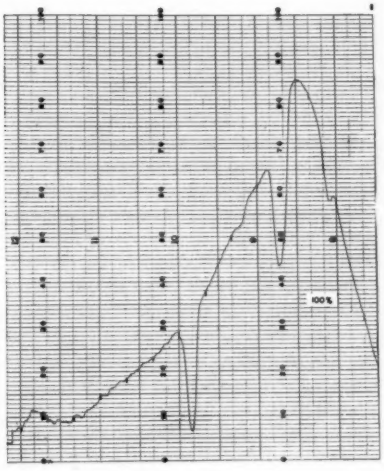

FIG. 4.

instrument is of two types: that resulting from the natural scattering of light from the optical surfaces and diaphragms, and the other caused by a re-entry of a portion of the spectrum into the system and leaving eventually through the exit slit. Elimination of the latter type is very necessary in infra-red spectrometry since the stray radiation due to this cause may under certain conditions amount to several times the intensity of the primary beam.

Figure 1 is a schematic diagram of the optical system of the spectrometer under consideration. The spectrum formed by the slit (*a*), the collimating mirror (*b*), the prism (*c*), and the mirror (*d*), is limited in length by the vignetting action between the prism and the collimating mirror. If the prism has been placed too near the slit-collimating mirror axis (*q*), as in this figure, the prism will intercept the rays forming the spectrum. Under these conditions the intercepted rays will appear as an out-of-focus image (*n*) centered on the exit slit.

Geometrical considerations will indicate that by placing the apex (*l*) of the prism outside the marginal radius line (*m*) of the collimating reflector, as in Fig. 2, there will not be any re-entry of spectral rays into the system.

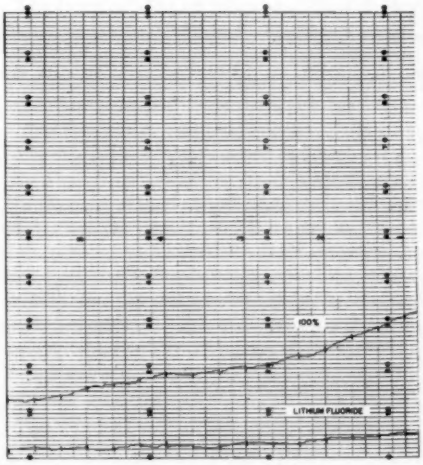

FIG. 5.

When stray light caused by a re-entry of spectral rays is present in an instrument, the apparent transmission of known non-transmitting samples may be very high. Figure 3 shows the false transmission of lithium fluoride in the 10.5-μ region where the material has no transmission. Under these conditions, however, lithium fluoride apparently transmits 75 percent of the incident radiation! A comparison of this graph with one made in the 2.5-μ spectral region with no sample in place, Fig. 4, will indicate that Fig. 3 is really a poorly dispersed record of the 2.5-μ region.

By suitably arranging the optical elements according to the condition shown in Fig. 2 the two peaks found in the 10.5-μ region were entirely eliminated. Figure 5 is a repeat run through the 10.5-μ region after this change had been made. Note that all suggestion of the 2.5-μ region has been eliminated.

In some instances it may not be desirable to rearrange the components of a system to fulfill the necessary conditions for the removal of stray light. However, by the insertion of diaphragms at (r) and (s) in Fig. 1 most of these advantages may be realized. In one particular optical arrangement these diaphragms caused a loss of only 5 percent of the light in the main beam while an enormous amount of stray light in the 10.5-μ region was completely eliminated.

Preparation by an Evaporation Technique of Correcting Elements for Refracting Optical Systems

L. G. Schulz
Department of Electrical Engineering, Ohio State University, Columbus, Ohio
April 7, 1947

IN the past, selective deposition of evaporated aluminum has been used to correct mirror defects and to parabolize spherical mirrors.[1] More recently improvements in technique and modifications of procedure together with quantitative test methods have been described.[2,3] This letter is to report that an evaporation method has been used successfully to correct defects of refracting systems. In particular, it has been used to eliminate spherical aberration of lens systems.

The principle of the method consists in forming a deposit of transparent dielectric on lenses so as to change the surfaces from spherical to aspherical. For the elimination of spherical aberration from a lens the deposit given by the following equation was used,

$$\text{Thickness} = K[Y_0^4/4 - Y^2(Y_0^2 - Y^2)].$$

Here Y_0 is the radius of the lens, Y is the distance from the axis, and K is a function of the focal length of the lens, its shape, and the indices of refraction of the glass and the dielectric used. In Fig. 1 is shown a diaphragm used to obtain the deposit required by the equation. This deposit can be made directly on the lens or on a plane piece of glass which is then used in combination with the lens as a correcting plate. In addition to correcting completely a single lens, it was also possible to over or under correct it so as to eliminate the aberration of the optical unit of which this lens was a part.

FIG. 1. Photograph of the diaphragm.

It was found necessary to design a special source for the evaporation of the dielectrics. It consisted of a thirty-degree cone about one inch deep, made of three-mil sheet molybdenum surrounded by a heating coil of twenty-mil tungsten wire covered with alundum cement to provide insulation. Initial evaporations were made on large sheets of glass to determine the radiation characteristics of the cone. Relative thicknesses of the deposits were determined by the position of the interference fringes. The lens to be corrected was mounted on the lower end of a vertical shaft in such a manner that the axis of the lens, shaft, diaphragm, and source were coincident. The diaphragm, illustrated in Fig. 1, was placed between the source and the lens, close to the surface of the lens. Evaporation operations were carried out in an eighteen-inch glass bell jar, the source and diaphragm being fixed and the lens rotated by motion brought into the vacuum through a Wilson-type seal.

The lenses were tested by both the Ronchi and the knife-edge tests. To eliminate chromatic aberration monochromatic light was used. Preliminary work has shown that lithium fluoride and magnesium fluoride are suitable dielectrics. A discussion of the theory for the calculation of various types of deposit with a detailed description of the experimental arrangement will be given later.

[1] John Strong, *Procedures in Experimental Physics* (Prentice-Hall, Inc., New York, 1945).
[2] L. G. Schulz, J. Opt. Soc. Am. **36**, 588 (1946).
[3] L. G. Schulz, J. Opt. Soc. Am. **37**, 349 (1947).

Minutes of the Twenty-Ninth Meeting of the Board of Directors of the Optical Society of America

HOTEL PENNSYLVANIA, NEW YORK, NEW YORK, FEBRUARY 19, 1947

IN addition to the transaction of routine business, the following items of general interest to members of the Society were considered.

Announcements by Secretary

Under authority conferred by a previous Board, the President and the Secretary had appointed Selig Hecht and H. E. Ives proxies for the Optical Society of America at the annual meeting of the American Institute of Physics, Inc., to be held on February 28, 1947.

Result of letter ballot:

Approval of appointment of Program Committee for winter meeting, 1947: O. S. Duffendack, Chairman, D. B. Judd, P. A. Lighty, S. L. Parsons, Norman Wright.

Appointments by President

Assistant to the Secretary to serve the special needs of the organizations which contemplate becoming local sections of the Optical Society of America:

Frederick W. Paul.

O.S.A. delegates on the A.A.A.S. committee to formulate plans that may lead to the establishment of a National Science Foundation:

Donald H. Andrews,
L. B. Tuckerman.

Program Committee for annual meeting in October, 1947:

Henry M. O'Bryan, Chairman,
S. S. Ballard, G. S. Monk,
S. Q. Duntley, Mary Warga.

Future Meetings of the Society

The Board of Directors approved resumption of the prewar schedule of holding the winter meeting of the Society in February or March in New York City and the annual meeting elsewhere during the month of October. The October, 1947, meeting will be held in Cincinnati, Ohio, if suitable accommodations can be arranged. The next winter meeting will be held in New York City on March 4, 5, and 6, 1948.

ARTHUR C. HARDY, *Secretary*

Annual Report of the Editor of Publications

STATEMENT OF OPERATIONS OF THE JOURNAL OF THE OPTICAL SOCIETY OF AMERICA FOR THE YEAR ENDING DECEMBER 31, 1946

Income			
Subscriptions			$10,125.34
Net income from published articles			1,493.31
Net income from sale of back numbers			6,075.77
Total Income Exclusive of Member Subscriptions			$17,694.42
Expense			
Printing and mailing			$11,752.87
Engraving			1,793.20
Editorial Mechanics:			
Salaries	$1,103.10		
Office expense	231.63		1,334.73
Subscription expense:			
Salaries	$1,465.84		
Office expense	260.98		1,726.82
Other expenses			86.74
Editorial Office, Cambridge:			
Salaries	$1,250.00		
Expenses	61.45		1,311.45
Total Cost of Editing and Publishing Journal			$18,005.81
Net Cost of Operating Journal and Furnishing it to Members			311.39

(Signed) GEORGE R. HARRISON, *Editor*

Annual Report of the Secretary of the Optical Society of America, Inc., for the Calendar Year 1946

Membership Record

January 1, 1946 to January 1, 1947

	Honorary	Regular Emeritus	Associate Emeritus	Regular Life Payment	Associate Life Payment	Regular Annual Payment	Associate Individual Annual Payment	Associate Corporation	Student	Total
Membership as of record in the books of the Secretary 1/1/46	4	18	1	8	1	546	927	29	3	1537
Gains During 1946										
By election as of 1/1/46	0	0	0	0	0	0	128	2	6	136
By election as of 1/1/47	0	0	0	0	0	0	28	1	4	33
By reinstatement	0	1	0	0	0	11	13	0	2	27
By transfer 10/2/46 as of 1/1/47	0	0	0	0	0	41	0	0	0	41
By transfer to regular life membership	0	0	0	2	0	0	0	0	0	2
Losses During 1946										
By death	1	1	0	0	0	3	1	0	0	6
By resignation as of 1/1/46	0	0	0	0	0	0	25	2	0	27
By resignation as of 12/31/46	0	0	0	0	0	7	18	0	3	28
By transfer 10/2/46 as of 1/1/47	0	0	0	0	0	0	41	0	0	41
By transfer to regular life membership	0	0	0	0	0	2	0	0	0	2
By separation for non-payment of dues	0	0	0	0	0	10	29	0	0	39
Membership as of 1/1/47	3	18	1	10	1	576	982	30	12	1633

New Members

Elected during 1946 as of January 1, 1946

Anderson, Scott (2511 A)
Applegate, C. E. (2440 A)
Arthur, Marion A. (2422 A)
Beck, William H. (2441 A)
Berg, O. (2414 A)
Berger, F. B. (2547 A)
Boyd, Bernard R. (2472 A)
Bragg, H. E. (2467 A)
Brown, Earle B. (2462 A)
Brunner, Adolphus J. (2448 A)
Buchele, Donald (2487 A)
Buck, G. B., Jr. (2475 A)
Burns, Loren V. (2510 A)
Burstein, Elias (2514 A)
Castle, John, Jr. (2559 S)
Chambers, Jack A. (2499 A)
Chikofsky, S. (2490 A)
Clarke, Richard G. (2554 A)
Clothier, R. F. (2500 A)
Clutz, Claude S. (2482 A)
Cohen, Ernest (2459 A)
Cohen, Jozef (2427 A)
Coleman, Howard S. (2478 A)
Creitz, E. Carroll (2449 A)
Cummings, C. E. (2481 A)
Damas, Leon (2520 A)
Darr, John E., Jr. (2450 A)
Davis, G. W. C. (2416 A)
Ditchman, J. P. (2480 A)
Dunham, Theodore, Jr. (2444 A)
Dunkelman, Lawrence (2515 A)
Dunn, Ray P. (2498 A)
Ehman, Roy G. (2493 A)
Ehrenfried, George (2425 A)
Engel, W. H. (2469 A)
Fearnley, George (2489 A)
Federer, Charles A. (2407 A)
Finch, Rogers B. (2457 A)
Frederick, G. W. (2430 A)
Fry, David L. (2445 A)
Furnas, Thomas C., Jr. (2497 S)
Garman, R. L. (2470 A)
Glasser, L. G. (2428 A)
Goodman, H. (2429 A)
Greenleaf, Allen R. (2488 A)
Greenspoon, R. (2446 A)
Hamly, D. H. (2543 A)
Hanson, W. T., Jr. (2474 A)
Hendley, Charles D. (2516 S)
Hill, William J. (2517 A)
Hillyer, Curtis (2483 A)

Homes, J. G. (2540 A)
Horscroft, W. F., Jr. (2417 A)
Howard, John N. (2458 A)
Howlett, Leslie E. (2519 A)
Hupman, George H. (2466 A)
Iredale, John R. (2471 A)
Jahn, Theodore L. (2473 A)
Kaplowitz, Morris (2492 A)
Kelley, W. F. (2501 A)
Kennard, Ralph B. (2535 A)
Kent, Rockwell, III (2438 A)
Knorr, H. V. (2439 A)
Kraft, Frank R. (2442 A)
Lapenas, Thorp A. (2505 A)
Lawson, W. L. (2534 A)
Lenz, Lester R. (2513 A)
Levin, Enrique (2486 A)
Levine, Louis (2419 A)
Li, Norman F. C. (2495 A)
Lord, Richard C. (2508 A)
Lyon, Donald W. (2521 A)
MacKenzie, James T. (2435 A)
Mader, William A. (2574 A)
Maerz, A. (2434 A)
Magliozzi, Joseph (2418 A)
Malcolm, Scott (2476 A)
Marron, T. U. (2463 A)
McAlister, E. D. (2451 A)
McReynolds, R. C. (2552 A)
Meyer, H. Sigmund (2420 A)
Mitchell, Donald E. (2415 A)
Mohn, Olof (2502 A)
Mollberg, Nils (2431 A)
Morgan, Raymond (2408 A)
Morris, Robert H. (2512 A)
Morse, Mark P., Jr. (2423 A)
Nachtrief, Norman H. (2522 A)
Nail, Nelson R. (2452 A)
Nat'l. Technical Laboratories (2523 AC)
Neill, Howard W. (2509 A)
Nitchie, Francis, Jr. (2507 A)
O'Grady, E. John (2568 S)
Otis, Marshall V. (2494 A)
Packer, Donald H. (2563 A)
Parsegian, V. L. (2460 A)
Patterson, W. A. (2524 A)
Pehta, Arnold John (2536 A)
Peridier, Julien (2566 A)
Pesce, Mario R. (2465 A)
Phillips, Sheldon (2561 S)
Pierce, Dorothea (2447 A)
Pitzer, L. E. (2503 A)
Plyler, Earle K. (2432 A)
Price, William B. (2426 A)
Proctor, Don R. (2453 A)
Ransom, Henry (2421 A)
Reilly, Frank J. (2532 A)
Rossmassler, Selma (2413 A)
Rubens, Sidney M. (2436 A)
Rusch, Mildred L. (2504 A)
Sandiford, Peter J. (2406 A)
Schaeffer, W. H. (2468 A)
Schatz, Frederick V. (2454 A)
Schultz, H. A. (2506 A)
Sharp, Howard M. (2433 A)
Sharp, J. W. (2496 A)
Small, John H. (2461 A)
Smith, Francis A. (2455 A)
Smith, Lothrop (2410 A)
Socony-Vacuum Labs. (2409 AC)
Spicer, W. M. (2484 A)
Strasser, Alexander (2485 A)
Sullivan, H. C. (2526 A)
Sziklai, George C. (2491 A)
Taylor, Harold H. (2477 A)
Terrio, Barbara W. (2424 A)
Tuttle, Henry A. (2437 A)
Vergbo, Joseph C. (2479 A)
Vine, Benjamin H. (2464 A)
Walton, Sam F., Jr. (2572 S)
Waring, Charles E. (2456 A)
Wasserstein, B. (2538 A)
Williams, Robley C. (2443 A)
Wing, Albert B. (2411 A)
Woodside, C. S. (2412 A)

Elected during 1946 as of January 1, 1947

Balcom, Margaret M. (2533 A)
Brant, Margaret (2570 S)
Castro, R. J. (2549 A)
Conklin, Doris E. (2530 A)
Dawson, Leo H. (2531 A)
Donnelley, R. R., & Sons Company (2575 AC)
Dust, Lambert C. (2569 A)
Eaton, William W. (2548 A)
Eichnor, L. C. (2546 A)
Gillette, R. H. (2544 A)
Hardy, J. D. (2537 A)
Harmon, Darell B. (2557 A)
Hechmer, Elizabeth (2560 A)
Hoffman, Charles W. (2518 A)
Horner, R. G. (2564 A)
Hughes, Harold K. (2553 A)
Jones, Llewellyn (2542 A)
Kadesch, Robert R. (2555 S)
Kennedy, Wm. R. (2539 A)
Koch, Donald A. (2571 S)
Krolak, Leo J. (2573 S)
Larsen, E. C. (2529 A)
Leverenz, H. W. (2558 A)
Nichols, Lawrence (2551 A)
Oldham, Max S. (2541 A)
Pfluger, Catherine (2525 A)
Ricksecker, R. E. (2567 A)
Riggs, Lorrin A. (2556 A)
Taylor, G. (2550 A)
Trusler, H. F., Jr. (2527 A)
Uhle, Otto D. (2528 A)
Vaile, C. A. (2565 A)
Winger, Edward H. (2562 A)

Associate Members

Elected to Regular Membership by Action of the Board of Directors October 2, 1946, effective as of January 1, 1947

Arthur, Marion A. (2422 A)
Billings, Bruce (2367 A)
Boettner, E. A. (1420 A)
Buck, G. B. Jr. (2475 A)
Coleman, Howard S. (2478 A)
Ditchman, J. P. (2480 A)
Dunham, Theodore, Jr. (2444 A)
Ellickson, Raymond (2374 A)
Federer, Chas. A. (2407 A)
Fry, David L. (2445 A)
Greenspoon, R. (2446 A)
Higgins, George C. (1783 A)
Jahn, Theo. L. (2473 A)
Knorr, H. V. (2439 A)
MacDonald, Duncan (2179 A)
Maerz, A. (2434 A)
McAlister, E. D. (2451 A)
Merritt, Thomas P. (2341 A)
Morgan, Raymond (2408 A)
Nahstoll, G. A., Jr. (1690 A)
Oetjens, Robert A. (2120 A)
Parsons, S. L. (1949 A)
Peckham, R. H. (2241 A)
Plyler, Earle K. (2432 A)
Richards, Llewellyn (2196 A)
Richardson, David (1386 A)
Robinson, Howard (2375 A)

Sheldon, John L. (2394 A)
Smith, Francis A. (2455 A)
Smith, Lothrop (2410 A)
Sterner, John (1042 A)
Strait, Louis A. (1359 A)
Strong, John (1599 A)
Sullivan, Francis J. (1547 A)
Tiedeman, John A. (2400 A)
Trimble, Frank H. (2321 A)
White, John U. (1278 A)
White, M. M. (2326 A)
Williams, Robley C. (2443 A)
Winter, Martin H. (2381 A)
Woodside, C. S. (2412 A)

Deaths Reported During 1946

Burgess, K. E. (994 A)
Cooke, H. L. (1398 R)
Fabry, Charles (88 H)
Rayton, W. B. (23 R)
Thwing, Charles B. (144 RE)
Zwillinger, Max (36 R)

(Signed) ARTHUR C. HARDY, *Secretary*

Annual Report of the Treasurer of the Optical Society of America for the Fiscal Year 1946

CASH TRANSACTIONS JANUARY 1, 1946 TO DECEMBER 31, 1946

Receipts		
Dues	$ 5,380.83	
Dues in Advance	6,986.19	
Income from Unallocated Securities	1,277.49	
Income from Ives Medal Fund Bonds	12.50	
Income from Adolph Lomb Fund Bonds	50.00	
Interest for Special Interest Account	51.49	
Total Receipts		$13,758.50
Disbursements		
Journal Publication Expense covered by Treasurer's office	279.25	
Journal Editorial Expense	1,350.00	
President's Expense	6.75	
Secretary's Expense	1,053.90	
Secretary's Travel Expense	68.71	
Treasurer's Expense	525.14	
Meetings and Programs	593.87	
Adolph Lomb Medal	24.16	
Contributions to the support of other organizations		
American Institute of Physics	1,657.53	
Inter-Society Color Council	25.00	
U. S. National Committee of International Commission on Illumination	50.00	
Total Expenditures		$ 5,634.31
Excess of Receipts over Normal Expenditures		$ 8,124.19
Investments		$ 7,416.71
Excess of Receipts over Total Expenditures		$ 707.48
Balances December 31, 1945		
Unallocated Cash	$10,047.60	
Ives Medal Fund	125.00	
Adolph Lomb Medal Fund	155.29	
		$10,327.89
Cash Balance, December 31, 1946		$11,035.37

Ives Medal Fund

Income		
Principal sum	$ 500.00	
Cash interest balance, January 1, 1946	125.00	
Bond interest accrued during 1946	12.50	
Total		$ 637.50
Disbursements		
None	0.00	0.00
Balance, December 31, 1946		$ 637.50

Note: The principal sum of $500.00 is invested in Series G War Bonds. They are included in the bonds reported in the accompanying Investment Statement.

Adolph Lomb Memorial Fund

Income		
Principal sum	$ 2,000.00	
Cash interest balance, January 1, 1946	155.29	
Bond interest accrued during 1946	50.00	
Total		$ 2,205.29
Disbursements		
Medal for Wayne G. Norton	24.16	24.16
Balance, December 31, 1946		$ 2,181.13

Note: The principal sum of $2000 is invested in Series G War Bonds. They are included in the bonds reported in the accompanying Investment Statement.

Investments

Investment Portfolio with market value of securities as of December 31, 1946.

		Book Value	Market Value	Annual Income
7M	U. S. Treasury Bonds 2¼% 59/56	$ 7,031.01	$ 7,368	$ 157.50
11.65M	U. S. War Savings Bonds "G" 2½%	11,600.00	11,600*	290.00
5M	Atch., Top. & Santa Fe 4% Gen. Mtge. 1995	5,000.00	6,475	200.00
3M	Consolidated Cigar Corp. 3¼% Deb.	3,156.47	3,090	97.50
15 Shares	El Paso Natural Gas Co. $4.10 Cum. Pref.	1,636.50	1,643	61.50
30 Shares	20th Century Fox Film $4.50 Pr. Pref.	3,077.80	3,075	135.00
10 Shares	Phillip Morris & Co. Ltd. 4% Pref.	1,098.10	1,063	40.00
65 Shares	General Electric Co. Common	2,544.23	2,332	104.00
10 Shares	Eastman Kodak Co. Common	1,718.19	2,245	60.00
35 Shares	Kennecott Copper Corp. Common	1,729.53	1,846	70.00
40 Shares	Standard Oil of N. J. Common	2,262.72	2,770	110.00
75 Shares	Indianapolis Power & Light Co. Common	2,543.81	2,203	90.00
		$43,398.36	$45,710	$1,415.50

* Maturity value.

The undersigned, having been duly appointed to audit the books of the Treasurer of the Optical Society of America, Inc. from January 1, 1946 to December 31, 1946, hereby certify that the Treasurer's report of receipts and disbursements is correct as shown by records, vouchers, bank statement, etc., and that his accounts check accurately with vouchers and bank statements.

(Signed) B. H. CARROLL, FRED W. PAUL, *Auditors*

Proceedings of the Winter Meeting of the Optical Society of America

HOTEL PENNSYLVANIA, NEW YORK, NEW YORK, FEBRUARY 20, 21, AND 22, 1947

THE winter meeting of the Optical Society of America was held at the Hotel Pennsylvania, New York, New York, on February 20, 21, and 22, 1947, with a registration of 650. The program consisted of eight sessions, simultaneous sessions being held on Friday morning and on Friday afternoon. The sessions on Thursday centered around papers on infra-red spectroscopy and spectroscopic equipment. The papers at Friday's sessions were divided between general optical and radiometric subjects and spectroscopy and spectrochemical analysis. At the close of the programs of contributed papers, Dr. E. O. Hulburt of the Naval Research Laboratory, read an invited paper on "The Upper Atmosphere of the Earth" and showed a motion picture film on the launching of V-2 rockets in New Mexico. Some results from measurements made with rocket-borne instruments were included in Dr. Hulburt's paper.

The most exciting part of the program followed the informal dinner on Friday evening, attended by over 400 members and guests. Mr. E. H. Land, President of the Polaroid Corporation, disclosed and demonstrated for the first time a new photographic process whereby a contact positive print is made in one minute in the camera itself. The exposure is made in the usual way except that paper can be used to support the silver bromide gelatin emulsion instead of glass or plastic film. After the exposure, the negative paper and a chemically treated sheet of paper are passed between rollers. In the process, a viscous substance having the consistency of vaseline is spread thinly between the two layers, and this substance contains the materials necessary to develop the negative image and to produce a positive image on the other layer. One minute is allowed for the chemicals to act, and then the camera is opened, the papers removed and separated, giving a negative and a positive print.

Prior to Mr. Land's demonstration, Dr. Max Herzberger and Dr. Mary Warga gave an account of their recent visits to optical and spectroscopic laboratories in England and France, and particularly of the Reunion d'Opticiens in Paris at which they represented the Optical Society of America. Dr. W. E. Meggers, of the U. S. Bureau of Standards contributed interesting anecdotes, as did Mr. N. A. Esserman of the Australian National Standards Laboratory, who had the distinction of having traveled the greatest distance to attend the meeting.

The sessions on Saturday were devoted to papers on vision and color. The high light of these sessions was an invited paper Saturday afternoon by Frank J. Reilly, entitled "Light and Shadow and Its Representation." Mr. Reilly explained and illustrated the use of scales of depth of shadow in painting.

CONTRIBUTED PAPERS

The abstracts of the contributed papers are appended.

MEETING OF THE BOARD OF DIRECTORS

A meeting of the Board of Directors was held on Wednesday, February 19. The minutes of this meeting appear on page 510 of this issue.

O. S. DUFFENDACK, *Chairman*
Program Committee

Program of Sessions

Titles and Abstracts of Papers

1. A Modulated Infra-Red Recording System. MAX D. LISTON, *The Perkin-Elmer Corporation.*

Drift in the recording of infra-red spectra can best be eliminated by the use of light modulation and a.c. amplification methods, but lack of sufficiently fast and sensitive detectors has greatly limited their general application. The signal-to-noise ratios of such systems have not been comparable to those obtainable from conventional thermocouple and galvanometer systems. A modulated system employing a new thermocouple and a breaker-type ampli-

fier has been tested in a Perkin-Elmer infra-red spectrometer and found to give performance comparable to that of a conventional d.c. system with the added advantage of not drifting. This thermocouple employs alloys with a thermoelectric power of more than 500 microvolts per degree assembled in a pin type of construction. A 10-ohm thermocouple of this type has a sensitivity of more than 5 microvolts per microwatt and a speed corresponding to 70 percent response with five-cycle modulation. The breaker amplifier is one of those currently used for d.c. amplification but employed in a special circuit to give five-cycle amplification. The equivalent input noise level of the whole system closely approaches the limits imposed by the thermal (Johnson) noise of the thermocouple.

2. An Infra-Red Recording Spectrophotometer. H. M. O'BRYAN, *Baird Associates.*

A spectrophotometer has been developed to give rapid transmission measurements of gases, liquids, and solids in the infra-red region of the spectrum. The "resolving power" of the recording system has been "matched" to the optical resolving power of the monochromator to obtain accurate and reproducible measurements. The optical system includes a 75-cm auto collimating mirror using a 10-cm 60° rocksalt prism in a Littrow-type mounting. The entrance and exit slits vary continuously to obtain approximately constant radiation incident on the receiving element as the spectrum is scanned. A wave-length cam is included to give a linear wave-length scale. The slit-width cam rotates in such a way that the region from 2 to 15 microns is recorded in 12 minutes and the instrument returned to its starting position in 6 minutes additional time. A double beam source system (patterned after those of N. Wright and J. D. Hardy) provides alternate illumination of the entrance slit by the sample and the reference beams at a frequency of 10 c.p.s. The radiation receiver is a blackened platinum-strip bolometer whose amplified (a.c.) output drives a control motor to equalize the source beams and to record the transmission of the sample as a function of wave-length. The transmission, as recorded by pen on a revolving drum, is continuously observable. The records are of convenient size for filing and can be read to a fraction of a percent transmission and to approximately 0.02-micron wave-length.

3. Analysis with a Double-Beam Infra-Red Spectrophotometer. N. WRIGHT AND L. W. HERSCHER, *The Dow Chemical Company.*

A spectrophotometer for the infra-red is described which consists of an external photometering system adapted to an ordinary rocksalt prism spectrometer equipped with a fast responding bolometer. Two radiation beams from the same source are made to fall alternately (at 6 cycles per sec.) upon the slit of the spectrometer while a variable diaphragm automatically balances one of the beams against the other. Electronic amplification and pen-type recording are employed to register the spectra, which appear directly as percent of radiation transmitted. Differential comparison of two samples, one placed in each beam, is an important capability of the instrument. When impure and pure samples are thus compared the spectrophotometer automatically records the spectrum of the impurity only. Similarly in the case of solution and solvent the spectrum of solute only is recorded. Recordings showing the performance of the apparatus are reproduced, and analytical applications are discussed.

4. The Infra-Red Spectra of Krypton and Argon. CURTIS J. HUMPHREYS AND EARLE K. PLYLER, *National Bureau of Standards Washington, D. C.*

The analysis of the spectra of the noble atmospheric gases, utilizing descriptive data covering the photographically accessible region, has long indicated the possibility of a considerable extension of most of these spectra into the infra-red region beyond 1.3 microns. Observations of the spectra of krypton and argon, in the region between 1 and 2 microns, have been made using a Perkin-Elmer spectrometer, fitted with a flint glass prism cut to an angle of 55°. The sources were Geissler tubes, used in previously reported work. More than 15 new lines of krypton have been observed. Part of these are blends of unresolved pairs or groups. The emission maxima have been determined in favorable cases to a precision of 2 wave numbers, roughly equivalent to $\frac{1}{10}$ of the smallest scale division on the wave-length drum. All observed lines have been classified, the most intense being represented by combinations of the type $2p-3d$, according to Paschen's notation. Two new levels from the configuration s^2p^5f have been found. The remaining unobserved combinations of the type $1s-2p$, occurring in this region, are with one exception too weak to be observed. The argon infra-red spectrum was observed by Paschen. More of its predicted combinations are in the photographic region than in the case of krypton. A few lines near 1.4 microns have been observed. This work is to be regarded as exploratory and is expected to be supplemented by use of more intense sources and grating instruments permitting higher resolution.

BIBLIOGRAPHY:
(1) William F. Meggers and C. J. Humphreys, Bur. Stand. J. Research 10, 427 (1933) RP 540.
(2) William F. Meggers, *Zeeman Verhandelingen* (1935), pp. 190–200.

5. Absorption Line-Width in the Rotation Spectrum of Atmospheric Water Vapor.* ARTHUR ADEL, *McMath-Hulbert Observatory of the University of Michigan, Ann Arbor, Michigan.*

Grating measurements at oblique incidence are employed as a means of obtaining the narrow slits essential to the direct observation of line-width. Correction for the finite width of slit is small. It is accomplished by empirical extrapolation to zero slit in one instance, and by numerical estimation of slit influence in another. The absorption coefficient half-width at half-height for the atmospheric water vapor lines at 18.64 mu and 15.99 mu is found to be 0.12 cm^{-1} and 0.11 cm^{-1}, respectively.

* This paper is based on work done for the Office of Scientific Research and Development under Contract OEMsr-1361 with the University of Michigan.

6. The Infra-Red Absorption of Carbonyl Groups in Steroids. NORMAN JONES, *The Division of Chemistry of the National Research Council of Canada,* M. J. WHALEN AND

V. Z. WILLIAMS, *The Physics Division of the American Cyanamid Company, Stamford, Connecticut,* AND KONRAD DOBRINER, *Sloan-Kettering Institute for Cancer Research, New York, New York.*

The basic ring structure of the steroid molecule consists of nineteen carbon atoms arranged as three six-membered and one five-membered rings. The introduction of certain substituent groups into this hydrocarbon skeleton yields a variety of substances of great physiological activity. Some of these concerned with male, female, and adreno-cortical hormone activity, together with certain of their metabolites which are excreted in the urine, will be described briefly. This will illustrate the fact that the introduction of ketonic or hydroxyl groups at positions conventionally numbered 3, 11, and 17 in the ring system, and at positions 20 and 21 in a two carbon atom side chain attached at position 17, is of special significance in connection with the various hormonal activities of these compounds. The biochemist is frequently confronted with the problem of locating the position of carbonyl substituents in newly isolated steroids, often where the quantities of the pure compound available may not exceed one milligram so that the ordinary methods of microorganic structural analysis cannot be applied. It has been found that the exact position of the carbon-oxygen stretching vibration which occurs between 1665 and 1770 cm^{-1} is critically dependent on the immediate molecular environment and can be used to locate the position of carbonyl substitution. For example, fourteen ketosteroids with a non-conjugated carbonyl group at position 17 all have the carbonyl stretching band at 1742 ± 3 cm^{-1} in carbon disulfide solution, while, under the same conditions, twenty-one ketosteroids with a non-conjugated carbonyl group at position 20 have a maximum at 1708 ± 3 cm^{-1}. Data for these and for other positions of substitution, based on an examination of some 120 steroids, will be presented. In cases where the molecule contains two or more carbonyl groups it is usually found that separate maxima corresponding to each carbonyl group occur, provided that the separation of the band positions exceeds the resolving power of the spectrograph. In a few cases of dicarbonyl compounds shifts from the anticipated band positions have been noted and may be attributed to a Fermi resonance effect. The carbonyl group of acetate and propionate esters of hydroxy steroids have been examined in a like manner but these do not show comparable positional shifts in the ester carbonyl maximum. They do show systematic shifts where there is unsaturation present at the point of attachment to the steroid ring system.

7. The Infra-Red Absorption Spectrum of Carbon Disulphide. EARLE K. PLYLER AND CURTIS J. HUMPHREYS, *National Bureau of Standards.*

The infra-red absorption spectrum of carbon disulphide has been remeasured in the region from 2 to 24 microns, using cells up to 5 mm in thickness. Fifteen bands were observed, some however being of low intensity. The strongest band for the liquid occurs at 6.64 microns, and the second harmonic of this band was observed at 2.23 microns, but the first harmonic, which should be at about 3.33 microns, was not observed, in accordance with the selection rules for a symmetrical linear molecule. Four combination bands were observed between 3 and 5 microns, whose wavelengths were in good agreement with the calculated values. A combination band which is represented by the difference between two fundamentals occurs as a broad moderately strong band in the region of 11.6 microns. A weak band was observed at 15.27 microns. This corresponds with the wavelength of the inactive vibration of the molecule. However, when this region was studied with a 140-cm cell filled with the saturated vapor of CS_2 at room temperature, no band was observed. In the vapor state a total of 6 bands were found at wave-lengths less than 20 microns. The fundamental band at 6.5 microns shows a side branch which is probably caused by the isotopic effect produced by C^{13}. Some small bands which were observed may be attributed to the $C^{12}S^{32}S^{34}$ molecule. As would be expected for this molecular configuration the spectrum of CS_2 as observed may be classified into an array of terms analogous to those of CO_2. A band at 12.7 microns has different intensities for samples obtained from two different sources and may be caused by an impurity. This band did not appear when using the cell containing the vapor.

8. Condensing Lenses for Raman Tubes of Small Volume. J. RUD NIELSEN, *Department of Physics, University of Oklahoma.*

A number of years ago the writer showed[1] that the most favorable focal length of the condensing lens in Raman apparatus is $F=hf/(b-s)$, where h is the radius of the Raman tube divided by the square root of 2, f the focal length of the collimator lens, $2b$ the height of the collimator aperture, and $2s$ the length of the spectrograph slit. With such a condensing lens, placed $(h+s)f/(b-s)$ from the slit, the largest possible length, $l_{max}=h^2f/sb$, of the Raman tube is fully effective in filling the spectrograph with light. This was proved for the case $h\gg s$. Often, however, only a small volume of the scattering material is available, necessitating the use of a Raman tube of small diameter. The case $h\leqq s$ has, therefore, been investigated. It has been shown that the theorem stated above holds also in this case. However, in order that the full amount of light may enter the spectrograph, some of the scattered light must pass out through the wall of the Raman tube and pass through the condensing lens at a distance from the center which is greater than the radius of the Raman tube. This has certain disadvantages. When $h=s$, it is found that the maximum length of the Raman tube can be utilized also by means of a condensing lens of focal length $sf/(b+s)$ placed immediately in front of the slit with the front end of the Raman tube right against the lens. This is usually the most satisfactory arrangement for liquids available in very small volume.

[1] J. Rud Nielsen, J. Opt. Soc. Am. **20**, 701 (1930).

9. Intensity Distribution in the Raman Bands of Six Hydrocarbons. J. RUD NIELSEN AND CHARLES M. RICHARDS, *Department of Physics, University of Oklahoma.*

The Raman spectra of cyclopentane, methylcyclopentane, ethylcyclopentane, cyclohexane, methylcyclohexane, and ethylcyclohexane were photographed with a

liquid-prism spectrograph of linear dispersion 13A/mm at 4400A. By means of a stepsector and a tungsten lamp of measured brightness temperature extinction marks were put on each film. Microphotometer records were made of the extinction marks at appropriate wave-lengths as well as of the Raman spectra. Characteristic curves were drawn for each Raman band or group of bands, and the intensity distribution in the Raman spectra was determined in terms of the known intensity distribution in the spectrum of the tungsten lamp. The results are presented in the form of intensity distribution curves covering all but the weakest Raman bands. The intensity per cm^{-1} used as unit is arbitrary but is constant over the entire spectrum. The accuracy of the procedure is illustrated by the agreement between intensity distribution curves obtained with widely different exposure times.

10. Microwave Absorption Spectroscopy and Some of its Techniques. DONALD K. COLES, *Westinghouse Research Laboratories.*

Very exact frequency measurements of the rotational absorption lines of gases provide correspondingly exact information about the molecular moments of inertia. For simple molecules the moment of inertia may be interpreted in terms of bond distances, provided frequency measurements can be obtained for molecules containing a sufficient number of different isotopes. Measurements of the absorption coefficient and of the splitting of a rotational line when an electric field is imposed on the gas provide information about the electric dipole moment of the gas and its orientation with respect to the axes of inertia of the molecule. Hyperfine structure in the rotational lines provides information about the nuclear spin and its coupling to the rest of the molecule. Realization of these results for most gases requires a rather long absorption cell and a method for detecting a very weak absorption. Methods for obtaining a sufficient sensitivity and of reducing the bothersome interference bands overlying the absorption spectrum will be discussed.

11. The Effect of Alkali and Alkaline Earth Salts on the Spectrographic Determination of Strontium. E. FAST* AND J. RUD NIELSEN, *Department of Physics, University of Oklahoma.*

In connection with an attempt to develop a method of quantitative spectrographic analysis of oil-field waters a detailed investigation has been made of the determination of strontium in the presence of alkali and other alkaline earth salts. The dried salts, together with a powdered graphite buffer and titanium as internal standard, were placed in cupped water-cooled graphite electrodes of a high voltage a.c. arc regulated by a variable inductance in the primary circuit. The spectrum was photographed with a Hilger E 1 quartz spectrograph, and the intensities of Sr 3380.7A, Ti 3383.8A, and Ti 3387.8A were determined by means of a step sector and a Dietert densitometer. With constant amounts of $SrCl_2$ and TiO_2 and various amounts of NaCl, KCl, $CaCl_2$, $BaCl_2$, and $MgCl_2$ short exposures were made at different times after the arc was started, and the intensities were determined. In all cases the intensity ratios between strontium and titanium lines were most constant during the period from 2 to 10 minutes after the arc was started. Hence, the weighted averages of the intensity ratios observed during this period have been studied as functions of the amount and composition of the extraneous salts. With NaCl added, the intensity ratio Sr 3380.7/Ti 3383.8 has a maximum value twice as great as when no extraneous element is present, with $MgCl_2$ sixteen times as great. When an alkaline earth is added, the concentration of the extraneous substance giving the maximum value of the Sr/Ti intensity ratio decreases with atomic weight. Alkalies show the opposite behavior. When the total concentration of $CaCl_2$+NaCl is kept constant a maximum of Sr 3380.7/Ti 3383.8 is found for a certain ratio of $CaCl_2$ to NaCl. On the other hand, when various mixtures of KCl and NaCl are added a minimum value of this intensity ratio is obtained for a certain ratio of KCl to NaCl. In neither case are the effects of the extraneous substances additive.

* Now with Phillips Petroleum Company at Bartlesville, Oklahoma.

12. The Spectrographic Analysis of Ferro Silicon. J. H. COULLIETTE, *Industrial Research Institute, University of Chattanooga.*

The mutual standard method of spectrographic analysis has been applied to the determination of eleven elements in commercial ferro-silicon alloys. The spectrum line-pairs and excitation methods are as follows:

Element	Wave-length	Iron Wave-length	Excitation
Al	3082.15	3083.74	spark
Ca	3968.5	3969.26	spark
Cu	3273.96	3286.75	spark
Cr	4254.34	4260.48	a.c. arc
Mg	2802.69	2806.98	spark
Mo	3170.34	3178.0	a.c. arc
Mn	2933.06	2941.34	spark
Ni	3492.9	3495.3	a.c. arc
Si	3905.53	3815.84	spark
Sn	3175.02	3178.0	a.c. arc
Ti	3372.80	3370.78	spark

Working curves were prepared by plotting line intensity ratios *vs.* concentration ratios, using iron as the reference element. Concentrations were computed from the ratios of concentrations.

BIBLIOGRAPHY:
(1) M. F. Hasler, C. E. Harvey, and H. W. Dietert, Ind. Eng. Chem. **15**, 102 (1943).
(2) C. B. Post, D. G. Schoffstall, and G. Hurley, Ind. Eng. Chem. **17**, 412 (1945).
(3) J. H. Coulliette, Ind. Eng. Chem. **16**, 653 (1944).
(4) J. R. Churchill and R. G. Russell, Ind. Eng. Chem. **17**, 24 (1945).
(5) C. H. Corliss, J. Opt. Soc. Am. **36**, 357(A) (1946).
(6) ASTM E-31, ASTM Methods of Chemical Analysis of Metals (1943).

13. Direct-Reading Spectrometer for Ferrous Analysis. R. O'B. CARPENTER, E. DUBOIS AND J. STERNER, *Baird Associates.*

The photoelectric direct-reading spectrometer* described by Saunderson, Caldecourt, and Peterson has been adapted for the determination of ten elements in ferrous materials. The spectrometer includes a three-meter concave grating of 15,000 lines per inch in a modified Paschen mounting and fixed entrance and exit slits. The instrument is stable

simple, and automatic in operation, producing measurements for eight elements simultaneously. Two successive exposures, one with an a.c. arc, the other with a spark source, are combined to cover both residual and alloying concentrations. Calibration curves have been made using samples calibrated by chemical means. Extensive tests have been made to determine analytical precision for Ni, Cr, Mo, V, Al, Cu, Sn, Si, Mn, and W in ferrous alloys. The condensed spark source is generally used in the range from 0.05 to 5 percent, giving an accuracy comparable to that obtained by spectrographic methods.

* Saunderson, Caldecourt, and Peterson, J. Opt. Soc. Am. **35**, 681 (November, 1945).

14. A Point-to-Plane Arcing Technique for the Spectrochemical Analysis of Monel. C. J. NEUHAUS, *The International Nickel Company, Inc., Huntington, West Virginia* AND PAUL E. LIGHTY, *Sperry Gyroscope Company, Great Neck, Long Island, New York.*

The requirement of determining, in addition to Mn, Si, Al, and Cr, Pb which is present in monel in the order of thousandths of percent indicated the use of d.c. arc excitation. The experimental conditions enumerated below were chosen to permit high sensitivity, a fair degree of precision, and short analysis time. The lower sample electrode which is the cathode consists of a casting $\frac{1}{4}$" diameter and 1" long. A high purity copper wire 0.07" diameter protruding $\frac{3}{16}$" from water-cooled clamps serves as the upper electrode, and is made the anode. The gap is held at 4 m/m, and the current through the arc is 10 amperes from a 220-volt d.c. line. The exposure time is 30 seconds with a 60 percent transmission filter interposed in the optical train. The region from 2400 to 3200A is photographed on Eastman Spectrum Analysis plates No. 1, using a Bausch & Lomb Littrow type spectrograph. The plates are developed in the Eastman formula D-8.

The analysis and control lines are as follows:

For Al	Al-3082	Ni-3125	Low concentration
	Al-2575	Ni-2559	High concentration
For Mn	Mn-2595	Ni-2559	
For Cr	Cr-2588	Ni-2841	
For Pb	Pb-2833	Ni-2559	

The standard deviations calculated from routine analyses of 100 samples run twice are:

For Al	3.6 percent,
For Mn	2.4 percent,
For Cr	1.7 percent,
For Pb	6.5 percent,
For Si	2.4 percent.

15. Instantaneous Spectrum Line Intensity Variations. J. H. ENNS AND R. A. WOLFE, *University of Michigan, Ann Arbor, Michigan.*

As a continuation of the study of spectrographic light sources, in part reported upon in an earlier paper, further observations have been made on the instantaneous intensity fluctuations of spectrum lines. The controlled spark source (air interrupted) and the alternating current arc source are used to excite the spectrum. By means of a direct pick-up (electron multiplier tube) and a two-gun oscilloscope, records are obtained to show spark to spark (spark source) and half-cycle to half-cycle (arc source) line intensity variations for pairs of lines. The effects of changing source conditions are interpreted from these intensity records.

16. Scattered Light in Microphotometer Systems. ROCKWELL KENT III, *Jarrell-Ash Company.*

During the process of developing a non-recording densitometer a number of experiments were undertaken to determine the importance of light scattered in microphotometric systems. A number of standard optical, illumination, and shielding systems were experimentally erected and tested. Data were collected showing (a) the effect of scattered light on the shape of emulsion H & D curves, (b) the effect of scattering from a neighboring line or lines, (c) the effect of other near-by spectra on the amount of scattered light, and (d) the magnitude of the error introduced to quantitative results by microphotometer systems with relatively high amounts of scattered light. The value of broad spectral lines for reducing errors from this effect also was investigated. With these experiments strongly in mind a densitometer to incorporate as well as possible comfort, ease of performance, speed, sensitivity, accuracy, and simplicity has been developed.

17. Light Absorption and Emission of Ions in Glasses and Crystals as Affected by Asymmetrical Electric Fields. W. A. WEYL, *Glass Science, State College, Pennsylvania.*

The environment of an ion strongly influences its light absorption and emission. The nature of the nearest neighbors of an ion, their number (coordination number) and their geometrical arrangement in space (crystal symmetry) are equally important for its color and fluorescence.[1,2] The differences in the optical properties between crystals and glasses are partly caused by the different symmetry of the electric fields surrounding the color centers. Ions or molecules which are adsorbed at the surface of an ionic crystal find themselves in strongly asymmetrical electric fields. The absorption of light by matter in the adsorbed state has been studied, especially by J. H. DeBoer[3] and his coworkers. Little is known about the influence of asymmetrical electric fields on the fluorescence of ions. Examples of this phenomenon will be discussed and a qualitative picture will be presented on the influence of one-sided polarization on the fluorescence of cadmium sulfide. One-sided polarization is accomplished by introducing cadmium ions into glasses where they are surrounded partly by oxygen and partly by sulfide ions. The same effect is accomplished by adsorbing cadmium sulfide molecules at the surface of alkali halides or oxides.

[1] W. A. Weyl, "Use of color and fluorescence indicators for determining the structure of glass," J. App. Phys. **17**, 628–639 (1946).
[2] J. H. Schulman, "Luminescence of $(Zn-Be)SiO_4$: Mn and other manganese phosphors," J. App. Phys. **17**, 902–908 (1946).
[3] J. H. DeBoer, *Electron Emission and Adsorption Phenomena* (Cambridge, At the University Press, 1935), pp. 181–204.

18. Fluorescence of Silicate Phosphors. KEITH H. BUTLER, *Sylvania Electric Products, Inc.*

A hypothesis is proposed for the fluorescence of silicate phosphors connecting the absorption and emission bands with the energy levels of the activator ions. The effect of

varying concentration of activator and modifier ions is discussed with particular emphasis on zinc beryllium silicate. The behavior of alkaline earth silicates is also discussed and an explanation of color differences under varying types of excitation is proposed.

19. General Correlations between the Efficiency Characteristics and Constitutions of Phosphors. H. W. LEVERENZ, *Radio Corporation of America, RCA Laboratories Division, Princeton, New Jersey.*

Phosphors with substitutional (*S*) activators (phosphorogens) are generally characterized by (1) invariant exponential decays of phosphorescence, (2) high optimum activator concentrations (up to about 10^{20} centers/cm^3), and (3) the appearance of a new emission band and suppression of the old band with increasing proportion of a new host-crystal ingredient. Phosphors with interstitial (*I*) activators generally have (1) variable power-law decays, (2) low optimum activator concentrations (about 10^{18} centers/cm^3), and (3) gradual shifts of old emission bands with increasing proportions of new host-crystal ingredients. The efficiencies of phosphors with *I* activators increase markedly with increasing density (intensity) of primary photons or electrons, whereas the efficiencies of phosphors with *S* activators are expected to increase little, if at all. The luminescences of phosphors with *I* activators saturate at a considerably lower level of excitation density than is the case for phosphors with *S* activators. These phenomena are interpreted in terms of the greater perturbability of *I* activator centers: (1) The lifetimes of the excited states of *I* activator centers decrease with increasing excitation density, thereby reducing the probability of losing excitation energy as heat. This effect accounts for the increasing efficiency of phosphors with *I* activators as the excitation density is raised. The efficiencies of phosphors with *S* activators should be relatively invariant with increasing excitation density up to the saturation limit, since the exponential decays of these phosphors are practically unaffected by changes in excitation or temperature. (2) The lower saturation limit of phosphors with *I* activators is a consequence of the lower optimum population density of *I* activator centers (about 10^{18}/cm^3) as contrasted with the 100-fold greater optimum population density of *S* activator centers (about 10^{20}/cm^3). The factor of 100 indicates that *I* activator centers are generally perturbed by impurities (including other identical *I* activator centers) which are, on the average, five times ($100^{\frac{1}{3}} \approx 5$) as remote as in the case of *S* activator centers.

BIBLIOGRAPHY:
(1) H. W. Leverenz, "Luminescence and tenebrescence as applied in radar," RCA Rev. **7**, No. 2, 199–239 (June, 1946).
(2) H. W. Leverenz, "Final report on research and development leading to new and improved radar indicators," Report PB25481, Office of the Publication Board, Department of Commerce, Washington, D. C., June 30, 1945.
(3) H. W. Leverenz, "Corpuscular vs. 'undulatory' excitation of phosphors," Phys. Rev. **69**, 686 (1946).
(4) W. B. Nottingham, "Electrical and luminescent properties of phosphors under electron bombardment," J. App. Phys. **10**, 73–83 (January, 1939).
(5) N. Riehl, "Ueber einen neuen Effekt an lumineszierenden Zinksulfid," Zeits. f. tech. Physik **20**, 152–155 (1939).

20. Method of Computing Correction Plate for Schmidt System for Near Projection, with Special Reference to System for Television Projection. HARRY S. FRIEDMAN, *Kollmorgen Optical Corporation, Brooklyn, New York.*

In an optical system for projecting the image of an object plane on a near screen, and employing spherical reflecting or refracting surfaces with a figured, aspherical refracting surface nearest to the image plane, a method is described for computing the coordinates of the figured surface so that the axial image point is freed from spherical aberration for all zones of the system. Only the computation of the figured surface is discussed. The tracing of the rays through the other part of the system is assumed to have been made by conventional ray trace methods. Special reference is made to Schmidt systems, in use for projection of television images from cathode-ray tubes. Also described are methods for computing the sine condition of the system and approximating the size of the blur circles produced at the center of the field by rays of wave-length different from that for which the system is corrected completely. A method of determining, in a section containing the optical axis, the nature of the imagery of extra-axial points in the object plane, and a means of determining the best curvature to be given the object plane in order to produce a flat image on the screen are also described.

BIBLIOGRAPHY:
(1) I. G. Maloff and D. W. Epstein, "Reflective optics in projection television," Proc. Nat. Elec. Conf., p. 190 (Oct. 5–7, 1944).
(2) Frank Allen Lucy, "Exact and approximate computation of Schmidt cameras. I. The classical arrangement," J. Opt. Soc. Am. **30**, 251 (1940).

21. Concentric Maksutov-Schmidt Reflecting Systems. HAROLD F. BENNETT, *Eastman Kodak Company.*

The meniscus type Schmidt camera has become familiar through several publications. The present paper will describe several forms not previously published which are chiefly elaborations of the concentric type briefly mentioned by Maksutov. Some of these forms are inherently easy to correct for color aberration, while others may be corrected by the method of Hawkins and Linfoot. Of especial interest is a form for which the zonal spherical aberration is highly corrected for apertures up to *f*:0.52. The outstanding feature of all strictly concentric systems is that the image is substantially as sharp at points off the axis as at the axial point, although it lies on a curved field.

BIBLIOGRAPHY:
Gabor, Br. Pat. 544,694 (January 28, 1941).
Maksutov, J. Opt. Soc. Am. **34**, 270 (May, 1944).
Rosch, Fr. Pat. 912,183 (February 9, 1945).
Hawkins and Linfoot, M. N. Roy. Astro. Soc. **105**, 334, No. 6 (1945).
Wynne, Nature **158**, 584 (October 26, 1946).

22. Structure of Evaporated Films as Determined by Electron Diffraction and Electron Microscopy. HENRY LEVINSTEIN AND ROBLEY C. WILLIAMS, *University of Michigan.*

For those who work with the optical, electrical, and thermal properties of thin films deposited in vacuum an adequate visualization of their micro-structure is important. Contrary to general belief, most films are discontinuous in internal structure and are far from smooth on

the surface. The magnitude of the discontinuities and surface features to be discussed is on the order of 10–1000A. Electron diffraction and electron microscope studies of some 35 elements have been made. The results indicate that with respect to internal structure the films may be placed in three categories: (1) those which are amorphous, (2) those which have crystallites of a size such as to exhibit sharp diffraction rings and to be visible in the microscope, and (3) those which have large crystallites and are preferentially oriented. Film structures in the three categories are functions of the melting point of the element, and are affected by the thickness of the film. Particle size is found generally to increase as the film is made thicker, but this effect is enormously enhanced in going from film type (1) to (3). Some work has been done with replicas of the surfaces of films and it is found that the degree of surface irregularity is roughly correlated with the internal irregularity. Photographic examples of different film structures will be shown.

23. Crystal Orientation and Refractive Index of Thick Evaporated MgF_2 Films. HOWARD S. COLEMAN, *Pennsylvania State College*, AND A. F. TURNER AND O. A. ULLRICH, *Bausch and Lomb Optical Company.*

X-ray analysis of thick vacuum evaporated films of MgF_2 shows them to be preferentially oriented. The films were of the order of 1.7 microns thick and were condensed on dense flint glass (Bausch & Lomb DF-2) at normal incidence. The orientation is a function of the temperature of the glass receiving surface during deposition. At 365°F the 111 planes are preponderantly parallel to the glass. As the temperature increases, the orientation changes continuously, and at 1000°F there is a preponderance of 110 planes oriented parallel to the glass. Changes in refractive index accompany these orientation effects. Indices were measured on the Abbe refractometer by determining the positions of at least two of the interference bands which appear when a film is contacted with a liquid to the Abbe prism. Actually each band is a doublet. Either component may be selected by a 90° rotation of a cap analyzer on the refractometer. Thus two refractive indices are associated with a film, corresponding to the vertical (v) and horizontal (h) settings of the analyzer. At a glass deposition temperature of 400°F they are $v=1.398$ and $h=1.394$, at 540°F they go through a minimum and are coincident, with $v=h=1{,}368$. Thereafter they increase up to 800°F where $v=1.379$ and $h=1.384$, and then remain constant to 1000°F. The $v-h$ difference is of opposite sign on the two sides of the minimum. Tentative explanations of these relations between refractometer and x-ray data will be discussed.

24. Electron Bombardment Cleaning. COLLIN H. ALEXANDER, *Bausch & Lomb Optical Company.*

The purpose of this paper is to present a new type of cleaning of optics in a vacuum before evaporation of antireflection films or first surface mirrors. A review of glow discharge cleaning in large systems with special emphasis on the voltage characteristics under various conditions will be given. A comparison of glow discharge cleaning with electron bombardment under high vacuum using a thermionic emitter as a source of electrons will be discussed. The electrical properties and effects on the glass to be coated will be presented. The description of a run using electron bombardment as a cleaning technique and the manufacture of ¼ wave-length magnesium fluoride anti-reflection films and first surface mirrors of aluminum plus ½ wave-length magnesium fluoride will be made. Some of the outstanding properties of films manufactured using electron bombardment cleaning will be given.

25. The Exact Solution of the Interference Filter as a Boundary Value Problem. P. J. LEURGANS, *Bausch & Lomb Optical Company.*

An interference filter[1] ordinarily consists of two semi-transparent metal films separated by a homogeneous transparent spacer. A complete solution for the transmission of the filter must take into account the optical thicknesses of all three layers, and the magnitude and phase of the reflections from each interface. A solution can be obtained from Maxwell's equations, the problem becoming a boundary value problem for three films, with the refractive indices of the two metal films being complex quantities. The transmitted intensity is found by solving eight simultaneous equations for the transmitted amplitude, and multiplying the transmitted amplitude by its complex conjugate. From the final equations, the effects of the various parameters (the optical constants and thicknesses of the films) on the filter properties can be investigated. To illustrate the effect of different thicknesses of the metal films, spectrophotometric curves have been computed for various thicknesses of silver ($n=.2$, $k=20$). The location of the peak of the transmission band indicates that the phase shift from a dielectric-metal interface is greater than 180°. To illustrate the effects of changing the optical constants of the metallic films, spectrophotometric curves have been computed for comparable filters with metallic films of aluminum, silver, and sodium.

[1] J. A. Sanderson and R. L. Ueberall, "German interference filters," Naval Research Laboratory Report H-2731 (January 5, 1946).

26. Tunable Narrow Passband Optical Filters. BRUCE H. BILLINGS, *Polaroid Corporation, Cambridge, Massachusetts.*

A polarization filter will be described which passes a region of the spectrum of the order of an angstrom in width and whose passband can be easily shifted to any wavelength in the visible spectrum. Previously, polarization filters have been designed which have a linear aperture of several centimeters and a transmission band an angstrom wide. The action of these filters depends on the superposition of the polarized channel spectra formed by X cut plates of quartz between parallel polarizers. Quartz plates were used whose thicknesses were in the ratios 1, ½, ¼, etc., the alternate passbands of each plate were cancelled out by the black bands of the succeeding plate. Since the passband of such filters was fixed in wave-length, they had limited application. Interest in filters of this type was restricted mainly to astronomers. Analysis shows that the 1, ½, ¼ retardation ratios in the fixed filter can be upset considerably without inducing any appreciable change in its optical

characteristics. Tuning is accomplished by altering the retardation of the successive filter elements so that transmission maxima in the individual channel spectra coincide at the desired passband wave-length. This retardation change can be made mechanically for example by stretching supplemental plastic sheets in series with the elements, or can be made electrically by using Kerr cells or crystals with high electro-optic coefficients such as ammonium dihydrogen phosphate. The additional retardation never has to exceed a full wave. In the electrical case, a network could be arranged so that with a single control the passband could be shifted through the spectrum. A tunable filter will be demonstrated.

27. The Photoelectric Measurement of Fluorescence Spectra. R. A. BURDETT AND L. C. JONES, JR., *Wood River Research Laboratory, Shell Oil Company, Inc., Wood River, Illinois.*

The Beckman quartz spectrophotometer[1] has been adapted to the determination of the fluorescence spectra of liquids and of solutions by means of a very simple attachment which may be interchanged with the usual light sources used for absorption studies. The attachment consists of a light-gauge sheet metal box housing a low pressure mercury arc, a filter cell containing a solution of nickel and cobalt sulfates, a quartz sample cell, and a condensing lens. The filter solution removes from the exciting radiation essentially all of the light of wave-lengths greater than 3200A. Alternatively a high pressure mercury arc in conjunction with a Corning Glass filter No. 5840 is used when 3650A excitation is desired. Fluorescent light originating in a thin layer at the front of the cell is focused on the entrance slit of the monochromator by means of a glass achromatic lens. Fluorescence bands may then be located by the measurement of photo-cell current as a function of wave-length using the measuring circuits supplied with the instrument. The conversion of photo-cell current to relative intensity of the fluorescent radiation is obtained by applying corrections for the effects of variations in photocell sensitivity, transmittancy of the lens, and linear dispersion with changing wave-length. In this manner the fluorescence spectra of a number of polynuclear aromatic hydrocarbons have been measured and found to be in good agreement with those obtained by the usual photographic techniques. The spectra of naphthalene, phenanthrene, and anthracene will be presented as typical data obtained with this apparatus.

[1] H. H. Cary and A. O. Beckman, J. Opt. Soc. Am. **31**, 682 (1941).

28. A Method for Automatically Recording Spectral Energy Distribution from Continuous Spectrum Sources. FRANK J. STUDER, *Research Laboratory, General Electric Company.*

The wide range of variation in the spectra of phosphors such as are used in fluorescent lamps and cathode-ray tubes has made it important to have available a means of making rapid determinations of spectral energy distribution of such light sources. Equipment to do this specifically for cathodoluminescent materials has been developed by Zworykin[1] and by A. E. Hardy.[2] The description of a method for point by point determination by the writer of spectral energy for low brightness sources is now in print. This paper will describe an arrangement of relatively simple construction with which it has been found possible to automatically record the spectral energy distribution of continuous spectrum sources within the visible range. There is no difficulty in working at brightness levels encountered with the common phosphors used in fluorescent lamps excited with a low pressure mercury arc (germicidal lamp), and it is possible to go to much lower brightness sources. The dispersion instrument used is a conventional constant deviation spectrometer, the wave-length drum being operated by a synchronous motor through a double cam to give a linear wave-length scale. The receiver is an electron-multiplier photo-tube (1P22). Correction for the spectral response of the cell and for the transmission of the spectrometer is made by means of a disk which varies the length of the exit slit. The output of the photo-multiplier feeds into a d.c. amplifier whose output goes to a photoelectric recorder, where the spectral distribution curve is drawn. The time required for drawing a curve can be varied from half a minute to two minutes. Tests made up to the present indicate that the instrument may be expected to repeat within 1 percent in successive measurements on a given light source. Checks made with Dr. B. T. Barnes at Nela Park, on several fluorescent lamps, have shown discrepancies of not more than 5 percent at any point in the spectrum.

[1] V. K. Zworykin, J. Opt. Soc. Am. **29**, 84 (1939).
[2] A. E. Hardy, to be published by the Electrochemical Society.

29. A Movable Unitized Beckman Spectrophotometer Installation. T. U. MARRON AND J. H. MUTH, *A. B. Dick Company, Chicago, Illinois.*

The utility and convenience of the Beckman model DU spectrophotometer can be considerably enhanced by the type of installation the instrument is given. From experience in using this instrument in several laboratories having a variety of use demands, the authors present a simple, practical design for a movable unit to contain the spectrophotometer, power pack, batteries, and constant voltage transformer. A table top of convenient height is provided for the spectrophotometer and accessories. A novel adjustable support for notebook or paper and a bracket light are mounted on the edge of this top. Underneath one end of the table a small cabinet houses the storage batteries in a lead tray on casters. On the outside of this cabinet are mounted constant voltage transformer, battery charger, automatic timer and switches. The wiring includes a switch for connecting the batteries in series for charging and in parallel for use, and a switch in the 110-v line to connect either the power pack or the charger. The whole unit on ball-bearing casters is compact and easily moved from one place to another for use. It is virtually independent of location except for a 110-v a.c. outlet.

30. Radiometry and Spectroscopy at Operation Crossroads. S. S. BALLARD, *Tufts College, Medford, Massachusetts,* E. O. HULBURT, J. A. SANDERSON, AND H. S. STEWART, *Naval Research Laboratory, Washington, D. C.*

This paper comprises a description of certain spectrographic and radiometric equipment used at the atomic

bomb tests at Bikini in July, 1946. Unusual features of the equipment and its installation will be discussed, and mention will be made of special technical and operational difficulties that were encountered. At shot *A*, the air burst, the following equipment was used: On the top deck of a surface ship eighteen miles distant from the explosion were installed one medium and two small quartz spectrographs fitted with infra-red sensitive plates and capable of photographing spectra in the wave-length range 2000A to 8200A. Also installed at this location were three unfocused thermocouples of the conventional type, one with a blue filter and two which accepted total received radiation. The thermocouple signals were recorded on wax paper by recording potentiometers which employed 10,000-fold logarithmic direct current amplification. These equipments were adapted especially for this use by the Farrand Optical Company of New York. Two similar radiometric equipments, one accepting total received radiation and the other equipped with a blue filter, were flown in an airplane at an altitude of ten thousand feet. The airplane was approximately eighteen miles from the burst. At shot *B*, the underwater explosion, the two small quartz spectrographs were carried in an airplane which was about seven miles from the explosion, and at ten-thousand foot altitude. This aircraft also carried the two unfocused thermocouples and amplifier-recorders referred to above. On the surface ship, located about ten miles from the explosion, there was a single focused thermocouple which employed an f:1 gold-surfaced parabolic mirror of 125-mm aperture, and the usual amplifier and recorder. This unit was carefully sighted on the ship under which the bomb was located.

* During the spring and summer of 1946 the authors served on the Technical Staff of the Commander, Joint Task Force ONE.

31. Solar Spectrograph for a V-2 Rocket. R. TOUSEY, C. V. STRAIN, J. J. OBERLY, F. S. JOHNSON, AND W. A. BAUM,* *U. S. Naval Research Laboratory.*

A vacuum grating spectrograph was designed for photographing the ultraviolet solar spectrum from a V-2 rocket. A 40-cm radius 15000 line/inch aluminized grating was used near normal incidence. The spectra were recorded on 35-mm film. A novel feature was the use of a 2-mm sphere of lithium fluoride instead of the usual slit and diffusing plate thus providing a wide field of view (140°) with high intensity. Because of astigmatism, a spectrum about 0.5 mm high was obtained from the small image of the sun produced by the sphere. An aluminum mirror between the sphere and the grating folded the light path so as to fit the instrument into the conical nose of the rocket. A second sphere and mirror were placed on the opposite side of the grating. This nearly doubled the field of view. The instrument was operated by electric motors and made a series of exposures of 0.1, 0.6, and 3 sec. in succession. The spectrograph was evacuated during flight by leaving a hole open to the outside. In the laboratory spectra were obtained down to 1100A, the transmission limit of lithium fluoride. The resolution of the instrument for a $\frac{1}{2}$° source, such as the sun, varied from 1 to 5A depending on the angle between the source and the optical axis. In an attempt to record the 1216A hydrogen line, provision was made for a single exposure of 55 seconds effective duration. To reduce the effects of scattered light during this exposure, one of the plane mirrors was made of crystalline quartz, whose reflectivity approaches that of aluminum at 1216A, but is only $\frac{1}{15}$ as great at the longer wave-lengths responsible for most of the scattering. Solar spectra from 3450 to 2100A obtained in flight will be shown. The instrument was manufactured by the Baird Associates.

* Now at the California Institute of Technology on leave of absence.

32. Invited paper, entitled "The Upper Atmosphere of the Earth," BY E. O. HULBURT, *Naval Research Laboratory.*

33. Improvements in Microscope Illumination. JAMES R. BENFORD, *Bausch & Lomb Optical Company.*

A number of recent improvements in microscope illumination are discussed. Several applications of complex shaped optical elements of transparent plastic are shown. A small fluorescent lamp designed for low power microscopy is described. Two applications of movable condenser lens systems are given in which the illuminated field and aperture are concurrently varied by the lens motion. Some applications of high and low index interference films and of evaporated metallic films are described. The use of the new zirconium oxide source in microscopy is discussed.

34. Factors in Fluorescence Microscopy and some Biological Applications. D. H. HAMLY, *Department of Botany, University of Toronto, Toronto, Canada* AND CHARLES SHEARD, *Division of Physics and Biophysical Research, Mayo Foundation, Rochester, Minnesota.*

This paper is concerned with an evaluation of the various factors governing successful observations with the fluorescence microscope. The primary considerations are: (1) brightness of the fluorescent image in absolute terms and (2) brightness level, image contrast, and resolving power of the eye. Various contributing elements, such as brightness of ultraviolet radiating sources, methods of illumination, selection of optical accessories, and filters for use with visible and ultraviolet radiations, and so forth, will be presented and discussed. The applications of fluorescence microscopy to biology will be concerned chiefly with the fluorescence of red blood cells. The presence of red fluorescing pigments in reticulocytes can be demonstrated with a suitable ensemble. Hence it is possible that the carriers of protoporphyrin may be identified. There are also evidences of a brightly fluorescing yellowish green pigment in reticulocytes, indicating the presence of some other modification of the normal hemoglobin of red blood cells.

35. The Theory of Measuring Unresolvable Particles with the Phase Microscope. HAROLD OSTERBERG, *Research Division, American Optical Company, Scientific Instrument Division, Buffalo, New York.*

The detection and measurement of small particles which lie in the submicroscopic region immediately below the Airy limit of resolution is of considerable importance. The

theoretical basis for a method by means of which it is proposed to measure both the area and optical path difference of an unresolvable particle will be discussed. This method depends upon the fact that for a given particle the character of the corresponding diffraction pattern which is produced by a phase or polanret microscope[1] varies not only with the phase difference and the amplitude ratio introduced by the phase or polanret system, but also with the area of the particle and its optical path difference and absorption relative to the surrounding medium. The center of the diffraction pattern can be brought to zero intensity by a suitable adjustment of the polanret system provided that scattering by the optical system is negligible. This adjustment provides two experimental parameters, specifically the phase difference between and the amplitude ratio of the conjugate and complementary[1] areas. These parameters determine the area and optical path difference of the particle. The polanret microscope is preferred because it allows continuous variation of the two experimental parameters. A simple optical arrangement will be described. The particle is illuminated by a narrow, oblique cone of light, and its diffraction pattern is viewed with suitably high magnification. When the optical path difference between the particle and its surround decreases to one-hundredth wave-length of the light, the corresponding variations in the above mentioned experimental parameters become small and difficult to measure, but these measurements appear to fall within the realm of physical possibility for submicroscopic particles whose effective radius is only one-fifth of that resolvable by the classical method.

[1] H. Osterberg, Paper No. 5, 31st Annual Meeting of the Optical Society of America, Oct. 3–5, 1946.

36. Compensation of the Aperture Ratio Markings of a Photographic Lens for Absorption, Reflection, and Vignetting Losses. IRVINE C. GARDNER, *National Bureau of Standards.*

The development of the modern photoelectric exposure meter and the more general dissemination of quantitative information regarding the properties of emulsions have made it possible not only for the professional but also for the skilled amateur to control his photographic work in a scientific manner. With this progress a demand has arisen for a more scientific method of marking the diaphragm openings of a lens. The method now in general use is based entirely upon the diameter of the entrance pupil and the equivalent focal length. It gives no consideration to the loss of effective light which arises because of absorption in the glasses of which the lens elements are made or because of reflection and scattering at the surfaces. Photographic objectives in common use may have from four to ten glass-air surfaces. The transmissions of such lenses may range from 50 percent to 80 percent if uncoated and may be as high as 95 percent if efficient low reflection coatings are applied to the surfaces. It is evident, therefore, that the effective exposures for different lenses with the iris diaphragm set for the same aperture ratio, may vary almost by a factor of 2, an uncertainty which is inconsistent with the precision with which the other factors governing exposure are controlled. Several methods for calibrating and marking the apertures of a photographic lens which will effect a correction for the varying light losses with different lenses have been proposed. A method is presented which is relatively simple and direct by which different laboratories may be expected to arrive at the same system of marking and equivalent values without the interchange of physical standards. The method is extended to apply to lenses when focused for infinity or for any finite distance and a system for marking the diaphragm scale is suggested. In order to distinguish between the older and newer systems of marking, the aperture ratio of the older system, based on geometrical measurements only, will be referred to as the *geometrical aperture ratio.* The new aperture ratio, which takes the absorption and reflection losses into consideration will, for present purposes, be designated the *equivalent aperture ratio.* Consideration is also given to the difference in effective exposure of different lenses because of vignetting.

BIBLIOGRAPHY:
Berlant, "Lens stop calibration by transmission," J. Soc. Mot. Pict. Eng. **46**, 17–25 (1946).
Daily, "A Lens Calibrating System," J. Soc. Mot. Pict. Eng. **46**, 343–356 (1946).
Murray, "The Photometric Calibration of Lens Apertures," J. Soc. Mot. Pict. Eng. **46**, 142–151 (1946).

37. A New Approach to the Problem of Granularity in Photographic Materials. JOHN V. ATANASOFF AND C. E. BARTHEL, JR., *Naval Ordnance Laboratory, White Oak, Maryland.*

Any method of measuring the granularity of photographic materials should fulfill two fundamental conditions: (a) the granularity indexes must correlate well with graininess numbers as determined by subjective methods, and (b) the granularity indexes must have direct significance in relation to the various physical applications of photographic materials. The formal mathematical postulates necessary to secure these conditions are given, an objective method of measuring granularity which satisfies these postulates is described, and preliminary experimental work using this method is discussed.

BIBLIOGRAPHY:
(1) L. A. Jones and G. C. Higgins, J. Opt. Soc. Am. **35**, 435–457 (1945).
(2) L. A. Jones and G. C. Higgins, J. Opt. Soc. Am. **36**, 203–227 (1946).

38. Submarine Binocular Telescope MK 90 and MK 91. WILLARD T. PERKINS, *Bausch & Lomb Optical Company.*

Some of the problems encountered during the design and manufacture of the Binocular Telescope MK 90 and 91 will be discussed. Particular emphasis will be given to several optical and mechanical features of construction as well as to methods of testing.

39. Recent and Unusual German Lens Designs. EDWARD K. KAPRELIAN, *Signal Corps Engineering Laboratories, Squier Signal Laboratory.*

A study of the photographic objectives in the Carl Zeiss collection now at Signal Corps Engineering Laboratories

reveals a number of interesting designs of large aperture or extreme angle of view. While a few of these are readily recognizable as belonging to some well-defined type, others are of unusual construction. Many of the lenses are experimental or trial objectives computed and built between 1936 and 1942 and are the prototypes of lenses used by the Germans for military photography from the ground and air as well as for infra-red photography and with infra-red image converting tubes. Constructional diagrams and formulas will be presented together with performance data.

BIBLIOGRAPHY:
Kingslake, J. Opt. Soc. Am. 36, 251 (1946).
Kingslake, J. App. Phys. 11, 56 (1940).

40. Infra-Red Response from Incandescent Lamps. BERNARD F. GREENE, *225 West 34 Street, New York.*

The type of light source which could be most readily adapted for use as a source of infra-red in signaling and recognition was the incandescent lamp. Data was obtained by calculation for the relative response of the incandescent source as a function of different variables. The calculations were made by relating the spectral response of the source to the response of the infra-red receivers. These calculations involved infra-red response per watt as a function of temperature and voltage. This procedure permitted the transposition of data obtained for visual response to the infra-red spectrum. Some of the information obtained in this manner was: the determination of incandescence and nigrescence of the incandescent source.

41. The Hololumen System for Rating Photo-Responsive Devices. GEORGE A. VAN LEAR,* *University of Michigan, Ann Arbor, Michigan.*

An outgrowth of the development of near infra-red military devices, the Hololumen System is a generalized photometry applicable to the consistent rating of photo-responsive devices and associated equipment. It is based on the spectral response curve characterizing the type of device dealt with, in precisely the same way as ordinary photometry is based on the spectral luminosity curve characterizing the human eye. The fundamental experiment is the usual one for determining the "sensitivity" of a photo-tube: the response of the device to a definite amount of the radiation from a tungsten lamp is measured. The Hololumen System is linked to ordinary photometry through the definition: *The hololumen measure, with respect to a given detector type, of radiant flux of any given spectral composition equals the lumen measure of the standard-distribution flux which evokes the same response from such a detector, the standard spectral distribution being that from a coil-filament tungsten lamp operated at a color temperature of 2870°K.* The various quantities of ordinary photometry, such as candlepower, brightness, etc., have their analogs in holocandlepower, holobrightness, etc. The only absolute radiation measurements required are those performed with ordinary photometric instruments and standards. Filters are characterized by holotransmission, defined in the usual way with reference to specified spectral distribution of incident radiation and the spectral response curve of the device. To avoid the confusion attendant upon use of the word "sensitivity" sometimes to mean response per unit of incident radiation and sometimes minimum signal required for operation, the word *responsivity* is assigned the former meaning and *threshold* the latter. Beacons are rated in holocandlepower, obtained as the product of the holocandlepower of the lamp and the holotransmission of the filter (the holocandlepower of a tungsten lamp is roughly equal to its candlepower). Thresholds of detecting devices are given in mile-holocandles. Threshold range is obtained as the square root of the quotient of beacon holocandlepower by detector holothreshold. The "system" is actually a multiplicity of systems, one for each type of spectral response curve. It is applicable and convenient whenever tungsten lamp radiation is appropriate as a basis for measuring responsivity. It is automatically as well-developed and as flexible in application to a wide variety of problems as is its prototype, visual photometry. This work was carried out under Contract NDCrc-185 between NDRC and the University of Michigan.

* Now with Lane-Wells Company, Ray Control Division, Pasadena, California.

42. A Method for Making Precise Resolution Measurements.* HOWARD S. COLEMAN AND SAMUEL W. HARDING, *The Pennsylvania State College.*

A method, based on a paper by Fabry,[1] for making precise resolving power measurements, has been developed. This method makes it possible to take into account the ill effects of stray light as well as the common optical aberrations. The method utilizes a device referred to as "the kinetic definition chart apparatus" (hereafter abbreviated to K.D.C. apparatus). The K.D.C. apparatus provides a means of continuously varying the angular subtense of the markings of a test object without changing the apparent distance between the test object and the optical device under test. Provision is made to vary the contrast and the brightness level of the test object. In order to simulate natural conditions, the test object is surrounded by a region, referred to as "the artificial sky," which may be illuminated to any desired brightness level. The artificial sky fixes the brightness level at which the observer's eye is adapted and provides a means of determining the ill effects on resolution caused by stray light that would normally be present in the optical device under consideration. Fixtures have been made which make it possible to measure the resolution at various field angles for an optical device under test. By means of auxiliary magnification, it is possible to test an optical device at full aperture and to practically eliminate differences among observers by reducing the diameter of the pupil of the observer's eye used to less than 1 mm. A quantity, referred to as "the K.D.C. efficiency," is introduced to describe the performance and the quality of optical devices. In predicting the performance of an optical device, such as the telescope, K.D.C. efficiency is a measure of how much farther a given object is visible using the instrument than with the unaided eye. The K.D.C. method described above has been used to determine

the performance and quality of telescopic systems, photographic systems, eyepieces, microscope objectives, and to measure the resolving power of the human eye under a variety of conditions.

* The work described in this paper was carried out, in part, under Contract OEMsr-1197 between the Office of Scientific Research and Development and The Pennsylvania State College.
[1] C. Fabry, Proc. Phys. Soc. London **48**, 747 (1935).

43. Photographic Measurements of Atmospheric "Boil."* LORRIN A. RIGGS, CONRAD G. MUELLER, CLARENCE H. GRAHAM, AND FREDERICK A. MOTE, *Brown University, Providence, Rhode Island.*

The character and extent of optical haze or "boil" have been studied with the aid of instantaneous photographs of outdoor targets. The targets, consisting of black-and-white striped patterns, are photographed against a reference scale by the use of a specially constructed telescopic camera. The "boil" effects are caused by the refraction by the atmosphere intervening between the scale and the targets. Such refraction produces differential shifts, from moment to moment, of points on the target along the reference scale. The amount of distortion so created has been determined for thirty or more successive exposures in each experiment by measuring the instantaneous deviation of any point on the target image from its mean position on the reference scale. It has been found that the average deviation due to "boil" is in excess of three seconds over level ground in bright sunlight; the maximum deviation may attain a value of nine seconds under these conditions. Two separate points on the target image are found to suffer the same kind of distortion at the same instant of time if the two points are very close together. The similarity is less marked, however, with points which are farther apart. With points whose angular separation is greater than about five minutes the effects of "boil" upon the two are essentially independent. The experiments described in this report were performed at Brown University for the Office of Scientific Research and Development.

44. Stray Light in Optical Instruments.* HOWARD S. COLEMAN, *The Pennsylvania State College.*

An objective method is described for measuring the stray light in optical instruments. This method utilizes an apparatus referred to as "the contrast rendition apparatus." The contrast rendition apparatus provides a means of measuring, photoelectrically, the contrast of an image formed by an instrument of an object of known contrast. The contrast of the image is compared on a percentage basis with the contrast of the object. This percentage is referred to as the "contrast rendition" of the instrument under consideration. Imperfection in the contrast rendition of an optical instrument is a measure of the reduction in contrast of the image caused by the presence of stray light. The importance of this imperfection has been evaluated by determining the loss in range at which objects are visible using the method described by Hardy.[1] Using the data published by Duntley[2,3] and Blackwell,[4] the loss in range caused by an imperfection in Contrast Rendition is compared with a corresponding loss caused by the same imperfection in light transmission and in the magnification for a number of typical telescopic instruments. In general, a greater loss in range was caused by the imperfection in contrast rendition. In determining the causes of imperfect contrast rendition each individual optical instrument must be considered on its own merits. In general, however, the stray light is associated with the mechanical as well as the optical parts. In addition the surface defects and cleanliness are important. For example a single thumbprint on the objectives of a good 7×50×7° binocular may reduce the range at which objects may be detected at night by as much as 50 percent.

* The work described in this paper was carried out under terms of Contract NOrd 7958 between the Bureau of Ordnance of the Navy Department and The Pennsylvania State College. This paper is by Howard S. Coleman, The Optical Inspection Laboratory of The Pennsylvania State College, State College, Pennsylvania.
BIBLIOGRAPHY:
[1] A. C. Hardy, J. Opt. Soc. Am. **36**, 283 (1946).
[2] S. Q. Duntley, J. Opt. Soc. Am. **36**, 359 (1946).
[3] S. Q. Duntley, "Contrast Reduction by the Atmosphere Along Inclined Paths of Sight," presented at the 31st meeting of the Optical Society of America, October, 1946.
[4] H. Richard Blackwell, J. Opt. Soc. Am. **36**, 624 (1946).

45. Spectral Transmissions of Some Eye Protective Glasses. EDWIN L. HETTINGER, *Willson Products, Inc., Reading, Pennsylvania.*

This paper is in the nature of a brief summary of the scientific background in the development of eye protective filters or glasses because literature on the subject is somewhat limited. The results, based on more than 30 years experience in the field of eye protection, may be of interest. This talk will be illustrated by slides of spectral transmissions, etc. One set of slides represents results of tests conducted at the University of Sheffield and published in 1938; another set more clearly shows the advances made in protective filters—these glasses were checked by the National Bureau of Standards and rechecked in our laboratory on a Beckman Quartz Spectrophotometer. Some reference to trade names is unavoidable because both the British and the American charts show names as a means of identification of samples, but there will be no mention other than stating basic composition of the various glasses. In addition to the eye protective properties, these glasses in finished form must meet certain optical requirements, as per Federal Specifications, to be satisfactory for use before the human eye. The early glasses were made for color only in the belief that all that was necessary was to cut down the amount of light with no thought to the invisible harmful rays contained in said light. Even now there is a division of opinion as to the necessity for protection against infra-red in ordinary sunlight, but it is a recognized fact that there must be such protection against the artificially created ultraviolet and infra-red rays present in certain industrial operations. Exposure to these rays would cause severe eyeburns. The iron green glasses, whether for sunglasses or industrial use, vary but slightly in the spectral transmissions. This variation is mostly caused by oxidizing or reducing conditions in the melting furnace, which is what swings the glass away from a true green to a yellowish-green or a bluish-green.

BIBLIOGRAPHY:
(1) W. W. Coblentz, "Recent progress in the manufacture of glasses for protecting the eyes from injurious radiations," reprint from J. Frank. Inst. (August, 1919).
(2) L. C. Martin, "Light Filters for Eye Protection," British Opt. Soc. (November, 1917).
(3) Charles Sheard, *Transmission of Radiant Energy by Ophthalmic Glasses.*
(4) Tech. Pap. Nat. Bur. Stand. Nos. 93, 119, 148, and 369.
(5) W. W. Coblentz, "Transmissive Properties of Tinted Lenses," reprint from J. Am. J. Ophthal. (October, 1932).
(6) Coblentz and Stair, "Spectral-transmissive properties and use of colored eye-protective glasses," Nat. Bur. Stand. Circular C421 (1938).
(7) Henry Laurens, *Physiological Effects of Radiant Energy.*
(8) J. Soc. Glass Tech. (October, 1938).
(9) Benj. F. Biser, *Elements of Glass and Glass Making.*
(10) Heyroth, *Chemical Action of Ultraviolet Rays.*
(11) Wood and Uhler, *Atlas of Absorption Spectra.*

46. An Infra-Red Pupillometer. M. J. KOOMEN, H. A. KNOLL,* AND R. TOUSEY, *U. S. Naval Research Laboratory.*

The eye pupil was illuminated with infra-red radiation and viewed with an infra-red image-forming telescope. The pupil was imaged at 1:1 magnification upon the photo-sensitive cathode of an RCA 1-*P*-25 image tube. The visible image emitted by the phosphor screen was observed through a 11-power eyepiece. A scale, having transparent graduations ½ mm apart, was illuminated with infra-red light and reflected into the objective lens of the telescope by means of a pair of small prisms. The eye pupil and surrounding area were illuminated by projecting an out-of-focus image of a 50-watt projection lamp filament upon the subject's eye. The beam was filtered through a Polaroid XR7X25 filter and water cell, and could not be seen by the subject. A red fixation point and dim white adapting field of variable brightness were presented to the subject by reflection from a glass plate. The eye pupil appeared dark and the iris bright, with the bright scale superimposed upon both. It was possible to measure the pupil diameter to an accuracy of 0.1 mm or better. Accuracy was limited chiefly by fluctuation of the eye pupil, and by involuntary eye movement. Since the photo-sensitive cathode resolved 15 to 20 lines per mm, accuracy was not limited on this account. Focusing was sufficiently critical so that errors due to incorrect positioning of the eye were avoided.

* Now at Ohio State University.

47. A Case of Unilateral Deuteranopia. LOUISE L. SLOAN AND LORRAINE WOLLACH, *Wilmer Institute, Johns Hopkins University School of Medicine.*

Studies are reported of a subject, D.D., having red-green color deficiency of the "deutan" type, complete in the right eye, slight in the left. A somewhat similar case, Dr. R., first reported by von Kries in 1919 as unilateral deuteranomaly, was recently re-examined by Trendelenberg,[1] who found evidence of slight color deficiency in the supposedly normal eye. On the Nagel anomaloscope, D.D., using the right eye, matched both spectral red and spectral green to yellow. The left eye did not differ from normal. Selected pseudo-isochromatic charts[2] and the Farnsworth-Munsell 100-Hue Test,[3] however, revealed in the left eye definite color deficiency of the "deutan" type. On these tests the right and left eyes gave essentially similar results. Scores on the Color Threshold Tester[4] indicated a marked defect in the right eye, slight in the left. When using the left eye, the subject arranged in the normal circular order a series of 21 colors taken from the 100-Hue Test (Nos. 1, 5, 9, etc.). With the right eye, however, he placed them in a linear series which he described as composed of light browns on the left, blues on the right and grays near the middle. Because of the relatively slight abnormality of the left eye, it is possible to obtain from this subject reliable information as to the colors perceived by the right eye.[5] In the spectrum the range from 501 to 505 millimicrons was reported as white; longer wave-lengths, as yellow; shorter ones, as blue. The spectral regions 584 and 451–453 appeared identical in hue to the right and the left eye. Similar tests were made with the 100-Hue series of Munsell papers. Those appearing gray to the right eye have dominant wave-lengths of 498 and 505 c. The blue and the yellow which were of the same hue with each eye have wave-lengths of 478 and 576.

BIBLIOGRAPHY:
(1) W. Trendelenberg, "Ueber Vererbung bei einem Fall von anomalen Farbensinn des einen und normalem Farbensinn des anderen Auges beim Mann," Klin. Mbl. Augenhk. **107**, 280 (1941).
(2) Louise L. Sloan, "An improved screening test for red-green color deficiency composed of available pseudo-isochromatic plates," J. Opt. Soc. Am. **35**, 761 (1945).
(3) Dean Farnsworth, "The Farnsworth-Munsell 100-hue and dichotomous tests for color vision," J. Opt. Soc. Am. **33**, 568 (1943).
(4) Louise L. Sloan, "A quantitative test for measuring degree of red-green color deficiency," Am. J. Ophth. **27**, 941 (1944).
(5) Deane B. Judd, "The color perceptions of protanopic and deuteranopic observers," J. Opt. Soc. Am. **34**, 351 (1944).

48. Stiles and Crawford Effect in Polarized Light. BRIAN O'BRIEN, *Institute of Optics, University of Rochester.*

Bárány has recently described experiments with a polarized pencil of rays entering the eye through the margin of pupil and illuminating the central retina obliquely. No fluctuation in sensation was observed with rotation of plane of polarization, and this has been interpreted by Bárány as contrary to proposal by Wright and Nelson[1] of multiple reflection within retinal element to explain the Stiles and Crawford effect. Since this also appeared contrary to the writer's more detailed theory,[2] an experimental test has been conducted with large scale models of retinal cones. Liquid tight cells in form of truncated cone with plane parallel windows have been made of a transparent plastic of known refractive index. When filled with liquid of higher refractive index than the cell wall, light entering at base is reflected within the cone. That which escapes into transparent wall is trapped, while that emerging at truncated end is received by photobarrier cell. If base of cone model is illuminated obliquely with collimated polarized light corresponding to Bárány's experiment, and the plane of polarization is rotated, then presence or absence of fluctuation in photo-cell indication will permit quantitative interpretation of Bárány's result. No fluctuation greater than 1 percent was observed for several values of refractive index difference between liquid and wall, and for two cells of cone included angles of 8 and 12 degrees, respectively. It is concluded that Bárány's experimental results are in complete accord with writer's theory of the Stiles and Crawford effect.[2] A similar result might be obtained entirely by calculation, by tracing a large number of skew rays through a transparent cone making due allowance by use of the Frésnel equations for reflection of the polarized beam at a number of orientations of the entering plane of polar-

ization. The experimental measurement was considered a simpler and much shorter procedure.

[1] E. Bárány, Acta Ophthalmol. **24**, 1 (1946).
[2] B. O'Brien, J. Opt. Soc. Am. **36**, 506–509 (1946).

49. Invited paper entitled "Light and Shadow and Its Representation," BY FRANK J. REILLY.

50. Reflex Glossmeter. RICHARD S. HUNTER, *Henry A. Gardner Laboratory, Inc.*

This new instrument has been built primarily to intercompare the specular reflectances of non-flat, high gloss surfaces. A collimated beam of light is directed onto a test surface at roughly 75°. In the path of the rays specularly reflected by the surface is placed a high grade retroreflector of the type widely used for night-visible traffic and vehicle markers. The merging cube corners of this retroreflector return each ray, striking it to that area of the test surface which first reflected it. Specular reflection occurs a second time with each ray taking the path of its first reflection in reverse direction. Thus deviations of rays due to sample curvature are compensated and the doubly reflected rays return through the collimating lens toward the small source. A thin beam-splitting pellicle[1] is interposed between collimating lens and source to divert a part of this reversed beam to one side where it is received for measurement by a photo-cell.

[1] F. S. Cooper, "Optical characteristics and applications of beam-splitting pellicles," J. Opt. Soc. Am. **36**, 363 (1946).

51. Goniophotometric Characteristics of Typical Diffuse Reflectors. SEIBERT Q. DUNTLEY, *Massachusetts Institute of Technology*, AND W. R. JACOBSON, *General Electric Company.*

The automatic recording photoelectric goniophotometer described in an earlier paper[1] has been used to measure a number of typical diffuse reflectors including magnesium carbonate, blotting paper, and ground vitrolite. In all instances the spatial distribution of reflected light was found to be approximately in accordance with Lambert's law when the light was incident normally, but large departures were found when the angle of incidence was increased. Extreme departures of a nature common to all of the diffuse reflectors tested were found when the angle of incidence was large. The assumption that such surfaces obey Lambert's law under all modes of illumination is seriously contrary to fact, and it should be avoided in lighting calculations. Speculations on the reasons for the observed departures from Lambert's law suggest coherent scattering as a possible mechanism. The goniophotometric investigation of diffuse reflectors was undertaken in the quest of a material suitable for use as a standard in goniophotometry. The authors will appreciate suggestions leading to the discovery of a surface producing a spatial distribution of reflected light in accordance with Lambert's law for all modes of illumination.

[1] S. Q. Duntley, J. Opt. Soc. Am. **36**, 367 (1946).

52. Correcting Filters for Photoelectric Photometry and Colorimetry. A. J. WERNER, *Corning Glass Works.*

In the practice of photoelectric photometry and photoelectric colorimetry it is necessary to employ auxiliary filters for correcting the spectral sensitivity of the photoelectric receiver to one or more of the spectral sensitivity curves of the normal eye. For realizing this the transmission of the filter must be such that the product of the transmission by the sensitivity of the receiver is proportional to the visibility function for each wave-length of luminous radiation. Glasses suitable for correcting the RCA photo-tube No. 926 are described and the departures of the filter transmission from the transmission for an ideal filter are discussed.

53. The Colors Due to Ideal Absorption and Transmission Bands. I. H. GODLOVE, *General Aniline and Film Corporation.*

Synthetic organic chemists have developed to a high state the art of prediction of changes in absorption spectra with changes in molecular architecture. But they are not able to visualize the colors resulting from specific changes. The colorimetrist is frequently asked what absorption spectra constitute ideal goals at which to shoot in a particular field of colors. Previously[1] the author had calculated the specifications of the colors due to a V shaped absorption band moving through the visible spectrum. More complete calculations have now been made for rectangular absorption and transmission spectra of two types having ideal cut-off (ordinates all zero or unity). Calculations were made for a number of different band widths and for variable wave-length centers, so that by interpolation all possible colors due to the indicated absorption curves have been mapped and plotted on the I. C. I. chromaticity diagram. Munsell renotations[2] of all the ideal colors have also been computed. Calculations by means of 30 selected ordinates, using the dozen supplementary wave-lengths recommended by the Colorimetry Committee,[3] were found insufficiently accurate. Calculations by means of 100 ordinates were found extremely simple and rapid, reducing to a mere counting of ordinates; and since this was done mechanically, the method was "fool-proof." As previously pointed out, true greens cannot be obtained with a single absorption band. Some other results were as follows. Saturation increases with width of absorption or narrowness of transmission bands; but a "law of diminishing returns" operates. A 5–10-mu shift in the yellow, for example, has more effect on the color than a 50-mu shift in the blue-green. In two spectral regions it makes little difference whether very wide or very narrow bands are used; in others the reverse is true. Saturation maxima were found at 3 absorption wave-length positions, and for transmission at 400–450 mu. The points representing the calculated colors lay on the surface defined by MacAdam[4] for maximally saturated pigment colors, but they are located with reference to a set of parameters of much more direct interest to chemists.

[1] Godlove, J. Opt. Soc. Am. **33**, 351–2 (1943).
[2] Munsell, J. Opt. Soc. Am. **33**, 385–418 (1943).
[3] Colorimetry Committee, J. Opt. Soc. Am. **34**, 653 (1944).
[4] MacAdam, J. Opt. Soc. Am. **25**, 249–52, 361–7 (1935).

54. Tetrahedral Representation of the Color Solid. CARL J. FOSS, *Princeton, New Jersey.*

It has been pointed out by Balinkin[1] that the vertices of a regular tetrahedron form a lattice of four colors which are visually equidistant from any one of the neighboring colors within a homogeneous and isotropic psychophysical color space. By tetrahedral representation of the color solid is meant a collection of chips whose colors may be represented at the vertices of a family of regular tetrahedrons so that the differences between each color in the manifold and its 12 nearest neighbors are all equally perceptible. This representation can be separated into four series of parallel planes yielding triangular arrays of points and into several series of parallel planes yielding rectangular arrays of points. In any of the planes yielding triangular arrays of points each point forms the center of a regular hexagon with its nearest neighbors at the vertices. A considerable fraction of the color solid has been represented by a tetrahedral array of chips in which planes of equally luminous colors correspond to triangular arrays. By observation of these chips of constant luminous reflectance the criterion of uniform representability of equally luminous colors on a plane, as stated by Silberstein,[2] has been applied. Preliminary observation of these chips by several observers indicates that the representation is at least approximately uniform, and similar studies have shown that the Munsell variables of hue, value, and chroma, are related in a simple way to the tetrahedral representation. This new method of representing the color space is valuable as an aid to visualization of color tolerances, and is startlingly successful in suggesting color harmonies. It is also the basis on which to assemble a collection of color chips of fixed total number that shall have the greatest possibility of including a near match for any color chosen at random. These three features will be illustrated, and plans disclosed for completing the assembly of such a collection of chips.

[1] I. A. Balinkin, "Solid geometry in color space," J. Opt. Soc. Am. **31**, 461 (1941).
[2] L. Silberstein, "Fundamental criterion of uniform representability of equiluminous colors on a geometrical surface," J. Opt. Soc. Am. **32**, 552–556 (1942).

55. Change in Object Colors by Passing from Daylight (Illuminant *C*) to Incandescent-Lamp Light (Illuminant *A*). JOSEPHINE GROVE* AND HARRY HELSON, *Bryn Mawr College.*

Hitherto no systematic investigation has been made of color matching under different illuminants. If the illuminants do not differ too much, such as Illuminants *C* and *A*, satisfactory matches of samples in the two can be made. 198 Munsell samples representing 13 hues at various value levels and chromas, including 9 neutrals, were viewed separately on black, gray, and white backgrounds under Illuminant *A* and matched by samples viewed in Illuminant *C* by 7 observers. Over 4000 observations yield the following general trends: Hues containing red and blue, i.e., from 10 *PB* to 5 *R*, become redder in Illuminant *A* as compared with Illuminant *C*, while hues between 5 *PB* and 5 *YR* shift in the opposite direction toward reddish-yellow. *G*, *GY*, and *Y* do not change as much as *B* and *BG*. Two invariant hues emerge: the first lies between 10 *R* and 5 *YR* on all three backgrounds, the second is between 5 *PB* and 10 *PB* with white background and between 5 *PB* and 10 *B* with gray and black backgrounds. Greatest hue shifts generally occur with black background, gray coming next, and white last. The lightest samples shift most on black and gray backgrounds. The greater the chroma of a sample the less does its hue change when compared under these two illuminants. Greatest loss in chroma occurs with the *PB* invariant and greatest increase with the *YR* invariant. Individual differences among the observers provide data for statistical treatment of range, variability, and reliability of the observations. The general trends are qualitatively in accord with the Helson-Judd principles of color conversion[1,2] and in the direction to be expected from the I.C.I. specifications of the samples in the two illuminants.[3] The changes in hue and chroma and the invariant hues as they appear in the I.C.I. plots are not far different from those observed but the computed changes are much greater than the observed because the I.C.I. computations are based on a completely non-reflecting background and observers screened from the illuminants. Further theoretical treatment of the data seems warranted. (*Acknowledgments:* The indebtedness of the authors to Miss Dorothy Nickerson and Dr. D. B. Judd for suggesting the problem, helping in the investigation, and in contributing to this report in various ways is gratefully acknowledged.)

* Now in the Color Control Department, Eastman Kodak Company, Rochester, New York.
[1] H. Helson, J. Exp. Psychol. **23**, 439 (1938).
[2] D. B. Judd, J. Opt. Soc. Am. **30**, 2 (1940).
[3] K. L. Kelly, K. S. Gibson, and D. Nickerson, J. Opt. Soc. Am. **33**, 355 (1943).

Author Index of Papers

Adel, Arthur—No. 5
Alexander, C. H.—No. 24
Atanasoff, John V. and C. E. Barthel, Jr.—No. 37
Ballard, S. S., J. A. Sanderson and H. S. Stewart—No. 30
Barthel, C. E., Jr.—see Atanasoff, John V.
Baum, W. A.—see Tousey, R.
Benford, James R.—No. 33
Bennett, Harold F.—No. 21
Billings, Bruce H.—No. 26
Burdett, R. A. and L. C. Jones—No. 27
Butler, Keith H.—No. 18
Carpenter, R. O'B., E. Dubois and J. Sterner—No. 13
Coleman, Howard S.—No. 44
—— **and Samuel W. Harding**—No. 42
—— **and A. F. Turner and O. A. Ullrich**—No. 23
Coles, Donald K.—No. 10
Coulliette, J. H.—No. 12
Dobriner, Konrad—see Jones, Norman
Dubois, E.—see Carpenter, R. O'B.
Duntley, Seibert Q. and W. R. Jacobson—No. 51

Enns, J. H. and R. A. Wolfe—No. 15
Fast, E. and J. Rud Nielsen—No. 11
Foss, Carl E.—No. 54
Friedman, Harry S.—No. 20
Gardner, Irvine C.—No. 36
Godlove, I. H.—No. 53
Graham, Clarence H.—see Riggs, Lorrin A.
Greene, Bernard F.—No. 40
Grove, Josephine and Harry Helson—No. 55
Hamly, D. H. and Charles Sheard—No. 34
Harding, Samuel W.—see Coleman, Howard S.
Helson, Harry—see Grove, Josephine
Herscher, L. W.—see Wright, N.
Hettinger, Edwin L.—No. 45
Hulburt, Edward O.—No. 32
Humphreys, Curtis J. and Earle K. Plyler—No. 4
—— see Plyler, Earle K.
Hunter, Richard S.—No. 50
Jacobson, W. R.—see Duntley, Seibert Q.
Johnson, F. S.—see Tousey, R.
Jones, L. C.—see Burdett, R. A.
Jones, Norman, V. Z. Williams and Konrad Dobriner—No. 6
Kaprelian, Edward K.—No. 39
Kent, Rockwell, III—No. 16
Knoll, H. A.—see Koomen, M. J.
Koomen, M. J., H. A. Knoll and R. Tousey—No. 46
Leurgans, P. J.—No. 25
Leverenz, H. W.—No. 19
Levinstein, Henry and Robley C. Williams—No. 22
Lighty, Paul E.—see Neuhaus, C. J.
Liston, Max D.—No. 1
Marron, T. U. and J. H. Muth—No. 29
Mote, Frederick A.—see Riggs, Lorrin A.
Mueller, Conrad G.—see Riggs, Lorrin A.
Muth, J. H.—see Marron, T. U.
Neuhaus, C. J.—No. 14
Nielsen, J. Rud—No. 8
—— **and Charles M. Richards**—No. 9
—— see Fast, E.
Oberly, J. J.—see Tousey, R.
O'Brien, Brian—No. 48
O'Bryan, H. M.—No. 2
Osterberg, Harold—No. 35
Perkins, Willard T.—No. 38
Plyler, Earle K. and Curtis J. Humphreys—No. 7
—— see Humphreys, Curtis J.
Reilly, Frank—No. 49
Richards, Charles M.—see Nielsen, J. Rud
Riggs, Lorrin A., Conrad G. Mueller, Clarence H. Graham and Frederick A. Mote—No. 43
Sanderson, J. A.—see Ballard, S. S.
Sheard, Charles—see Hamly, D. H.
Sloan, Louise L. and Lorraine Wollach—No. 47
Sterner, J.—see Carpenter, R. O'B.
Stewart, H. S.—see Ballard, S. S.
Strain, C. V.—see Tousey, R.
Studer, Frank J.—No. 28
Tousey, R., C. V. Strain, J. J. Oberly, F. S. Johnson and W. A. Baum—No. 31
—— see Koomen, M. J.
Turner, A. F.—see Coleman, Howard S.
Ulrich, O. A.—see Coleman, Howard S.
Van Lear, George A.—No. 41
Werner, A. J.—No. 52
Weyl, W. A.—No. 17
Williams, Robley C.—see Levinstein, Henry
Williams, V. Z.—see Jones, Norman
Wolfe, R. A.—see Enns, J. H.
Wollach, Lorraine—see Sloan, Louise L.
Wright, N. and L. W. Herscher—No. 3